Innovative polymer-based membrane materials containing reactive (RILs) and polymerizable (PIL) ionic liquids

Edyta Rynkowska

THESE

Pour obtenir le diplôme de doctorat

Spécialité : Chimie

Préparée au sein de l'Université de Rouen Normandie

En partenariat international avec Nicolaus Copernicus University in Toruń, Poland

Innovative polymer-based membrane materials containing reactive (RILs) and polymerizable (PIL) ionic liquids

Présentée et soutenue par
Edyta RYNKOWSKA

Thèse soutenue publiquement le 14 Fevrier 2019 devant le jury composé de		
Mme Aleksandra WOLIŃSKA-GRABCZYK	dr hab. inż. / Professeur / Centre of Polymer and Carbon Materials of the Polish Academy of Sciences	Rapporteur
Mr Jean-François FELLER	Professeur / Professeur / Université de Bretagne-Sud	Rapporteur
Mme Magdalena REGEL-ROSOCKA	dr hab. inż. / Assistant Professeur / Poznan University of Technology	Examinateur
Mr Stéphane MARAIS	Professeur / Professeur / Université de Rouen Normandie	Examinateur
Mr Edward SZŁYK	Professeur / Professeur / Nicolaus Copernicus University in Toruń	Examinateur
Mme Kateryna FATYEYEVA	dr HDR / McF / Université de Rouen Normandie	Codirecteur de thèse
Mr Wojciech KUJAWSKI	dr hab., HDR / Associated Professeur / Nicolaus Copernicus University in Toruń	Codirecteur de thèse

Thèse dirigée par Dr. Wojciech KUJAWSKI du Membranes and Membrane Techniques Research Group (Pologne) et Dr. Kateryna FATYEYEVA du laboratoire Polymères, Biopolymères et Surfaces, UMR CNRS 6270 (France)

Uniwersytet Mikołaja Kopernika w Toruniu
Wydział Chemii
Katedra Chemii Fizycznej i Fizykochemii Polimerów
we współpracy z
Université de Rouen Normandie (France)
Laboratoire Polymères, Biopolymères et Surfaces, UMR CNRS 6270

Edyta Rynkowska
nr albumu 502089

doktorat realizowany w trybie "co-tutelle" – podwójnego dyplomu
na kierunku chemia

Innovative polymer-based membrane materials containing reactive (RILs) and polymerizable (PIL) ionic liquids

Promotorzy

dr hab. Wojciech Kujawski, prof. UMK w Toruniu
Wydział Chemii UMK w Toruniu

dr hab. Kateryna Fatyeyeva
Université de Rouen Normandie

Toruń 2018

Pracę przyjmuję i akceptuję:

……
data i podpis opiekuna pracy

Potwierdzam złożenie pracy dyplomowej:

……
data i podpis pracownika dziekanatu

To my Mother,

who supported me for all these years

Contents

Acknowledgements

A PhD counts for more than to gain the precious experience in solving the scientific problems. Equally important is the way we shape our characters. We learn how not to give up, and if we maybe resign from something for a while, we learn how to get back on track. We learn how to be patient and persistent. We learn how to work in a group, first a group of colleagues, then a group of friends. I am very grateful for all these experiences!

I would like to express my thanks to many people who contributed to the course of this PhD. This thesis work would have not been possible without the guidance and the help of several individuals who in one way or another contributed and extended their valuable assistance in the preparation and completion of this study. Words are not able to express my gratefulness, but at least I will try.

First and foremost, I would equally like to express my profound gratitude to prof. Wojciech KUJAWSKI and dr. Kateryna FATYEYEVA – the co-directors of my cotutelle PhD thesis for giving me the opportunity to conduct my research in Zespół Membran i Technik Membranowych at the NCU in Toruń (Poland) and PBS Laboratory at the University of Rouen Normandy (France), respectively. For their invaluable help, assistance and guidance, meaningful discussions, suggestions, and their effort to review the manuscripts of the PhD thesis and articles. To prof. Wojciech KUJAWSKI, who taught me many things during my PhD. His excellent writing and presenting oral communications experiences, as well as his worldwide expertise became an invaluable inspiration for me. I am truly grateful for all the opportunities and challenges I had for all those years. To dr. Kateryna FATYEYEVA whose constant advice, constructive criticism, and encouragement immensely helped me in the continuation of this research work. Her great knowledge and experience helped me to develop my skills as a scientist. For her valuable suggestions and unfailing support throughout the course of my thesis work. For her patience, always friendly attitude, and numerous help with French bureaucracy over all those years.

I would also like to record my sincere thanks to prof. Stéphane MARAIS for contributing to the articles and the results discussion in this thesis with his expertise, effort, and enthusiasm, which helped many times in the troubleshooting of various issues encountered during my PhD thesis.

Dr Joanna KUJAWA for sharing her vision, and giving suggestions on the interpretation of the results and corrections of the articles' manuscripts. Special thanks for the help to prepare for the entrance exam for the PhD study and to prepare for the interview in the French Embassy before starting the cotutelle PhD thesis.

Dr. Andrzej WOLAN for the discussions about ionic liquids and sharing his organic chemistry knowledge.

Prof. Quang Trong NGUYEN for his kind concern, valuable advices, and discussions from time to time about PVA crosslinking.

I would like to thank all members of Zespół Membran i Technik Membranowych and MPBM team, especially, the members of PBS laboratory for their support, help and creating a great atmosphere in the department. For being my "expat family" for the last couple of years! For the possibility to blend in a little, by getting to know the customs and traditions, the language and the cuisine of France and your native countries.

To my teammates in Poland: Kasia, Ewelina, Ania, Asia for their help, the mutual support in our ups and downs, for all the laughter and optimism, fruitful discussions about science and life, conferences we attended together (especially the one in Zakopane), to mention a few. And most of all, for making me feel, on my returns, like I have never left.

To my former and present officemates: Sebastien, Raphaël, Vincent, Ferhat, Bassidi, Tiphaine, Etienne, Julien for all the good times we had in our too cold/too hot office (delete where inapplicable). For all countless unforgettable memories.

To my floormates: Jorge, Naila, Nagihan, Quentin, Elias, Aracelys, Clement, Julie, Sara for making those years what they were.

To all the 3rd floor team including dr. Corinne CHAPPEY, Laurent COLASSE, dr. Nadege FOLLAIN, prof. Laurent LEBRUN, it was my great pleasure to work with you. Thank you for the time we shared in PBS. To dr. Chappey, for all the talks we had, and her artistic talents she shared with me.

To the members of Chair of Physical Chemistry and Physicochemistry of Polymers at the NCU in Toruń: dr Piotr ADAMCZAK, dr Magdalena GIERSZEWSKA, prof. Stanisław KOTER, dr Izabela KOTER, dr. Jacek NOWACZYK, dr. Ewa OLEWNIK-KRUSZKOWSKA, dr Piotr SZCZEPAŃSKI for all the comments, suggestions, and fruitful discussions during our numerous seminars.

To all my friends, Gabi, Naila, Cedric, Jorge, Seb, Magda, Gosia, Ola, Julita, Bartek, Kasia, Ewelina, Nagihan, for great moral support in better and worse times, friendly discussions, steadfast encouragement.

This thesis and the work behind it were financed by the Harmonia research project that received the funding from the Polish National Science Centre (grant agreement 2015/18/M/ST5/00635). It was also supported by Hubert Curien's Partnership Program "Polonium" (35501/2016). I would like to acknowledge the financial support of the French Government and the French Embassy in Poland (scholarship 848642E, 878205J, 912422E).

Last but not the least, I wish to acknowledge the support provided by my Mom and my Family. Dziękuję Wam za to, że dzielicie ze mną momenty szczęścia i jesteście bezcennym i niezastąpionym wsparciem w trudnych chwilach!

List of Figures

List of Tables

Abbreviations & Nomenclature

Abbreviations

[AMIM][Cl]	1-allyl-3-methylimidazolium chloride
[BMIM][BF4]	1-butyl-3-methylimidazolium tetrafluoroborate
[BMIM][Cl]	1-butyl-3-methylimidazolium chloride
[BMIM][PF6]	1-butyl-3-methylimidazolium hexafluorophosphate
[BMIM][Tf2N]	1-butyl-3-methylimidazolium bis(trifluoromethanesulfonyl)imide
[EMIM][PF6]	1-ethyl-3-methylimidazolium hexafluorophosphate
[EMIM][Tf2N]	1-ethyl-3-methylimidazolium bis(trifluoromethanesulfonyl)imide
AFM	atomic force microscopy
AGU	anomeric glucose unit
ATBC	acetyltributyl citrate
BMI	1-butyl-3-methyl-imidazolium cation
BMPyr	1-butyl-1-methyl-pyrrolidinium cation
CA	cellulose acetate
CAB	cellulose acetate butyrate
CAM	contact angle measurements
CAP	cellulose acetate propionate
CNCs	cellulose nanocrystals
CNTs	carbon nanotubes
CTA	cellulose triacetate
CTR	citric acid
DEP	diethyl phthalate
DIDP	di-isodecyl phthalate
DINP	di-isononyl phthalate
DIPS	diffusion-induced phase separation
DOA	dioctyl adipate
DOP	dioctyl phthalate
EIPS	evaporation-induced phase separation
ENR	epoxised natural rubber
EtAc	ethyl acetate
ETBE	ethyl *tert*-butyl ether

EtOH	ethanol
FAP	tris(pentafluoroethyl)trifluorophosphate anion
FTIR-ATR	Fourier transform infrared spectroscopy with attenuated total reflectance
FTMs	facilitated transport membranes
GA	glutaraldehyde
HMI	1-hexyl-3-methyl-imidazolium cation
HSP	Hansen's solubility parameters
ILs	ionic liquids
IPA	propan-2-ol
LOD	limit of detection
LOQ	limit of quantification
MOFs	metal organic frameworks
NIPS	nonsolvent-induced phase separation
NMR	nuclear magnetic resonance
PAA	poly(acrylic acid)
PDLLA	poly(D,L-lactide)
PDMS	polydimethylsiloxane
PEG	poly(ethylene glycol)
PIL	polymerizable ionic liquids
PIL1_Cl	1-methyl-3-(4-vinylbenzyl)-imidazolium chloride
PILMs	polymerized ionic liquid membranes
PIMs	polymer inclusion membranes
PLA	polylactic acid
PMMA	poly(methyl methacrylate)
PTFE	poly(tetrafluoroethylene)
PTG	poly(tetramethylene glutarate)
PTS	poly(tetramethylene succinate)
PV	pervaporation
PVA	poly(vinyl alcohol)
PVC	poly(vinyl chloride)
RH	relative humidity
RIL1_Br	3-(1,3-diethoxy-1,3-dioxopropan-2-yl)-1-methyl-1H-imidazol-3-ium bromide
RIL2_Br	1-(2-ethoxy-2-oxoethyl)-3-methylimidazolium bromide

RIL3_BF4	1-(2-ethoxy-2-oxoethyl)-3-methylimidazolium tetrafluoroborate
RILs	reactive ionic liquids
RSD_r	relative standard deviation for the repeatability
RSD_R	relative standard deviation for the reproducibility
RTILs	room-temperature ionic liquids
SA	succinic acid
SEM-EDX	scanning electron microscopy coupled with energy-dispersive X-ray
SGPV	sweeping gas pervaporation
SLMs	supported liquid membranes
SPEEK	sulfonated poly(ether ether ketone)
SSA	sulfosuccinic acid
TBC	tributyl citrate
TCD	thermal conductivity detector
TEC	triethyl citrate
TEOS	tetraethoxysilane
TGA	thermogravimetric analysis
TIPS	temperature-induced phase separation
TPV	thermopervaporation
TSILs	task-specific ionic liquids
UV	ultraviolet light
VIPS	vapor-induced phase separation
VOCs	volatile organic compounds
VPV	vacuum pervaporation
WAXD	wide angle X-ray diffraction
WPU	waterborne polyurethane
βCD	β-cyclodextrin

Symbols

A	membrane area [m^2]
a_i	activity of compound i ($a_i = \gamma_i c_i$) [-]
c_i	molar fraction of compound i [-]
D	diffusion coefficient [$cm^2\ s^{-1}$]
d	thickness of membrane sample [μm]
D_0	diffusion coefficient for a permeant concentration equals to zero [$cm^2\ s^{-1}$]

DS	degree of substitution [-]
DS_{max}	maximum theoretical degree of substitution [-]
E	total cohesion energy of a liquid [eV]
E_D	activation energy of diffusion [kJ mol^{-1}]
E_P	activation energy of permeation [kJ mol^{-1}]
F	Faraday constant [C mol^{-1}]
J	flux or transfer rate per unit area of material [kg m^{-2} h^{-1}]
$J_{N,i}$	thickness-normalized permeate flux [µm kg m^{-2} h^{-1}]
J_{stat}	thickness-normalized stationary state flux [µm kg m^{-2} h^{-1}]
J_t	total permeate flux [kg m^{-2} h^{-1}]
k	factor dependent on membrane morphology [-]
M_{AGU}	average molar mass of the anhydroglucose unit in CAP [g mol^{-1}]
m_{CAP}	weight of CAP [g]
M_{RIL}	molar mass of ionic liquid [g mol^{-1}]
m_{RIL}	weight of RIL [g]
M_{sol}	solvent molecular mass [g mol^{-1}]
P	permeability coefficient [1 Barrer = $\frac{10^{-10} cm^3(STP)\cdot(cm\ membrane\ thickness)}{(cm^2\ membrane\ area)\cdot(cmHg\ pressure)\cdot s}$]
$p_{i,l}$	partial pressures of component i on either side of the membrane [Pa]
P_i/l	permeance [1 gpu = $\frac{10^{-6} cm^3(STP)}{cm^2\ s\ cmHg}$]
PSI	pervaporation separation index [kg m^{-2} h^{-1}]
PSI_N	thickness-normalized pervaporation separation index [µm kg m^{-2} h^{-1}]
Q_{exp}	amount of diffusing molecules accumulated in the downstream compartment [mmol]
R	gas constant [J mol^{-1} K^{-1}]
r	pores radius [nm]
R_a	arithmetic average height [nm]
R_q	root mean square roughness [nm]
S	solubility coefficient [$\frac{cm^3(STP)\ cm^3}{cmHg}$]
$S1$	integral of the resonance of the imidazolium ring proton (7.81 ppm) [-]
$S2$	integral of the proton resonance of AGU (5.10 ppm) [-]
S_a	solubility in the amorphous phase [m^3 cm^{-3} cmHg^{-1}]
SD_M	molar swelling degree [mol solvent/g dry membrane]

SFE	surface free energy [mJ·m^{-2}]
S_i	molar entropy of compound [J mol^{-1} K^{-1}]
s_o	total surface area of the pores [m^2 g^{-1}]
T	temperature [°C]
T_c	critical temperature [°C]
T_g	glass transition temperature [°C]
t_l	time called “time-lag” [s]
T_m	melting temperature [°C]
T_{onset}	onset temperature [°C]
V	volume of the downstream compartment [cm^3]
V_i	molar volume of compound [m^3 mol^{-1}]
V_m-*VdW*	Van der Waals molar volume [cm^3 mol^{-1}]
$V_{permeant}$	partial volume of permeant [cm^3]
W_{dry}	mass of the dry membrane [g]
W_{wet}	mass of the equilibrated membrane [g]
x_i	mass fraction of component *i* in the feed [g g^{-1}]
y_i	mass fraction of component *i* in the permeate [g g^{-1}]
YM	Young’s modulus [MPa]
z_i	valence of the compound [-]

Greek symbols

γ^D	dispersive component [mJ·m^{-2}]
γ_i	activity coefficient of compound *i* [-]
γ^P	polar component [mJ·m^{-2}]
μ_i^0	electrochemical potential [J mol^{-1}]
$\alpha_{i/j}$	membrane selectivity [-]
β	separation factor [-]
γ	plasticization factor [-]
γ	surface tension [J m^{-2}]
γ_L	surface free energy of liquid used in measurements [N m^{-2}]
γ_{LV}	interfacial surface free energy between liquid and vapor [N m^{-2}]
γ_S	surface free energy of solid in vacuum [N m^{-2}]
γ_{SL}	interfacial surface free energy between solid and liquid [N m^{-2}]

γ_{SV}	interfacial surface free energy between solid and vapor [N m^{-2}]
δ	Hansen's solubility parameter [$MPa^{1/2}$]
Δa	difference of water activity between upstream and downstream compartment [-]
ΔC	difference of concentration [-]
δ_d	dispersion interactions [$MPa^{1/2}$]
ΔE	difference of electric potential [V]
δ_h	hydrogen bonding interactions [$MPa^{1/2}$]
ΔH_{cond}	permeant molar enthalpy of condensation [kJ mol^{-1}]
ΔH_m	melting enthalpy [kJ·mol^{-1}]
ΔH_{mix}	partial molar enthalpy of permeant/polymer mixing [kJ mol^{-1}]
ΔH_s	partial molar enthalpy of dissolution [kJ mol^{-1}]
$\Delta_{I,II}P$	pressure difference [Pa]
$\Delta_{i,j}$	distance parameter [$MPa^{1/2}$]
Δm_t	permeate mass [g]
Δp	difference of pressure [Pa]
δ_p	polar interactions [$MPa^{1/2}$]
ΔT	difference of temperature [°C]
$\Delta\mu$	difference in chemical or electrochemical potential [V]
ε	volume porosity [-]
ε_{max}	elongation at break [%]
ε_{pow}	surface porosity [-]
η	viscosity [Pa s]
θ	contact angle [°]
σ_{max}	stress at break [MPa]
τ	tortuosity factor [-]
Φ	electric potential in a given phase [V]
ϕ_d	dynamic diameter [Å]
$\phi_{polymere}$	polymer volume fraction in the mixture [-]
χ_c	degree of crystallinity [%]

Introduction

Originating from biological membranes in living organisms to synthetic membranes used in industry, membranes are of essential importance in our everyday life. Over the last decades, membrane processes made a great contribution to the improvement and development of many industrial separation technologies due to their versatility, low-energy demand, and opportunity to work with thermolabile compounds. Membrane separation technologies constitute a viable alternative or complement technique to the conventional energy-consuming methods, such as distillation, evaporation, liquid-liquid extraction. Pervaporation process is an important example of membrane techniques providing the diverse possibility of liquid-liquid separation, e.g. dewatering, separation of azeotropic mixtures or removal of volatile organic compounds (VOCs).

Membranes for the pervaporation should possess chemical stability and mechanical strength at elevated temperatures, and be highly selective. Membrane properties determine the overall efficiency of the separation process. There is a wide variety of possible materials (e.g. ceramics, zeolites, polymers) used for the membrane elaboration. The significant attention of researches has been attracted by polymer materials, particularly the ones that are biodegradable and derived from the renewable resources. Recently, research has been also focused on the development of polymer membranes filled with ionic liquids (ILs) that are characterized by numerous interesting properties. Due to the polymer plasticizing effect and ion-exchange capability, various ILs are intensively used as components of polymer membranes [1].

Polymer membranes containing ILs possess wide range of advantages over the classical polymer membranes. Molecular diffusion is much higher in ionic liquid than in polymers; therefore, the use of polymer-IL membranes in separation processes can result in a much better separation and higher fluxes. Such membranes can be successfully applied in liquid separation by pervaporation, in gas separation, in separation of metal ions as well as separators in fuel cells. However, the main disadvantage of already used polymer-IL membranes is the leaching out of ILs from the membrane during the process.

Therefore, the purpose of this study is to obtain new stable composite materials by combining IL with polymers in order to take advantage of properties of both kind of materials. Two kinds of ILs (reactive and polymerizable) and two kind of polymers (cellulose acetate propionate, CAP and poly(vinyl alcohol), PVA) are used and

characterized by different techniques. The membrane efficiency is discussed in terms of preparation conditions and transport and separation properties.

The research work was conducted in the Membranes and Membrane Techniques Research Group at the Faculty of Chemistry of Nicolaus Copernicus University in Toruń (Poland) and in the Laboratory of Polymers, Biopolymers, Surfaces (PBS) UMR CNRS 6270 at University of Rouen Normandie (France). This cooperation resulted from bilateral research in the frame of the Harmonia 7 program (2015/18/M/ST5/00635) financed by the National Science Centre and the joint (co-tutelle) PhD thesis with the financial support of the French Government and the French Embassy in Poland (scholarship 848642E, 878205J, 912422E). The research groups from Poland and from France have been working together since 2007 in the frame of basic research including structural material properties [2-5].

This PhD thesis is divided into four chapters. Chapter 1 “Bibliography” is devoted to the literature review of the separation membranes and introduces the principles of transport through dense polymer membranes, and the basics of the pervaporation process.

Chapter 2 “Materials & Characterization” gives the detailed information about studied materials, methods of IL and polymer-IL membranes preparation, as well as the detailed description of characterization methods used.

Chapter 3 and Chapter 4 present the physicochemical, equilibrium, and transport properties of PVA-IL and CAP-IL membranes, respectively. The special attention is paid on the hydrophilic pervaporation, as the incorporation of IL into the polymer structure makes such membranes potential candidates for dehydration.

The last part “Conclusions & Prospects” summarizes the main results obtained during the study and gives possible prospects for the future research.

CHAPTER 1

Bibliography

In this chapter a general introduction into the membrane separation processes will be given. Special attention will be paid to the key requirements of the membrane materials and their transport and barrier properties.

1.1 Basics of Membrane Separation Processes

Membrane-based technology provides essential and efficient separation methods characterized by multiple advantages over conventional separation processes, such as distillation or chemical extraction [6]. The application of membranes offers higher separation efficiency, relatively lower cost and energy consumption, tunable design, and possibility of operation at the ambient temperature [6-8]. As a consequence, membrane technology is nowadays a wide area comprising various industries: water treatment (desalination of sea and brackish water), biotechnology (purification of bioproducts), food and beverage (processing of dairy and fruit juice) [9], medical (artificial kidneys, blood oxygenators, controlled release of pharmaceuticals) [10], as well as energy generation and storage (fuel cells, supercapacitors) [11]. The aforementioned industrial exploitation of synthetic membrane materials is based on the following main processes that diverse in terms of different criteria (e.g. driving force, membrane type, size of separated molecules): reverse osmosis, ultrafiltration, microfiltration, gas separation, pervaporation, and electrodialysis (Table 1) [11]. Despite the variety of membrane processes, in each case the membrane is the key component. Therefore, the design, elaboration, and comprehensive investigation of membrane materials with the improved or novel characteristics have been driving the current research in membrane technology field.

1.1.1 Membrane Definition

In general, membrane is a solid, liquid or gas barrier that separates two phases and actively or passively allows the selective transport of various chemical species [12]. The membrane separation is characterized by the transport rates and separation effectiveness. The transport through the membrane occurs by applying a given driving force (Table 1).

Table 1. The characteristics of some membrane separation techniques [11, 13].

Technique	Driving force	Feed/permeate phase
Microfiltration	Pressure difference	Liquid/liquid
Pervaporation	Chemical potential difference	Liquid/vapor
Membrane distillation	Vapor pressure difference	Liquid/vapor
Vapor permeation	Chemical potential difference	Vapor/vapor
Gas separation	Pressure difference	Gas/gas

In general, the driving force is defined as a difference in chemical or electrochemical $\Delta\mu$ potential on both sides of the membrane caused by the difference of pressure (Δp), concentration (ΔC), temperature (ΔT) or electric potential (ΔE). Solvents or solutes can be selectively transported through the membrane from feed to permeate side or they can be retained by the membrane depending on its inner structure and nature as well as on various physical and chemical properties of separated species, e.g. size, charge, or activity (Figure 1) [6, 14].

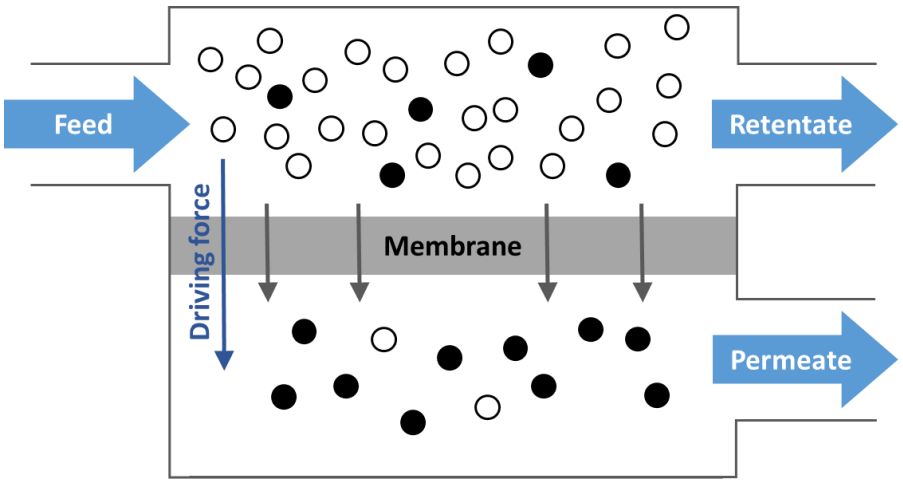

Figure 1. Scheme of species separation through the membrane.

The selective separation occurs due to different transport rates between separated components as well as the various affinity between the membrane and the separated species.

1.1.2 Membrane Types

Depending on the origin, nature, morphology, or elaboration method, various kinds of membranes exist (Figure 2).

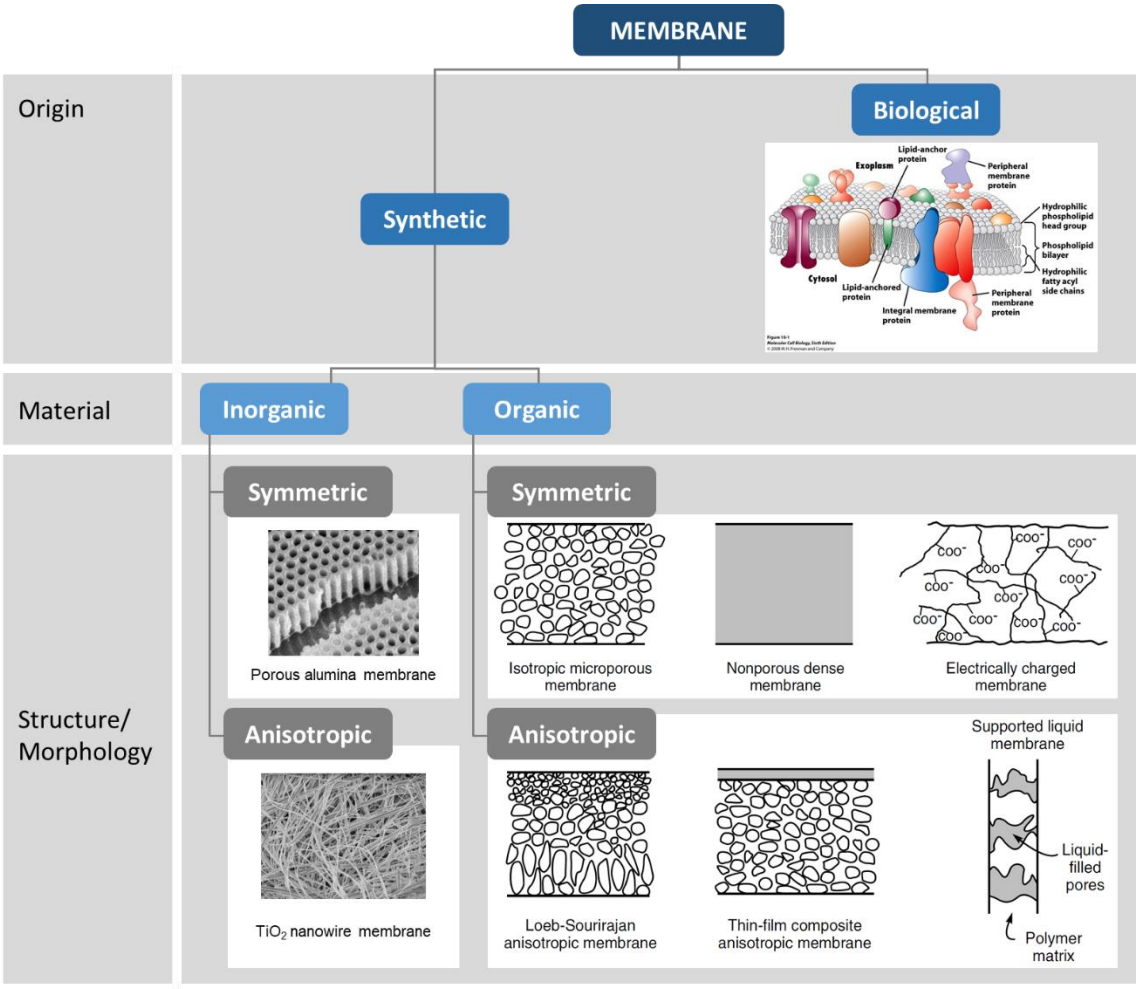

Figure 2. General membrane classification (based on Figure 1.1 in Membrane Technology and Applications with permission of Baker et al. [11]).

Two main classes of the synthetic membranes can be distinguished: organic (polymer) and inorganic. The latter one is typically based on zeolites and ceramics, e.g. alumina, zirconia or titania. Inorganic membranes are characterized by the high tensile strength, superior chemical stability and resistance to applied temperature or pressure

compared to organic membranes. However, inorganic membranes are still expensive, that restricts their industrial application. The synthetic membranes based on polymers are the major class of materials designed for the membrane-based technologies due to the extensive variety of their properties and structures [15].

Taking into account the membrane structure and morphology, the membrane can be either homogenous with uniform structure and composition or heterogeneous possessing pores or a layered structure (Figure 2). Microporous, nonporous, dense, and electrochemically charged membranes can be distinguished among the symmetrical (isotropic) membranes. Anisotropic membranes can be divided into integrally asymmetric (Loeb-Sourirajan), composite, and supported liquid membranes.

1.1.2.1 Isotropic (Symmetrical) Membranes

Nonporous dense membranes. Generally, nonporous membranes consist of a dense film that transports the permeants by a solution-diffusion mechanism under driving force induced by concentration, pressure, or electrical potential difference. The separation of permeants depends on their various solubility and diffusivity in the membrane material. Therefore, polymer materials can be used to separate molecules with comparable size. Dense membranes are used in pervaporation, gas separation, and reverse osmosis. On the laboratory scale, they can be prepared by solution casting or thermal melting extrusion [11]. The melting extrusion technique is used to prepare nonporous membrane films based on polymers that do not dissolve in any solvent, and, thus, cannot be prepared by using the solution casting method.

Solution casting combined with phase-inversion is one of the most commonly used technique for elaboration of single- or multi-layered dense or porous membranes in wide variety of fields, including membrane separation techniques, such as pervaporation [16, 17]. In general, the dense membranes are formed due to the solvent evaporation from the binary solution consisting of polymer and solvent, whereas porous membranes are obtained during the phase separation of polymer solution in the presence of non-solvent. These type of membranes will be described more in detail in the section related to anisotropic membranes (Section 1.1.2.2). The membrane preparation by a solution casting method consists of preparing the homogenous solution by dissolution of polymer and other chosen ingredients in the common solvent; spreading of the given polymer solution across a leveled flat plate using a casting knife (Figure 3). The casting knife possesses the

stainless steel blade that provides the precise slit of a desired thickness. The cast solution is left for the solvent evaporation that results in a formation of a thin polymer film.

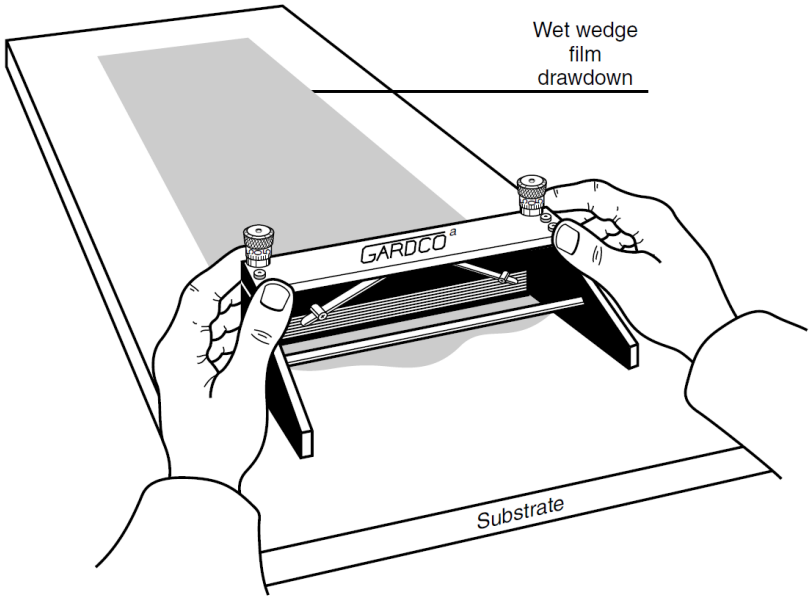

Figure 3. Scheme of membrane casting with manual casting knife (reprinted with permission from ref. [11]).

In principle, the polymer solution used for casting should be sufficiently viscous in order to avoid its leaking from the casting plate. The solvents used for the polymer solution preparation should be moderately volatile such as acetone or cyclohexane that would allow obtaining a dry membrane film within few hours. During the prolonged time of solvent evaporation, the cast polymer film can absorb moisture that can lead to the polymer precipitation, and, thus, opaque surface of the polymer film. In the case of rapid evaporation of very volatile solvents, the polymer gelation takes place that results in the mottled surface. After complete solvent evaporation, the dry nonporous polymer film can be removed from the casting plate [10, 11]. Dense polymer membranes, which are the subject of research in this thesis, will be described more in detail in the Chapter 3 and Chapter 4.

Isotropic microporous membranes. The isotropic microporous membranes possess rigid and isotropic structure containing interconnected pores with the diameter varied from 0.001 to 10 μm. Thus, the separation of permeants by this membrane is affected by their molecular size and pore size distribution. The use of such membranes ensures higher fluxes in comparison to isotropic dense membranes. This kind of membrane is widely used in microfiltration, in battery and fuel cell applications as inert

spacers, and in drug delivery systems as a rate-controlling element. The majority of isotropic microporous membranes is prepared by the phase separation techniques. In addition, different special techniques developed by industrial companies can be used: track etching, expanded-film, and template leaching.

Electrically charged membranes. Electrically charged membranes, known as ion-exchange membranes, possess the dense or microporous structure with fixed negatively (cation-exchange membrane) or positively (anion-exchange membrane) charged ions. The separation through ion-exchange membranes is determined by the charge and concentration of ions.

1.1.2.2 Anisotropic (Asymmetrical) Membranes

Anisotropic (asymmetric) membranes have a layered structure varying in composition, porosity, or pore size. Such membrane materials consist of a very thin surface layer deposited on a significantly thicker porous support. In this case, the membrane separation properties are exclusively dependent on the surface layer, whereas the porous layer plays a role of a mechanical support [10, 11, 17]. Due to the very thin selective layer, such materials provide the improved membrane fluxes.

Integrally asymmetric (Loeb-Sourirajan) membranes. The characteristic example of anisotropic membrane is the integrally asymmetric membrane developed by Loeb–Sourirajan (Figure 4).

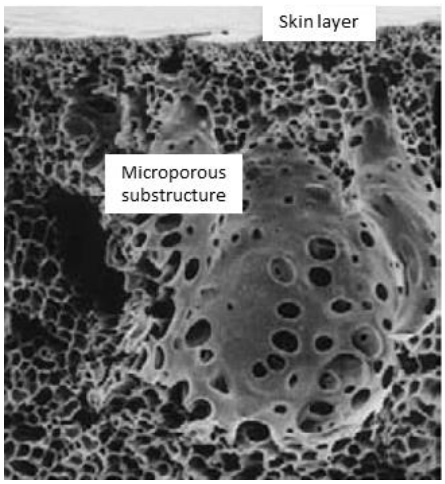

Figure 4. Scanning electron micrograph of anisotropic polysulfone membrane obtained by the Loeb–Sourirajan phase separation process (reprinted with permission from [11]).

This membrane type is prepared by a phase separation technique [18]. The resultant membrane possesses coupled asymmetric structure consisting of the either porous or dense “skin” layer and the highly porous support as shown in Figure 4. Integrally asymmetric membranes with a porous skin layer have found applications in dialysis, ultra-, and microfiltration, whereas the ones with dense skin layer can be used in reverse osmosis or gas separation [19].

Phase separation (known as phase inversion or polymer precipitation process) is the most common technique to prepare anisotropic and isotropic polymer membranes. This technique is based on the precipitation of an initially homogenous polymer solution into two phases, namely polymer- and solvent-rich phases. The polymer-rich phase (solid phase) is a basis of the membrane matrix, whereas the membrane pores originate from the solvent-rich phase (*i.e.* polymer-lean phase). In the phase separation process, the precipitation of the polymer solution can be achieved by various factors, therefore, the following types of the phase separation method can be distinguished [11, 17]:

1. nonsolvent-induced (or diffusion-induced) phase separation (NIPS or DIPS) known as the Loeb–Sourirajan membrane process, where the precipitation is induced by immersion into a nonsolvent bath (usually water);
2. temperature-induced phase separation (TIPS), where precipitation of polymer solution is obtained by cooling of the casing solution layer;
3. evaporation-induced phase separation (EIPS), where the precipitation is achieved by evaporation of a volatile solvent from the casting polymer solution;
4. vapor-induced phase separation (VIPS), where polymer solution precipitation is caused by the adsorption of the nonsolvent from the vapor phase.

Thin-film composite membranes. Composite membranes are composed of at least two layers based on various membrane materials: the selective skin layer and the porous support that plays a role of a mechanical substrate. Different methods of the thin-film deposition on porous support were developed, such as solution coating technique (in this case the thin dense polymer layer on the microporous polymer support is obtained by the solution casting) or interfacial polymerization (*i.e.* the polymerization of an extremely thin monomer solution layer on a microporous polymer support). The composite membranes can be exploited in the reverse osmosis, gas separation or pervaporation [19].

Supported liquid membranes. Supported liquid membrane is composed of a porous solid support filled with a selective liquid carrier. Porous membrane matrix provides a mechanical support for the liquid carrier immobilized in pores by capillary

forces. The separation process is dependent on the liquid carrier characteristics and the permeate transport is based on the facilitated mass transfer [18].

The polymer-based membranes, due to their remarkable properties, are suitable for wide range of application, such as biomaterials [20], electrolytes in fuel cells [21], sensors [11], selective barrier used in separation of gas and liquid mixtures (pervaporation, gas separation, reverse osmosis, nano-, micro-, ultrafiltation) [15, 22], and recovery of metal ions [23]. However, their efficiency is still limited because of the moderate functionalization [6]. Thus, the design and elaboration of the polymer membrane material with the improved or novel characteristics attract the researchers' attention in the membrane technology field.

1.2 Membrane Transport Theory

In order to describe the transport of permeants through the membrane, three mechanisms can be distinguished depending on the membrane type: pressure-driven convective flow, molecular diffusion, and facilitated transport mechanism [11, 24].

A solution-diffusion model is based on a solution and diffusion phenomena that describe the transport in nonporous dense and composite membranes (Figure 5A). According to a solution-diffusion model, the transport and separation of permeants result from the various affinity and physicochemical properties of components in respect to a polymer membrane. Due to their various solubility in the membrane and different diffusion rates, the permeants separation occurs. Dense nonporous membranes are the subject of this research, therefore, the solution-diffusion model is described more in detail in section 1.2.1.

Pressure-driven convective flow is the basis of the pore-flow model describing the transport of permeants in porous membranes (Figure 5B). The transport and separation of molecules through the porous membranes are mainly influenced by the molecular size, weight, and shape of components in relation to the dimensions of membrane pores. As a result, a given permeant can move through membrane pores, while other permeants are rejected by the membrane. The transport through porous membranes can be described by the Hagen-Poiseuille (Eq. (1)) or Carmann-Kozeny (Eq. (2)) equations:

$$J_v = \frac{\varepsilon_{pow} * r^2}{8 * \eta * \tau} \Delta_{I,II} P \qquad (1)$$

$$J_v = \frac{1}{\eta * l * k * s_0^2} * \frac{\varepsilon^3}{(1-\varepsilon)} \Delta_{I,II} P \quad (2)$$

where $\Delta_{I,II}P$ is the pressure difference, r is the pores radius, η is the viscosity, τ is the pores tortuosity factor, ε_{pow} is the surface porosity, k is the factor dependent on membrane morphology, ε is the volume porosity, and s_0 is the total surface area of the pores.

The facilitated transport mechanism describes the transport and separation of permeants in supported liquid membranes. The permeants transport occurs due to the complexation of a given permeant by a carrier immobilized in the porous membrane support (Figure 5C).

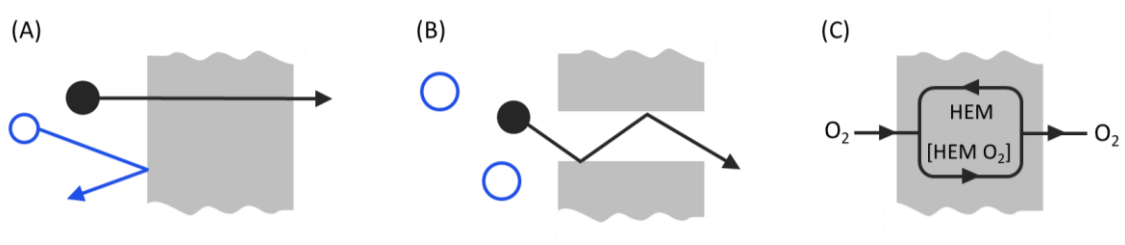

Figure 5. General scheme of permeants' transport through membranes according to the following models: (A) solution-diffusion, (B) pore-flow, and (C) facilitated transport.

1.2.1 Solution-Diffusion Model

As it was mentioned, the transport of permeant molecules (gas, vapor, or liquid) through a dense nonporous polymer membrane is described by the solution-diffusion model [25] (Figure 6). As a result, this model is used to describe the following membrane separation processes: pervaporation, gas separation, and reverse osmosis.

According to this mechanism, the permeation of individual molecules (gas, vapor, or liquid) through the membrane involves three consecutive steps:

(i) permeant sorption into the membrane on the feed side,

(ii) diffusion of permeant through the membrane,

(iii) desorption of permeant at the permeate side [26].

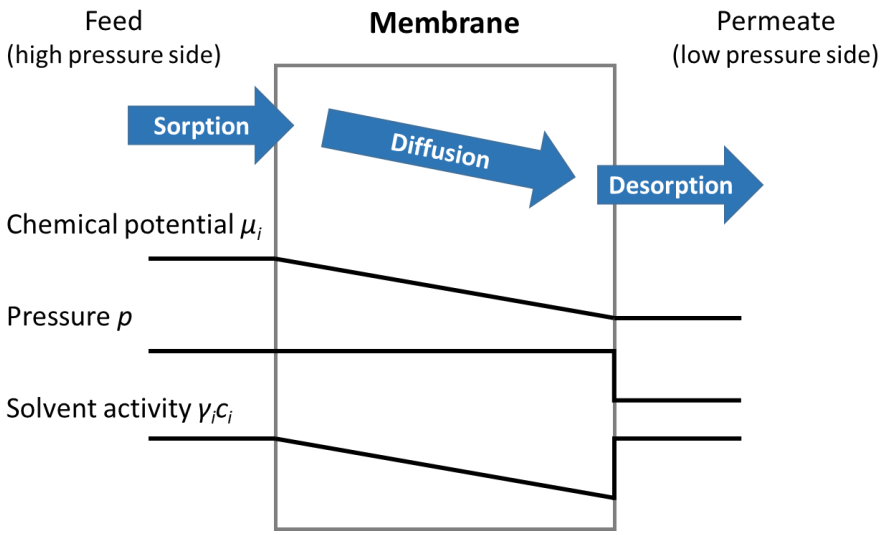

Figure 6. Scheme of permeants' transport through the membrane according to the solution-diffusion mechanism (based on Figure 2.12 in Membrane Technology and Applications of Baker et al. [11]).

The solution-diffusion model assumes that the pressure across the membrane is uniform, whereas the difference of the chemical potential through the membrane is expressed only by the concentration difference as depicted in Figure 6 [16]. The chemical potential is defined as follows:

$$\tilde{\mu}_i = \mu_i^0 + RT \ln a_i + z_i F \Phi \tag{3}$$

where μ_i^0 is the electrochemical potential, R is the gas constant, T is the temperature, a_i is the activity of compound i ($a_i = \gamma_i c_i$, where γ_i – activity coefficient of compound i, c_i – molar fraction of compound i), z_i is the valence of the compound i, Φ is the electric potential in a given phase, and F is the Faraday constant.

The change of the chemical potentials is described according to the following expression:

$$\Delta\tilde{\mu}_i = -S_i \Delta T + V_i \Delta p + RT \ln a_i^{II}/a_i^{I} + z_i F \Delta\Phi \tag{4}$$

where S_i is the molar entropy of compound i and V_i is the molar volume of compound i. Eq. (4) shows that the solution-diffusion process can be induced by the increase of temperature, pressure, electrical potential and activity, as well as by the increase of volatility in the case of a mixture of gaseous components. In practice, the separation is carried out under the influence of one specific stimulus.

Desorption is a very fast stage due to the decreased pressure at the permeate side, therefore, it is considered that desorption does not affect the membrane performance. Sorption (quantified by a solubility coefficient *S*) and diffusion (quantified by a diffusion coefficient *D*) phenomena have a crucial influence on the permeation process according to the following expression [27]:

$$P = S \cdot D \text{ [Barrer]} \quad (5)$$

where P is a permeability coefficient, usually expressed in Barrer (1 Barrer = $\frac{10^{-10} cm^3(STP) \cdot (cm\ membrane\ thickness)}{(cm^2\ membrane\ area) \cdot (cmHg\ pressure) \cdot s}$ or $\frac{m^2}{s}$ (SI units)), S in $\frac{cm^3(STP)\ cm^3}{cmHg}$, and D in $\frac{cm^2}{s}$. STP corresponds to the standard temperature (T = 273.15 K) and pressure (p = 1.013 10^5 Pa) conditions.

1.2.1.1 Sorption

The sorption is a thermodynamic process described by the solubility coefficient *S*, corresponding to the initial penetration and dispersion of permeant molecules into the polymer matrix due to the absorption and dissolution of molecules in a given polymer. The solubility coefficient is influenced by the concentration gradient created when the given component of a feed solution is sorbed preferentially on the membrane surface. The equilibrium state during sorption occurs when the concentration of sorbed molecules in the polymer is equal to their concentration in bulk liquid. As a result of the concentration gradient, the sorbed molecules subsequently diffuse to the opposite membrane surface. The sorption selectivity is a key factor in order to explain the selective transport in membrane separation process. Moreover, it provides the crucial information during the selection of a suitable membrane material for a given separation process.

Sorption of molecules depends on their solubility in the polymer structure that is described by the solubility parameter theory using Hansen's solubility parameters (HSP). Due to the sorption process, the interaction between the polymer chains changes, resulting in the membrane swelling, which facilitates the permeant diffusion through the membrane [28]. In some cases, the affinity between a polymer matrix and liquid permeate is strong enough, so the preliminary polymer crosslinking is required in order to avoid its dissolution.

HSP refers to a cohesive energy that involves hydrogen bonding δ_h, polar δ_p, and dispersion δ_d interactions. Solubility parameters δ_i can be used to calculate the distance

parameter $\Delta_{i,j}$ (Eq. (6)) that provides information about the affinity between permeates as well as between permeates and membrane. Moreover, the distance parameter explains the preferential sorption of a given component of a liquid mixture into the membrane matrix [11, 16]. The lower value of distance parameter $\Delta_{i,j}$ corresponds to the higher affinity between two components.

$$\Delta_{i,j} = \left[\left(\delta_{d,i} - \delta_{d,j}\right)^2 + \left(\delta_{p,i} - \delta_{p,j}\right)^2 + \left(\delta_{h,i} - \delta_{h,j}\right)^2\right]^{0.5} \quad (6)$$

The permeant solubility is influenced also by temperature and by the permeant size. Van Krevelen [29] pointed out that the solubility of a given gas does not change extensively; however, the gas nature and its dynamic diameter affects the solubility of different gases in a given polymer. Generally, the solubility increases with the increasing gas permeant size and the solubility parameter *S* value changes in the following order:

$$S_{H2}\ (0.75) < S_{N2}\ (1) < S_{O2}\ (2.2) < S_{CO2}\ (24)\ [29].$$

Naylor indicated that the doubling of the gas molecular volume increases the solubility value by a factor of about 200 [25]. Houde and Stern [30] also observed the increase of the solubility coefficient *S* value for the ethyl cellulose membranes at 35°C and at around 3.040 kPa in the following row:

$$S_{He} << S_{N2} < S_{O2} < S_{CH4} < S_{CO2}$$

that was correlated to the increase of the critical temperature (T_c) of the tested gases [30]:

$T_{c,He}$ (–298.0°C) < $T_{c,N2}$ (–146.9°C) < $T_{c,O2}$ (–118.6°C) < $T_{c,CH4}$ (–82.6°C) < $T_{c,He}$ (31.0°C)

Also, the solubility depends on the temperature according to the Arrhenius-type dependence:

$$S = S_0 e^{\frac{-\Delta H_S}{RT}}, \quad (7)$$

where S_0 is the constant, T is temperature, R is a gas constant, and ΔH_s is a partial molar enthalpy of dissolution:

$$\Delta H_s = \Delta H_{cond} + \Delta H_{mix}, \quad (8)$$

where ΔH_{cond} is permeant molar enthalpy of condensation and ΔH_{mix} is the partial molar enthalpy of permeant/polymer mixing. ΔH_{mix} value can be estimated from permeate and polymer solubility parameters according to the Hildebrand equation:

$$\Delta H_{mix} = V_{permeant}\left(\delta_{permeant} - \delta_{polymere}\right)^2 \phi_{polymere}^2, \quad (9)$$

where $V_{permeant}$ is a partial volume of permeant, δ_i is solubility parameter, and $\phi_{polymere}$ is a polymer volume fraction in the mixture.

The value of ΔH_{cond} is negligible for not very condensable gases such as N_2 or O_2, and, thus, the enthalpy of dissolution ΔH_s is determined by ΔH_{mix}. Additionally, the interactions between gas molecules and polymer are weak; therefore, ΔH_{mix} and, hence, ΔH_s value is positive (endothermic effect), so the gas permeate solubility increases with the temperature raise [25, 29]. On the other hand, ΔH_s for more condensable gases such as CO_2, SO_2, or hydrocarbons is negative (exothermic effect) due to the large contribution of ΔH_{cond}, and, thus, the gas permeate solubility decreases with the increasing temperature [25, 29]. In the case of liquid permeates, their solubility in polymers generally tends to increase with the increasing temperature [25].

The solubility can be also influenced by the degree of crystallinity of semi-crystalline polymers and it changes according to the dependency proposed by Michaels and Bixler [31] that is valid for a significant number of gases [29]:

$$S = S_a(1 - \chi_c), \quad (10)$$

where S_a is the solubility in the amorphous phase and χ_c is the degree of crystallinity. The gas solubility in fully crystalline polymers is close to zero [29]. Michaels and Bixler [31] indicated no detectable solubility of tested gases in the crystalline form of polyethylene even in the case of small helium molecules.

1.2.1.2 Diffusion

Diffusion is the kinetic process based on the molecules transport through the membrane due to the concentration gradient. It is quantified by the diffusion coefficient *D*. This coefficient corresponds to the rate of diffusing permeate, that, in its turn, is proportional to the amount of permeate molecules going through an active membrane area per second due to the driving force caused by concentration gradient according to the first Fick's law [25, 29]:

$$J = -D\frac{\partial C}{\partial x} \quad (11)$$

where *J* is the flux or transfer rate per unit area of material, *C* is the concentration of diffusing molecules, *x* is the membrane thickness, and *D* is the diffusion coefficient or diffusivity.

In cases, when the concentration gradient of permeate varies across the membrane with time, the second Fick's law is applied:

$$\frac{\partial C}{\partial t} = D\frac{\partial^2 C}{\partial x^2}. \tag{12}$$

The interactions between gases and polymer are rather weak, thus *D* is considered to be independent on the concentration of gas permeate. In the case of the strong interactions between polymer and permeate (*e.g.* organic vapor), *D* is influenced by the permeant concentration (second Fick's law – Eq. (12)), as well as by the size and shape of permeant, temperature, glass transition temperature of polymer [25, 29]. As indicated by Van Krevelen [29] and Merkel et al. [32], the decrease of the gas dynamic diameter raises the gas diffusion though the membrane, and, thus, permeability increases in the well-known tendency:

$$P_{N2} < P_{O2} < P_{CO2}.$$

This phenomenon is also related to the higher critical temperature value of CO_2 (31.15°C), than that of N_2 (−146.94°C) and O_2 (−118.56°C) [29, 33].

The characteristics of polymer matrix have also a great influence on the *D* value [11]. The diffusion is totally different in rubbery polymers, where polymer chains can rotate around their axis, and glassy polymers, where steric hindrance of polymer chains restricts their movement. Taking this fact into account, the thermal motion of chains in rubbery polymers leads to the high value of *D*; whereas the thermal motion in glassy polymers, that are tough and rigid, is limited, thus low value of *D* is observed [11].

Additionally, the permeate solubility *S* and diffusivity *D* can be influenced by the polymer free volume. Houde and Stern [30] indicated the increase of solubility *S* and diffusivity *D* with the increase of the ethoxy content from 42.2 to 49.6 % for the ethyl cellulose membranes, that was correlated with the increase of the polymer free volume.

Diffusion of gases is also thermally activated process according to the Arrhenius-type equation:

$$D = D_0 e^{\frac{-E_D}{RT}}, \tag{13}$$

where D_0 is a diffusion coefficient for a permeant concentration equal to zero and E_D is the activation energy of diffusion. The activation energy of diffusion E_D is the most important parameter in the diffusion process, and it refers to the energy required to move the dissolved permeate molecules in the polymer structure. In general, the diffusion of larger permeate molecules requires the greater free volume between the polymer chains and higher activation energy, and, therefore, the diffusivity of bigger molecules is found to be smaller [25, 29].

1.2.1.3 Permeation

As it was mentioned, permeation of a given permeant through the nonporous membrane, quantified by permeability coefficient *P*, depends on both *D* and *S* (Eq. (5)). Nevertheless, diffusion process is found to have the dominant influence on the membrane permeability [25]. The contribution of sorption and diffusion to permeation can be expressed by the Arrhenius-type equation:

$$P = P_0 e^{\frac{-E_P}{RT}}, \tag{14}$$

where E_P is the activation energy of permeation, that correlates permeant sorption and diffusion phenomena:

$$E_P = \Delta H_{cond} + \Delta H_{mix} + E_D - yRT \tag{15}$$

In this work, the permeation kinetics was studied basing on two different approaches: (i) variable pressure method, so-called “time-lag” method, for the gas permeation measurements performed in the closed circuit, and (ii) differential permeation for liquid water and water vapor measurements based on the principle of the sweeping gas permeation performed in open circuit (Figure 7) [34]. In general, the membrane sample was sealed in the membrane permeation cell between the upstream (feed) and downstream (permeate) compartments.

In the case of variable pressure method (time-lag method) the quantity of the permeating gas molecules was calculated for a membrane based on the stationary flux J_{st} determined from the slop α of the kinetic curve according to:

$$J_{st} = \frac{\alpha \cdot V}{A \cdot R \cdot T}, \tag{16}$$

where V is volume of the downstream compartment [cm^3], A is membrane area surface in the direct contact with gas [cm^2], R is ideal gas constant, T is temperature of experiment [°C].

Permeability coefficient (P) and diffusion coefficient (D) were calculated based on Eq. (17) and Eq. (18), respectively.

$$P = \frac{J_{st} \cdot d}{\Delta p} = \frac{L}{A \Delta p} \frac{dQt}{dt}, \tag{17}$$

where d is thickness of membrane sample, Δp is difference of pressure between upstream (p_1) and the downstream (p_2) compartments of permeation module.

$$D = \frac{d^2}{6 \cdot t_l}, \tag{18}$$

where t_l is time, called "time-lag", determined from the intercept of the asymptotic straight line of the stationary flux with the time axis (Figure 7A).

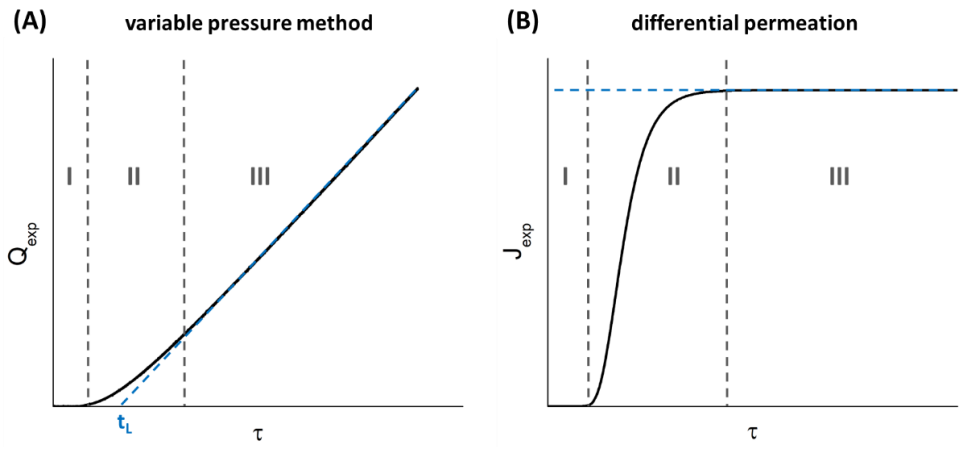

Figure 7. Representation of the curves obtained by (A) variable pressure method and (B) differential permeation.

Solubility coefficient (S) of permeating molecules was determined according to:

$$S = \frac{P}{D} \tag{19}$$

During the differential permeation, the flux was measured as a function of time and estimated from the increase of the dew point value in the downstream compartment detected by a chilled mirror hygrometer (Figure 7B). The permeation flux J_{st} reached at

the stationary state is directly proportional to the permeability coefficient *P* (expressed in Barrer) according to:

$$P = \frac{J_{st} L}{\Delta a}, \quad (20)$$

where *L* is the membrane thickness and Δa is the difference of water activity between upstream and downstream compartment (Δa = 1 in the case of liquid water permeation).

The permeation curves obtained by the two methods can be divided into three sections (Figure 7). At short transient times (I), there is no variation of Q_{exp} or J_{exp}, namely no molecule has yet passed the total membrane thickness. Subsequently, the desorption phenomenon in the downstream compartment (II) starts, and the increase Q_{exp} or J_{exp} is observed that follows by the stationary state reaching (III). The permeability coefficient *P* is determined from the stationary section (III), in contrast to the diffusion coefficient *D* that is determined from the transient section (I and II).

1.2.2 Pervaporation

The progressive interest in the comprehensive understanding and subsequent amelioration of the permeation properties of polymers resulted in the development of wide variety of applications involving polymer materials, such as food and drinks packaging, coatings, and controlled release. Pervaporation (PV) is applied for the molecular-scale separation of binary or multicomponent liquid mixtures including azeotrope, isomer, enantiomer, and close-boiling systems. The use of pervaporation is beneficial compared to the conventional separation processes, like distillation, thanks to its low energy consumption, superior selectivity offered by membranes, safe and ecofriendly characteristics.

The dehydration of organic solvents is the main industrial application of pervaporation. During pervaporation dehydration, hydrophilic membranes that are selective towards water are generally used. One of the most common polymer membranes used for dehydration on the industrial scale are based on PVA, polyimides, or polyacrylonitrile [28, 35].

The pervaporation process can be influenced by factors determined by the membrane (polymer material, membrane thickness, swelling resistance, membrane morphology) or the process conditions (feed concentration, feed pressure, permeate pressure, concentration polarization, temperature). Taking into account the

aforementioned factors, the solution-diffusion mechanism in the case of pervaporation process consists of the several consecutive steps (Figure 8) [36]:

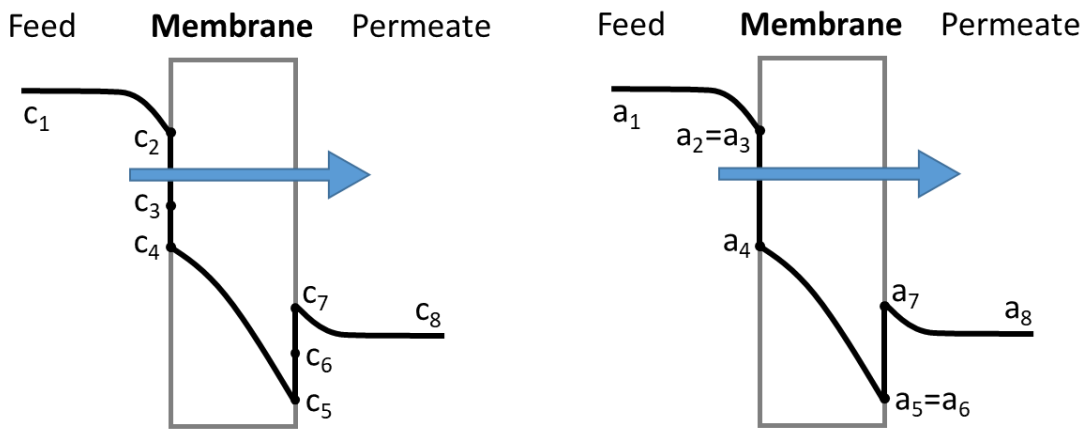

Figure 8. Scheme of the concentration and activity profiles of the component, which is preferentially transported from the bulk feed to the bulk permeate side during pervaporation [36].

1. in the case of the occurrence of the concentration polarization phenomena on the feed side of the membrane, the decrease of the concentration of the preferentially transported molecules is observed (from c_1 to c_2; $a_1 \rightarrow a_2$). It is a result of the component diffusion in the boundary layer of the membrane;
2. the transported molecules are absorbed in the polymer membrane according to the thermodynamic equilibrium ($c_2 \rightarrow c_3$; $a_2 = a_3$);
3. in the case of not reaching the swelling equilibrium, the concentration of the transported molecules at the membrane surface is noticed ($c_3 \rightarrow c_4$; $a_3 \rightarrow a_4$) due to the membrane swelling resistance;
4. the transported molecules diffuse through the membrane as a result of the concentration gradient in the membrane ($c_4 \rightarrow c_5$; $a_4 \rightarrow a_5$);
5. the transported molecules desorb on the permeate side according to the thermodynamic equilibrium ($c_5 \rightarrow c_6$; $a_5 = a_6$);
6. in the case of not reaching the thermodynamic equilibrium, the concentration (or activity) drops at the membrane surface due to the membrane desorption resistance ($c_6 \rightarrow c_7$; $a_6 \rightarrow a_7$). This step refers to the slow evaporation of the transported molecules into a vapor phase;

7. in the case of the observed pressure loss at the permeate membrane side or the hindered permeate removal, the concentration (or activity) at the membrane surface increases compared to the concentration (or activity) determined by the applied driving force ($c_7 \rightarrow c_8$; $a_7 \rightarrow a_8$).

Generally, the step 1 should be taken into account in the practical application of membranes due to the non-ideal mixing conditions. However, in the laboratory conditions, this step can be avoided or neglected. In the case of the permeation of pure solvents step 1 does not exist. In addition, the step 3 and 6 can be also neglected, whereas the influence of the step 7 can be diminished by the improved design of the membrane module. As a result, the steps 2, 4, and 5 commonly present the solution-diffusion mechanism of molecules transport in the pervaporation process.

1.2.2.1 Basics of Pervaporation Process

The name of this separation technique originates from the permeation of molecules through the membrane and their subsequent evaporation on the permeate side as a vapor phase. In general, pervaporation process involves the physical change of liquid phase to a vapor one, therefore, this technique is unique among membrane separation processes [14]. During PV the permeants' molecules are in the direct contact with one side of a nonporous membrane and they are selectively transported from the feed to the permeate side (Figure 6).

The mass transfer is ensured by the driving force created due to the difference in chemical potentials of separated species induced by vacuum (vacuum pervaporation, VPV), temperature difference (thermopervaporation, TPV) or using sweep gas (sweeping gas pervaporation, SGPV) [37, 38]. The heat transfer is a concomitant process of vaporization of feed components; consequently, the drop of the feed temperature takes place. The thermostated feed stream ensures the energy (the enthalpy of vaporization) required for the physical change from liquid to vapor phase [36]. In the case of pervaporation, gas separation, and vapor permeation using nonporous polymer membranes, the mechanism of separation is based on the solution-diffusion model (Figure 6) [2, 11].

1.2.2.2 Membrane Performance in Pevaporation

The membrane performance in the pervaporation process refers to the quantity of the components transported through the membrane and it is commonly assessed based on the total flux J_t (Eq. (21)), partial fluxes J_i (Eq. (22)), and separation factor β (Eq. (24)).

The total flux J_t is determined based on the mass weight of permeate collected for a given membrane area over a specified time according to Eq. (21) [39]:

$$J_t = \frac{\Delta m_t}{A\Delta t} \text{ [kg m}^{-2}\text{ h}^{-1}\text{]} \quad (21)$$

where Δm_t is permeate mass [g] collected over time Δt [h], A is membrane area [m^2].

The partial flux J_i of component i can be calculated taking in to account the total flux J_t and permeation composition y_i [39]:

$$J_i = J_t y_i \text{ [kg m}^{-2}\text{ h}^{-1}\text{]} \quad (22)$$

where y_i is the mass fraction of component i in the permeate.

Taking into account the varied thickness of studied membranes, the thickness-normalized permeate fluxes ($J_{N,i}$) can be calculated as:

$$J_{N,i} = J_i d_i \text{ [µm kg m}^{-2}\text{ h}^{-1}\text{]} \quad (23)$$

where d_i is the thickness of the membrane [µm].

Separation factor (β) is calculated according to Eq. (24) [40]:

$$\beta = \frac{y_i/(1-y_i)}{x_i/(1-x_i)} \quad (24)$$

where y, x are mass fractions of compound i in permeate and feed, respectively.

Pervaporation separation index (*PSI*) is also used to compare the effectiveness of membranes with varied selectivity and permeability [26]. Generally, higher value of *PSI* parameter corresponds to the better membrane efficiency in PV process. Considering different membrane thickness, thickness-normalized pervaporation separation index (PSI_N) may be calculated using Eq. (25):

$$PSI_N = J_t d_i(\beta - 1) \text{ [µm kg m}^{-2}\text{ h}^{-1}\text{]} \quad (25)$$

Baker et al. [40] proposed another approach based on using permeability (P_i), permeance (P_i/l), and selectivity ($\alpha_{i/j}$) coefficients in order to evaluate the pervaporation performance of membranes. The use of P_i and $\alpha_{i/j}$ allows comparing the properties of

different studied membranes without taking into consideration the experimental conditions or physicochemical properties of solvents [41]. This results from the fact that P_i and $\alpha_{i/j}$ refer to the intrinsic properties of the tested membrane.

The membrane permeability (P_i) is described by the component flux normalized by membrane thickness and driving force:

$$P_i = J_i \frac{l}{p_{i,o} - p_{i,l}} \tag{26}$$

where $p_{i,o}$ and $p_{i,l}$ are the partial pressures of component *i* on either side of the membrane (surfaces *o* and *l*), *l* is the membrane thickness. In case if the membrane thickness is not known, the membrane permeance (P_i/l) can be used:

$$\frac{P_i}{l} = \frac{J_i}{p_{i,o} - p_{i,l}} \tag{27}$$

The membrane selectivity refers to the ratio of the permeabilities or permeances of components *i* and *j* through the membrane:

$$\alpha_{ij} = \frac{P_i}{P_j} = \frac{P_i/l}{P_j/l} \tag{28}$$

1.2.3 Gas Separation

The important applications of gas separation membranes are the removal of hydrogen from nitrogen, separation of argon and methane in ammonia plants, the production of nitrogen from air, and the separation of carbon dioxide from methane in natural gas operations [11]. The production of acid gases is a great concern regarding the environmental protection and the problems of the global warming. Therefore, the sweetening of natural gas, particularly the removal of carbon dioxide from natural gases, is one of the most extensively studied membrane separation processes. The investigation regarding the development of the membrane materials for the CO_2 capture has been carried out since the early 1980s [42]. Such membrane materials expect to have the high permeability $P(CO_2)$ and separation factors $\alpha(CO_2/N_2)$. The supported liquid membranes (SLMs) containing ILs are promising composite materials in the separation of CO_2 from CH_4 and CO_2 from N_2 [43, 44].

1.2.3.1 Basics of Gas Separation

In general, the separation of binary gas mixtures is driven by the difference in the partial pressures of gas between two sides of the membrane. The membranes used for the gas separation can be dense and porous; therefore, the membrane morphology strongly influences the gas separation mechanism. The separation of gas mixture components using dense membranes is based on the solution-diffusion model. The separation involves the consecutive steps: the preferential gas solubility in the upstream membrane side, the gas diffusivity through the membrane, and the gas desorption at the downstream membrane side [41, 42]. The gas solubility and diffusivity phenomena determine the efficiency of the separation process. In the case of the porous membranes, various separation mechanisms can be distinguished depending of the membrane porosity: Knudsen's diffusion, molecular sieving, Poiseuille flow, and/or capillary condensation [45].

1.2.3.2 Membrane Performance in Gas Separation

The membrane performance in gas separation process is generally considered in terms of the selectivity and the permeability and additionally assessed based on the Robeson plot [46]. The Robeson plot comprises the upper bound representing the experimental results for the nonporous polymer membranes obtained for the numerous pairs of gases including: He, H_2, O_2, N_2, CO_2, and CH_4.

The characteristic feature of the Robeson plot is the empirically defined upper bound based on the experimental results for the polymeric dense membranes obtained for the multitude pairs of the following gases: He, H_2, O_2, N_2, CO_2, and CH_4. The permeability (P_i) (Eq. 29) and the selectivity ($\alpha_{i/j} = P_i/P_j$) (Eq. 30) referring to a given gas pair determines the upper bound. The gas permeability is described as a thickness-normalized stationary state flux (J_{stat}) that is acquired for the given pressure difference (Δp) between two membrane sides [47].

$$P_i = \frac{J_{stat} \times L}{\Delta p} \tag{29}$$

Membrane selectivity (α_{ij}) refers to a ratio of a permeability of two various gases investigated for a given membrane, which can be also calculated as a product of the solubility and diffusivity ratios (Eq. 30). The transport of gas molecules through the

membrane material is also described by the solution-diffusion mechanism; therefore, gas solubility (S) and diffusivity determine the membrane permeability (Eq. 5) [42, 48].

$$\alpha_{i/j} = \frac{P_i}{P_j} = \frac{S_i}{S_i}\frac{D_i}{D_j} \tag{30}$$

The development of the novel membranes for the gas separation processes aims to obtain materials enabling to exceed the upper bound [46, 49].

1.2.4 Membrane Materials

The membrane for separation processes should possess high selectivity and transport efficiency. However, the increase of the separation is frequently accompanied by simultaneous drop of permeability [17, 50]. The transport and separation effectiveness of a membrane is influenced by the structure and properties of the membrane material, as well as by the characteristics of permeating molecules. The membrane for industrial separation processes should also have high chemical resistance, good mechanical and thermal stability [17, 50]. Moreover, it is expected that the membrane fabrication will be reproducible and relatively inexpensive [19].

Polymer-based separation membrane materials can be elaborated from different polymers including polysulfone, polystyrene, polyesters, and polyamides, poly(vinylidene fluoride), poly(dimethylsiloxane), cellulose, cellulose esters, and poly(vinyl alcohol) [6, 48, 51-54]. Cellulose esters and PVA have attracted the special attention due to their biodegradable and harmless nature. “Green” polymers based on the renewable natural resources become more and more popular as they constitute an alternative for the non-degradable polymers manufactured from fossil fuels [55, 56]. Among all green polymers, membranes based on cellulose esters possess numerous advantages such as moderate flux, relatively easy manufacture, and cost effectiveness [57]. Such materials are successfully used in pervaporative separation of aqueous solutions of ethanol, acetic acid, dimethyl sulfoxide, or cyclohexane/benzene mixture revealing the correlation between the membrane transport and separation behavior, and membrane physicochemical characteristics [58]. Also, PVA-based membranes are found to be suitable for pervaporation dehydration due to their hydrophilic properties, high chemical resistance, good film forming capacity [59].

1.2.4.1 Cellulose Acetate Propionate (CAP) Based Membranes

Cellulose is generally considered as one of the most abundant polymer that can be obtained from wood and plant fibers as well as algae or fungi bacteria [60, 61]. Due to the fact that this polysaccharide is available, renewable, non-toxic, biodegradable, and biocompatible, as well as it is characterized by thermal and chemical stability, and possibility of derivatization, therefore, cellulose and its derivatives are widely studied and used [61]. However, the application of cellulose is restricted because of its limited solubility, related to compact, mainly crystalline packing with single amorphous region that results from the van der Waals interactions and strong hydrogen bonds between –OH groups [60, 62, 63]. Moreover, cellulose is low dimensionally stable, highly hydrophilic, and no thermoplastic [64]. As a consequence, cellulose esters were elaborated [58, 65], for example, cellulose acetate (CA) [66, 67], cellulose triacetate (CTA) [68, 69], cellulose acetate butyrate (CAB) [70, 71], and cellulose acetate propionate (CAP) [66, 72]. In general, cellulose-based polymers are characterized by good solubility, facile film forming, good structure stability, resistance to light, and high optical properties [58, 62, 69]. Nevertheless, cellulose triesters (CAP and CAB) reveal enhanced properties, e.g. better solubility, improved structure stability, and higher light resistance, compared to the cellulose monoesters [53, 62]. It is due to the increased number of acyl groups and length of their chain as well as to the polymerization degree.

Taking into account the attractive properties, cellulose esters are one of the oldest polymers widely used in different fields, as plastics, coatings, composites, laminates, optical films [73-75]. They are also utilized in medical application (hemodialysis, blood filtration) and separation (reverse osmosis, pervaporation, gas separation, metal ions separation) [58, 73, 76]. Luo et al. [77] studied CAP-based membranes for the pervaporation separation of ethanol (EtOH) and ethyl *tert*-butyl ether (ETBE) mixture. It was found that the transport and separation properties of tested membranes depend on feed composition and temperature of experiment. The increase of the ethanol content (from 2.5 to 32.5 wt.% at 40°C) and temperature (from 40 to 60°C) resulted in the raise of the ethanol flux – from around 100 to 1700 g $h^{-1}m^{-2}$ [77].

The use of cellulose ester in film application is also restricted because of its inadequately low elastic modulus and high elongation at break [78, 79]. This issue of cellulose ester polymers can be overcome by using plasticizers that induce the softening of the polymer material due to the reduction of the glass transition temperature T_g and

elastic modulus, and to the diminishing intermolecular forces between polymer chains [79], which also enhances the flexibility of polymer material [80, 81]. Moreover, the suitable plasticizer should be compatible with polymer, non-toxic, resistant to UV radiation, and it should possess high boiling point and low volatility in order to avoid its leaching from the polymer matrix. The use of many common plasticizers, including phthalate esters, such as dioctyl phthalate (DOP), di-isononyl phthalate (DINP), or di-isodecyl phthalate (DIDP) underlines the effective plasticization of membrane material; however, their application has been questioned because of the recorded release from the polymer matrix [82]. Vieira et al. [82] emphasized that the most suitable plasticizer is the one with the lowest volatility, that provides the higher stability of plasticized membrane materials during their storage and exploitation. Among the tested plasticizers with minimized toxicity are adipic or citric acids, alkyl esters, or more recently ionic liquids [80, 81]. Bendaoud and Chalamet [83] pointed out the better plasticization effect of 1-butyl-3-methylimidazolium chloride [BMIM][Cl] ionic liquid than with diethyl phtalate (DEP) in the case of CA-based membranes prepared by the melting technique at 150°C. This result is related to the strong interactions between IL and CA that are correlated to the electrostatic nature of ionic liquid and the presence of hydrogen bonding and van der Waals interactions [83]. Liu et al. [84] and Ning et al. [85] reported that 1-allyl-3-methylimidazolium chloride ([AMIM][Cl]) ionic liquid can successfully replace conventional plasticizers. [AMIM][Cl] used for cornstarch revealed the plasticization effect simultaneously with the improvement of conductive properties [85]. Cellulose nanocrystals (CNCs) with [AMIM][Cl] resulted in the material with tuned coloration and pliability. The addition of 1-ethyl-3-methylimidazolium bis(trifluoromethanesulfonyl)imide [EMIM][Tf2N] ionic liquid up to 40 wt.% to the epoxy resins resulted in improved mechanical properties due to the plasticization confirmed by the high Young's modulus values (650-800 MPa) [86]. Schmidt et al. [87] reported that the incorporation of imidazolium- and pyrrolidinium-based ionic liquids containing cations with flexible butyl (1-butyl-3-methyl-imidazolium (BMI), 1-butyl-1-methyl-pyrrolidinium (BMPyr)) and hexyl (1-hexyl-3-methyl-imidazolium (HMI)) side chains to Nafion® 117 membrane matrix decreased the Young's modulus with increasing ionic liquid content whatever used anion (tris(pentafluoroethyl)trifluorophosphate (FAP), Tf2N, PF_6^-, or BF_4^-).

1.2.4.2 Poly(Vinyl Alcohol) (PVA) Based Membranes

PVA is a semi-crystalline synthetic polymer characterized by numerous properties, such as water-solubility, good film/gel-forming, adhesive and emulsifying properties [88-90]. Moreover, PVA is a non-toxic, biocompatible, and biodegradable polymer with high barrier properties towards oxygen that make it suitable for many industrial applications [88, 91-93]. Due to PVA highly hydrophilic character, its properties are strongly affected by the humidity level. PVA swells or even can be dissolved during the contact with the liquid water, which is its main drawback [90]. In order to diminish PVA-based materials solubility in water, the chemical and/or thermal crosslinking of the hydroxyl groups of PVA can be performed. Additional benefit of PVA crosslinking is the improvement of its mechanical properties, thermal stability, and the separation properties [91, 93-96]. The PVA crosslinking have been already carried out by using glutaraldehyde (GA) [97, 98], glyoxal [99], maleic acid [20], citric acid [100], succinic acid (SA) [101], or sulfosuccinic acid (SSA) [101, 102]. Mahdi Dadfar et al. [93] confirmed the improvement of PVA-based membrane resistance towards water after crosslinking with GA that was reflected by the significant decrease of the PVA water solubility (from 59 to 40 % for pure PVA and PVA with 4 % GA, respectively), the water swelling (from 350 to 250 %), and the water uptake (from 53 to 38 %) [93]. Researchers indicated the decrease of free volume space in the membrane structure and, thus, the reduction of the amount of the water molecules passing through the PVA membranes with the increase of the crosslinking degree [93]. Wang and Hsieh [95] revealed that the use of poly(ethylene glycol) (PEG) diacylchloride as a crosslinking agent minimized the PVA solubility in water by affecting the crystalline structure and causing lower porous volume than that obtained during the reaction with GA [95]. In addition to the water resistance, Mahdi Dadfar et al. indicated the change of PVA thermal behavior as a result of crosslinking [93]. Kim et al. [97] showed a strong changes of the PVA structure due to the crosslinker type and the conditions of the membrane preparation. For example, the crystallinity of PVA increased after crosslinking using GA in ethanol solution, which was confirmed by the increase of the 2θ peak intensity at 20° obtained by wide angle X-ray diffraction (WAXD) analysis and by the increase of the melting enthalpy ΔH_m from 39 to 41 $J \cdot g^{-1}$ compared with the pure PVA membrane [97]. Wang et al. [103] revealed also the impact of the crosslinking with GA of PVA-based membranes containing poly(acrylic acid) (PAA) on membranes transport and separation properties during pervaporative

separation of dimethyl carbonate/methanol mixture. The increase of the GA content from 3 to 9 mol% GA per mole of the PVA repeating unit enhanced the affinity of PVA-PAA membranes to methanol. This fact was related to the increase of the crosslinking degree as well as to the amount of the unreacted aldehyde groups [103]. The gradual increase of the methanol flux from 154 to 366 $g \cdot m^{-2} \cdot h^{-1}$ was observed with the GA content increasing from 3 to 9 mol%. The maximum separation factor equal to 37 was obtained for the membrane with 6 mol% GA [103].

Various approaches were also studied to improve the crosslinking efficiency of PVA-based membranes. Kumeta et al. [104] investigated the influence of the heat-treatment conditions and the effect of the neutralization degree for the PVA-based membranes crosslinked with the PAA, taking into account that the PVA:PAA weight blend ratio equals 8:2. It was pointed out that the use of the non-neutralized PAA resulted in drop of the crosslinking performance. This fact was related to the increased number of hydroxyl groups as a result of the oxidation reaction instead of the esterification reaction [104]. Wang et al. [105] reported a significant difference in mechanical properties between the chemically crosslinked membranes with GA and heat-treated porous PVA membranes [105]. The crosslinking of PVA membranes with 3 wt.% GA during 5-30 min enhanced the membranes' tensile strength with the increase of the crosslinking degree. Also, the tensile strength and strain of the crosslinked membranes were found to be higher and lower, respectively, compared to those of membrane heated at 120°C during 1-3h with 3 wt.% GA. The chemically crosslinked PVA membranes studied in wet state showed the decrease of both the tensile strength and strain at break. When polymer is solvated with the water molecules, the polymer chains are extended. However, the mobility of the polymer chains is restricted by the presence of the crosslinking bonds, which contribute to the increasing of the inner stress with increasing crosslinking degree during swelling process. On the contrary, the heat-treated membranes in wet state possessed superior mechanical properties in comparison with those in dry state [105]. For example, strain at break of the heat-treated membranes investigated in wet state was around twice higher than that for the membranes in dry state [105]. Furthermore, it is shown that the thermal treatment of the PVA-based membranes combined with the chemical crosslinking leads to the enhancement of the crosslinking efficiency and water resistance of the PVA-based membranes. Thus, the crosslinking appears to be a promising approach for the improvement of the membrane performance in separation processes.

The application of CAP and PVA as membrane materials and the additional modification or reinforcement of CAP and PVA can provide the functionalized composite materials with improved physicochemical properties and separation performance.

1.3 Composite Membranes

The selection of a suitable polymer material is an important step in the design and elaboration of the desired membrane. However, the separation performance or physicochemical properties of a membrane material are often insufficient. In general, to meet all necessary requirements of a well-suited membrane for a given separation, the membrane modification is needed in order to improve the membrane selectivity and/or flux, as well as its chemical resistance. There are two main approaches used for the elaboration of the novel membrane materials with enhanced efficiency as well as with superior or novel functions, such as: the alteration of a membrane surface or the modification of the bulk structure of the polymer prior to the membrane formation [6]. Moreover, the synthesis of new polymers and the elaboration of composite membranes can be also used for the preparation of membranes with tailored structure and properties [106]. The most common strategies of pristine membrane modification include the polymer blending, crosslinking (photo, chemical, or thermal), the use of the inorganic (e.g. carbon nanotubes (CNTs), metal organic frameworks (MOFs), zeolites) or organic (e.g. ionic liquids) additives [50] (Figure 9).

ILs are an exceptional class of salts composed of the relatively large organic cation and inorganic or organic anion of various sizes. ILs possess a melting point usually lower than 100°C, and ILs that are liquids at/or below room temperature are classified as a room-temperature ionic liquids (RTILs). Due to the large size, ions of ILs are dissociated without the use of a solvent, in contrast to conventional ionic salts, like sodium chloride (NaCl) or potassium chloride (KCl) (Figure 10) [107].

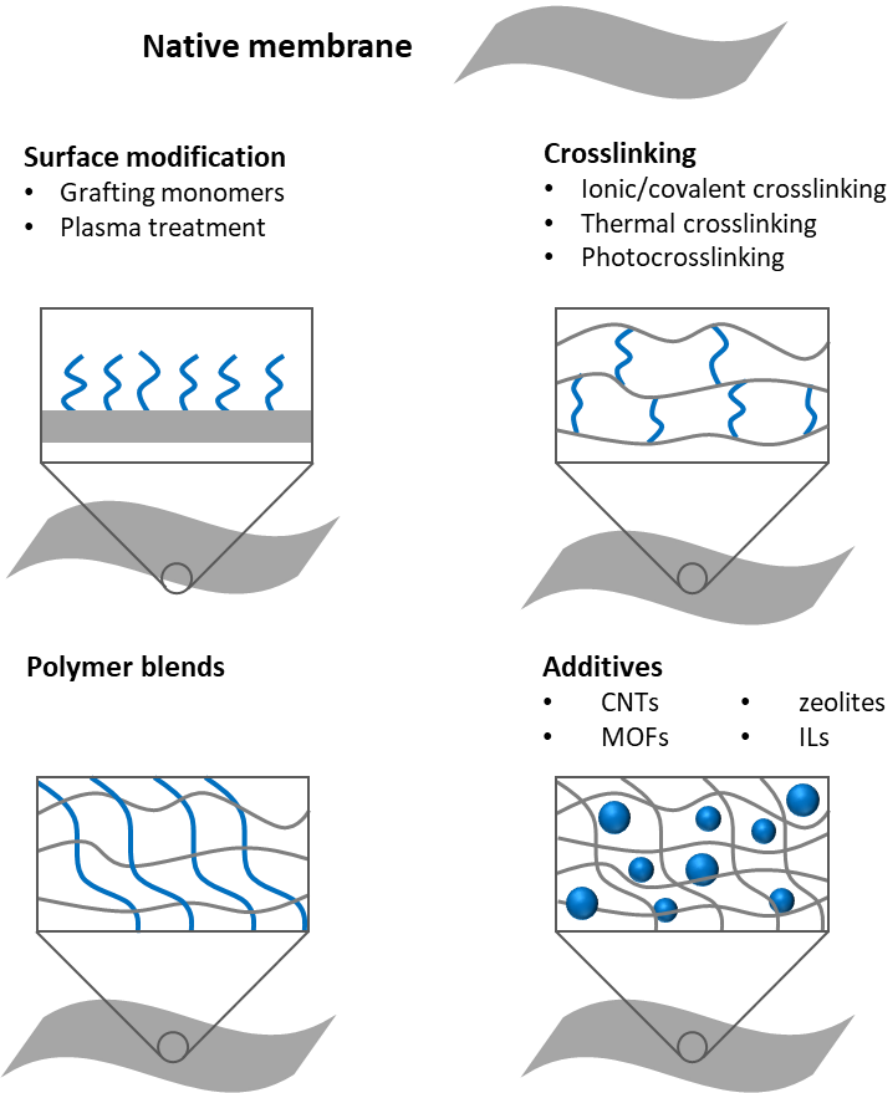

Figure 9. Various elaboration methods of novel or improved polymer membrane materials.

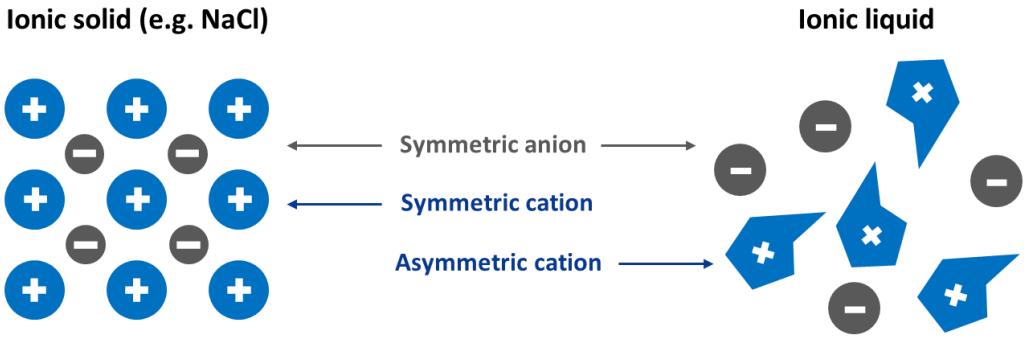

Figure 10. Comparison of ionic solid and ionic liquid structure.

ILs can be designed through combining cations and anions in almost unlimited configurations provided by the wide variety of potentially available ions. Figure 11

presents the various commonly used cations, including imidazolium, pyrrolidinum, pyridinium, phosphonium, ammonium, and anions including bromide (Br^-), chloride (Cl^-), tertafluoroborate (BF_4^-), trifluoromethanesulfonate (TfO^-).

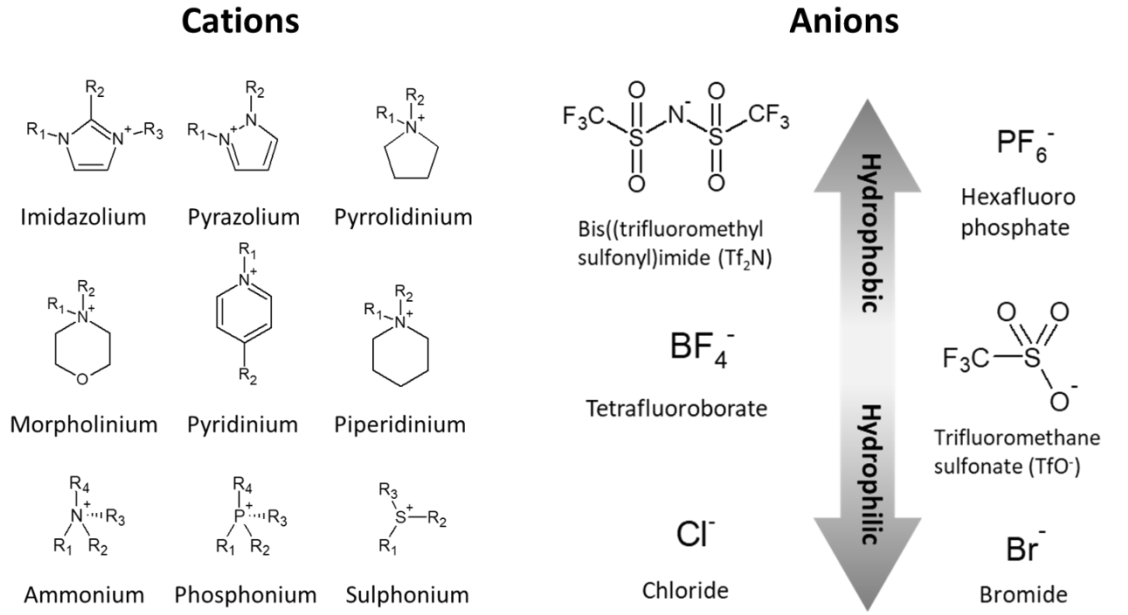

Figure 11. Chemical structures of cations and anions used for the synthesis of ionic liquids.

ILs are generally composed of ions with single charge, however, ILs can also possess cations or anions with double positive or negative charge, respectively [108, 109].

Polymerizable ionic liquids (PILs) are another group of ILs that possess the functional groups, such as acrylate, vinylbenzyl, and N-vinylimidazolium (Figure 12A), that can be polymerized *via* free radical polymerization or UV photopolymerization [63, 110-112]. The characteristics of PIL are comparable to conventional RTIL, namely, PILs possess the enhanced stability, better processability, improved flexibility and durability [47, 113]. The obtained polymerized ionic liquids (poly(ILs)) can possess variety of structures including: poly(cation) and poly(anion) type IL, poly(zwitterion), copolymer, and network (Figure 12B) [21, 113].

By functionalization and changing the type of cation and anion, the properties of ILs can be dramatically altered and tailored according to their further specific applications. Consequently, such functionalized ILs are classified as “task-specific ionic liquids” (TSILs) [114, 115]. The nature of IL ions affects their melting point, viscosity,

thermal stability, ionic conductivity, polarity, hydrophilic/hydrophobic properties, or ability of solvation [116-118].

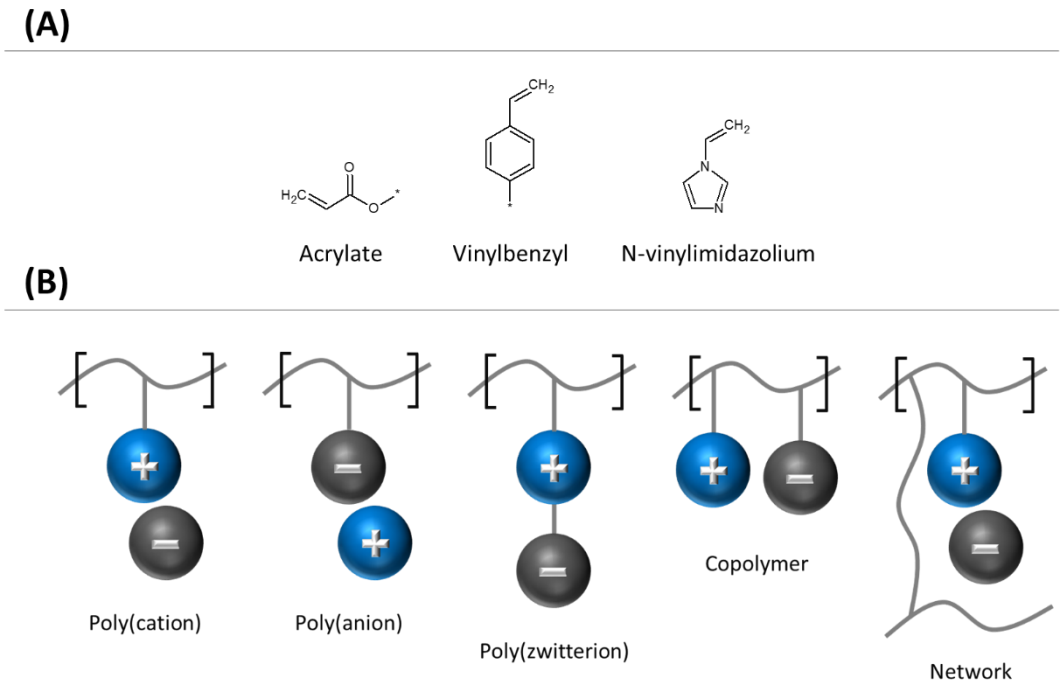

Figure 12. Variation of (A) functional groups commonly used in polymerizable ionic liquids and (B) polymerized ionic liquids.

ILs attract the special attention of the researchers due to their excellent and potentially useful properties, such as negligible vapor pressure, high chemical and electrochemical stability, superior ionic conductivity, and non-flammability [21, 107, 119, 120]. Moreover, ILs possess low melting point and high viscosity [119]. Due to their outstanding properties, ILs are used in a wide range of applications, e.g. as a solvent in organic synthesis, catalysis, or extractive media replacing VOCs [1, 121-123]. Moreover, ILs have been used as a plasticizer or an additive for the elaboration of new membranes or to tailor the properties of membrane materials applied in separation of metal ions [124-126], gaseous mixtures [43, 127, 128], and liquid mixtures in pervaporation [72, 129, 130]. ILs are also used as additives in polymer electrolyte membranes for fuel cells, as well as in other electrochemical devices, such as lithium batteries, sensors, or solar cells [113, 128, 131, 132].

Imidazolium-based ionic liquids were chosen in this study due to the tunable structure of imidazolium cation. The tunable structure of imidazole ring results from its amphoteric behavior enabling to act as both donor and acceptor of protons. Such behavior

allows the SN_2 substitution reaction at the position 3 in the imidazole ring (Figure 13). Imidazole ring possesses multiple active sites, particularly the secondary amine group at the position 1 (Figure 13) that can undergo different reactions resulting in various IL structures. The carbon at the position 2 can be deprotonated in the presence of strong base that allows undergoing a chemical modification of the resulting carbene. Moreover, the imidazole cation interacts with the mobile anion that can be substituted changing the physicochemical properties of ionic liquid [133, 134].

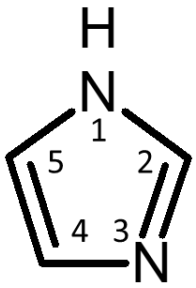

Figure 13. Scheme of imidazole ring.

1.3.1 Polymer-Ionic Liquid Membranes

Depending of the elaboration procedure and the IL immobilization method, the utilization of IL as a component of a polymer matrix leads to various types of IL-based membranes, e.g. ionic gels, facilitated transport membranes (FTMs) including supported liquid membranes (SLMs) and polymer inclusion membranes (PIMs) [21, 123] (Figure 14). Based on the current state of art, the possible approaches to obtain IL-based membranes can be classified as follows [107, 123, 124]:

(A) polymer doping with IL,

(B) polymer impregnation with IL,

(C) IL grafting onto polymer,

(D) polymerization of polymerized IL monomers,

(E) polymerization/crosslinking of polymer monomers in IL.

Dispersion of IL in polymer solution prior to the membrane formation results in the ion gels formation (Figure 14A) [135, 136]. The functional properties of ion gels and their fabrication method are determined by the ratio between IL and polymer as well as their compatibility. The ion gels are characterized by superior ionic conductivity (from 10^{-1} to 10^{-2} S cm^{-1}) [111]. However, this kind of material can suffer from the diminishing

mechanical stability or the leaching of IL [123]. Lodge [136] reports that ion gels used as a membrane material in gas separation do not withstand the applied pressure.

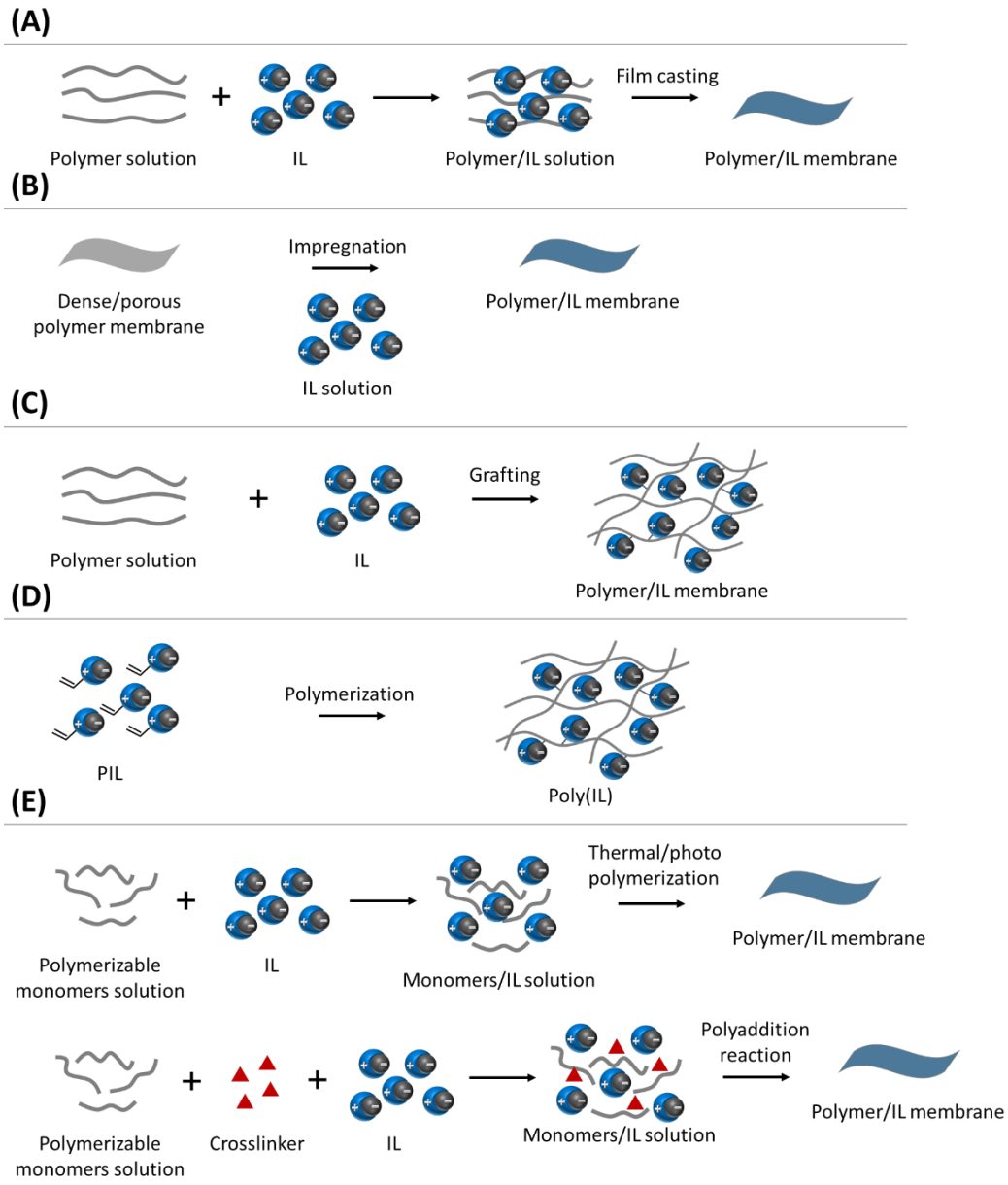

Figure 14. Scheme of possible strategies of the preparation of IL-based polymer materials (based on Ye et al. [21]).

Another approach to immobilize IL inside the polymer membrane is the soaking of the native dense polymer membrane (Figure 14B) or the IL confinement into the pores of polymer matrix in the case of porous structure (Figure 14B). The pristine dense or porous polymer membrane can be elaborated by phase inversion method enhanced by solvent evaporation. In this case, the homopolymers or blends of polymers, copolymers,

or blockpolymers can be used. In such membrane materials, IL is trapped by physical forces. Therefore, this approach restricts tuning the interactions between polymer and IL phases. Moreover, the amount of IL that can be sorbed into the polymer matrix is limited by the given free volume in the pristine membrane [21].

Nevertheless, polymer membranes with immobilized IL are an important group of materials that either possess the high proton conductivity [137] or provide the facilitated transport due to the IL presence. IL plays a role of carrier or complexing agent that selectively transports given components across the membrane during separation process as a result of a reversible reaction between IL functional groups and separated species [11]. FTMs have been investigated in gas or metal ions separation on the laboratory scale achieving high selectivity of the separation [11, 115, 138, 139]. Kasahara et al. [140] investigated FTMs based on poly(tetrafluoroethylene) (PTFE) with tetrabutylphosphonium amino acid ionic liquids containing glycine, alanine, proline, and serine as the anion for the CO_2 permeation. It was found that PTFE membranes with ionic liquid containing proline anion possessed superior CO_2 permeability of 14000 Barrer and CO_2/N_2 selectivity of 100 at 373 K under dry conditions [140].

The particular example of FTMs is SLMs and PIMs. SLMs consist of the porous solid membrane support (polymer or ceramic) filled with the organic carrier phase (solvent or IL) [126]. PIMs are composed of the polymer matrix (generally CTA or poly(vinyl chloride) (PVC)), carrier/extractant (IL), and the plasticizer [141]. Ong and Tan [130] reported that PVA-based SLM containing [BMIM][BF4] possess high efficiency of pervaporation dehydration of the ethyl acetate (EtAc)/ethanol (EtOH)/water (H_2O) azeotrope mixture (EtAc/EtOH/H_2O composition equal to 82.6/8.4/9.0 wt.%). The separation factor β (Eq. 24) and the total permeate flux J_t (Eq. 21) during dehydration at 30°C were equal to 247 and 385 g m^{-2} h^{-1}, respectively. Matsumoto et al. [142] studied PIMs based on the PVC membrane doped with Aliquat 336, Cyphos 101, 102, and 104 ionic liquids prepared on the hydrophobic PVDF support. The membranes were investigated in the pervaporative separation of butan-1-ol and propan-2-ol from their aqueous solutions. The membrane containing 70 wt.% of Aliquat 336 was found to be the most efficient achieving the highest butan-1-ol flux (26.08 g m^{-2} h^{-1}) and total flux J_t (1193 g m^{-2} h^{-1}) for the 5 g L^{-1} of propan-2-ol and butanol concentrations in feed mixture. Researchers pointed out that membranes containing 60 and 70 wt.% of IL were stable, and no IL leaching from the membrane was observed during pervaporation. However, the membranes containing more than 70 wt.% of IL were not stable during the pervaporation.

The application of aforementioned membranes on the industrial scale in various fields (e.g. separation of gases, metal ions, liquids in pervaporation, as well as fuel cells) has been limited because of the losses of the unbound ionic liquid during the exploitation [48, 54, 111, 113, 143-151]. This drawback results from the insufficient physical stability of the polymer-IL system that is related to the physical interactions between polymer matrix and IL. Therefore, other possible approaches have been studied in order to permanently entrap IL inside the polymer structure. Taking into consideration the promising achievements of IL-based membranes in the field of membrane separation techniques, the research towards development of new methods for polymer-IL membrane elaboration is indispensable.

The potential strategies for diminishing the IL leaching include the grafting of IL onto the polymer matrix (Figure 14C) [81, 152] or the use of polymerizable ionic liquid (PIL) monomers [111, 113, 153, 154] (Figure 14D). Hassan Hassan Abdellatif et al. [152] proposed the sequential synthesis route for grafting IL containing bromide anion and various cations (imidazolium, pyrodinium, and ammonium) onto CA in order to minimize the leaching and extraction of IL as well as to enhance the membrane performance in the ETBE biofuel purification using pervaporation. Researchers reported the efficient modification of CA with IL confirmed by ^{1}H NMR analysis allowing to avoid the release of IL from the membrane due to the covalent bonds between IL and CA. Simultaneously, it was found that CA-based membranes chemically modified with ammonium-based IL revealed the best performance in the pervaporative separation of ethanol-ETBE mixture at 50°C reflected by the highest normalized flux equal to 0.182 kg m^{-2} h^{-1} for the membrane thickness of 5 μm [152].

The utilization of PIL monomers followed by their polymerization is another approach for the preparation of IL-based membranes (Figure 14D). PIL monomers can be either blended with the polymer [155] or used to prepare polymerized ionic liquid membranes (PILMs) [156, 157]. Polymerization of PIL monomer increases the IL-based membrane stability by minimizing the loss of IL from the polymer matrix. Simultaneously, it restricts the mobility of IL ions, what results in the drop of the ionic conductivity from ca. 10^{-2} S cm^{-1} (which is an usual order of ionic conductivity of IL) to ca. 10^{-6} S cm^{-1} [158]. This disadvantage can be avoided by combining polymerizable PILs with non-polymerizable ILs [143, 158, 159]. Murakami et al. pointed out that blonding of cellulose with the polymerizable ionic liquid followed by the *in situ* polymerization resulted in the interpenetrating polymer-IL network [155].

Another method for the preparation of membranes containing ILs is based on the polymerization or crosslinking of polymer monomers in IL (Figure 14E). The *in situ* polymerization or crosslinking is preceded by the blending of IL with all necessary reactants: generally vinyl-based polymer monomers and initiator of polymerization as well as polymer monomers with crosslinking agent, respectively [21, 160]. Such approach leads to obtain ion gels with controlled physicochemical properties [160].

The use of ILs for the membrane preparation and modification is a very promising approach that allows us achieving tailored physicochemical properties and separation effectiveness of polymer membranes. Due to the low volatility, ILs can replace conventional plasticizers. The polymer-IL membranes are characterized by the improved selectivity and transport properties in liquid and gas separation; however, the leaching of RTIL from polymer membranes may be observed. According to the state-of-art, the promising approach that allows minimizing IL migration during the membrane exploitation is the use of IL grafting or PIL. The research on ionic liquids carried out up to now proved that the choice of the suitable ionic liquid in a given separation process requires to find a compromise between the IL properties and the desired efficiency of the material. Based on the distinguished properties of the composite ionic liquid/polymer membranes, it can successfully replace the conventional membranes for the membrane separation techniques.

1.4 Research Motivation

As it has been shown, polymer membranes containing ILs play an important role in the field of membrane separation processes. The continuous interest in the use of ILs arises from their excellent properties and wide possibility to modify their properties depending on the final application. The incorporation of IL into polymer structure enables to alter properties of existing polymer membranes. On the other hand, the application of IL can provide the membrane materials of new quality. The research carried out up to now shows that design of polymer-IL systems results in the membrane materials with tailored properties that meet the requirements of good separators. The particular attention should be paid on the fact that the incorporation of IL into the polymer structure results in the facilitated transport of separated molecules through the membrane that is observed for polymer-IL membranes used in pervaporation, metal ions separation, or gas separation.

Nevertheless, the commercial application of polymer-IL membranes has been restricted due to the progressive release of the unbound IL during the utilization. The leaching of IL from the membrane structure is related to physical interactions within polymer-IL system. Hence, the aim of the present PhD thesis is to elaborate novel membranes based on PVA and CAP filled with various reactive (RILs) and polymerizable (PILs) ionic liquids. The investigation of physicochemical characteristics and study of the equilibrium, barrier and transport properties of the obtained membranes will be subsequently carried out. Furthermore, the obtained membranes will be tested in pervaporation process in contact with water-propan-2-ol mixture. The novelty of research is the application of RILs and PILs for the preparation of composite polymer membranes.

The scope of the research includes the influence of the following factors:

- the nature of polymer matrix (PVA and CAP),
- the type of ionic liquid (hydrophilic and hydrophobic),
- the type of crosslinking agent (nature and concentration) and conditions of crosslinking (time and temperature),
- the type of plasticizer.

The research work was conducted in the Membranes and Membrane Separation Processes Research Group at the Faculty of Chemistry at Nicolaus Copernicus University in Toruń (Poland) and in the Polymers, Biopolymers, Surfaces (PBS) Laboratory CNRS UMR 6270 at the University of Rouen Normandy (France).

Performed complementary studies widen the knowledge of the new polymer materials due to the correlation between the morphology and the structure of prepared membranes and their separation, transport, and barrier properties.

CHAPTER 2

Materials & Characterization Methods

In this chapter, a brief description of the materials used throughout this work will be provided. Also, this chapter presents the experimental procedures used for the ILs synthesis, membrane preparation and characterization methods.

2.1 Materials

2.1.1 Polymer Matrices

In this study, two types of polymer matrices are used: CAP and PVA.

2.1.1.1 Cellulose Acetate Propionate (CAP)

Cellulose acetate propionate (CAP-482-20) (Figure 15) with M_w = 75,000 g mol^{-1} (acetyl group content: 1.3 wt. %, propionyl group content: 48.0 wt. %, hydroxyl group content: 1.7 wt. %) was kindly provided by Eastman, Kingsport, Tennessee, USA.

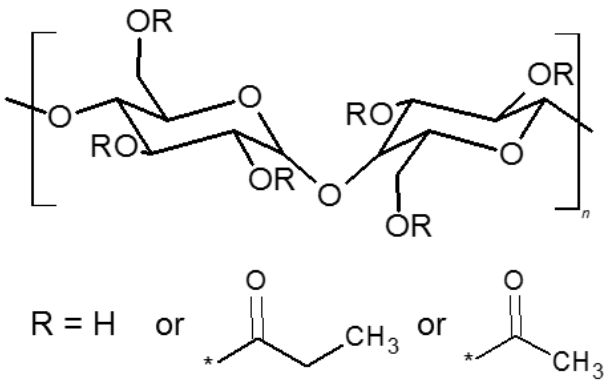

Figure 15. Chemical structure of cellulose acetate propionate (CAP).

2.1.1.2 Poly(Vinyl Alcohol) (PVA)

PVA powder (Elvanol 71-30, fully hydrolyzed, a molecular weight of 100 000 kDa) was kindly provided by DuPont, USA. Figure 16 demonstrates the chemical structure of PVA.

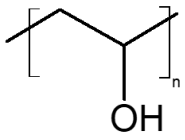

Figure 16. Chemical structure of poly(vinyl alcohol) (PVA).

2.1.2 Sulfosuccinic Acid (SSA)

SSA (Figure 17) was purchased from Merck as 70 wt.% solution in water. It was utilized as a crosslinking agent.

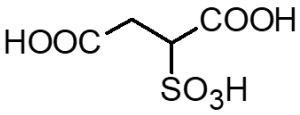

Figure 17. Chemical structure of SSA.

2.1.3 Plasticizers – Tributyl Citrate (TBC) and Acetyltributyl Citrate (ATBC)

TBC and ATBC (Figure 18) were purchased from Acros Organics.

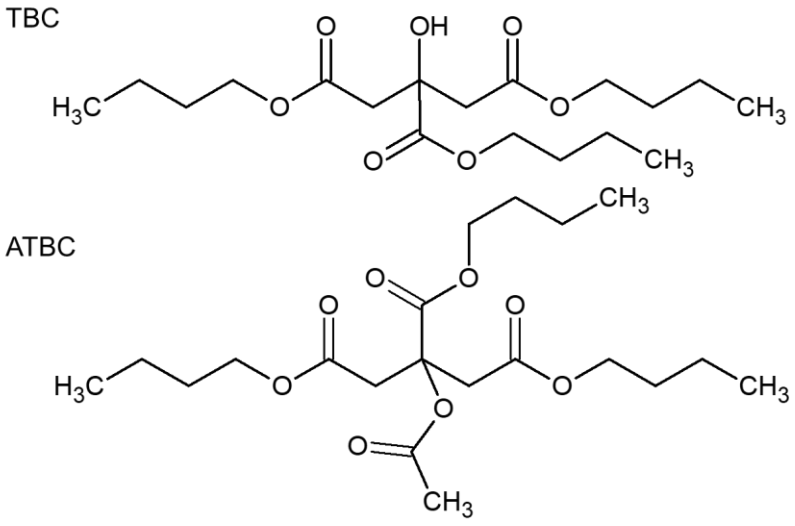

Figure 18. Chemical structure of tributyl citrate (TBC) and acetyltributyl citrate (ATBC).

2.1.4 Solvents

Following solvents: acetone, chloroform, diethyl ether, ethyl acetate, ethanol and propan-2-ol were delivered by Avantor Performance Materials Poland S.A. (Gliwice, Poland). Methanol as well as glycerol and diiodomethane were delivered by Fischer Chemical, France. Solvents of the analytical reagent grade and the ultrapure water deionized by Milli-Q system (18.2 MΩ·cm, Millipore®, Fontenay-sous-Bois, France) were used.

2.2 Ionic Liquids Synthesis

All studied RILs and PILs were synthesized by Synthex Technologies Ltd. (Toruń, Poland).

2.2.1 Reactive Ionic Liquids (RILs)

2.2.1.1 3-(1,3-diethoxy-1,3-dioxopropan-2-yl)-1-methyl-1H-imidazol-3-ium bromide, RIL1_Br

A 50 mL flask was charged with *N*-methylimidazole (0.80 mL; 10 mmol; Sigma-Aldrich, Poznań, Poland) and chloroform (10 mL). Diethyl 2-bromomalonate (1.70 mL; 10 mmol, Sigma-Aldrich, Poznań, Poland) was added under inert atmosphere of argon and slightly yellow solution was heated under reflux for 24 hours (Figure 19). Solvent was removed using rotary evaporator. The yellow liquid was washed with diethyl ether (3 x 20 mL). Residual solvents were removed under vacuum (66.7 Pa; 5 hours). The yield of the synthesis reaction was equal to 98.8%. The structure of RIL1_Br was confirmed by ^{1}H and ^{13}C NMR analysis. ^{1}H NMR (400 MHz, DMSO-d_6) δ ppm 10.55 (s, 1 H), 7.83 (t, J = 1.8 Hz, 1 H), 7.58 (t, J = 1.8 Hz, 1 H), 7.07 (s, 1 H), 4.34 (dqt, J = 15.9, 7.1, 3.7 Hz, 4 H), 4.13 (s, 3 H), 1.33 (t, J = 7.2 Hz, 6 H). ^{13}C NMR (101 MHz, $CDCl_3$) δ ppm 163.11, 138.42, 123.24, 122.99, 64.16, 62.93, 37.12, 13.90.

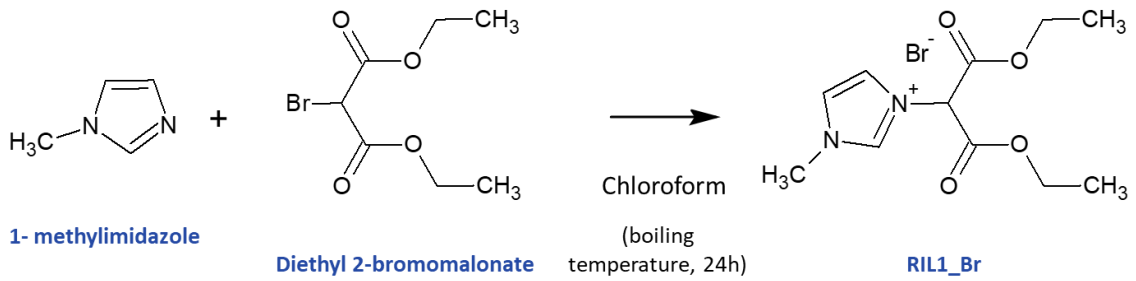

Figure 19. Scheme of RIL1_Br synthesis.

2.2.1.2 1-(2-ethoxy-2-oxoethyl)-3-methylimidazolium bromide, RIL2_Br

Ethyl bromoacetate (8.20 g; 100 mmol; Sigma-Aldrich, Poznań, Poland) was added to a solution of *N*-methylimidazole (16.7 g; 100 mmol; Sigma-Aldrich, Poznań, Poland) in tetrahydrofuran (100 mL). Reaction mixture was stirring for 2 hours at room temperature (21 ± 3°C) (Figure 20A). Solvent was evaporated under reduced pressure. Residual solvent was removed under vacuum (0.1 Pa; 5 hours). The yield of the synthesis reaction was equal to 95.0%. The structure of RIL2_Br was confirmed by ^{1}H and ^{13}C NMR analysis. ^{1}H NMR (400 MHz, DMSO-d_6) δ ppm 10.17 (s, 1 H), 7.63 (t, J = 1.8 Hz, 1 H), 7.48 (t, J = 1.8 Hz, 1 H), 5.48 (s, 2 H), 4.07 (s, 3 H), 4.25 (q, J = 7.1 Hz, 2 H), 1.30 (t, J = 7.2 Hz, 3 H). ^{13}C NMR (176 MHz, $CDCl_3$) δ ppm 165.69, 138.08, 123.44, 122.52, 62.60, 49.95, 36.52, 13.67.

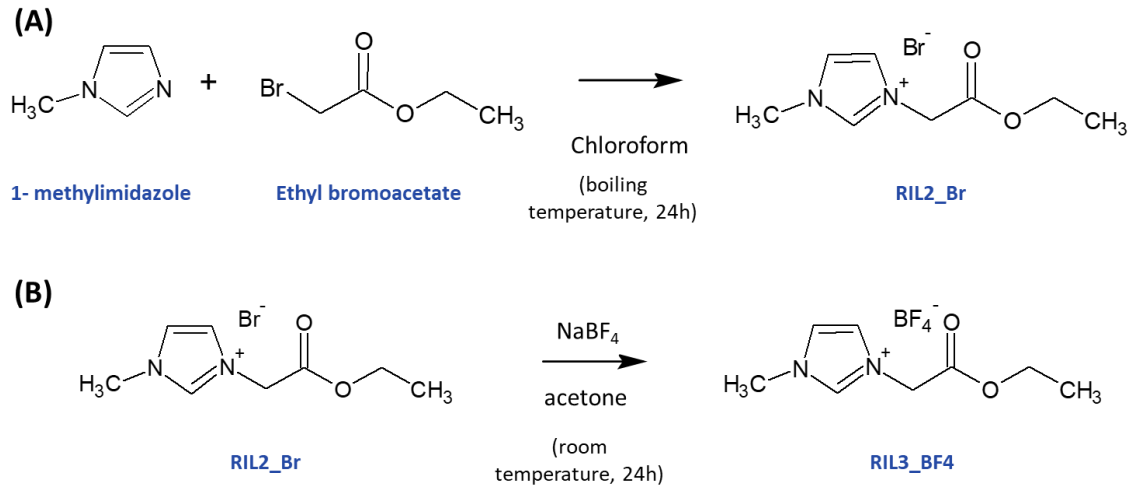

Figure 20. Scheme of (A) RIL2_Br and (B) RIL3_BF4 synthesis.

2.2.1.3 1-(2-ethoxy-2-oxoethyl)-3-methylimidazolium tetrafluoroborate, RIL3_BF4

A 50 mL round-bottom flask was charged with RIL2_Br (7.41 g; 30 mmol) and acetone (30 mL). Sodium tetrafluoroborate (3.96 g; 36 mmol; Sigma-Aldrich, Poznań, Poland) was added. The reaction mixture was stirred at room temperature (21 ± 3°C) for 48 hours (Figure 20B). White crystal precipitate of sodium bromide was filtered off. Solvent was evaporated using rotary evaporator. Residual solvent was removed under vacuum (0.1 Pa; 5 hours). The structure of RIL3_BF4 was confirmed by ^{1}H and ^{13}C NMR analysis. ^{1}H NMR (700 MHz, DMSO-d_6) δ ppm 9.08 (d, J = 0.4 Hz, 1 H), 7.73 (dt, J = 6.2, 1.7 Hz, 2 H), 5.24 (s, 2 H), 4.20 (q, J = 7.1 Hz, 2 H), 3.91 (s, 3 H), 1.24 (t, J = 7.1 Hz, 3 H). ^{13}C NMR (176 MHz, DMSO-d_6) δ ppm 166.95, 137.79, 122.78, 123.49, 61.98, 49.60, 36.08, 14.07.

2.2.2 Polymerizable Ionic Liquid (PILs)

2.2.2.1 1-methyl-3-(4-vinylbenzyl)-imidazolium chloride, PIL1_Cl

A 1000 mL flask was charged with 1-(chloromethyl)-4-vinylbenzene (90.9 mL; 660 mmol; Sigma-Aldrich, Poznań, Poland) and chloroform (500 mL). *N*-methylimidazole (68.2 mL; 860 mmol; Sigma-Aldrich, Poznań, Poland) was added under inert atmosphere of nitrogen and slightly yellow solution was heated at 50°C for 24 hours (Figure 21). Solvent was removed using rotary evaporator. The yellow liquid was washed with ethyl acetate (3 x 200 mL). Residual solvents were removed under vacuum (66.7 Pa; 5 hours). The yield of the obtained PIL was equal to 91.5%. The structure of PIL was confirmed by ^{1}H and ^{13}C NMR analysis. ^{1}H NMR (400 MHz, DMSO-d_6) δ ppm 9.25 (s, 1 H), 7.80 (t, J = 1.8 Hz, 1 H), 7.73 (t, J = 1.8 Hz, 1 H), 7.53 (d, J = 8.3 Hz, 2 H), 7.41 (d, J = 8.1 Hz, 2 H), 6.75 (dd, J = 17.6, 11.0 Hz, 1 H), 5.88 (dd, J = 17.7, 0.9 Hz, 1 H), 5.42 (s, 2 H), 5.31 (dd, J = 11.0, 0.7 Hz, 1 H), 3.86 (s, 3 H). ^{13}C NMR (176 MHz, DMSO-d_6) δ ppm 139.34, 139.02, 137.44, 130.26, 128.10, 125.42, 123.77, 116.71, 52.95, 37.33.

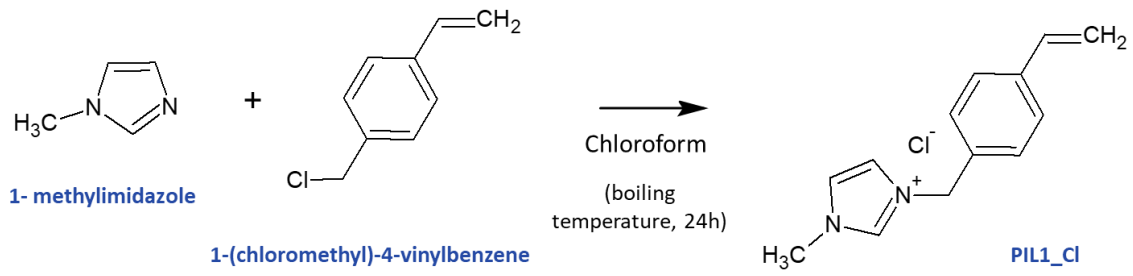

Figure 21. Scheme of PIL1_Cl synthesis.

2.3 Membrane Elaboration

2.3.1 PVA-Crosslinked Membranes

Initially, aqueous 10 wt.% PVA solution was prepared by dissolving the PVA powder in deionized water by stirring under the reflux at 100°C for at least 6 h under an ambient atmosphere in order to obtain the solution which was subsequently used to prepare native PVA and PVA-based membranes. The various amounts of SSA (5-50 wt.%) were added to the solution after cooling of PVA solution to the room temperature and the obtained mixture was followed by vigorous stirring at the room temperature (21 ± 3°C) during 24 h. The solution was degassed and cast on a hydrophobized glass plate using the Doctor Blade with slit varied from 1500 to 2300 μm in order to obtain membranes with comparable thickness. Higher concentration of the crosslinking agent in PVA-based solution corresponds to higher value of applicator's slit used. The cast polymer films were dried in the oven at 30°C for at least 24 h. The dried membranes were stored in a desiccator over P_2O_5 and treated under following conditions: (1) 1 h at 25°C, (2) 6 h at 80°C, (3) 1 h at a given crosslinking temperature (120°C, 140°C or 160°C) under the vacuum. The thickness of the prepared membranes, determined by micrometer, varied from 170 to 190 μm.

2.3.2 Plasticized CAP-based Membranes

Initially, 10 g of CAP were dissolved in 90 g of chloroform at room temperature (21 ± 3°C) for at least 12 h to obtain the solution used to prepare native CAP and CAP-based membranes. Various amounts of TBC or ATBC (weight fraction of plasticizer was equal to 9; 23; 50 wt.%) were added to CAP solution followed by vigorous stirring at the room temperature (21 ± 3°C) during 24 h. The portion of around 5 g of the obtained solution was poured onto glass Petri dish, covered and placed under the hood at ambient

temperature (21 ± 3°C) during 24 h for slow solvent evaporation. The thickness of the prepared membranes varied from 100 to 130 µm.

2.3.3 IL-based Membranes

CAP-IL and PVA-IL membranes were prepared by blending of the polymer solution with IL followed by membrane casting involving phase-inversion technique enhanced by the solvent evaporation. Various amounts of ILs were added to the previously prepared polymer solution. In general, membrane elaboration used in this work involves a number of sequential steps (Figure 22):

- dissolving of IL in the previously prepared polymer solution using solvent compatible with both polymer and IL;
- casting of polymer-IL solution on a glass plate or a Petri dish;
- evaporation of a solvent;
- drying of the obtained membrane under the fume hood at the ambient temperature (21 ± 3°C). PVA-based membranes were additionally dried an the oven at 30°C for at least 24 hours;
- peeling off the membrane sample from a glass support.

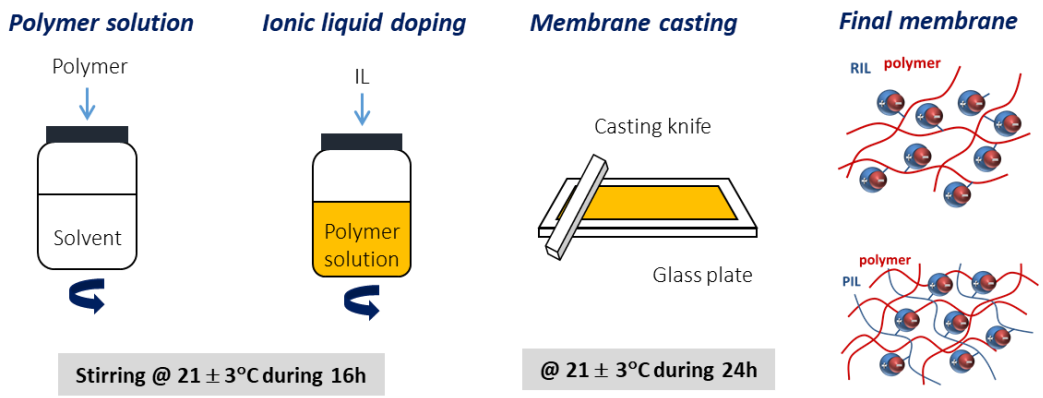

Figure 22. Scheme of CAP-IL and PVA-IL membrane preparation.

The elaborated polymer-IL membranes are presented in Table 2.

Table 2. Specification of the prepared CAP- and PVA-based membranes containing RILs and PILs.

	CAP	PVA
	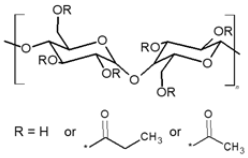	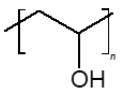
RIL1_Br 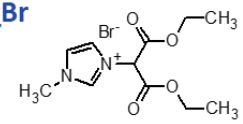	✓	✓
RIL2_Br 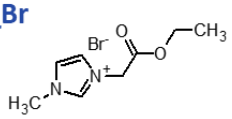	✓	✓
RIL3_BF4 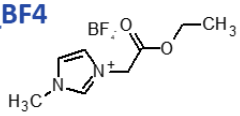	✓	✗
PIL1_Cl 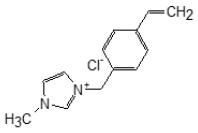	✓	✗

In the case of CAP, the membranes were successfully prepared with all synthesized ILs. However, PVA-based membranes containing RIL3_BF4 and PIL1_Cl were not prepared as these ILs are not soluble in water.

2.4 Characterization Methods

2.4.1 Nuclear Magnetic Resonance (NMR) Spectroscopy

The ^{1}H NMR and ^{13}C NMR spectra were recorded by a 400 MHz Bruker Avance III spectrometer and Bruker Avance III 700 MHz (Rheinstetten, Germany), respectively, at 25°C using DMSO-d_6 as a solvent. The degree of substitution (*DS*) of the obtained CAP-RIL membranes was determined on the basis of the ratio of the proton integrals of the imidazolium ring and anomeric glucose unit (AGU) according to:

$$DS = \frac{S1}{S2}, \tag{31}$$

where *S1* is the integral of the resonance of the imidazolium ring proton (7.81 ppm) and *S2* is the integral of the proton resonance of AGU (5.10 ppm) [161]. The maximum theoretical degree of substitution (DS_{max}) was calculated as a ratio of RIL and AGU molar masses taking into account the weight of RIL and CAP used to prepare CAP-RIL membranes according to:

$$DS_{max} = \frac{M_{RIL} m_{RIL}}{M_{AGU} m_{CAP}}, \quad (32)$$

where M_{AGU} is the average molar mass of the anhydroglucose unit in CAP (325.67 g mol^{-1}), M_{RIL} is the molar mass of ionic liquid, m_{CAP} and m_{RIL} is the weight [g] of CAP and RIL, respectively, in a given CAP-RIL membrane. M_{AGU} was calculated based on CAP data provided by the producer concerning the acetyl, propionyl, and free –OH groups content equal to 1.3 wt.%, 48.0 wt.%, and 1.7 wt.%, respectively.

2.4.2 Fourier Transform Infrared Spectroscopy with Attenuated Total Reflectance (FTIR-ATR)

FTIR-ATR analysis was performed using the Nicolet FT-IR apparatus (ThermoFischer, Avatar 360 Omnic Sampler) in the range of 4000-500 cm^{-1} with a resolution of 4 cm^{-1} and 256 scans using germanium crystal.

2.4.3 Scanning Electron Microscopy (SEM) Coupled with Energy-Dispersive X-Ray (EDX) Spectroscopy

The distribution of chemical elements was observed using SEM microscope (LEO 1430 VP, LEO Electron Microscopy Ltd. Cambrigde, England) with energy dispersive X-ray (EDX) spectrometer (Quantax 200, Bruker AXS Microanalysis GmBH, Germany) and EDX detector (XFlash 4010, Bruker AXS Microanalysis GmBH, Germany) at 28 kV. The morphology of the prepared membranes was studied using SEM microscope (Quanta 3D FEG) at 30 keV. In order to obtain cross-section images, the membrane samples were prepared by fracturing them in liquid nitrogen. Prior to SEM analysis, membrane surface was sputtered with a conductive layer of Au/Pd (80/20) with the thickness equal to 2-6 nm.

2.4.4 Atomic Force Microscopy (AFM)

The surface topography of CAP-RIL membranes was also studied using an atomic force microscope with a NanoScope MultiMode SPM System and NanoScope IIIa and Quadrex controller (Veeco, Digital Instrument, UK). Root mean square roughness (R_q) and arithmetic average height (R_a) were evaluated based on tip scanning mode for scanned sample area (10μm×10μm and 5μm×5μm) using Nanoscope v6.11 software (Bruker Corporation).

2.4.5 Thermogravimetric Analysis (TGA)

The thermal behavior was studied using the TGA thermogravimetric analyzer (TGA Q 500, TA Instruments). The TGA measurements were carried out from 25°C to 800°C under the nitrogen atmosphere. The heating rate and the nitrogen flow rate were 10°C min^{-1} and 90 mL min^{-1}, respectively.

2.4.6 Contact Angle Measurements (CAM)

In order to determine the hydrophobic/hydrophilic character of membrane surface, the direct (i.e. contact angle measurements, drop shape analysis) and indirect (i.e. the Owens-Wendt method for the determination of the membrane total surface free energy) methods were used. The contact angle was determined by aligning a tangent between the surface of the sessile drop and the contact outline with the surface. The drop angle value indicates the affinity between the membrane and water, namely the decreasing contact angle reflects a higher compatibility of the water molecules and membrane due to the presence of polar groups. In general, the contact angle values lower than 90° are characteristic of the hydrophilic surface [35, 162].

The membrane surface properties were also characterized by the total surface free energy (*SFE*) value, *i.e.* a surface tension γ determined using the contact angle values for two or three solvents. The *SFE* value provides the information about the surface physicochemistry as well as the evaluation of the membrane ability for adsorption, wettability, and adhesion [163].

In this study water (Milli-Q), glycerol, and diiodomethane were chosen for the contact angle measurements performed at 22 ± 3°C and around 50% RH (Table 3). The contact angle was measured with an accuracy of ± 3° using the Multiscope apparatus (Optrel, Sinzing, Germany) and applying the sessile drop method. The contact angle of

each drop of a given liquid was measured after 5 sec after the drop deposition. The *SFE* value was calculated by means of the least-squares fit taking contact angles of each liquid and applying the Owens-Wendt method [164].

Table 3. Dispersive γ^D and polar γ^P components of water, glycerol, and diiodomethane [162, 163].

Liquid	γ mN·m^{-1}	γ^D mN·m^{-1}	γ^P mN·m^{-1}
Water	72.8	21.8	51.0
Glycerol	63.4	37.0	26.4
Diiodomethane	50.8	50.8	0.0

According to Young's equation (Eq. (33)), there is a relationship between the contact angle θ and the interfacial tension between solid and liquid (γ_{SL}), liquid and vapor (γ_{LV}) as well as solid and vapor (γ_{SV}) (Figure 23).

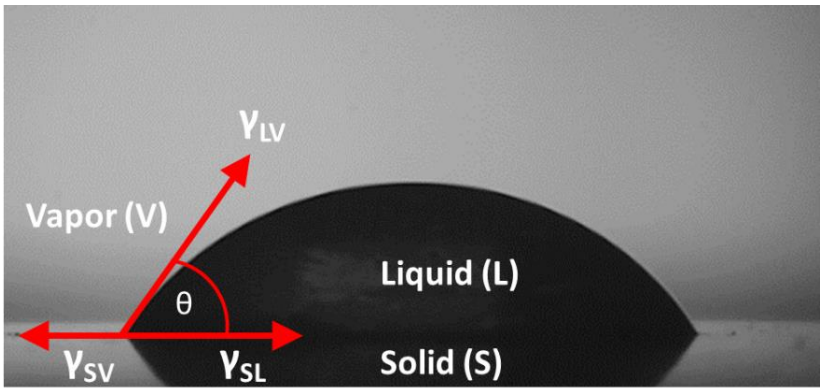

Figure 23. Schematic diagram of contact angle measurement.

$$\gamma_{SV} = \gamma_{SL} + \gamma_{LV} \cos\theta, \tag{33}$$

where γ_{SV} is the interfacial surface free energy between solid and vapor [N m^{-1}], γ_{SL} is the interfacial surface free energy between solid and liquid [N m^{-1}], γ_{LV} is the interfacial surface free energy between liquid and vapor [N m^{-1}], θ is the contact angle.

The γ_{SL} and γ_{SV} values cannot be determined directly by experiment; however, they can be calculated using Dupré's Eq. (34) defining the reversible thermodynamic adhesive work as equal to the surface free energy (*SFE*):

$$W_{SL} = \gamma_S + \gamma_L - \gamma_{SL}\,, \tag{34}$$

where γ_S is the surface free energy of solid in vacuum and γ_L is the surface free energy of liquid used in measurements.

Combining the Eq. (33) and Eq. (34), the following expression is obtained:

$$W_{SL} = \gamma_L(1 + \cos\theta) + \gamma_S - \gamma_{SV}\,. \tag{35}$$

The part ($\gamma_S - \gamma_{SV}$) is equal to π_e which is a spreading pressure defined as a reduction of γ_S as a result of the adsorption of vapor on the solid surface. π_e is very often negligibly small [165] and, thus, the Young–Dupré's equation can be written as follows:

$$W_{SL} = \gamma_L(1 + \cos\theta). \tag{36}$$

In general, Owens–Wendt method used to determine *SFE* assumes that *SFE* is a sum of a polar part component γ_i^P and a disperse part component γ_i^D:

$$\gamma_c = \gamma_c^D + \gamma_c^P, \tag{37}$$

where *c* refers to a liquid or solid phase. Eq. (37) for the liquid (L) and solid (S) can be expressed as follows:

$$\gamma_L = \gamma_L^D + \gamma_L^P, \tag{38}$$

$$\gamma_S = \gamma_S^D + \gamma_S^P. \tag{39}$$

Based on the Owens-Wendt's assumption, *SFE* can be described as:

$$W_{SL} = 2\sqrt{\gamma_S^D\gamma_L^D} + 2\sqrt{\gamma_S^P\gamma_L^P} = \gamma_L(1 + \cos\theta). \tag{40}$$

After combining and transforming the Eqs. (38) and (40), the following expression is obtained:

$$(1 + \cos\theta) = 2\sqrt{\gamma_S^D}\,\frac{\sqrt{\gamma_L^D}}{\gamma_L^D + \gamma_L^P} + 2\sqrt{\gamma_S^P}\,\frac{\sqrt{\gamma_L^P}}{\gamma_L^D + \gamma_L^P}. \tag{41}$$

Eq. (41) can be simplified assuming that $1 + \cos\theta = T_i$, $2\sqrt{\gamma_S^D} = a_1$, $\frac{\sqrt{\gamma_L^D}}{\gamma_L^D + \gamma_L^P} = X_i$, $2\sqrt{\gamma_S^P} = a_2$, $\frac{\sqrt{\gamma_L^P}}{\gamma_L^D + \gamma_L^P} = Y_i$ and the following expression is obtained:

$$T_i = a_1 X_i + a_2 Y_i, \tag{42}$$

where *i* refers to a given solvent: water, glycerol, and diiodomethane.

Eq. (42) is a basis for the calculations of *SFE* by means of the least-squares fit taking contact angles of three liquids of different polarity and applying the Owens-Wendt method. Because the various solvents were taken for the contact angle measurements, Eq. (42) will be expressed as follows:

$$\sum T_i = a_1 \sum X_i + a_2 \sum Y_i \tag{43}$$

Based on the assumptions of the least-squares fit, Eq. (43) can be multiplied by X_i

$$\sum X_i T_i = a_1 \sum X_i^2 + a_2 \sum X_i Y_i \tag{44}$$

or by Y_i

$$\sum Y_i T_i = a_1 \sum X_i Y_i + a_2 \sum Y_i^2 \tag{45}$$

Eq. (44) and (45) can be written in the form of the matrix:

$$\begin{bmatrix} \sum X_i^2 & \sum X_i Y_i \\ \sum X_i Y_i & \sum Y_i^2 \end{bmatrix} \begin{bmatrix} a_1 \\ a_2 \end{bmatrix} = \begin{bmatrix} \sum X_i T_i \\ \sum Y_i T_i \end{bmatrix} \tag{46}$$

Assuming that $\begin{bmatrix} \sum X_i^2 & \sum X_i Y_i \\ \sum X_i Y_i & \sum Y_i^2 \end{bmatrix}$ matrix is expressed as A, Eq. (46) was subsequently multiplied by the inverse matrix A (A^{-1}):

$$A\, A^{-1} \begin{bmatrix} a_1 \\ a_2 \end{bmatrix} = A^{-1} \begin{bmatrix} \sum X_i T_i \\ \sum Y_i T_i \end{bmatrix} \tag{47}$$

That resulted in the following expression:

$$\begin{bmatrix} a_1 \\ a_2 \end{bmatrix} = A^{-1} \begin{bmatrix} \sum X_i T_i \\ \sum Y_i T_i \end{bmatrix} \tag{48}$$

Remembering that $2\sqrt{\gamma_S^D} = a_1$ and $2\sqrt{\gamma_S^P} = a_2$, the γ_S^D and γ_S^P values can be calculated:

$$\gamma_S^D = \left(\frac{a_1}{2}\right)^2 \tag{49}$$

$$\gamma_S^P = \left(\frac{a_2}{2}\right)^2 \tag{50}$$

The sum of Eq. (49) and Eq. (50) is the total *SFE* γ_S:

$$SFE = \gamma_S^D + \gamma_S^P \quad (51)$$

2.4.7 Tensile Tests

The mechanical properties of membranes were studied using Instron 5543 machine. Tensile deformation was determined at a crosshead speed of 1mm min^{-1}. The tests were carried out at 23 ± 2°C and relative humidity of 43 ± 5 %. The dimensions of the sample were as follows: length 30 mm and width 5 mm.

The tensile behavior of tested membranes was evaluated in terms of the Young's modulus (E), elongation at break (ε_{max}), and stress at break (σ_{max}) parameters. The E parameter known as an elastic modulus corresponds to the material stiffness towards deformation under applied loading, and it is calculated from the slope of the straight-line part of the stress-strain curve in the elastic deformation region. The elongation and stress at break are the elongation (ε_{max}) and maximum tensile stress (σ_{max}) values required by the tested sample during the tensile test. In general, high values of E, ε_{max} and σ_{max} display the hard and tough behavior of the material, while their low values characterize the soft and weak behavior [88].

2.5 Swelling Measurements

The sorption behavior of membranes was studied at 25 ± 1°C in contact with pure water, ethanol, and propan-2-ol. Swelling of the investigated membranes was evaluated gravimetrically on the basis of the membrane solvent uptake estimated from the change of the mass between the dry membrane (W_{dry}) and membrane equilibrated in a given solvent (W_{wet}). For this, the dried membrane sample was immersed into the solvents. After a given period of time, the membrane sample was taken out, wiped with tissue to remove the excess of solvent from the membrane surface, and weighed. This step was repeated 3-4 times per day for at least 48 hours until the constant mass of swelled membrane sample was reached (W_{wet}). Thus, the value of membrane mass equilibrated in a given solvent was determined. The degree of swelling was assessed by the amount of solvent absorbed by polymer and, thus, it was calculated according to Eq. (52) and Eq. (53) [4].

$$SD_W = \frac{W_{wet} W_{dry}}{W_{dry}} \text{ [g solvent/g dry membrane]} \quad (52)$$

$$SD_M = \frac{SD_W}{M_{sol}} \text{ [mol solvent/g dry membrane]} \quad (53)$$

where W_{dry} and W_{wet} are the mass of the dry membrane and equilibrated membrane, respectively; M_{sol} is the solvent molecular mass.

2.6 Gas Permeation Measurements

Gas permeation measurements were performed at 25 ± 1°C based on variable pressure method, known as "time-lag" method, using a home-made setup [166] schematically depicted in Figure 24. Gas permeation properties of investigated membranes were evaluated for nitrogen (N_2), oxygen (O_2), and carbon dioxide (CO_2). Initially, a membrane sample (with the active area surface equal to 4.94 cm^2) was sealed between upstream and downstream compartment of the permeation module. Afterwards, the high vacuum purge step was carried out. Subsequently, the stream of given gas (N_2, O_2, or CO_2) with an absolute pressure of 4 bar was injected to the upstream compartment. The pressure increase in the downstream compartment was monitored as function of time using a pressure sensor (Druck, Effa AW-10-TA, Germany). The permeation measurements were performed at least for three various samples per tested membrane and repeated at least four times per tested gas for the reproducibility.

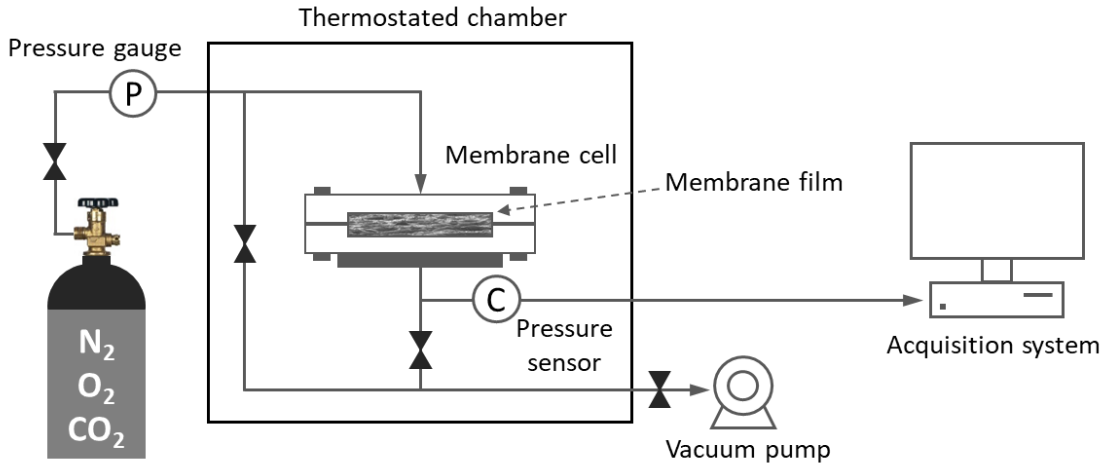

Figure 24. Scheme of gas permeation setup.

2.7 Water Permeation Measurements

Water permeation measurements were performed at 25 ± 1°C using a home-made setup presented in Figure 25 [34]. Prior to the measurements, a membrane sample (with

the active area surface equal to 2.5 cm^2) was sealed in the permeation cell and dried by circulating dry nitrogen (Alphagaz 2, Air Liquide®, France) on both sides of the film till the lowest constant value of dew point (corresponding to the lowest amount of moisture in the system) was reached (ca. -70°C).

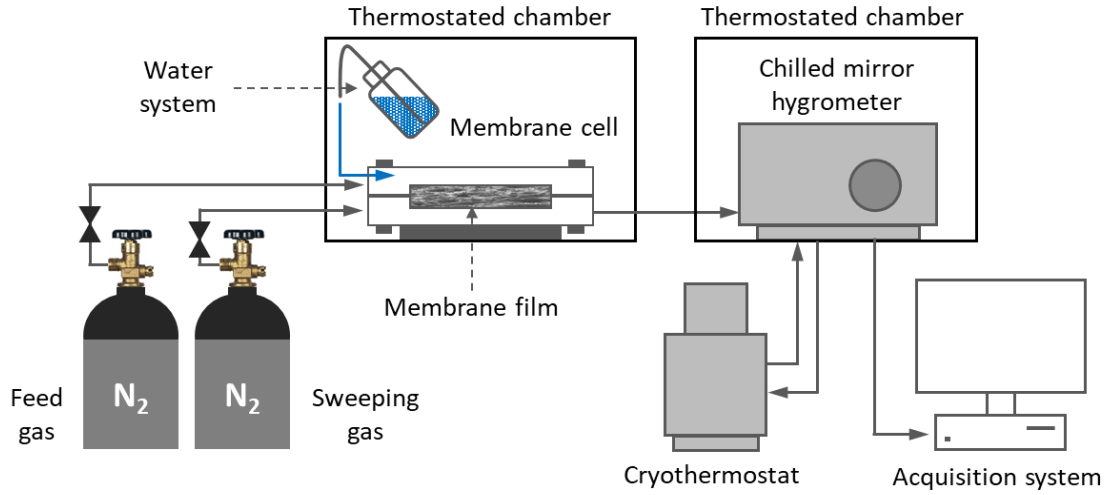

Figure 25. Scheme of water permeation setup.

Subsequently, a stream of liquid water (or water vapor) as a feed was injected into the upstream compartment while the downstream compartment was continuously swept out by the stream of dry nitrogen. Due to the difference in water activities on both sides of membrane, water molecules diffused through the membrane. The amount of vapors transported into the downstream compartment was monitored by using a chilled mirror hygrometer (General Eastern Instruments, Elcowa®, France) connected to the data acquisition system (Figure 25). The experiments were performed at water vapor activities of feed stream increasing up to the saturation vapor pressure. The data were collected until the stationary state in the system was reached.

2.8 Pervaporation

The vacuum pervaporation (VPV) measurements of the elaborated polymer-IL membranes were performed using the standard experimental setup depicted schematically in Figure 26 [26]. The effectiveness of the tested membranes was evaluated for water–propan-2-ol mixture (H_2O-IPA) at 35°C. The water content in the feed mixture varied within the concentration range 0-13 wt.% depending on the studied membrane.

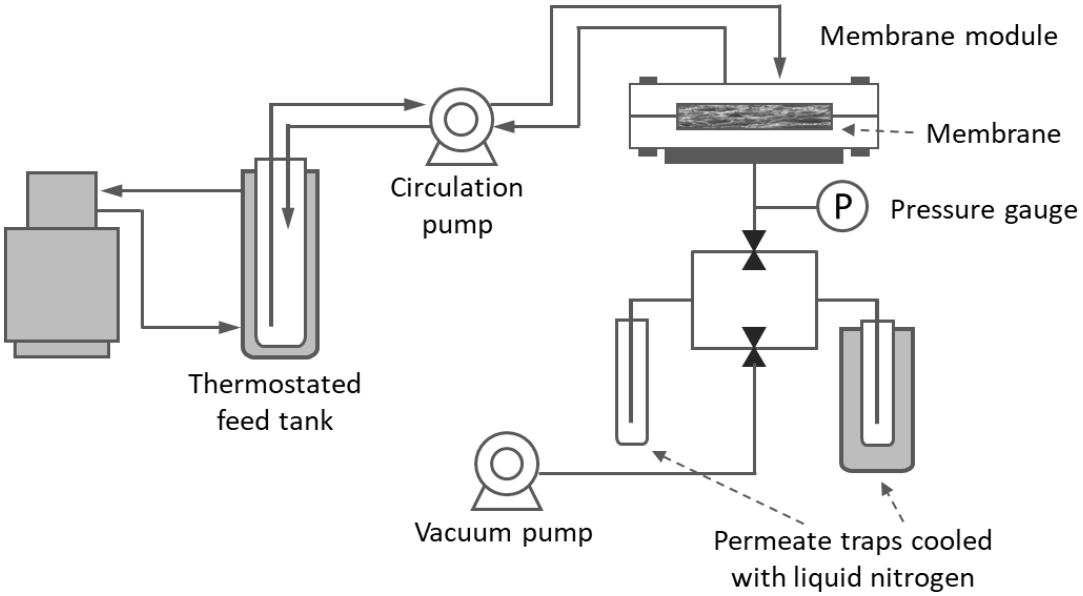

Figure 26. Scheme of vacuum pervaporation setup.

The membrane sample (with the active area surface equal to 2.25 10^{-3} m^2) was sealed on a porous stainless steel support in the membrane module. A circulating feed pump ensured the continuous circulation of a thermostated feed between the feed tank and the membrane module. The low pressure (below 2 mbar) on the permeate side was retained by a vacuum pump (Alcatel 2015 Pascal, France). In order to maintain the continuous work of the pervaporative measurement, permeate was collected alternately into two parallel permeate traps cooled with liquid nitrogen.

The composition of feed and permeate for VPV measurements was analyzed using Varian 3300 gas chromatograph with thermal conductivity detector (TCD) (Varian, Inc., Walnut Creek, CA, USA) and Porapak Q packed column (injection port temperature at 200°C, detector temperature at 220°C, column temperature at 180°C). The volume of analyte injected into the column was in the range of 0.2–0.4 μL. The acquired data were processed using BORWIN software (version 1.21.07, JMBS, Grenoble, France).

The validation of gas chromatography analysis of feed and permeate composition was performed in terms of following parameters: limit of detection (LOD), limit of quantification (LOQ), relative standard deviations for the repeatability (RSD_r) and the reproducibility (RSD_R) [4, 167, 168]. LOD is defined as the minimum concentration of water and referred to the signal-to-noise (S/N) ratio equal to 3. LOQ is calculated as a S/N ratio equal to 10. LODs and LOQs of water were as follows: LOD=0.02 wt.%,

LOQ=0.07 wt.%. RSD_r for n=5 and RSD_R for n=11, 4 operators in the investigated range of water content were following: $RSD_r < 0.8\%$, $RSD_R < 6.2\%$.

CHAPTER 3

Elaboration and Characterization of PVA-Based Membranes

For the present study, PVA was chosen because of good properties and wide application in separation technologies as it was mentioned in Chapter 1. Chapter 3 is subdivided into two distinct parts. In the first part, the characterization of chemically and thermally crosslinked PVA-based membranes is presented. The second part is devoted to the study of PVA-based membranes with incorporated imidazolium-based ionic liquids.

The main objective of this chapter is to evaluate the influence of the crosslinking agent and conditions of crosslinking on the properties of PVA-based membranes in order to select the membranes with reinforced mechanical properties and improved resistance towards liquid water. Furthermore, PVA-RIL membranes are prepared and investigated taking into account the influence of the RIL presence on the physicochemical and transport properties of the elaborated membranes.

3.1 Cross-linked PVA Membranes

Because of the solubility of PVA-based materials in water, PVA-SSA membranes were prepared by two-step crosslinking approach involving chemical crosslinking of PVA using SSA as a crosslinking agent (the SSA weight fraction range varied from 5 to 50 wt.%) and the subsequent thermal treatment. The thermal treatment at different temperature (from 120 to 140°C) was performed in order to improve the membrane crosslinking process.

3.1.1 Effectiveness of Crosslinking

The possible chemical reaction between PVA and SSA is shown in Figure 27.

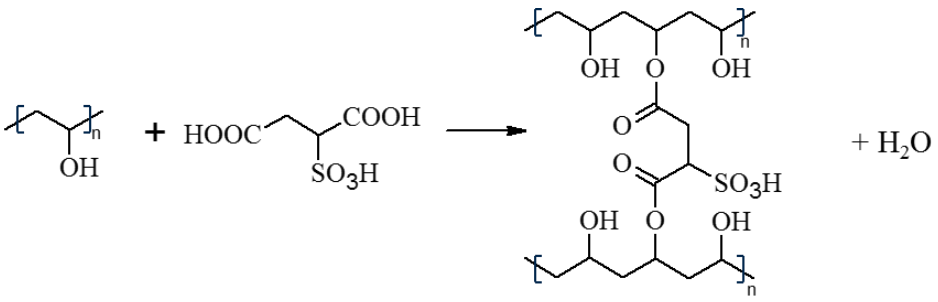

Figure 27. Scheme of the crosslinking reaction between PVA and SSA.

The effectiveness of the crosslinking reaction is assessed based on the FTIR-ATR analysis of the pure and crosslinked PVA membranes. The spectra of native PVA, pure SSA, and PVA-SSA membranes crosslinked using various concentrations of SSA and heated at different crosslinking temperature are presented in Figure 28. The spectra were normalized with respect to the -CH_2- stretching vibration band in the PVA backbone (ν = 2939 cm^{-1}) [91]. The spectrum of pristine PVA membrane reveals characteristic bands assigned to -OH stretching vibration (3685-3010 cm^{-1}), -CH_2- symmetric (2929-2915 cm^{-1}) and asymmetric (2854 cm^{-1}) stretching vibrations, as well as to C-O stretching vibration (1238 cm^{-1}) (Table 4) [91, 169].

Table 4. Band assignments of pristine PVA and SSA.

Band assignments	Wavenumber [cm^{-1}]	
	PVA	SSA
O–H stretching	3685-3010	3675-3000
CH_2 symmetric stretching	2929-2915	-
CH_2 asymmetric stretching	2854	-
C=O stretching vibration (from -COO- ester group)	-	1714
C-O stretching vibration	1238	1215
sulfonate groups (SO_3^-) stretching	-	1038
skeletal and C–O stretching	825	-

The spectrum of SSA solution (Figure 28A) presents the -OH stretching vibration band in the range from 3675 to 3000 cm^{-1} due to the presence of the water molecules and the carboxylic acid groups (-COOH). Also, the stretching vibration band of sulfonate groups (SO_3^-) is seen at 1038 cm^{-1}. The presence of the sulfonate groups band in the FTIR-ATR spectrum results from the dissociation of -SO_3H in the SSA structure [91]. The

bending band of the water molecules can be distinguished at around 1640 cm^{-1} which confirms the high water content in the SSA solution; however, this band is overlapped with the C=O stretching vibration band at 1714 cm^{-1} (Figure 28).

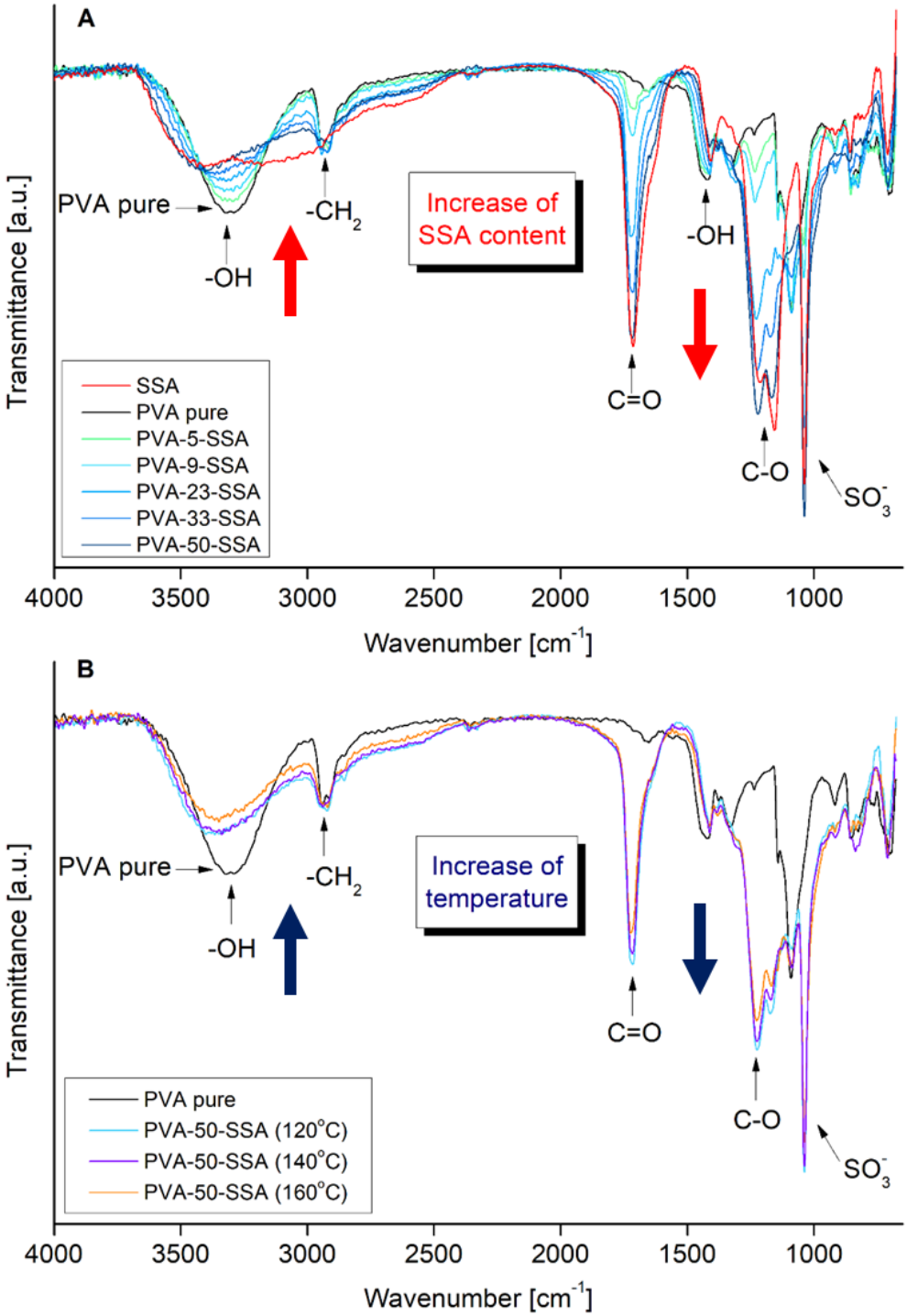

Figure 28. FTIR-ATR spectra of crosslinked PVA-based membranes: (A) heat-treated at 120°C as a function of the SSA content (5-50 wt.%) and (B) containing 50 wt.% SSA as a function of the crosslinking temperature (120-160°C).

The FTIR-ATR spectra of the PVA-SSA membranes revealed significant changes of bands' intensity and position compared to the native PVA membrane confirming the influence of the SSA addition (Figure 28A). The raise of the SSA content at a given crosslinking temperature led to the intensity increase of C=O and C-O stretching vibration bands of -COO- ester groups in PVA-based membranes. The C=O stretching vibration band was found at around 1718 cm^{-1} whatever the SSA concentration, whereas the C-O stretching vibration band observed at 1240 cm^{-1} for pristine PVA was shifted to lower wavenumber value with the increasing SSA content (up to 1217 cm^{-1} for the PVA-SSA membrane containing 50 wt.% SSA). Furthermore, the reduced intensity of the -OH stretching vibration band was observed with the increasing SSA content. The aforementioned changes are related to the crosslinking reaction based on the esterification reaction between -OH groups in PVA and -COOH groups in SSA (Figure 27) [92, 169, 170]. Simultaneously, the increasing content of SSA increases the intensity of the $-SO_3^-$ symmetric stretching vibration band at ~ 1040 cm^{-1} (Figure 28A).

The crosslinking temperature (120°C, 140°C, and 160°C) also possesses the important influence on the spectral behavior of the PVA-SSA membranes (Figure 28B). It can be seen that the raise of the curing temperature from 120°C to 160°C results in the decrease of the intensity of stretching vibration bands of -OH group. As a result, the intensity of the C=O and C-O symmetric stretching vibration bands increases. Therefore, it can be concluded that the thermal curing can reinforce the effect of the chemical PVA crosslinking.

The influence of the crosslinking on the properties of PVA membranes used as polyelectrolyte membranes was examined and reported by Martínez-Felipe et al. [91], Rhim et al. [92], and Kudoh et al. [101]. Researchers presented the significance of the thermal treatment for PVA-based membranes reinforced with SSA as a crosslinker. Martínez-Felipe et al. indicated that the crosslinking based on the esterification reaction occurred in all tested PVA-SSA membranes containing SSA in the concentration range from 5 to 30 wt.% [91]. The further membrane heating at 110°C enhanced their thermal stability. The crosslinking of PVA-based membranes with SSA was confirmed by the decreased intensity of -OH vibrational stretching band in the 3600-3000 cm^{-1} region and by simultaneous increased intensity of C=O vibrational stretching band. The intensity of SO_3^- group bands was also increased. As a result, the raise of the proton conductivity was observed confirmed by an increase of the ion-exchange capacity from 0.052 $meq \cdot g^{-1}$ to 0.141 $meq \cdot g^{-1}$ for membranes containing 5 wt.% and 30 wt.% SSA, respectively [91].

3.1.2 Thermal Stability

The thermal stability of the pristine PVA and crosslinked PVA-SSA membranes was examined using the TGA analysis. The obtained TGA and derivative thermogravimetric (DTG) curves are presented in Figure 29. The thermal degradation of pristine PVA follows three sequential degradation steps. The first stage at around 100°C refers to the loss of the water molecules entrapped in the hydrophilic PVA structure. The second intensive peak in the range of 200-380°C is due to the loss of -OH groups and the deacetylation of PVA chains. The third degradation step observed at 400-500°C is assigned to the degradation of the PVA backbone [91, 98].

In the case of PVA-SSA membranes, three main degradation steps can be also distinguished. The first strong weight loss observed at around 100°C can be attributed to the loss of the water molecules strongly bounded to the polymer structure. The peak at 200-300°C corresponds to the desulfonation as well as to the loss of -OH and acetate groups related to the break of ester bonds between PVA and SSA. The weight loss in this range increases with the increasing concentration of a crosslinking agent and shifts to a lower temperature for PVA-SSA membranes in comparison with native PVA (Figure 29). The degradation of the PVA-SSA main chains is observed in the temperature range of 400-500°C [91, 92], and it is more pronounced than in the case of pure PVA (Figure 29).

It was also noticed that the increase of the crosslinking temperature from 120°C to 160°C led to a slight increase of the degradation temperature at a given weight loss (Table 5), thus indicating the improvement of the thermal stability of elaborated PVA-SSA membranes. Indeed, for the PVA-SSA membrane containing 33 wt.% SSA and annealed at 120°C and 160°C, the 5 % weight loss is observed at 111°C and 127°C, respectively.

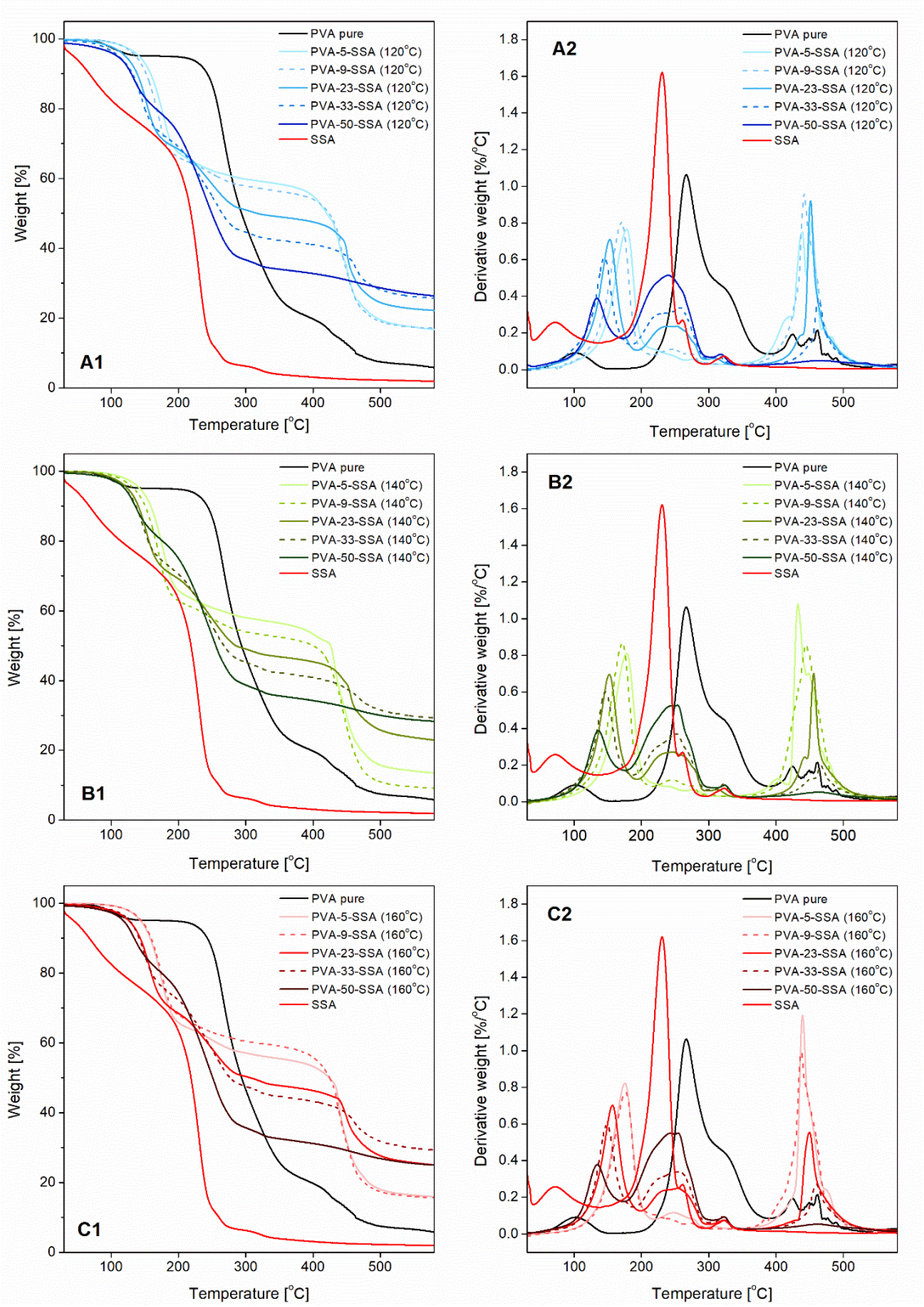

Figure 29. TG (A1, B1, C1) and DTG (A2, B2, C2) curves of heat-treated PVA-based membranes containing 5-50 wt.% SSA as a function of crosslinking temperature.

Table 5. Characteristic degradation temperature of studied PVA-SSA membranes.

Membrane	Degradation temperature [°C]	
	at 5% weight loss	at 10% weight loss
PVA pure	163 ± 2	243 ± 2
PVA-5-SSA (120°C)	142 ± 2	159 ± 2
PVA-5-SSA (140°C)	143 ± 2	159 ± 2
PVA-5-SSA (160°C)	144 ± 2	158 ± 2
PVA-9-SSA (120°C)	137 ± 2	152 ± 2
PVA-9-SSA (140°C)	134 ± 2	150 ± 2
PVA-9-SSA (160°C)	145 ± 2	159 ± 2
PVA-23-SSA (120°C)	121 ± 2	139 ± 2
PVA-23-SSA (140°C)	125 ± 2	140 ± 2
PVA-23-SSA (160°C)	126 ± 2	143 ± 2
PVA-33-SSA (120°C)	111 ± 2	132 ± 2
PVA-33-SSA (140°C)	120 ± 2	137 ± 2
PVA-33-SSA (160°C)	127 ± 2	142 ± 2
PVA-50-SSA (120°C)	109 ± 2	130 ± 2
PVA-50-SSA (140°C)	120 ± 2	136 ± 2
PVA-50-SSA (160°C)	118 ± 2	134 ± 2

PVA membranes containing 23 and 33 wt.% SSA and crosslinked at 140°C were found to provide the favorable balance between crosslinking and the membrane thermal stability. The thermal stability up to around 120°C of PVA-23-SSA and PVA-33-SSA membranes annealed at 140°C is sufficient for their potential further application in pervaporation. Therefore, these membranes were chosen for the further analysis.

3.1.3 Morphology and Surface Characterization

The morphology of the pristine PVA and heat-treated PVA-SSA membranes was examined by the SEM analysis. The SEM images of the cross-section view of the pure PVA and PVA-based membranes containing 23 wt.% and 33 wt.% SSA heated at 140°C are presented in Figure 30.

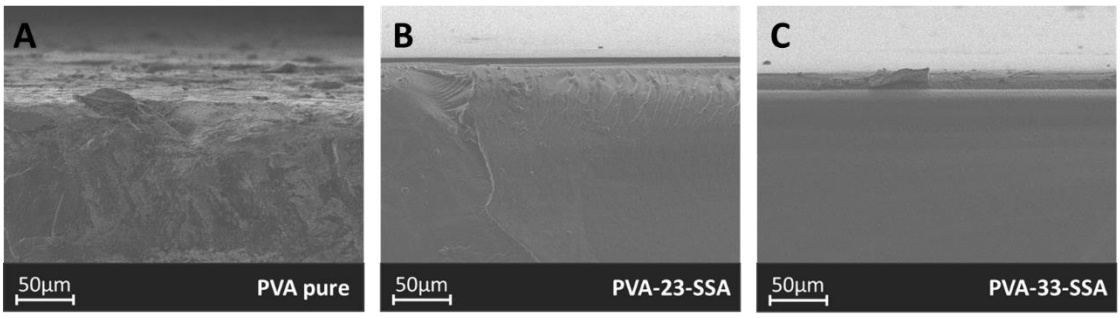

Figure 30. SEM cross-section micrographs of: (A) pristine PVA membrane, (B) PVA-SSA membrane containing 23 wt.% SSA heated at 140°C, and (C) PVA-SSA membrane containing 33 wt.% SSA heated at 140°C.

The cross-section SEM images of the elaborated membranes indicate that PVA-based membranes are dense and nonporous. The cross-section of the native PVA membrane is uniform (Figure 30A). The addition of 23 wt.% and 33 wt.% of a crosslinking agent (SSA) into the PVA membrane matrix did not change the membrane homogeneity (Figure 30B and Figure 30C, respectively) that confirmed the good compatibility between the polymer and the used crosslinking agent. The compatibility of the polymer matrix and the crosslinking agent is indeed a key factor for further possible incorporation of the chosen additives into the crosslinked membrane structure. Riyajan et al. reported that the crosslinking of PVA-based membranes containing maleic acid enhanced the compatibility of PVA and the used epoxised natural rubber (ENR) [94]. The pristine PVA-ENR blend revealed numerous microphase separations highlighted by the SEM analysis. The crosslinking of PVA with maleic acid resulted in the significant increase of the compatibility between PVA and ENR what was reflected by the decrease of microphase separations [94].

3.1.4 Mechanical Properties

The mechanical strength and elasticity are important parameters of polymer materials used in membrane separation processes driven by the chemical potential difference, such as VPV studied in this work. Thus, the influence of the crosslinking agent content and temperature on the mechanical properties of PVA-SSA membranes was studied by tensile test and assessed based on the Young's modulus (E) (Figure 31A), elongation at break (ε_{max}) (Figure 31B), and stress at break (σ_{max}) (Figure 31C) parameters.

The Young's modulus, stress at break, and elongation at break values for the pristine PVA membrane are E = 1266 ± 168 MPa, σ_{max} = 42 ± 4 MPa, and ε_{max} = 315 ± 63 %, respectively. The raise of the SSA content up to 9 wt.% for the membranes crosslinked at 140°C increased the value of Young's modulus parameter up to 3196 ± 338 MPa and the stress at break parameter up to 46 ± 3 MPa compared to the pristine PVA membrane. Simultaneously, the elongation at break value decreased (176 ± 61 %) that was correlated with the reduced polymer chains' flexibility and, thus, enhanced membrane stiffness [88, 100, 171]. The further increase of a SSA content resulted in the drop of Young's modulus (Figure 31A) and the stress at break (Figure 31C) parameters. The elongation at break remained at the constant level of about 200 % up to 33 wt.% of SSA in PVA membranes followed by the sharp decrease to ~50 % for the PVA-50-SSA membrane containing 50 wt.% od SSA (Figure 31B).

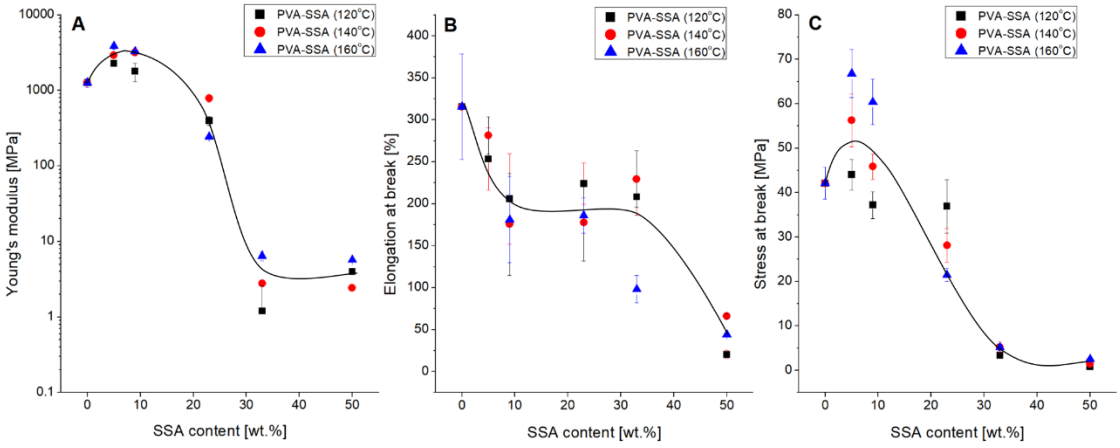

Figure 31. Influence of the crosslinking temperature and SSA content on the mechanical properties of PVA-SSA membranes: (A) Young's modulus, (B) elongation at break, and (C) stress at break. The solid lines are only to guide an eye.

PVA-50-SSA membrane revealed a brittle behavior, whatever the crosslinking temperature, what was reflected by the remarkable decrease of the elongation at break and stress at break values – ε_{max} = 66 ± 2.9 % and σ_{max} = 1.4 ± 0.1 MPa. This result can be explained by the high crosslinking density, which hinders the plastic deformation of the studied membrane [100]. Dadfar et al. [93] reported the increased tensile strength (from 8 MPa to 13 MPa) and the decreased elongation at break (from 270 % to 200 %) for PVA-based membrane with the raise of the GA content from 3 wt.% to 9 wt.%. Vashisth and Pruthi [172] indicated that the two-step crosslinking combining the heat

treatment as well as the exposure to methanol and $CaCl_2$ improved the tensile strength of the PVA-gellan nanofibers. The similar behavior can be noticed in this work for annealed PVA-SSA membranes with a low content of SSA characterized by the increased values of stress at break parameter with increasing the crosslinking temperature (Figure 31C).

The degree of the PVA crosslinking depends on both the chemical and thermal crosslinking. Riyajan et al. [94] reported that the increase of the maleic acid content (from 10 wt.% to 60 wt.%) and the time of crosslinking (from 10 min to 60 min at 120°C) enhanced the crosslinking degree of PVA-based membranes. For example, the increasing content of maleic acid (from 10 wt.% to 60 wt.%) improved the tensile strength (from 12 MPa to 32 MPa) of the studied PVA-based membranes and this effect was more pronounced when the membrane was heated at 120°C. Birck et al. discovered that the PVA-based membranes crosslinked with 10 wt.% and 40 wt.% of citric acid (CTR) required heating for 40 min and 120 min at 130°C, respectively, in order to reach the complete crosslinking reaction between PVA and CTR [100]. The tensile measurements testified that the studied PVA-CTR membranes containing 40 wt.% CTR and heated at 130°C during 40 min were brittle because of the high crosslinking density hindering the plastic deformation, reflected by the nominal stress and nominal strain equal to around 40 MPa and 0.01, respectively. In the case of PVA-based membranes crosslinked with 10 wt.% CTR, it was shown that the increase of the annealing time up to 360 min decreased the nominal strain from around 2 to 0.3 and increased the nominal stress from around 18 MPa to 23 MPa as compared with the non-heated PVA-CTR membrane.

In general, the hydrogen bonds and hydrophobic interactions stabilize the pristine PVA membrane. The crosslinking of PVA with SSA results in the creation of covalent bonds between the PVA chains and crosslinking agent (Figure 27), which leads to the increase of the stress at break value (Figure 31C). However, the increase of the SSA concentration over 10 wt.% causes the progressive deterioration of the mechanical properties as observed by the drop of the stress at break, elongation at break, and Young's modulus values (Figure 31) due to the exceeded inner stress in PVA-SSA membranes [94, 105]. It is known that in the case of the excessive crosslinking the internal stresses occur and deteriorate the mechanical properties of polymer membranes [173-175]. This phenomenon was widely studied in the case of the epoxy polymers and acrylate networks showing that the internal stress was extended through the membrane thickness from the surface to the center [175]. Such behavior was also observed for PVA-based membranes crosslinked with GA [173]. It was shown that the increase of the GA content from 16

wt.% to 25 wt.% decreased the flexural strength and modulus. Korsmeyer et al. noticed that the crosslinking with a high GA content and subsequent drying of the PVA-based gels could create the microvoids and cracks due to the pronounced inner stress inside the highly crosslinked polymer networks [174]. Rey et al. pointed out the significance of the inner stress after annealing and post-annealing treatment for the dimethacrylate/styrene films [175]. The value of the internal stress was associated with the double bond conversion and crosslinking density.

Based on the aforementioned findings, it can be seen that the crosslinking reinforces membrane mechanical properties. However, one should remember that the exceeded increase of the membrane crosslinking raises its density and, thus, the membrane becomes more rigid and brittle. Taking into account the obtained results it can be noticed that PVA membranes with the 9-23 wt.% SSA content crosslinked at 140°C reveal sufficient mechanical strength for the subsequent application in VPV.

3.1.5 Equilibrium Properties

In order to evaluate the effect of PVA crosslinking on the membrane surface wettability, the contact angle measurements using solvents with different polarity (water, glycerol, diiodomethane) were performed. The analysis of water contact angles allowed assessing additionally the effectiveness of the PVA crosslinking. The performed measurements revealed that the values of water contact angle increased with the increasing SSA concentration for heat-treated PVA-SSA membranes (Table 6). This fact is resulted from the reduced hydrophilic character of the membrane surface due to a decreased amount of hydroxyl groups after the esterification reaction with a SSA crosslinking agent (Figure 27). This result is in a good agreement with the results obtained by FTIR-ATR analysis (Figure 29). The average values of water contact angle obtained for the PVA-5-SSA and PVA-33-SSA membranes heated at 140°C are equal to 75° and 89°, respectively (Table 6). The increase of the water contact angles as a result of crosslinking was also observed by Vashisth and Pruthi for the PVA-gellan nanofibers indicating the improved stability of the PVA-based materials in contact with water [172].

Penkova et al. [176] reported slight increase of the water contact angle as a result of the increase of the annealing temperature testifying the reduction of the membrane surface hydrophilicity. PVA-SSA membranes containing 5 wt.% of a crosslinker and heated at 140°C and 160°C show the water contact angle values equal to 75° and 80°,

respectively (Table 6). It was shown that the thermal annealing at 140°C during 100 min diminished the surface hydrophilic character of PVA-based materials containing fullerenol as a crosslinker [176]. However, the incorporation of fullerenol caused the increased hydrophilic character of the film surface compared to the pristine PVA membrane. The water contact angle of the pristine PVA membrane was equal to 66°, whereas the addition of 5% of fullerenol decreased the contact angle value to 45° [176]. Zhou et al. pointed out that the reduction of the hydrophilic character of the membrane surface can also be achieved by increasing the UV irradiation dose for the thermoplastic starch-PVA blend films due to the consumption of hydroxyl groups during the crosslinking reaction [171].

Table 6. Water contact angle, dispersive γ^D and polar γ^P components, and surface free energy (*SFE*) of crosslinked PVA-SSA membranes.

Membrane	Crosslinking temperature [°C]	Water contact angle [°]	γ^D [mJ·m^{-2}]	γ^P [mJ·m^{-2}]	*SFE* [mJ·m^{-2}]
PVA	-	64 ± 3	41.1 ± 2.1	9.5 ± 0.5	50.7 ± 2.6
PVA-5-SSA	120	86 ± 3	33.2 ± 2.0	1.3 ± 0.4	34.5 ± 2.4
PVA-9-SSA		91 ± 3	34.7 ± 1.7	0.8 ± 0.5	35.5 ± 2.2
PVA-23-SSA		96 ± 3	29.4 ± 1.8	0.7 ± 0.5	30.1 ± 2.2
PVA-33-SSA		92 ± 3	31.0 ± 2.2	0.8 ± 0.3	31.8 ± 2.4
PVA-5-SSA	140	75 ± 3	33.1 ± 1.8	2.8 ± 0.7	35.9 ± 2.5
PVA-9-SSA		84 ± 3	32.6 ± 1.1	1.5 ± 0.7	34.1 ± 1.7
PVA-23-SSA		98 ± 3	31.2 ± 2.1	0.3 ± 0.3	31.5 ± 2.3
PVA-33-SSA		89 ± 3	29.2 ± 1.3	1.3 ± 0.6	30.5 ± 1.8
PVA-5-SSA	160	80 ± 3	33.6 ± 1.4	1.8 ± 0.7	35.4 ± 2.0
PVA-9-SSA		89 ± 3	33.5 ± 1.9	0.9 ± 0.4	34.3 ± 2.3
PVA-23-SSA		87 ± 3	29.0 ± 2.1	2.3 ± 0.5	31.3 ± 2.6
PVA-33-SSA		91 ± 3	30.5 ± 2.3	2.7 ±0.4	33.1 ± 2.7

Taking into account measurement errors, the *SFE* results indicate the slight influence of thermal and chemical crosslinking on both polar γ^P and dispersive γ^D

components (Table 6). Moreover, the predominant influence of the London dispersive interactions [165] is clearly observed, as a result of a much higher dispersive component value γ^D in comparison to the polar component γ^P. It is known that materials with a low surface energy (30-35 $mJ \cdot m^{-2}$) demonstrate great water repellency [35-38], which explains their water resistance and makes them popular for the wettability researches.

The influence of the crosslinking on the swelling behavior of PVA-based membranes was evaluated in contact with pure water, methanol, and propan-2-ol. The results of the swelling measurements are a good indication of the crosslinking effect. The values of the molar swelling degree SD_M of PVA-SSA membranes annealed at 120°C, 140°C and 160°C in contact with different solvents are calculated according to Eq. (53) and gathered in Table 7. The obtained results reveal the significantly higher membrane sorption in water than in methanol and propal-2-ol whatever the crosslinking temperature. For example, SD_M of PVA-9-SSA membrane heated at 140°C is equal to 362.4 mol solvent/g dry membrane in the case of the water swelling, whereas SD_M for the same membrane swelled in methanol and propan-2-ol is equal to 1.7 mol solvent/g dry membrane and 0.12 mol solvent/g dry membrane, respectively. Thus, much higher membrane swelling degree in water compared to the swelling degree in the solvents of a lower polarity (methanol and propan-2-ol) was noticed.

Moreover, it was found that the membrane swelling degree in water is inversely proportional to the SSA content for all studied membranes except the PVA-5-SSA membrane whatever the crosslinking temperature (Table 7). The highest swelling degree in water was observed for PVA-9-SSA membrane, whereas this value decreased with the increasing content of a crosslinking agent. Such behavior is related to the decrease of the free volume of polymer network, namely, the capability of polymer to swell in water progressively decreases with the crosslinking density increase [176]. It should be also taken into account that the amount of the crosslinking agent influences the polymer hydrophilic character (Table 6), and, consequently, contributes to the swelling ability of the membrane.

As expected, the alcohol swelling behavior of the PVA membrane is also influenced by the crosslinking reaction (Table 7). The swelling measurements revealed a higher methanol swelling as compared with propan-2-ol swelling. This result is in agreement with the swelling results for the PVA membranes crosslinked with GA obtained by Farid et al. [177]. It was reported the higher swelling of the PVA-GA membrane in ethanol than in propan-2-ol that was correlated with a smaller molecular

size and higher polarity of ethanol. Farid et al. stated that the membrane free volume decreased with the raise of the crosslinking agent content and, hence, the sorption of solvent molecules with higher molecular size would be difficult [177].

Table 7. The molar swelling degree SD_M of heat-treated PVA-SSA membranes in water, methanol and propan-2-ol as a function of the SSA concentration and crosslinking temperature.

Membrane	Crosslinking temperature [°C]	SD_M [mol solvent/g dry membrane]		
		Water	Methanol	Propan-2-ol
PVA-5-SSA	120	179.3	0.9	0.01
PVA-9-SSA		402.9	4.2	0.01
PVA-23-SSA		224.6	4.1	0.04
PVA-33-SSA		166.4	3.4	0.01
PVA-50-SSA		89.4	-	-
PVA-5-SSA	140	149.1	0.9	0.03
PVA-9-SSA		362.4	1.7	0.12
PVA-23-SSA		237.6	6.0	0.01
PVA-33-SSA		149.4	11.9	0.05
PVA-50-SSA		122.2	-	3.67
PVA-5-SSA	160	174.0	0.4	0.05
PVA-9-SSA		369.6	2.0	0.04
PVA-23-SSA		264.0	6.9	0.01
PVA-33-SSA		75.4	11.3	0.03
PVA-50-SSA		-	-	4.18

Penkova et al. [176] noticed the remarkable effect of the thermal annealing on the properties of crosslinked PVA-fullerenol membranes equilibrated with water and ethanol. The swelling measurements revealed the reduced water and ethanol sorption capacity for PVA membranes heat-treated at 140°C for 100 min. The membrane annealing led to the decrease of the water sorption degree from 310% to 87% for the membrane containing 5% of fullerenol. In the case of the ethanol sorption, the heat-treatment resulted in the decrease of the sorption degree from 8.6 % to 2.6 % for the PVA-based membrane

containing 5% of fullerenol [176]. This phenomenon was related to the fact that heat-treated PVA-fullerenol membranes revealed the presence of ether bonds of covalent character compared to non-heat-treated membranes possessing the extensive hydrogen bonding between PVA and fullerenol. The crosslinking due to the covalent ether bond formation resulted in the increased packaging, decreased free volume of PVA membranes, and their more rigid structure that contributed to the decreased swelling in ethanol [176].

Kudoh et al. studied the PVA crosslinking using SA and SSA [101]. Researchers reported that the efficiency of PVA crosslinking increased with increasing the SA content and the crosslinking temperature. In the case of SSA, the crosslinking reaction was effective at the low SSA content (5-10 wt.%) in the whole investigated temperature range (from 140°C to 200°C), that was testified by the low dissolution rate of the obtained PVA-SSA membranes in water. It was noticed that the dissolution rate of membranes containing 20 wt.% SSA and heated at 180°C and 200°C was nearly two-fold higher than that of the pure PVA membrane. It was pointed out that the excess amount of SSA was used; therefore, the unreacted SSA molecules were dissolved while swelled in hot water. SSA is found to be more reactive than SA even if the increase of the SA content and the crosslinking temperature decrease the dissolution rate of crosslinked PVA-based membranes. For example, the dissolution rate of PVA-SSA membranes containing 5 or 10 wt.% SSA does not exceed 10%, whereas the membranes crosslinked with 6 wt.% SA and heated at 140°C exhibit the dissolution rate around 55% [101].

The difference in the swelling behavior of PVA-SSA crosslinked membranes can be also explained by the molecular size of a solvent [178] as well as correlated to the covalent bonds formation. The size of the studied solvent molecules decreases in the following order:

propan-2-ol (5.12 Å) > methanol (4.10 Å) > water (3.40 Å).

Consequently, the membrane swelling capacity is found to increase in the same order (Table 7). Simultaneously, the reduced membrane free volume as a result of the covalent ester bond formation between PVA and SSA hinders the penetration of methanol and propan-2-ol molecules possessing bigger molecular size. Thus, the penetration of polymer membrane with small water molecules is facilitated and more rapid.

The studies of the equilibrium properties revealed the resistance of crosslinked PVA-SSA membranes towards liquid water reflected by the decreasing water contact angle and the water swelling ability. It is found that the PVA-23-SSA membrane heat-

treated at 140°C possesses the highest difference of the swelling ability between water and organic solvents (Table 7) as well as it has a good mechanical stability (Figure 31). Thus, taking these results into account, the behavior of the PVA-23-SSA membrane towards water is investigated by means of the water vapor permeation kinetics measurements. The water permeation measurement of pure PVA was not possible to perform due to the rapid solubility of PVA in contact with pure water.

3.1.6 Transport Properties

The preferential membrane swelling in water as well as the great difference of the membrane swelling ability between water and organic solvents testifies to the promising membrane application in separation process. Consequently, the water permeation measurements were carried out at different RH level in order to assess the water transport properties of the crosslinked membrane as a function of the moisture content surrounding the membrane. The values of water permeability coefficient obtained for the membrane investigated at varied RH in the range from 24 % to 91 % are presented in Table 8. The obtained results indicate the strong influence of the RH level on the membrane moisture resistance. The increase of the water activity causes the greater water permeation of the investigated membrane and, hence, the increase of the membrane permeability coefficient *P* from 16.6 Barrer at 24 % RH to 63865.1 Barrer at 91 % RH is observed.

Table 8. Water vapor permeability coefficients of the PVA membrane containing 23 wt.% SSA and heat-treated at 140°C.

Water activity [-]	*P* [Barrer]*	$P \cdot 10^{-4}$ [$g \cdot mm \cdot m^{-2} \cdot kPa^{-1} \cdot h^{-1}$]	$P \cdot 10^{-4}$ [$g \cdot m \cdot m^{-2} \cdot atm^{-1} \cdot d^{-1}$]
0.24	17	4	9
0.41	18	4	10
0.59	2742	596	1451
0.68	9312	2022	4928
0.76	13759	2981	7264
0.85	32762	7113	17335
0.91	63865	13819	33675

*1 Barrer = 10^{-10} $cm^3 \cdot cm \cdot cm^{-2} \cdot s^{-1} \cdot cm\ Hg^{-1}$

Such significant dependence of the water permeability on the water activity is in agreement with the results of López-de-Dicastillo et al. [90]. The PVA/β-cyclodextrin (βCD) composites crosslinked with glyoxal revealed strong influence of the water vapors presence in the whole investigated RH range (35-70 % RH) as a function of the crosslinking method. It was stated that the films prepared by the addition of the βCD solution to the previously crosslinked PVA solution (PVA*.CD) and by the crosslinker addition to the aqueous solution containing PVA-βCD ((PVA.CD)*) possessed the highest barrier properties and the best physical properties among tested composites. The asterisk * refers to the crosslinked material. The water permeability coefficient *P* of the pristine PVA membrane was equal to $116.0 \cdot 10^3$ $g \cdot m \cdot m^{-2} \cdot day^{-1} \cdot atm^{-1}$ at 70 % RH, whereas the *P* values for the PVA*.CD and (PVA.CD)* membranes were much lower – $87.5 \cdot 10^3$ $g \cdot m \cdot m^{-2} \cdot day^{-1} \cdot atm^{-1}$ and $37.5 \cdot 10^3$ $g \cdot m \cdot m^{-2} \cdot day^{-1} \cdot atm^{-1}$, respectively [90]. These results exhibit the great improvement of the water barrier properties due to the crosslinking reaction. Moreover, it was observed that for all studied composite membranes the permeability increased with the RH increasing. For example, *P* raised from $2.0 \cdot 10^3$ $g \cdot m \cdot m^{-2} \cdot day^{-1} \cdot atm^{-1}$ to $37.5 \cdot 10^3$ $g \cdot m \cdot m^{-2} \cdot day^{-1} \cdot atm^{-1}$ for the PVA*.CD membrane with the RH increasing from 35 % to 70 % RH, respectively.

Mahdi Dadfar et al. also reported the improved water barrier properties of PVA crosslinked with GA during the permeation measurements at 25°C and 60 % RH [93]. It was found that the raised GA content caused the decrease of the water permeability of PVA-based membranes. This behaviour was related to the increased crosslinking degree, that led to the enhanced network density and, consequently, the hindered transport of the water molecules through the membrane was observed. The water permeability of the membranes decreased from 0.4 $g \cdot mm \cdot m^{-2} \cdot kPa^{-1} \cdot h^{-1}$ to ~0.15 $g \cdot mm \cdot m^{-2} \cdot kPa^{-1} \cdot h^{-1}$ for the pristine PVA membrane and the PVA membrane containing 4 % GA, respectively [93].

The water permeability results obtained in the present work clearly testify to the improved barrier performance of PVA membranes after the crosslinking reaction. At the same time, the obtained results seem to be higher than those presented by other researchers. This fact may be explained by the difference in the structure of a used crosslinking agent (SSA, GA, and glyoxal).

3.1.7 Conclusions

PVA-based membranes were crosslinked using a two-step approach: the esterification reaction and the subsequent heat-treatment. The membrane crosslinking was evidenced by the FTIR-ATR analysis and reflected by the decreased intensity of bands corresponding to the vibration of -OH groups and increased intensity of ester bond created between PVA and SSA. As a result of the SSA content increase, the crosslinking density raised significantly, that was confirmed by the decrease of Young's modulus, stress at break, and elongation at break parameters for all studied crosslinking temperatures. Moreover, the increase of the SSA concentration and annealing temperature increased the water contact angles by 15° and 7°, respectively, due to the decreased hydrophilic character of the PVA-SSA membrane surface. The swelling studies of PVA-SSA membranes in contact with pure water, methanol and propan-2-ol reveal that the membrane swelling diminishes with the raised SSA concentration for all studied crosslinking temperatures, whereas the highest swelling is observed for the membranes equilibrated with pure water. The elaborated membranes are characterized by a very low swelling capacity in the organic solvents in comparison with water, which indicates that PVA membranes crosslinked with SSA possess a high potential for the pervaporative separation processes with the purpose of the alcohol dehydration.

The two-step approach combining chemical crosslinking and the thermal treatment is an efficient, but relatively time-consuming method for the reinforcement of PVA-based membrane material and tailoring its physicochemical properties. Therefore, the other approach, namely, the use of ILs was also studied in this work. Besides, the influence of the IL structure on the membrane properties was investigated.

3.2 PVA-RILs Membranes

Recently, it has been shown that polymer membranes containing ILs possess wide range of advantages and better separation properties than the classical polymer membranes [179]. As the molecular diffusion is much higher in ionic liquid than in polymers, thus, the use of polymer-ILs systems in separation processes should result in much better separation and higher fluxes. Besides, the structure and physicochemical properties of ionic liquids can be modified depending on the separated system. Therefore, ILs can be used to "tailor" a suitable polymer material for a given separation process without preparation of a chemically new membrane. For this purpose, PVA-based

membranes blended with different RILs (RIL1_Br and RIL2_Br) (Figure 19 and Figure 20, respectively) in the weight fraction range from 9 to 28.6 wt.% were prepared.

3.2.1 Polymer-RIL Interactions

FTIR-ATR analysis was performed in order to study the possible interactions between the polymer and ionic liquids. The spectra of native PVA, pure ionic liquids (RIL1_Br and RIL2_Br), and PVA-RIL membranes are presented in Figure 32. The spectra were normalized with respect to the -CH_2- stretching vibration band in the PVA backbone ($\nu = 2939$ cm^{-1}) [91]. The analysis of the vibration bands of pure RIL1_Br and RIL2_Br revealed their characteristic absorption bands of the imidazolium (Im) ring stretching at 1556 and 1572 cm^{-1} and bending at 1182 and 1174 cm^{-1} (Table 9) [180].

Table 9. Band assignments of RIL1_Br and RIL2_Br vibrational modes.

Band assignments	Wavenumber [cm^{-1}]	
	RIL1_Br	RIL2_Br
Water presence in a sample	-	3425
Imidazolium (Im) C–H stretching	3070	3082
Alkyl C–H stretching	2993	2982
C=O stretching vibration (from -COO- ester group)	1759	1745
Imidazolium (Im) ring stretching	1556	1572
C–O stretching vibration (from -COO- ester group)	1221, 1263	1225
C–H scissoring deformation (CH_2 from methylene group)	1471	1470
C–H asymmetric deformation (CH_3 group)	1444	1439
H–C–C and H–C–N bending (imidazolium ring)	1182	1174
C–H in-plane deformation (imidazolium ring)	839	876
C–H out-of-plane deformation (imidazolium ring)	750	766

The FTIR spectra of PVA membranes blended with RIL1_Br and RIL2_Br indicated the alteration of some absorption bands as a result of the interactions between the membrane components. It can be noticed that the raise of RIL content leads to the intensity increase of C=O and C-O stretching vibration bands of -COO- ester groups in PVA-RIL membranes. The doping of PVA with RIL1_Br and RIL2_Br increases also the

intensity of the stretching vibration band of -OH groups attached to the main chain of PVA. This band shifts to higher frequency values (from 3313 cm^{-1} for pure PVA to 3344 and 3334 cm^{-1} for PVA-28.6-RIL1_Br and PVA-28.6-RIL2_Br, respectively).

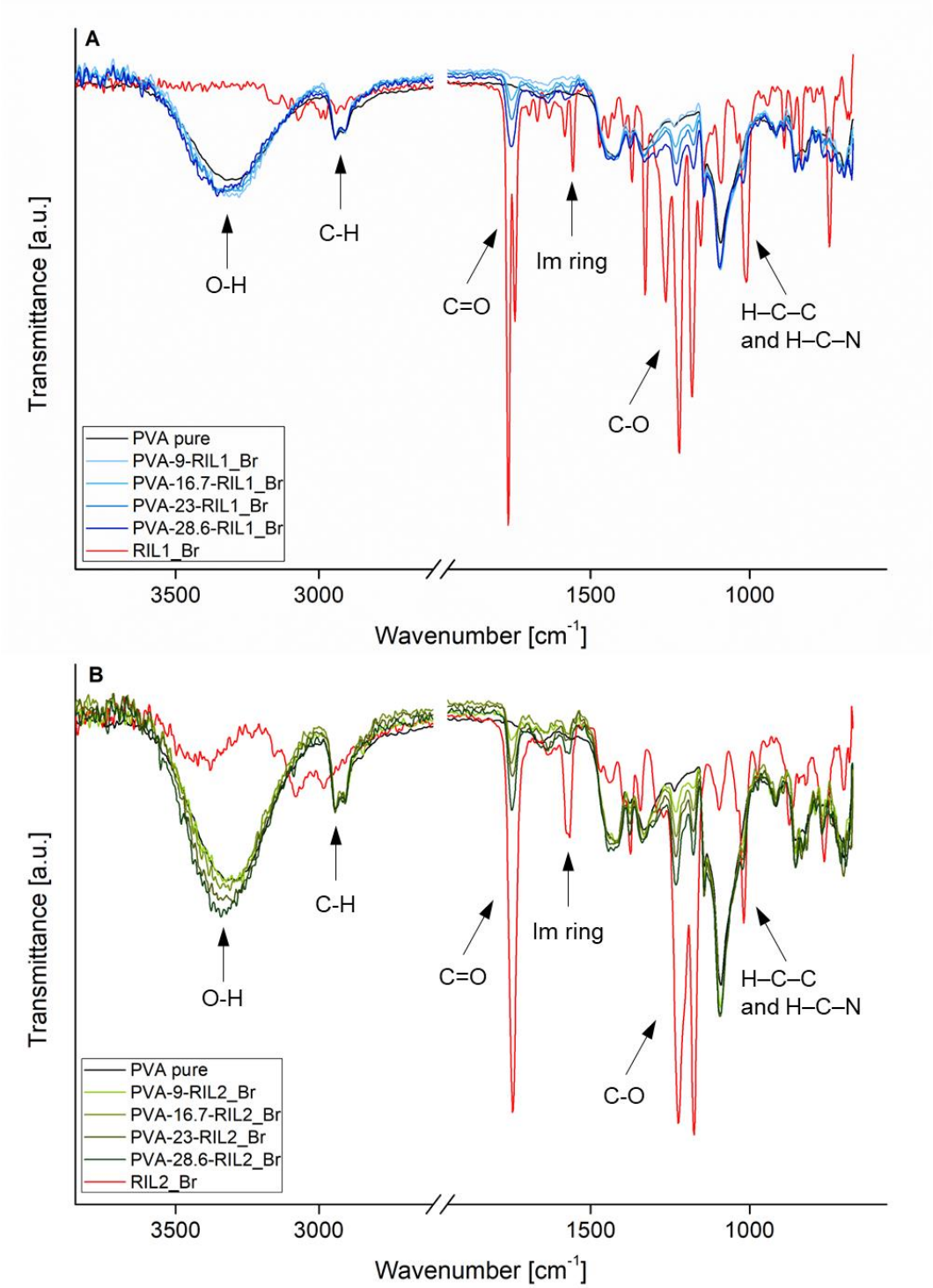

Figure 32. FTIR-ATR spectra of PVA-based membranes containing different concentrations of (A) RIL1_Br and (B) RIL2_Br.

This result can be explained by the strong interactions between imidazolium-based cations of RILs and hydroxyl groups of PVA. Thus, O-H bond in PVA becomes stronger, and its band shifts to higher frequencies [181]. Similar behavior was also found by Patachia et al. [182] as well as by Rozik and Ward [183].

Moreover, the skeletal and C–O stretching band of PVA is shifted from 825 to 835 cm^{-1} for PVA-RIL membranes. This behavior underlines the increased stiffness of the PVA chain due to the hydrogen bonding interactions between hydroxyl groups that is in accordance with the results of Patachia et al. [182]. In addition, the band related to the bending of H–C–C and H–C–N in imidazolium ring shifts from 1182 cm^{-1} (for pure RIL1_Br) and 1172 cm^{-1} (for pure RIL2_Br) to 1170 cm^{-1} (for PVA-RIL membranes) as a result of the ionic interactions between imidazolium cation and bromide anion. The proposed scheme of the interactions is presented in Figure 33.

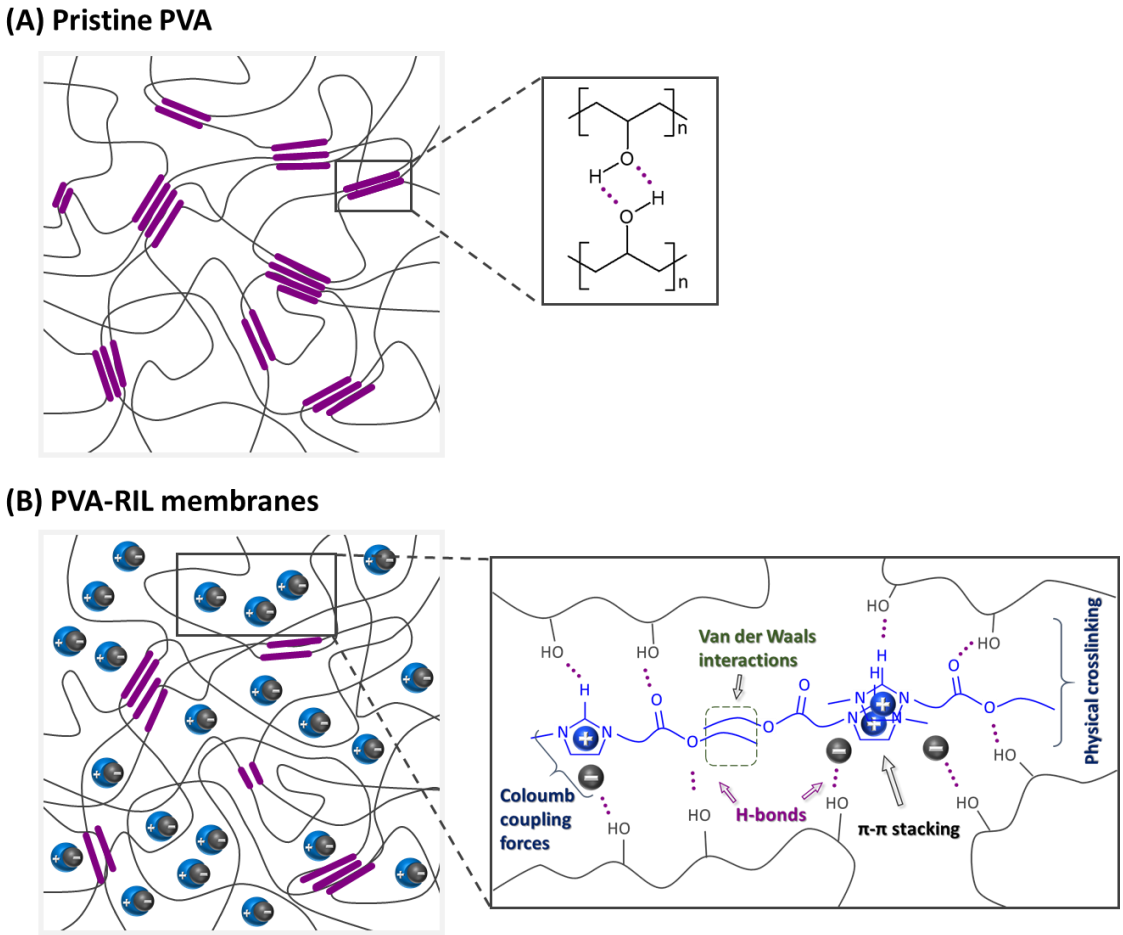

Figure 33. Scheme of the proposed interactions in (A) PVA and (B) PVA-based membranes blended with RILs (RIL1_Br and RIL2_Br).

Patachia et al. [182] studied the interactions between PVA gel and 1-butyl-3-methylimidazolium tetrafluoroborate ionic liquid [BMIM][BF4]. Researchers presented the IL concentration influence on FTIR spectra of PVA/[BMIM][BF4] gels. It was found that the spectrum of PVA/[BMIM][BF4] gels reveals the C–O stretching band shifted to 844 cm^{-1} comparing to pure PVA (830 cm^{-1}). This result was explained by the PVA stiffening due to the enhanced hydrogen bonding. Rozik and Ward [183] noted that doping of PVA by 3-N-tetradecyl-1-vinylimidazolium bromide PIL resulted in the spectral intensity increase and in the decrease of the -OH stretching band as a consequence of the interactions between the PIL cation and PVA hydroxyl groups.

The interactions between PVA and RILs result from following aspects:

- PVA chains contain numerous hydroxyl groups that enable the intramolecular interactions between PVA as well as between PVA and RILs-based on the hydrogen bonds (Figure 33) [181, 184];
- imidazolium-based cations in studied RILs (RIL1_Br and RIL2_Br) possess the amphiphilic nature that is related to the presence of the hydrophobic ethyl substituents attached to the hydrophilic ester-functionalized imidazolium ring;
- the presence of hydrophobic aliphatic substituents in RIL predicts the occurrence of the van der Waals interactions [117, 185];
- RILs possess C–H units in the imidazolium ring which can play role of donors in hydrogen bond as well as they are involved in the face to face π-π stacking interactions (Figure 33B) [185-187]. Moreover, the functionalization of the RIL structure with ester groups intensifies the hydrogen bond interactions between RIL and PVA;
- the interactions between imidazolium-based cation and bromide anion are based on the Coulomb coupling forces [185].

The non-covalent interactions in polymer-RIL composite membranes influence the compatibility between RILs and polymer matrix and the membrane performance in the separation process. Schäfer et al. [188] indicated that RTILs behave like electrolytes while being in contact with Nafion® or polydimethylsiloxane (PDMS) membranes due to the presence of the interactions between ILs and polymers. Xi et al. [189] found that the hydrogen bonding interactions between 1-ethyl-3-methylimidazolium hexafluorophosphate ([EMIM][PF6]) and waterborne polyurethane (WPU) influenced the benzene permeability. Such hydrogen bonding interactions hindered the interactions between WPU-[EMIM][PF6] composite membrane and benzene, that led to its lowered

permeability at the low IL content. On the other hand, the increased permeability was observed due to the increase of IL concentration and simultaneously to the formation of the phase separation. In this case, the IL-rich phases were created, thus facilitating the benzene permeability [189].

3.2.2 Thermal Stability

The thermal stability of the pristine PVA, pure RILs, and PVA-RIL membranes was examined using the TGA analysis and the obtained results are depicted in Figure 34. The thermal degradation of pristine PVA was described in details in section 3.1.2.

The thermal degradation profile of RIL1_Br shows four degradation steps (Figure 34A), whereas three degradation stages are visible for RIL2_Br (Figure 34B). The presence of the first peak at the onset temperature T_{onset} at ca. 54 °C for both RILs is related to the release of the moisture absorbed by pure ionic liquids [190]. In the case of RIL1_Br, the subsequent steps (at T_{onset} equal to 115, 192, and 250°C) are presented due to the decomposition of ester groups and imidazole ring [180]. The second step at 115°C can also correspond to the nucleophilic attack of ester groups in RIL1_Br that leads to the bromomethane or diethyl-2-bromomalonate formation [191]. Ohtani et al. [191] reported that the presence of bromide anion in 1-ethyl-3-methylimidazolium bromide ionic liquid results in nucleophilic attack of IL by anion that leads to the cleavage of the C-N bonds at the ethyl group. Consequently, the formation of bromomethane and ethyl imidazole or bromoethane, ethylene and HBr was observed during the IL thermal degradation studied by pyrolysis-gas chromatography [191].

TGA analysis of RIL2_Br reveals the decomposition of ester groups (T_{onset} = 196°C) and imidazole ring (T_{onset} = 274°C). The initial temperature of RIL1_Br decomposition is slightly lower comparing to 3-methyl-1-hexyloxycarbonylmethylimidazolium bromide [C_6EMeIm][Br] ionic liquid (T_{onset} = 210°C) studied by Garcia et al. [192]. The researchers found that the decrease of the alkyl group length in ester-functionalized imidazolium-based ionic liquids from 14 to 6 carbon atoms (from R=$C_{14}H_{29}$ to R=C_6H_{13}) slightly decreased the T_{onset} degradation temperature (from 228 to 210°C) [192].

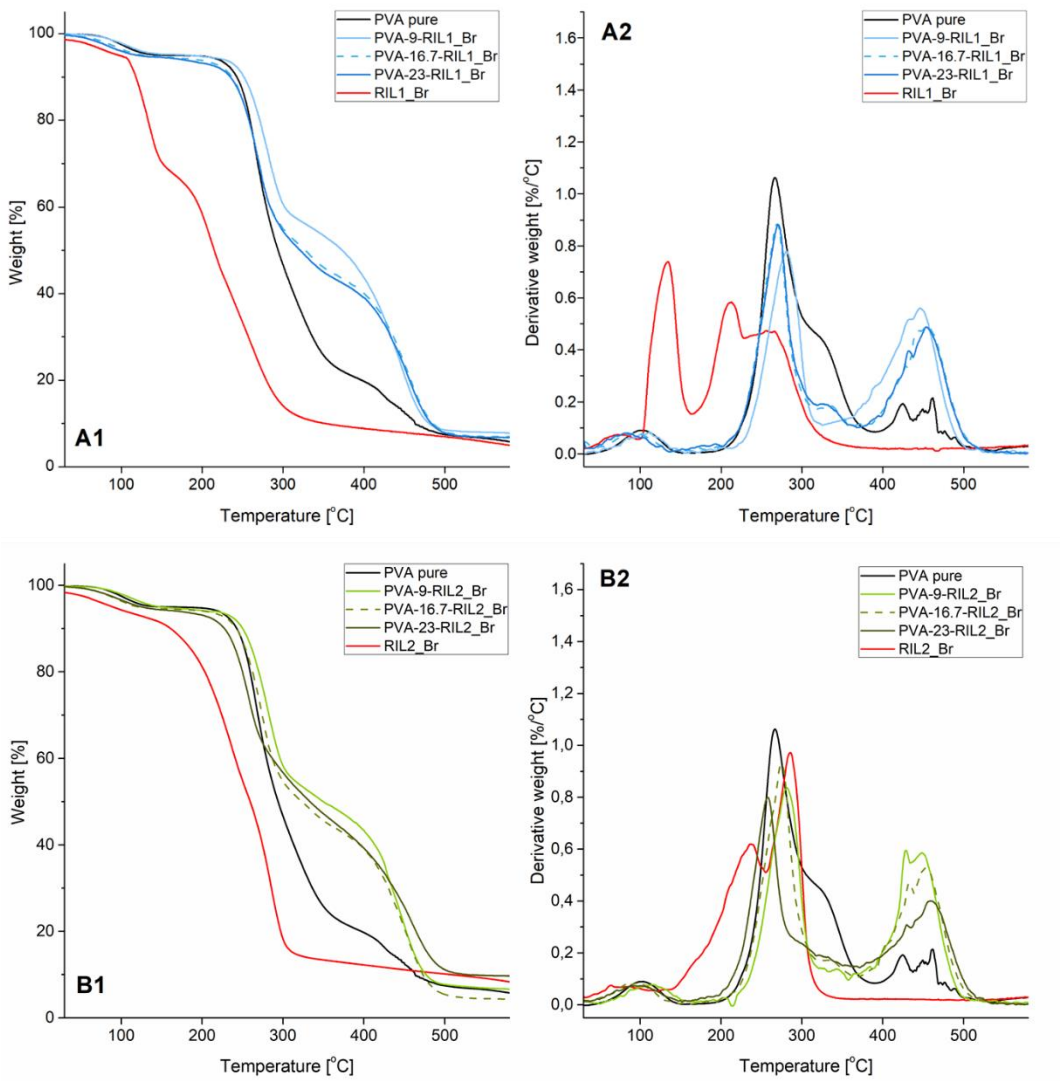

Figure 34. Thermogravimetric analysis of (A) PVA-RIL1_Br and (B) PVA-RIL2_Br membranes: (A1, B1) TG and (A2, B2) DTG curves.

Thermograms of PVA-RIL membranes reveal three main decomposition steps (Figure 34). The first peak at T_{onset} = 65°C that corresponds to ca. 5% weight loss can be attributed to the removal of the water molecules bounded to the polymer and ionic liquid structure due to the hydrophilic nature of PVA and used RILs (RIL1_Br and RIL2_Br) [183]. The weight loss in the temperature range between 200-300°C corresponds to loss of -OH and acetate groups due to the break of ester bonds of PVA and RILs. It can be seen that the peak intensity in the temperature range 200-300°C decreases and shifts to a lower temperature values for PVA-RIL membranes comparing to native PVA membrane. Such behavior confirms the presence of strong interactions between PVA and RILs. This can also indicate the plasticization effect of RIL on PVA. The weight loss in the

temperature range between 400-500°C corresponds to the degradation of the PVA main chain.

It can be seen that PVA-based membranes with 9 wt.% of RIL possess the improved thermal stability compared to pure PVA that is reflected by the raised degradation temperature at 10% weight loss up to 251 and 250°C for PVA-9-RIL1_Br and PVA-9-RIL2_Br membranes, respectively, comparing to pure PVA (243°C) (Table 10). The further increase of the RIL content shifts the degradation temperature to lower values. Besides, this shift is more pronounced in the case of PVA-RIL1_Br membranes (Table 10) that corresponds to the lower thermal stability of pure RIL1_Br compared to RIL2_Br. This result correlates with the RIL increased influence on the thermal stability of PVA-based membranes with higher RIL content. Nevertheless, all tested PVA-RIL membranes are stable up to T_{onset} equal to ca. 230°C. Such thermal stability is sufficient for their potential further application in the pervaporation process.

Table 10. Characteristic degradation temperature of studied PVA-RIL1_Br and PVA-RIL2_Br membranes.

Membrane	Degradation temperature [°C]	
	at 5% weight loss	at 10% weight loss
PVA pure	163 ± 2	243 ± 2
PVA-9-RIL1_Br	183 ± 2	251 ± 2
PVA-16.7-RIL1_Br	126 ± 2	234 ± 2
PVA-23-RIL1_Br	120 ± 2	235 ± 2
PVA-9-RIL2_Br	148 ± 2	250 ± 2
PVA-16.7-RIL2_Br	122 ± 2	242 ± 2
PVA-23-RIL2_Br	126 ± 2	228 ± 2

3.2.3 Morphology and Surface Characterization

The results of the SEM analysis for the pristine PVA and PVA-RILs membranes as a function of the RIL content are presented in Figure 35. The cross-section view of PVA-RIL1_Br and PVA-RIL2_Br membranes confirms the dense and nonporous morphology of membranes. The incorporation of RIL1_Br and RIL2_Br does not

influence the membrane homogeneity that reflects good compatibility between polymer matrix and used RIL.

The surface roughness of the pure PVA and PVA-based membranes with RIL1_Br and RIL2_Br was studied based on the AFM analysis (Figure 36) and assessed by the roughness parameters: root mean square roughness (R_q) and arithmetic average height (R_a). The calculated values of R_a and R_q parameters [193] for various scanning membrane area are gathered in Table 11. These parameters provide the quantitative information about the difference in PVA-RILs membranes morphology.

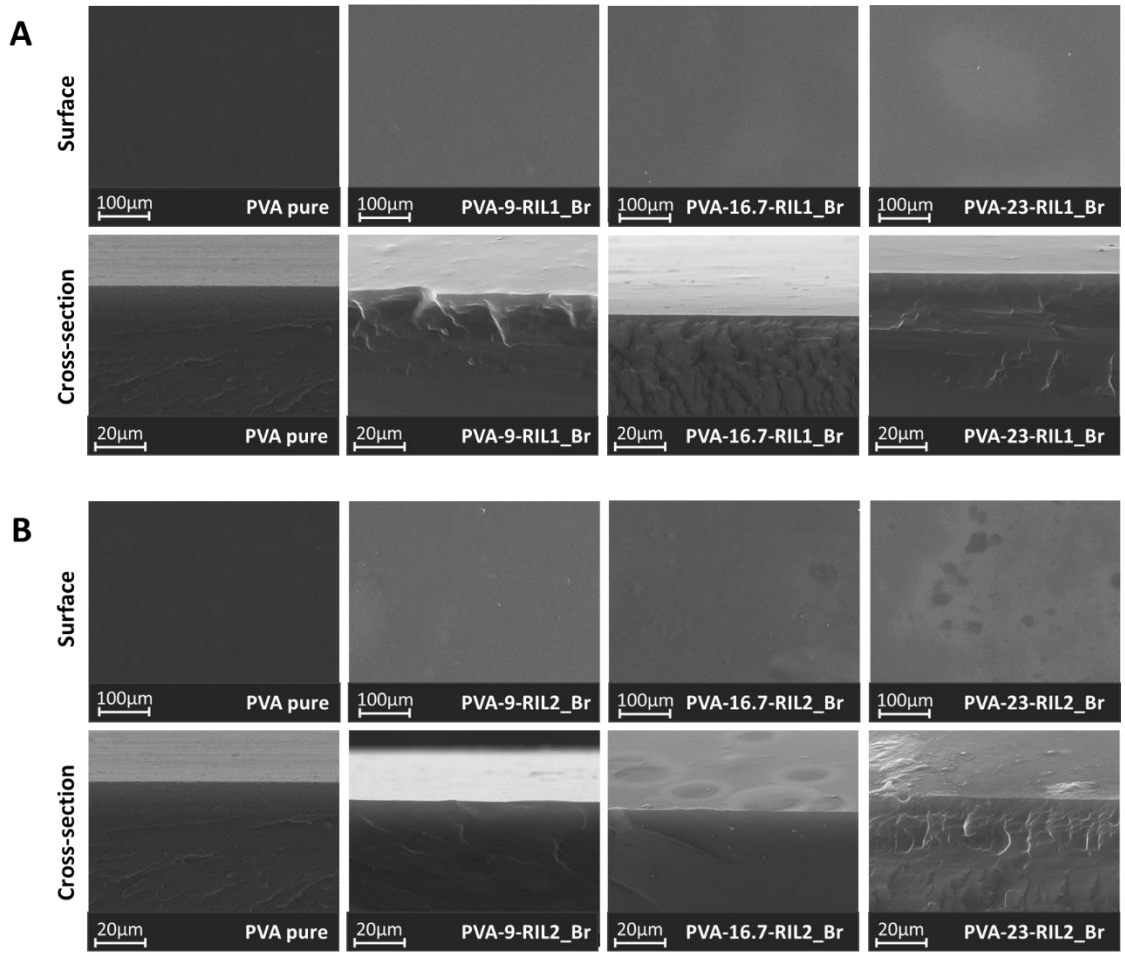

Figure 35. Surface and cross-section SEM images of (A) PVA-RIL1_Br and (B) PVA-RIL2_Br membranes.

It can be seen that PVA-based membranes blended with RILs possess higher roughness of the membrane surface comparing to the pristine PVA membrane whatever the RIL type. This result is confirmed by the increased height of RIL-rich domains and the greater R_a and R_q values (Table 11). The increase of the RIL content (from 9 to 23

wt.%) results in the smoothening of the PVA-RIL membrane surface (Figure 36) that is in accordance with decreasing R_a and R_q values (Table 11). Higher RIL content smoothes the PVA-RIL membranes surface which is in agreement with the results of Deng et al. for CA-based membranes blended with ether-functionalized pyridinium ionic liquids ($[E_nPy][NTf_2]$) [194]. Researchers found that the CA membranes with the $[EnPy][NTf_2]$ content higher than 20 wt.% possess smoother membrane surface. The decrease of the roughness of the membranes surface is correlated with the liquid nature of IL.

Table 11. Roughness parameters (R_q and R_a) of pristine PVA and PVA-based membranes with RIL1_Br and RIL2_Br.

Parameter	R_q [nm]	R_a [nm]	R_q [nm]	R_a [nm]
Scanning area	5 μm x 5 μm		10 μm x 10 μm	
PVA pure	3.2 ± 0.8	2.3 ± 0.5	9.3 ± 0.6	6.0 ± 0.1
PVA-9-RIL1_Br	14.0 ± 1.3	10.2 ± 1.1	15.1 ± 2.8	11.0 ± 1.8
PVA-16.7-RIL1_Br	7.5 ± 2.7	5.6 ± 2.6	6.0 ± 2.3	4.4 ± 1.3
PVA-23-RIL1_Br	4.4 ± 2.5	2.7 ± 1.7	4.2 ± 0.3	2.2 ± 0.2
PVA-9-RIL2_Br	7.9 ± 3.4	6.5 ± 2.8	11.5 ± 1.8	9.3 ± 1.6
PVA-16.7-RIL2_Br	6.8 ± 3.2	5.1 ± 2.4	9.3 ± 1.7	7.2 ± 0.9
PVA-23-RIL2_Br	6.3 ± 1.1	5.1 ± 0.8	6.5 ± 1.9	4.3 ± 1.0

It can be also seen that R_a and R_q values for PVA-16.7-RIL1_Br, PVA-23-RIL1_Br, and PVA-23-RIL2_Br membranes are lower comparing to the pristine PVA membrane (Table 11). This result can be related to the fact that higher IL content allows filling the voids in the polymer membrane surface, thus resulting in the wetting of the membrane surface [194].

The raised roughness of polymer membranes surface increases its active surface area that, in its turn, can enhance the membrane performance in separation processes or fuel cell applications. Hooshyari et al. pointed out that the increased surface roughness of polybenzimidazole (PBI) membranes enhanced the membrane ionic conductivity [195].

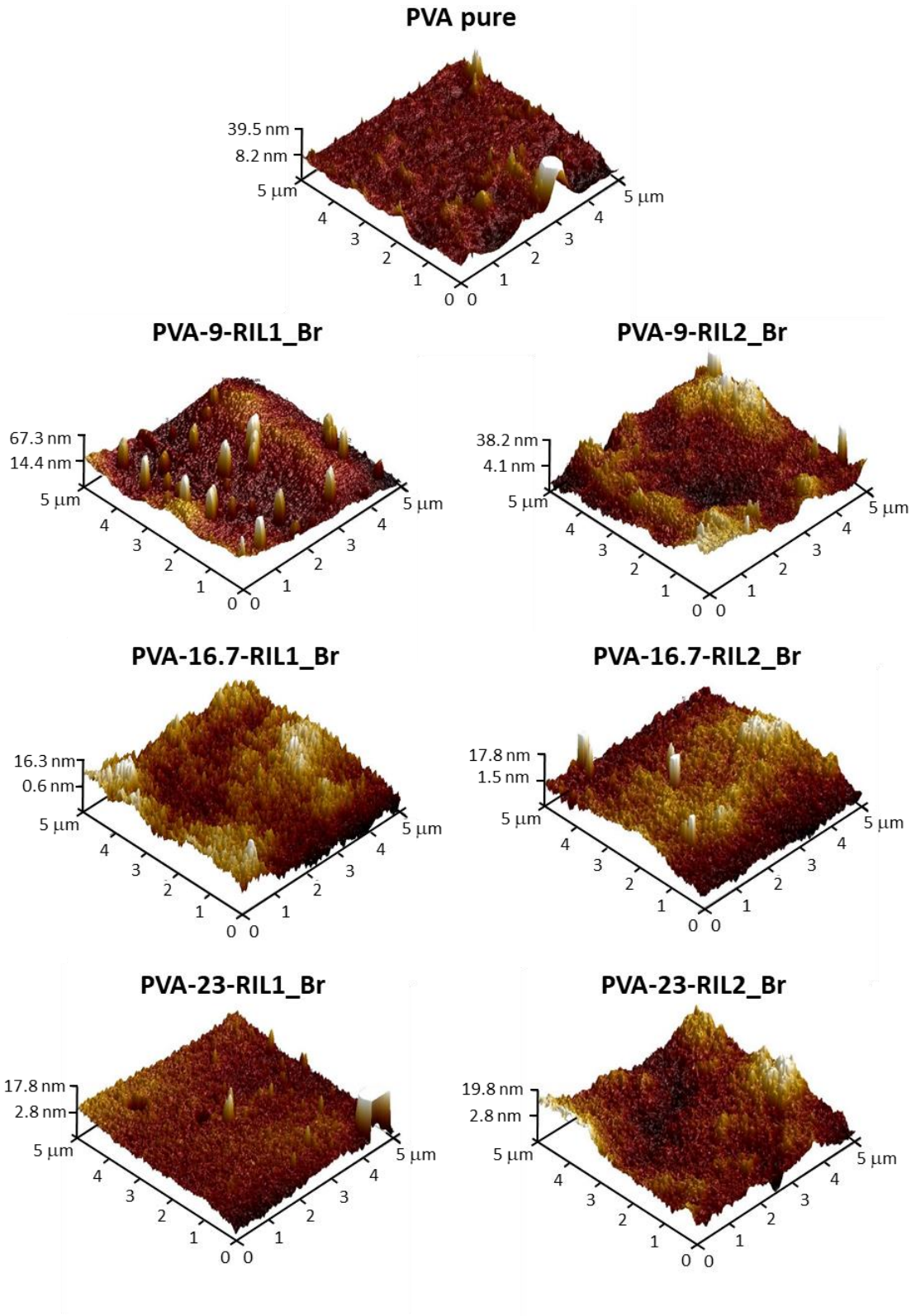

Figure 36. 3D surface profile of pristine PVA and PVA-based membranes blended with RIL1_Br and RIL2_Br at different concentrations.

3.2.4 Mechanical Properties

The mechanical strength and elasticity of pure PVA and PVA-RIL membranes (RIL1_Br and RIL2_Br) were studied by tensile test and assessed based on *E* (Figure 37A), ε_{max} (Figure 37B), and σ_{max} (Figure 37C) parameters.

In general, it is found that the type of RIL does not have a significant influence on mechanical properties of PVA-based membranes; however, the RIL content plays the key role on the membrane ductility. The addition of low RIL1_Br and RIL2_Br content (9 wt.%) into PVA-based membranes results in the simultaneous increase of Young's modulus parameter and decrease of elongation at break value comparing to pure PVA (Figure 37A). This behavior results in the enhanced membrane stiffness due to the reduced polymer chains' flexibility. The introduction of RILs into PVA matrix interrupts the PVA chains mobility and interactions between PVA chains by creating the intramolecular interactions between RIL and PVA (Figure 33B). The addition of the low RIL content increases the hydrogen bonding between RIL imidazolium cations and PVA hydroxyl groups as it is shown in FTIR spectra (Figure 32). The enhanced hydrogen bonding acts as a physical crosslinking between PVA and RILs (Figure 33B), thus PVA-RIL membranes become more rigid.

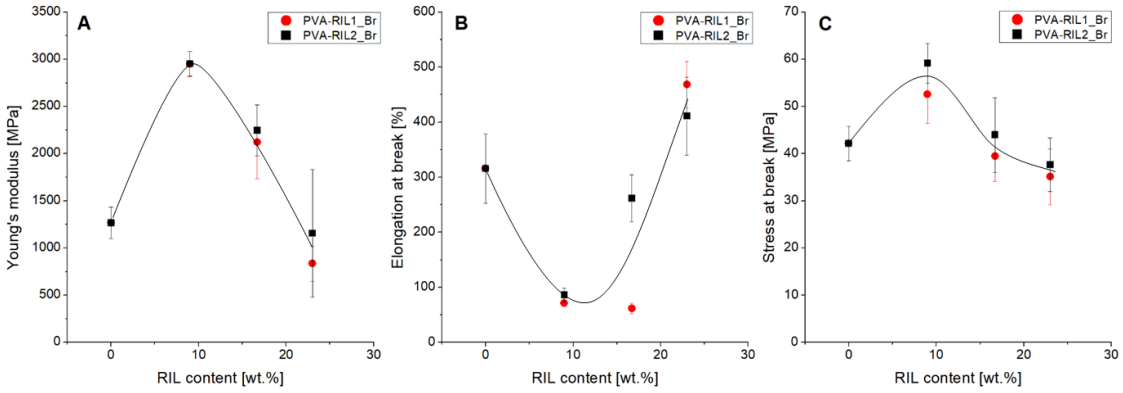

Figure 37. Young's modulus (A), elongatıon at break (B), and stress at break (C) of PVA-RIL1_Br and PVA-RIL2_Br membranes. The solid lines are only to guide an eye.

The further increase of the RIL1_Br and RIL2_Br content leads to the decrease of the *E* value and to the increase of the ε_{max} value (Figure 37A and Figure 37B, respectively). The higher content of RIL (16.7 and 23 wt.%) promotes the interactions between RIL molecules, that can result in the formation of RIL-rich domains. As a result, the enhanced flexibility and reduced stiffness of PVA-23-RIL1_Br and PVA-23-RIL2_Br

membranes was observed. It can be pointed out that the presence of the high RIL content (23 wt.%) in the PVA membrane has the predominant influence on the membrane softness and elasticity. Simultaneously, the addition of 16.7 and 23 wt.% of RIL1_Br or RIL2_Br does not have a significant influence on the stress at break parameter (Figure 37C).

Based on the mechanical properties of PVA-RILs membranes it can be noted that RILs can exhibit the dual function: as a physical junction promoter and as a plasticizer:

- the initial increase of the PVA-RILs membrane stiffness reflected by the increase of *E* and σ_{max} and the decrease of ε_{max} values compared to pristine PVA and combined with the observed shifts of the vibrational bands of PVA (Figure 32) indicates the influence of the RIL doping on the PVA chains mobility. This behavior corresponds to the enhanced hydrogen bond interactions between PVA hydroxyl groups and RIL cations that promotes the physical crosslinking between PVA and RIL;
- the reversed mechanical properties at the high RIL content corresponding to the decrease of *E* and σ_{max} and to the increase of ε_{max} indicate the influence of RILs on PVA-RILs membranes elasticity. Simultaneously, the good compatibility between PVA and RIL evidenced by SEM (Figure 35) and AFM (Figure 36) analysis is found confirming that RIL acts as a plasticizer.

The obtained results for PVA-RILs membranes are in accordance with findings of Yoon et al. studying properties of thermoplastic elastomer composed of PVA and 1-ethylpyridinium bromide ionic liquid [181]. Researchers found that blending of PVA with pyridinium-based ionic liquid shifted the -OH stretching vibration band to higher frequency values as a function of the IL content, thus confirming the presence of interactions between PVA and IL. Additionally, the use of 1-ethylpyridinium bromide ionic liquid resulted in the decrease of *E* from around 4000 MPa for pristine PVA membrane to around 300 MPa for the PVA membrane containing 70% of pyridinium-based IL [181].

3.2.6 Conclusions

PVA membranes were blended with compatible ester-functionalized imidazolium-based ionic liquids containing bromide anion. The results of FTIR analysis evidenced the presence of the physical PVA-RILs junctions induced by the hydrogen bond interactions between PVA and RILs (RIL1_Br and RIL2_Br) which partially replaced the intermolecular interactions of PVA chains. As a result of the RIL content

increase, the altered mechanical properties of PVA-RILs membranes were found. In the presence of RIL with low content stiffened PVA-RILs membranes were obtained, whereas PVA-RILs membranes with high RIL content (23 wt.%) exhibited increased elastic properties. It was found that PVA-9-RIL membranes possessed the improved thermal stability among all tested membranes. The observed dual functions of RIL (as a promoter of physical crosslinking and plasticizer) depending on the RIL content provide the possibility for obtaining of PVA-RIL materials with tailored mechanical and thermal properties.

CHAPTER 4

Elaboration and Characterization of CAP-based Membranes

Chapter 4 is divided into two parts. The first part is devoted to the plasticized CAP-based membranes elaborated with commercial plasticizers (TBC and ATBC). In the second part, CAP-based membranes modified with imidazolium-based reactive and polymerizable ionic liquids are characterized. The studied membranes were prepared by applying a phase inversion method – the solvent evaporation technique.

The interest of study presented in this chapter is focused on the evaluation of the effect of the plasticizer on the mechanical properties of the CAP-based membranes in order to select the membranes with the reinforced mechanical properties. Furthermore, the CAP-based membranes were investigated taking into account the IL incorporation influence on the physicochemical, separation, and transport properties of the elaborated membranes.

4.1 CAP-Based Membranes with Plasticizers

The phthalate plasticizers are widely used for cellulose ester-based plastics, however, their toxicity and poor compatibility causing the plasticizer migration arouse serious environmental and health concerns in terms of long-term use [55]. Citrate esters plasticizers, such as tributyl citrate (TBC) and acetyl tributyl citrate (ATBC), are derived from natural citric acid and, thus, they constitute the non-toxic alternatives for the phthalate esters [196]. TBC and ATBC possess a good compatibility with cellulose ester polymers due to the interactions between ester groups of plasticizers and polymer [197]. Therefore, CAP-TBC and CAP-ATBC films were prepared using TBC and ATBC (in the concentration range from 9 to 50 wt.% of the plasticizer).

4.1.1 Polymer-Plasticizer Interactions

The FTIR spectra of native CAP, pure plasticizers (TBC and ATBC), and plasticized CAP membranes are presented in Figure 38. The assignments of characteristic bands in pristine CAP and plasticizers are gathered in Table 12. The analysis of the pure CAP vibration bands revealed hydroxyl -OH vibrational stretching band at 3500 cm^{-1}, carbonyl C=O stretching vibration bands of -COO- ester group at 1741 cm^{-1}, whereas two peaks at 1165 and 1070 cm^{-1} were ascribed to C–O stretching vibration bands of -COO- ester group and pyranose ring COC stretching band [61, 69, 198].

Table 12. Assignments of vibrational modes for CAP and plasticizers (TBC and ATBC) [61, 69, 199].

Band assignments	Wavenumber [cm^{-1}]		
	CAP	TBC	ATBC
O–H stretching	3500	-	-
C–H stretching (CH_3)	2945	2933	2937
C–H stretching (CH_2)	2889	2875	2873
C=O stretching vibration (ester group)	1741	1738	1741
CH_2 bending	1462	1464	1463
C–H bending	1350	1344	1348
CO symmetric stretching (ester group), asymmetric bridge COC stretching (pyranose ring in CAP)	1165	1184	1180
CO symmetric stretching (ester group), COC stretching (pyranose ring in CAP)	1070	1062	1064

The FTIR spectra of TBC and ATBC possess the characteristic peaks corresponding to the C–H stretching and bending vibration bands (CH_3, CH_2), as well as carbonyl C=O and C–O stretching vibration bands of -COO- ester group (Table 12). The obtained results are in accordance with the findings of Wang et al. [199]. The FTIR-ATR spectra of CAP-based films blended with TBC and ATBC plasticizers possess minor changes comparing to pure CAP (Figure 38). The shift of the C–O vibrating band from 1163 cm^{-1} for pure CAP to 1172 cm^{-1} and 1169 cm^{-1} for CAP-23-ATBC and CAP-23-TBC, respectively, is observed. The change in the spectra of plasticized CAP-based

membranes can be influenced by the attractive interactions between dipoles in ester groups of CAP and plasticizers, namely between the oxygen in the carbonyl group and the polarized hydrogen in aliphatic substituents [200].

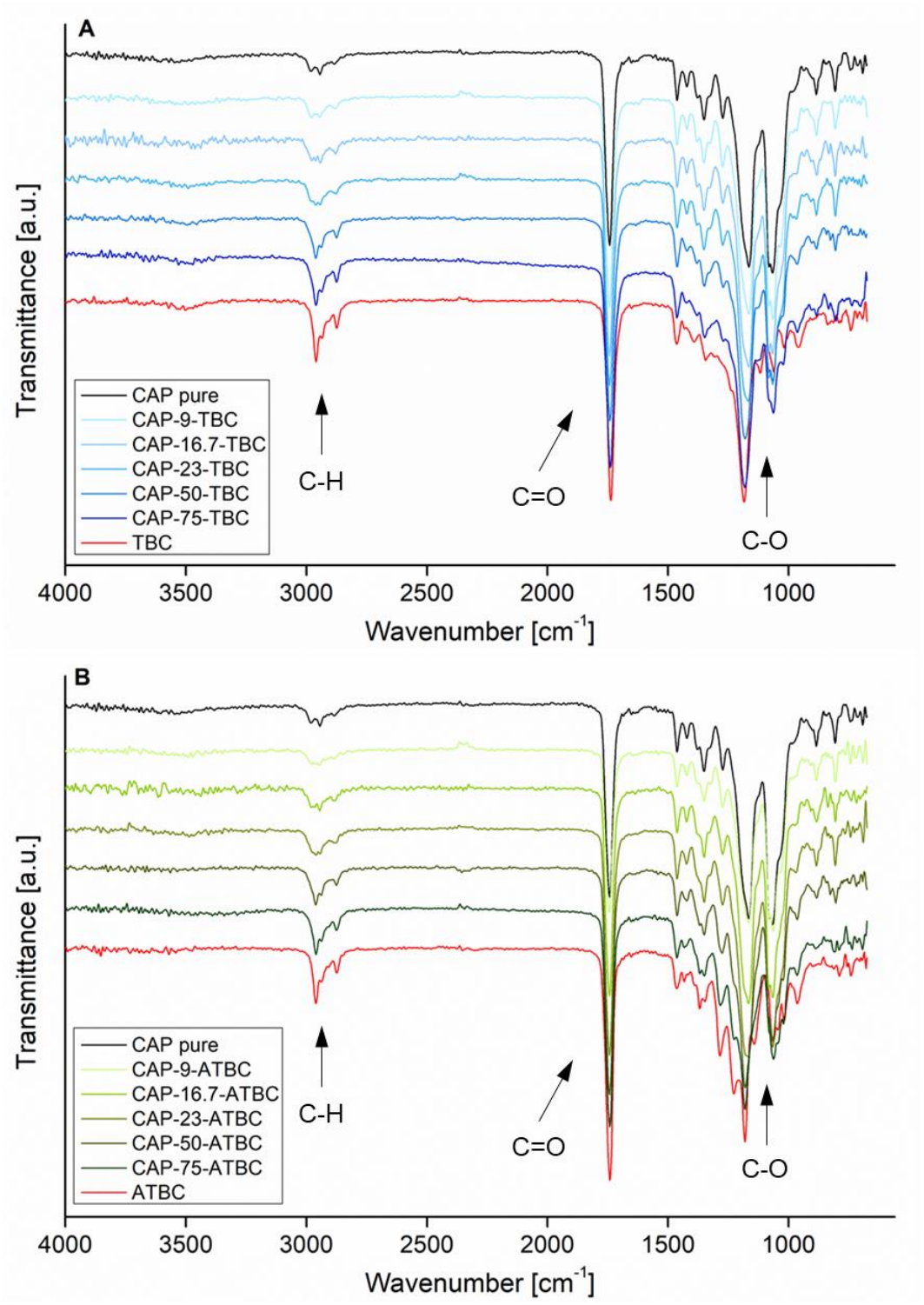

Figure 38. FTIR-ATR spectra of CAP-based films containing (A) TBC and (B) ATBC.

4.1.2 Mechanical Properties

The good elasticity and mechanical strength are important properties of polymer membranes used in separation processes. The efficiency of the plasticization is studied by the tensile tests of the pure and plasticized CAP membranes and assessed based on Young's modulus (E), elongation at break (ε_{max}), and stress at break (σ_{max}) parameters. In general, the decreasing Young's modulus value reflects the diminishing of polymer rigidity and increasing polymer soft character [66, 80]. On the other hand, the increasing elongation at break values correlate with the enhanced plastic deformation of the polymer material.

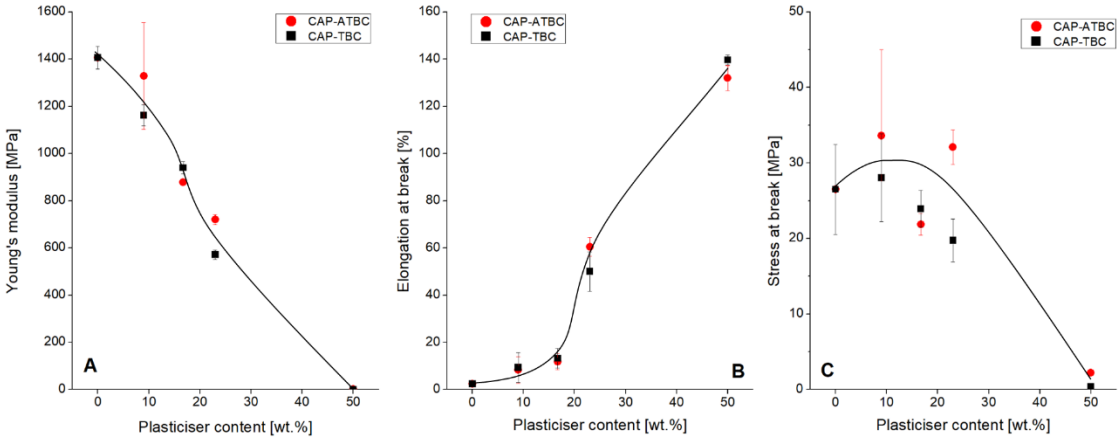

Figure 39. Young's modulus (A), stress at break (B), and elongation at break (C) of the CAP-based membranes modified with TBC and ATBC.

The pristine CAP film is brittle which is reflected by the Young's modulus, stress at break, and elongation at break values equal to E = 1406 ± 48 MPa, σ_{max} = 26 ± 6 MPa, and ε_{max} = 2.4 ± 0.4 %, respectively (Figure 39). The pristine CAP film studied in this research is less brittle than CAP film studied by Bastos et al. [66]. The researchers reported higher values of E and σ_{max} (E = 2624 ± 169 MPa and σ_{max} = 34 ± 2 MPa), whereas the ε_{max} value was lower (ε_{max} = 1 ± 0 %) [66]. The difference in the mechanical properties of pristine CAP membrane used in this work (MW = 75,000) and CAP membrane studied by Bastos et al. (MW = 25,000) may result from the various molecular weight of polymers. In general, a higher molecular weight enhances the chain entanglement that increases the tensile strength and elastic modulus due to the fact that more energy is required to break the entangled chains. It is found that membrane based on CAP with higher MW possesses higher tensile strength (49 MPa compared to 34 MPa

for membrane with lower MW) and higher elongation at break (53 % compared to 1 % for membrane with lower MW). However, contrary to what could be expected, the elastic modulus of CAP membrane (MW = 75,000) is lower compared to the CAP membrane (MW = 25,000) prepared by Bastos et al [66]. This result may be explained by the fact that in addition to polymer molecular weight, the polymer structure (liner or branched) as well as the molecular chain organization should be also taken into account.

An addition of TBC or ATBC plasticizers to CAP reveals the high dependence of film mechanical properties on the plasticizer content. The increasing content of TBC and ATBC results in the decrease of Young's modulus (Figure 39A) and in the increase of the elongation at break (Figure 39B) values compared to pure CAP, confirming that CAP-based membranes are plasticized [80]. In the case of CAP-TBC membranes, the decrease of stress at break values as a function of TBC content can be seen (Figure 39C). This behavior corresponds to the reduced rigidity of CAP-based membranes with simultaneous improvement of their elongation. It can be noticed, however, that CAP films modified with the highest content of TBC and ATBC (~50 wt.%) possess deteriorated mechanical properties compared to other CAP-based membranes, due to the enhanced inner stress in the membrane. This fact was reflected by the very low values of E and σ_{max}, namely the increased content of the incorporated TBC and ATBC of up to 50 wt.% resulted in the drop of E to 1.6 ± 0.2 MPa and σ_{max} to 2.2 ± 0.1 MPa (Figure 39). CAP-based membranes with TBC and ATBC have the extended elongation at break that is in the accordance with studies of cellulose acetate butyrate (CAB) membranes containing TBC as plasticizer performed by Wojciechowska [80]. It is found that the increase of TBC content from 25 to 35 wt.% causes a raise of the elongation at break value from 24.3 ± 2.3% to 38.1 ± 4.4% [80].

The plasticization effect of TBC and ATBC on CAP-based membranes is also in accordance with the findings of Bastos et al. [66] and White et al. [201], who studied the mechanical properties of CAP-based membranes plasticized with essential oils [66] or aliphatic polyesters [201]. Bastos et al. [66] reported the plasticization of cellulose esters due to the incorporation of essential oils such as lemongrass, basil, and rosemary pepper. It was found that the addition of essential oils decreases the Young's modulus for CA-, CAP-, and CAB-based membranes, what is characteristic for the plasticized membrane materials. In the case of CAP, the highest decrease of Young's modulus to 1603 ± 35 MPa compared to pure CAP (2624 ± 169 MPa) was observed for CAP-based membranes containing 20 % (v/w) of basil oil [66]. White et al. [201] compared the influence of

aliphatic polyesters (poly(tetramethylene succinate) (PTS), poly(tetramethylene glutarate) (PTG)) and dioctyl adipate (DOA) on the mechanical properties of CAP-based blends. It was reported that the increase of the elongation at break was correlated with the increased content of PTS, PTG, and DOA used as plasticizers. For example, the value of the elongation at break parameter raised from 11% for pure CAP up to 27% for CAP blend containing 12 wt. % of DOA.

The plasticization effect of TBC and ATBC was also studied for other polymer-based films. Harte et al. [202] found that the poly(D,L-lactide) (PDLLA) plasticized with TBC and ATBC (in the concentration range of plasticizer from 10 to 30 wt.%) possessed the increased ε_{max} and decreased E values.

4.1.3 Thermal Stability

Thermogravimetric analysis was used to investigate thermal properties of pure CAP, CAP-TBC, and CAP-ATBC membranes. TG and DTG curves shown in Figure 40 reveal a single degradation for pure CAP membrane (at T_{onset} = 348°C) that corresponds to the simultaneous degradation of acetate and propionate functional groups as well as pyrolysis of cellulose rings [66]. The thermal degradation of pure plasticizers (TBC and ATBC) also takes place in a single degradation step at T_{onset} = 181°C.

In the case of CAP membranes with plasticizers, the degradation is observed at T_{onset} = 165°C whatever the plasticizer (Figure 40). This result corresponds to the plasticizers' evaporation as the boiling point is equal to ca. 170°C [197]. The further thermal degradation of CAP-based membranes observed at T_{onset} equal to around 290 and 353°C is due to the break of ester bonds and pyrolysis of the main polymer chain, respectively. The thermal degradation of CAP membranes with TBC and ATBC plasticizers is concentration-dependent (Figure 40 and Table 13). The obtained results are in accordance with the findings of Maiza et al. [197] who studied the influence of ATBC and triethyl citrate (TEC) incorporation on the thermal stability of polylactic acid (PLA). It was pointed out that the PLA materials plasticized with ATBC and TEC possessed diminished thermal stability comparing to pristine PLA. The incorporation of ATBC and TEC results in the shift of the initial degradation temperature to lower values as a function of plasticizer content. For example, the increase of ATBC content from 10 to 30% results in the drop of the onset degradation temperature from 214 to 146°C [197].

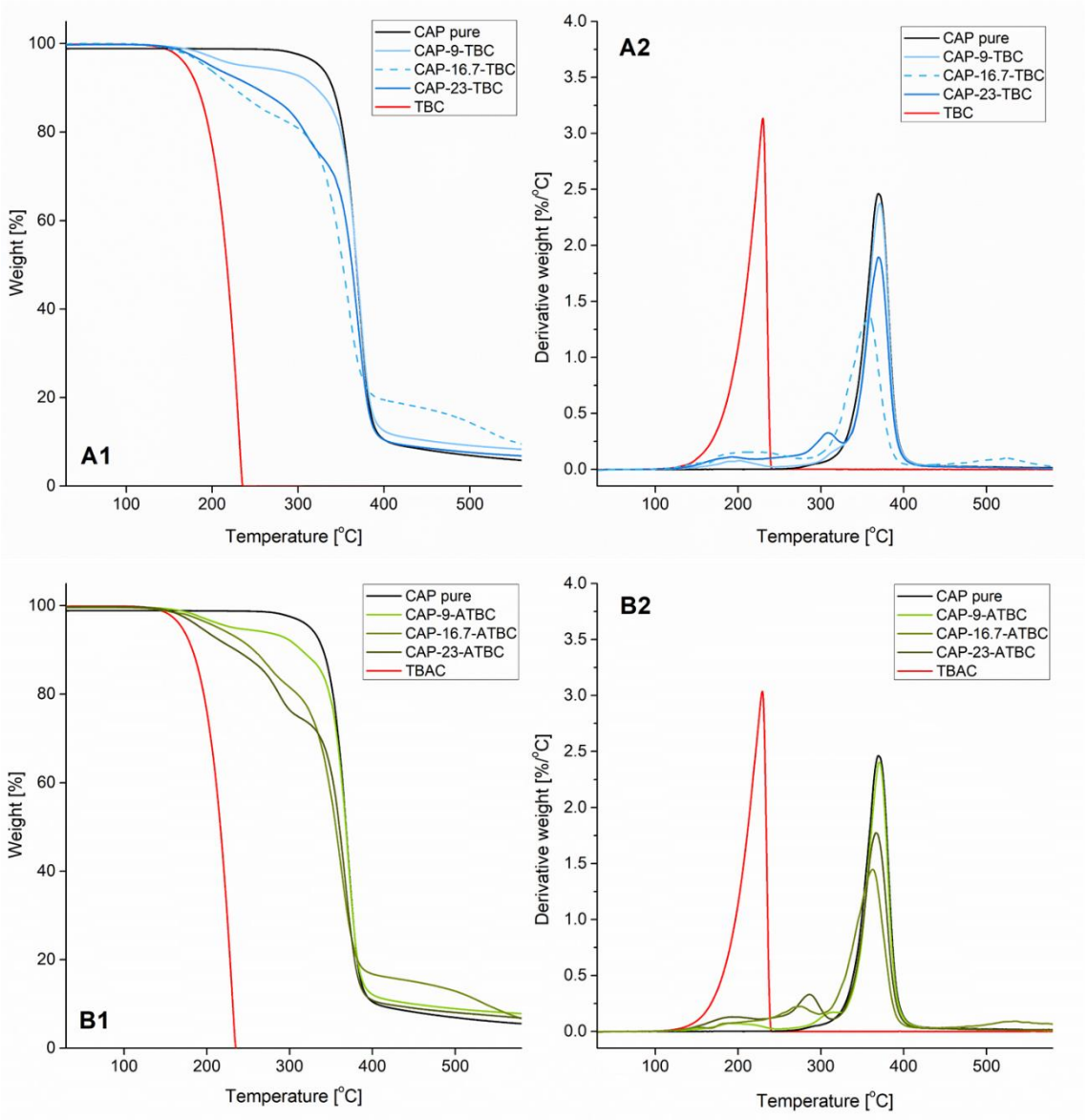

Figure 40. Thermogravimetric analysis of (A) CAP-TBC and (B) CAP-ATBC membranes: (A1, B1) TG and (A2, B2) DTG curves.

The dependence of plasticizer concentration on the thermal stability of CAP membranes with TBC and ATBC was evidenced (Table 13). It can be seen that the incorporation of plasticizer into CAP-based membranes decreases the decomposition temperature of CAP-TBC and CAP-ATBC comparing to pure CAP. Moreover, it was found that the degradation temperature at 5 and 10% weight loss is shifted to lower values due to the increase of the TBC and ATBC content. For example, the raise of TBC content from 9 to 23 wt.% results in the decreased initial degradation temperature from 238 to 192°C, respectively. These findings are in accordance with the results obtained by Maiza et al. for PLA membranes plasticized with TEC, TBC, and ATBC [197]. The addition of

citrate esters decreased the degradation temperature of PLA. For example, the thermal degradation at 5% weight loss of PLA with 20wt.% of ATBC decreased to 254°C comparing to neat PLA (249°C) [197].

Table 13. Characteristic degradation temperature of studied CAP, CAP-TBC, and CAP-ATBC membranes.

Membrane	Degradation temperature [°C]	
	at 5% weight loss	at 10% weight loss
CAP pure	325 ± 2	340 ± 2
CAP-9-TBC	238 ± 2	321 ± 2
CAP-16.7-TBC	199 ± 2	250 ± 2
CAP-23-TBC	192 ± 2	225 ± 2
CAP-9-ATBC	233 ± 2	314 ± 2
CAP-16.7-ATBC	214 ± 2	256 ± 2
CAP-23-ATBC	193 ± 2	235 ± 2

4.1.4 Morphology Characterization

The morphology of the pure CAP and plasticized CAP films containing TBC and ATBC was examined by the SEM analysis. The SEM images of the cross-section view of the pristine CAP and CAP-based membranes containing 23 wt.% of TBC and ATBC are presented in Figure 41. The cross-section view of the CAP-based membranes confirmed their dense structure. The cross-section of the native CAP membrane is uniform. The addition of 23 wt.% TBC and ATBC into the CAP membrane matrix did not change the membrane homogeneity that confirmed the good compatibility between the polymer and the used plasticizers.

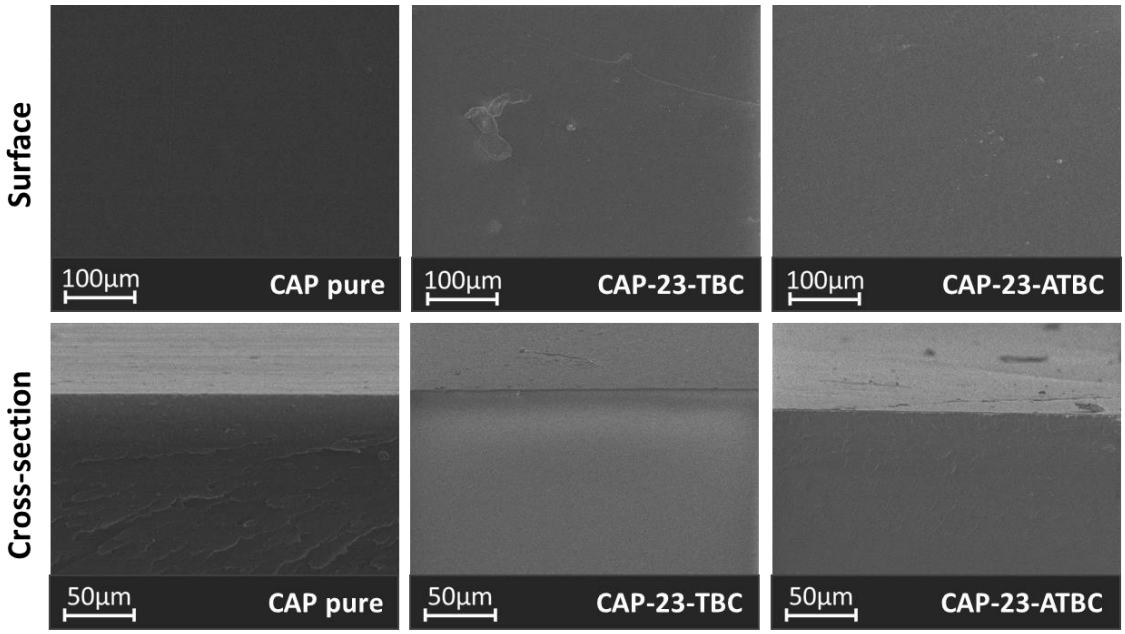

Figure 41. SEM images of surface and cross-section of pristine CAP and CAP-based membranes with 23 wt.% of TBC and ATBC.

4.1.5 Equilibrium Properties

The contact angle measurements were performed for CAP-based membranes using water, glycerol, and diiodomethane. The obtained results confirmed the hydrophilic character of pure CAP membrane as the obtained water contact angle was equal to 84° (Figure 42). The addition of TBC and ATBC resulted in the decrease of the water contact angle to 70° compared to the native CAP. Such behavior is related to the enhanced hydrophilic nature of the CAP-TBC and CAP-ATBC membrane surface due to the higher amount of hydrophilic hydroxyl groups in the prepared films after the addition of plasticizer. Simultaneously, it was observed that the addition of 9 and 16.7 wt.% of TBA or ATBC plasticizer led to the increase of polar part comparing to values for the native CAP (Figure 42) whatever the used plasticizer. Such an effect confirms additionally the plasticizer influence on the membrane surface hydrophilicity.

The swelling ability of pure CAP membrane and CAP-based membranes with TBC and ATBC in water, ethanol, and propan-2-ol, expressed as molar swelling degree SD_M value (Eq. (53)), is presented in Figure 43. It can be found that the lowest SD_M value is found in the case of CAP membrane equilibrated with water, which is in accordance with the significantly higher distance parameter $\Delta_{i,j}$ between CAP and water as compared to ethanol and IPA. On the other hand, it can be seen that SD_M of pure CAP membrane

equilibrated with IPA is the highest one, despite the higher affinity between CAP and IPA reflected by the lowest distance parameter. This difference can be related to the lower molar volume of ethanol and, thus, to the better accessibility to the CAP functional groups for ethanol molecules. In general, CAP possesses higher affinity to organic solvents compared to water due to the hydrophobic character of the polymer associated with low dielectric constant of CAP varying in the range of 3.4-3.7 [203].

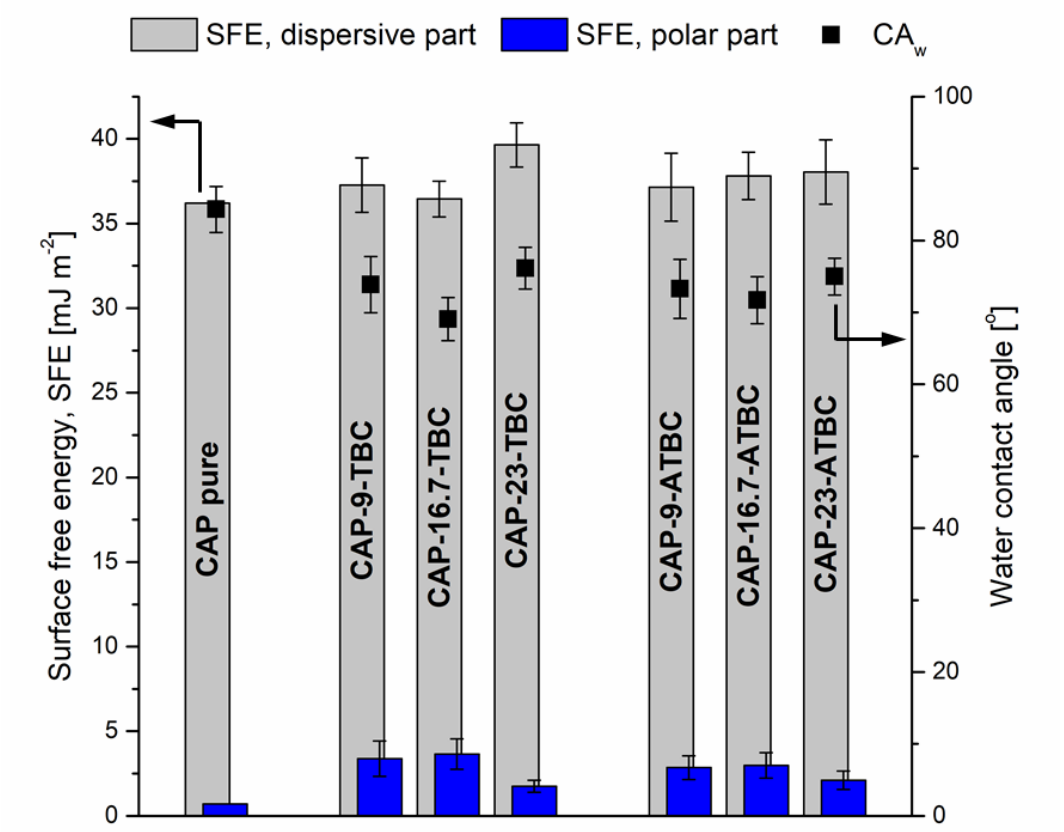

Figure 42. Water contact angle, dispersive γ^D and polar γ^P components, and surface free energy (SFE) of CAP-TBC and CAP-ATBC membranes.

The addition of citric esters as plasticizers did not affect the swelling ability of CAP-9-TBC and CAP-9-ATBC membranes in water, despite of the improved surface hydrophilicity comparing to the pristine CAP membrane. The further increase of the plasticizer content resulted in the diminished swelling of plasticized CAP-based membranes. The addition of plasticizers enhances the interactions between the hydrophilic ester groups of CAP and plasticizers reducing the interactions between water molecules and the hydrophilic ester groups in CAP. The similar results were also reported by Kalachandra and Turner [204] for poly(methyl methacrylate) (PMMA) films

placticized with DOP and diethyl phthalate (DEP) as well as by Sanyang et al. [205] for sugar palm starch-based films plasticized with glycerol and sorbitol.

Considering the swelling ability of the CAP-TBC and CAP-ATBC membranes in solvents of lower polarity, it was noticed that plasticized CAP-based membranes possess the decreased swelling in the contact with ethanol and propan-2-ol compared to native CAP. Simultaneously, it can be seen that the swelling of all tested membranes is higher in ethanol and propan-2-ol. It is related to the presence of the long hydrophobic substituents in the structure of TBC and ATBC (Figure 18) that can be solvated by the ethanol and propan-2-ol. As a result, the swelling ability of CAP-based membranes is enhanced in contact with organic solvents.

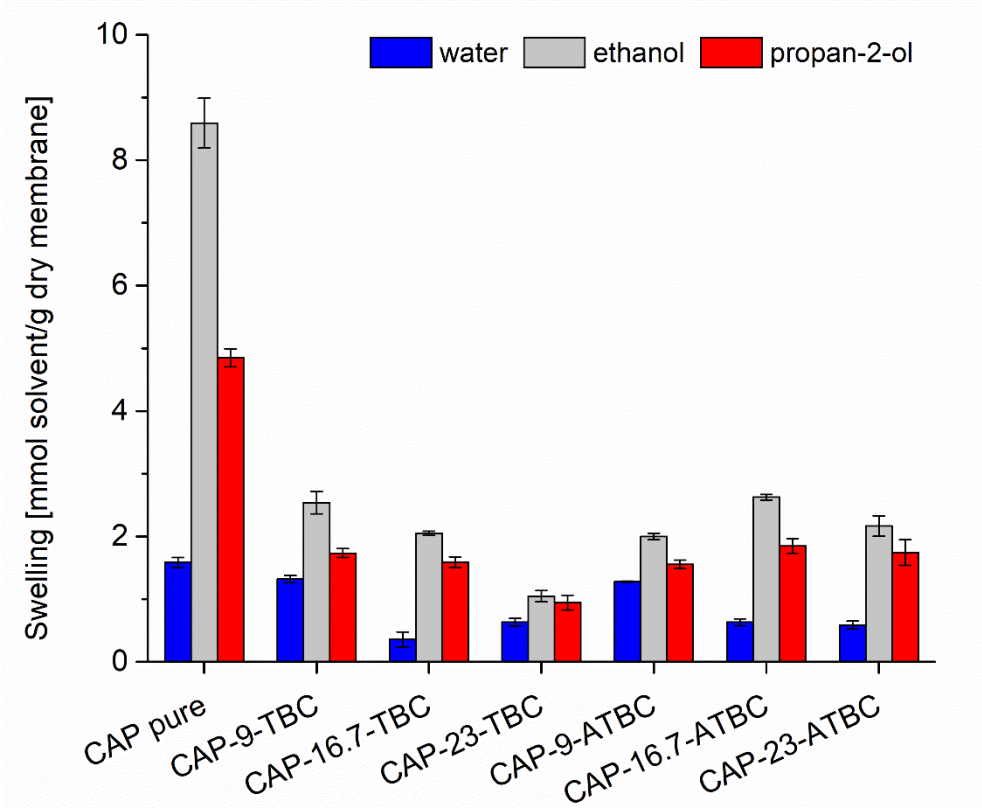

Figure 43. The molar swelling degree SD_M of CAP, CAP-TBC, and CAP-ATBC membranes.

4.1.6 Conclusions

The CAP-based membranes were plasticized using citrate esters as reflected by the increase of the elastic properties of tested films. The decrease of Young's modulus and stress at break, and increase of the elongation at break parameters was observed for

these membranes. TBC and ATBC plasticizers possessed the influence on the CAP-based membranes' surface hydrophilicity. The addition of plasticizers decreased the water contact angle of the plasticized CAP-based films compared to the native CAP membrane.

The use of commercial plasticizers is an efficient method for the plasticization of CAP-based membrane material. However, the addition of TBC and ATBC does not influence the CAP-based membranes swelling in water that restricts their further application in hydrophilic pervaporation. Moreover, it is known that citrate esters can migrate and they can be released from the polymer-based materials [55]. Therefore, the other approach, namely, the use of ILs was also studied in this work. The mixing of polymer with ILs is a facile and efficient method for the alteration of the polymer membrane properties.

4.2 CAP-ILs Membranes

The use of ILs alters the physicochemical properties of polymer based materials as well as improves the membrane separation efficiency due to wide variety of ILs properties. ILs can be also the alternative for the commonly used plasticizers [80, 206, 207]. Therefore, ILs were also used to "tailor" properties of CAP-based membrane materials. For this purpose, CAP-based membranes blended with different RILs (RIL1_Br, RIL2_Br, and RIL3_BF4) (Figure 19 and Figure 20) and PIL monomer (Figure 21) were prepared.

4.2.1 Effectiveness of Modification

The effect of CAP mixed with various amounts of ILs and possible interactions between CAP and ILs were studied by FTIR-ATR analysis. The spectra of native CAP and pure RIL1_Br and RIL2_Br ionic liquids were described in the section 4.1 and 3.2.1, respectively. The bands assignments of pure RIL3_BF4 and PIL are gathered in Table 14. The vibration bands analysis of pure RIL3_BF4 revealed the characteristic absorption bands of the imidazolium (Im) ring stretching at 3087 and 1556 cm^{-1} and bending at 1174 cm^{-1} (Table 14) [180]. Since the studied RILs contain the similar functional groups, the FTIR-ATR spectra of CAP-RIL membranes are very close. The spectra of CAP-RIL membranes possess characteristic vibrational bands of carbonyl (C=O) and C–O groups (Figure 44). The intensive band at 1741 cm^{-1} corresponds to the symmetric stretching vibration bands of the C=O groups. Two symmetric stretching vibration bands of C–O

groups are present at 1167 cm^{-1} and 1063 cm^{-1}. It is found that the increasing RILs content increases the intensity of stretching and bending vibration bands of imidazolium ring at around 1560 cm^{-1} and 1175 cm^{-1}, respectively. The obtained FTIR-ATR spectra confirmed the structure of studied pure RILs and pristine CAP. On the other hand, the RIL presence did not affect the position of characteristic bands observed for CAP-RIL membranes in comparison to pristine CAP and RILs. As both CAP and RIL possess ester groups in their structure, FTIR-ATR analysis did not allow to evidence the chemical reaction between polymer and RILs.

Table 14. Band assignments of RIL3_BF4 and PIL ionic liquids [180].

Band assignments	Wavenumber [cm^{-1}]	
	RIL3_BF4	PIL
Water in a sample	3429	3373
C–H stretching (aromatic, alkene)	-	3136, 3053, 3006
Imidazolium (Im) ring C–H stretching	3087	2975
Alkyl C–H symmetric stretching	2982	2950
C=O stretching vibration (from -COO- ester group)	1745	-
C=C stretching (Ar conjugated)	-	1629
Imidazolium ring stretching	1574	1573
C=C skeletal vibrations (aromatic)	-	1560, 1514
C–H scissoring deformation (CH_2 from methylene group)	1438	1449
C–H asymmetric deformation (CH_3 group) and C–H in-plane deformation (CH from vinyl group)	-	1409
H–C–C and H–C–N bending (imidazolium ring)	1174	1161
C–H out-of-plane deformation (CH from vinyl group)	-	995
C–H out-of-plane deformation (CH_2 from vinyl group)	-	909
C–H in-plane deformation (imidazolium ring)	870	859
C–H out-of-plane deformation (aromatic)	-	830
C–H out-of-plane deformation (imidazolium ring)	762	780

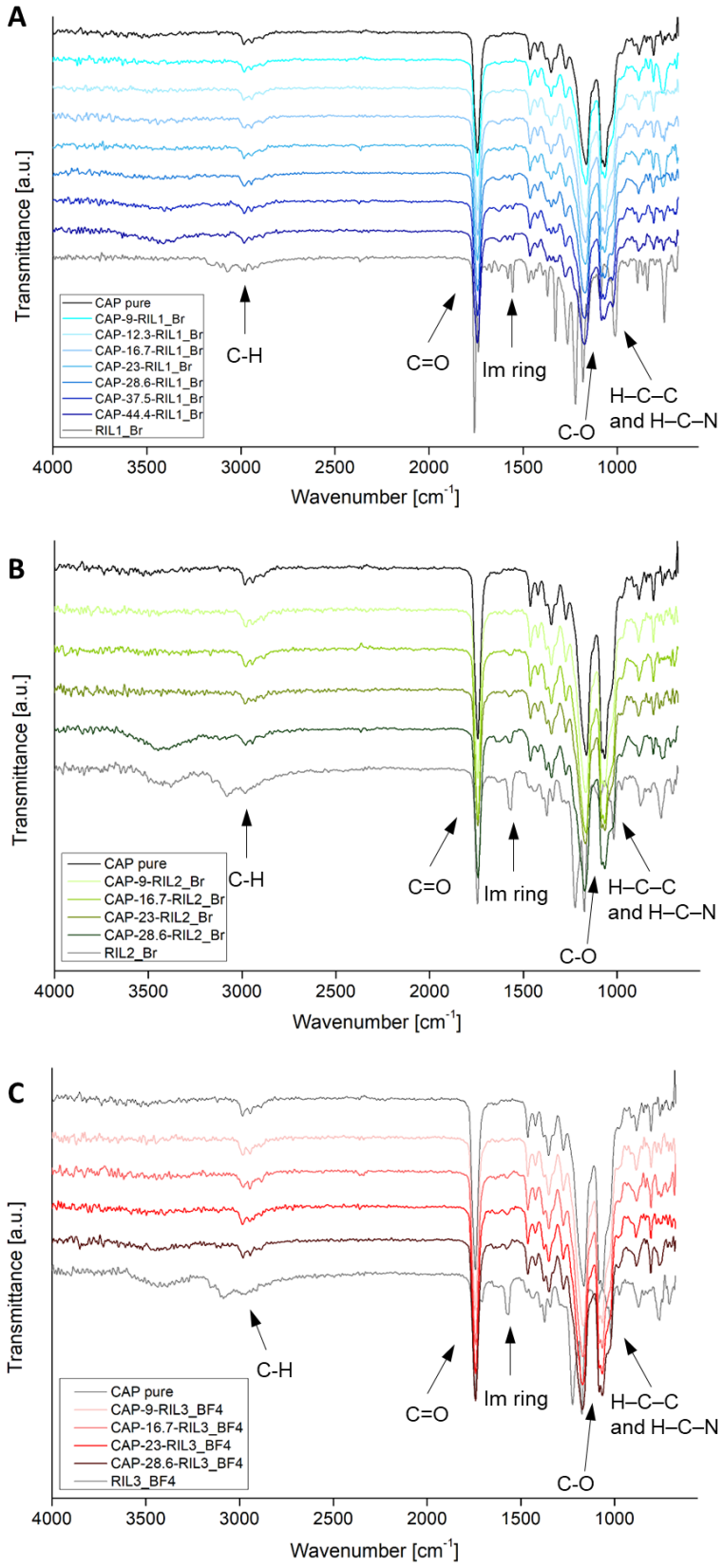

Figure 44. FTIR-ATR spectra of CAP-based membranes containing (A) RIL1_Br, (B) RIL2_Br, and (C) RIL3_BF4.

The spectra of CAP-PIL membranes are presented in Figure 45. The performed analysis shows the increasing intensity of stretching bands at around 3050 cm^{-1} (C–H group) and at 1573 cm^{-1} (imidazolium ring) with the increasing content of PIL monomer. The another characteristic vibration band at 1161 cm^{-1} corresponding to H–C–C and H–C–N imidazolium ring bending is overlapped with C–O symmetric stretching vibration band from ester groups and pyranose ring (Figure 45). The addition of PIL to CAP also influences the position of characteristic bands comparing to pure CAP and PIL.

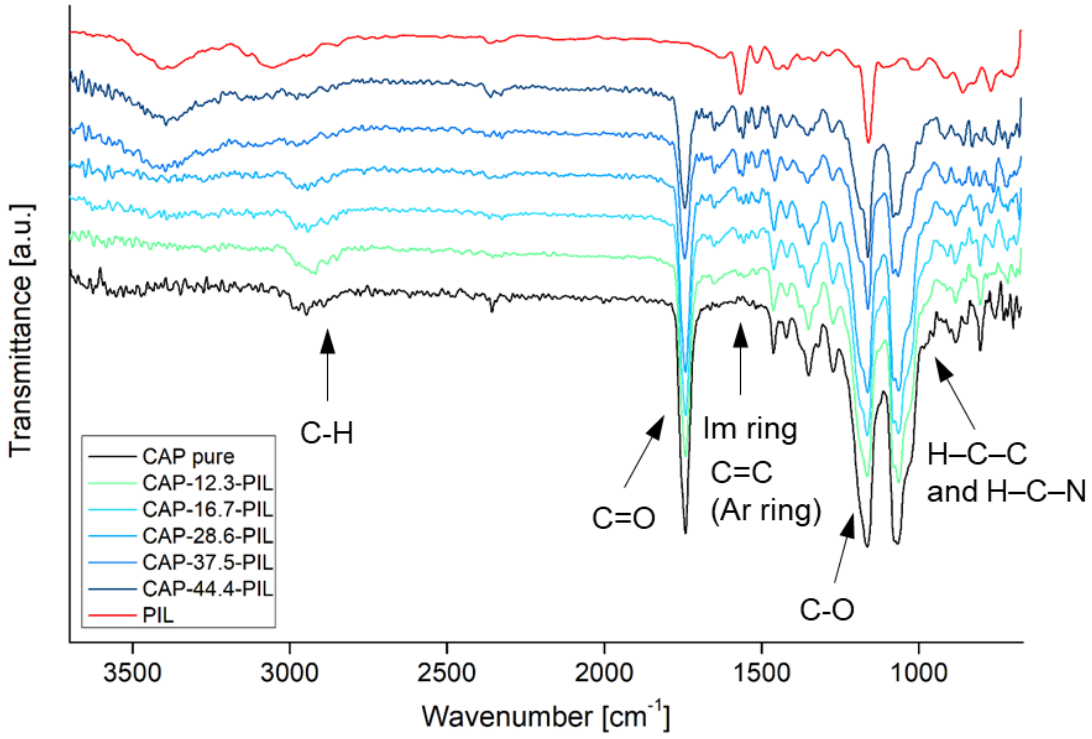

Figure 45. FTIR-ATR spectra of CAP-PIL membranes.

The chemical structure of the CAP and pure IL was confirmed using NMR analysis (Figure 46 and Figure 47). ^{13}C NMR spectrum of pure CAP presents the shifts δ 60-110 ppm corresponding to the signals of AGU carbonate region (Figure 46A). The shifts δ 170-180 ppm correspond to signals of the carbonyl carbon, whereas the shifts δ 0-30 ppm correspond to the signals of the acyl carbon [62]. The proton signal peaks for CAP were as follows: δ 3.2-5.9 ppm (protons of the cellulose backbone, 7H), δ 2.3 ppm (methyl protons of acetyl, 3H), δ 1.1 ppm (methyl protons of propionyl, 3H), and δ 2.2 ppm (methylene protons of propionyl, 2H) (Figure 46B).

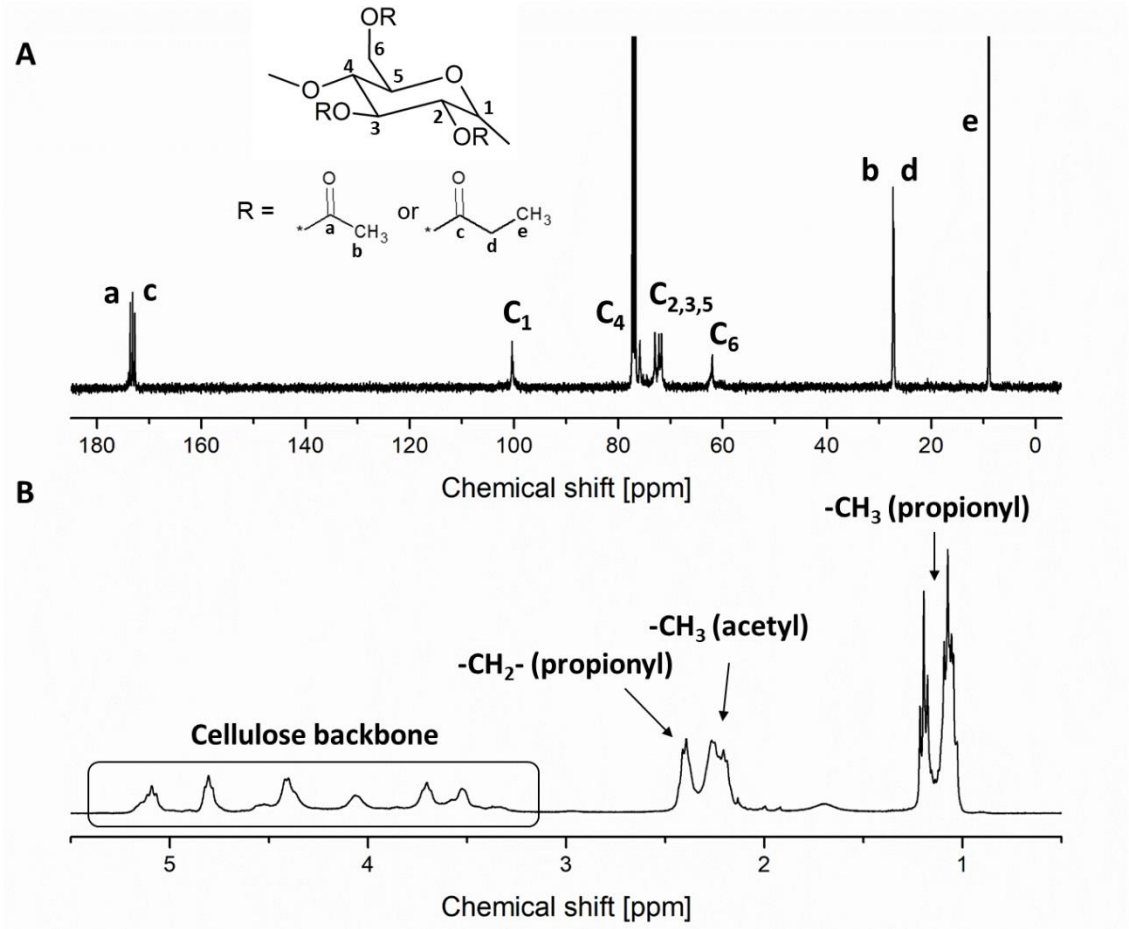

Figure 46. ^{13}C (A) and ^{1}H (B) NMR spectra of pristine CAP membrane.

NMR analysis was also used to investigate the possible interactions between the imidazolium ring and its local vicinity based on the changes of the chemical shifts in the NMR spectra [208]. The effectiveness of the transesterification reaction between polymer and studied RILs was evaluated based on the magnitude of chemical shifts in the NMR spectra of CAP-RIL membranes compared to the NMR spectra of pure RILs (Figure 47, Table 15). In general, the chemical shifts magnitude is affected by the changes in the chemical structure of the given molecule, and it strongly depends on the substituents nature and position with respect to the discussed nucleus [42]. Chen et al. [208] emphasized that protons of the imidazolium ring are notably sensitive to their environmental changes, which can be observed in NMR spectra [208].

The presence of RILs influenced the ^{1}H NMR spectra of CAP-RIL membranes (Figure 47). The comparison of the spectra of CAP-RIL1_Br and CAP-RIL2_Br with the spectra of pure RILs shows the shift of the signal corresponding to the proton at C2 carbon in the imidazole ring (Table 15).

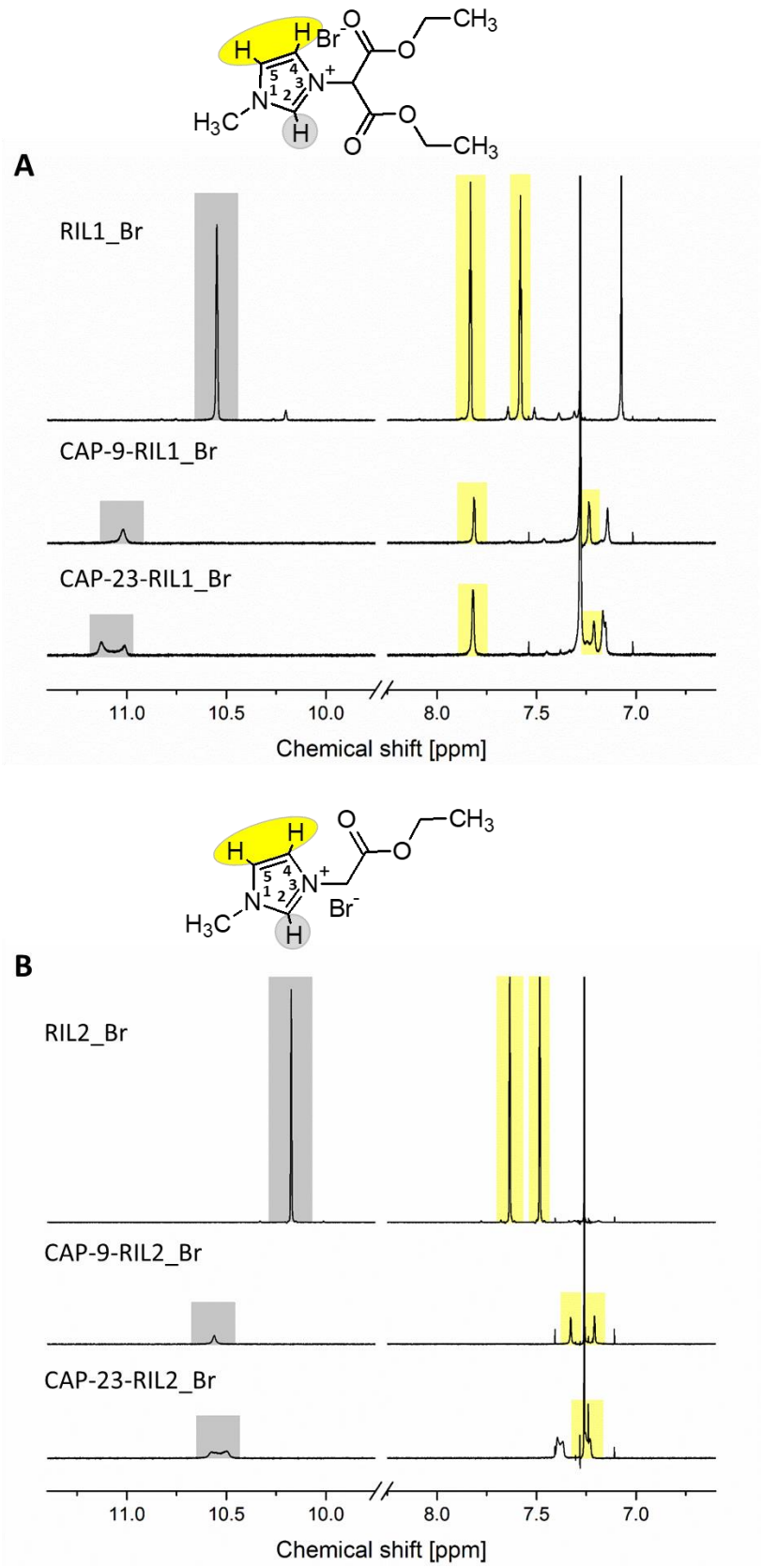

Figure 47. ^{1}H NMR spectra of (A) CAP-RIL1_Br and (B) CAP-RIL2_Br membranes.

The characteristic peaks of CAP below 5.5 ppm did not changed after the transesterification reaction. The H2 proton in the imidazole ring was de-shielded, therefore, the chemical shift of H2 proton in CAP-9-RIL1_Br was observed from 10.55 to 11.02 ppm in comparison to RIL1_Br (Table 15) [209]. Simultaneously, one of the protons at C4 and C5 positions in the imidazole ring is shielded and shifted from 7.58 to 7.24 ppm in the case of CAP-RIL1_Br membrane (Figure 47, Table 15). Shin et al. [210] also noted that only one of the H4 and H5 protons shifted as a result of the change from ethyl to butyl substituent in the structure of the imidazolium-based ionic liquid. The aforementioned changes confirm the successful transesterification reaction between the RIL and CAP (Figure 48).

Table 15. The NMR signals position of H2, H4 and H5 protons of imidazole ring in CAP-RIL1_Br and CAP-RIL2_Br membranes.

	Signal position of proton [ppm]	
	H2	H4 and H5
Pure RIL1_Br	10.55	7.58
CAP-9-RIL1_Br	11.02	7.24
CAP-23-RIL1_Br	11.01	7.21
Pure RIL2_Br	10.17	7.48
CAP-9-RIL2_Br	10.56	7.21
CAP-23-RIL2_Br	10.58	7.24

The quantitative assessment of the transesterification reaction between propanoyloxymethyl group in CAP and 2-etoxy-2-oxoethyl in RILs was also performed based on the substitution degree (*DS*) and discussed from the point of view of RILs. The effectiveness of the substitution reaction was evaluated based on the RIL amount undergoing the transesterification reaction with CAP (Table 16, Eq. (31)). The substitution reaction possesses a significant impact on the characteristics of cellulose derivatives, like solubility, thermal, and mechanical properties [74, 161, 211].

Generally, the CAP ester groups in the C2, C3, and C6 positions in AGU unit can undergo the substitution reaction. However, the primary carbon atom at C6 position is the most reactive CAP substituent. In the case of RIL1_Br possessing two ester groups, it is assumed that the transesterification reaction takes place only with one ester group due to

the steric hindrance. Therefore, the *DS* and DS_{max} values were calculated taking into account the 1:1 molar ratio between CAP and RILs.

It can be noticed that reaction between CAP and RIL leads to the various partial substitution of ester groups in RILs as different *DS* vales are obtained (Table 16). The calculated degree of substitution is equal to 0.087 and 0.283 for CAP-9-RIL1_Br and CAP-23-RIL1_Br, and 0.027 and 0.076 for CAP-9-RIL2_Br and CAP-23-RIL2_Br, respectively (Table 16). The comparison of the obtained *DS* with the DS_{max} allows to calculate the amount of RIL attached to the polymer chain. For example, the *DS* = 0.087 for CAP-9-RIL1_Br means that 87% of ionic liquid are substituted to the CAP chain. The calculated *DS* values for CAP-RIL1_Br films are comparable to the values of the DS_{max} that testifies to the high efficiency of the transesterification reaction between RIL and CAP. It was also found that *DS* is higher in the case of the membranes modified with the RIL1_Br possessing two active sites, *i.e.* two ester groups.

Table 16. Degree of substitution *DS* calculated based on ^{1}H NMR data for pure RILs and CAP-RIL membranes.

	Integral of resonance [-]	
Film	CAP-9-RIL1_Br	CAP-23-RIL1_Br
S1	1.00 (at 7.81 ppm)	1.00 (at 7.82 ppm)
S2	11.43 (at 5.10 ppm)	3.53 (at 5.09 ppm)
DS	0.087	0.283
DS_{max}	0.099	0.295
Film	CAP-9-RIL2_Br	CAP-23-RIL2_Br
S1	1.00 (at 7.41 ppm)	1.00 (at 7.24 ppm)
S2	36.88 (at 5.07 ppm)	13.10 (at 5.07 ppm)
DS	0.027	0.076
DS_{max}	0.076	0.229

The transesterification reaction starts by the protonation of the carbonyl group by the acid protons, thus activating it towards the nucleophilic attack. Then, the carbonyl group undergoes the nucleophilic attack by the CAP molecule. Subsequently, the proton transfer takes place. The charge displacement from the –OH group to $–O^+$ results in the

removal of the ethanol molecule. Finally, the deprotonation of the resultant molecule occurs and the final product of the transesterification reaction is obtained (Figure 48).

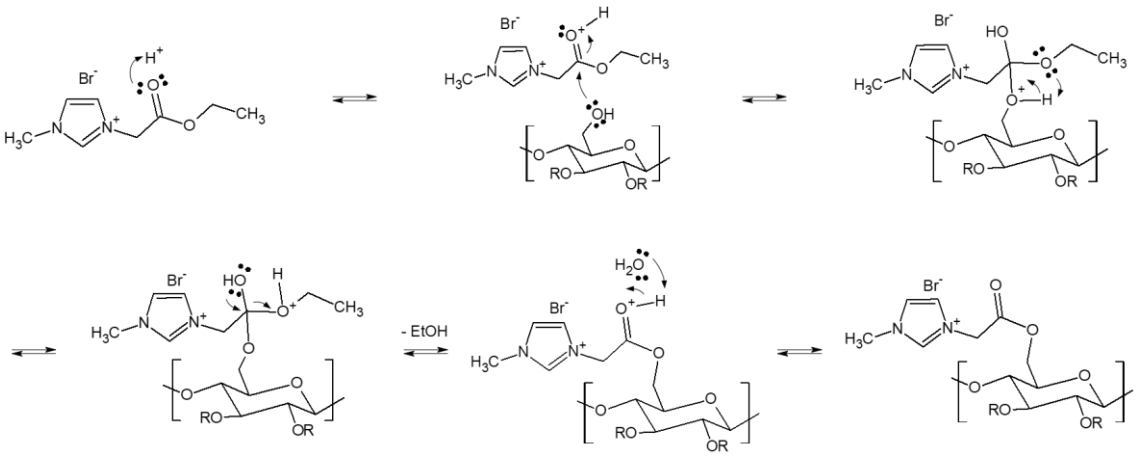

Figure 48. Proposed scheme of the transesterification reaction between CAP and RIL2_Br.

4.2.2 Mechanical Properties

The effect of ionic liquids (RILs and PIL) incorporation on mechanical properties of CAP-based membranes was also studied by tensile tests and was evaluated in terms of the Young's modulus (E), stress at break (σ_{max}), and elongation at break (ε_{max}) parameters.

The incorporation of RILs results in the significant alteration of the mechanical properties of CAP-based membranes compared to the pure CAP as the enhanced elongation and reduced brittleness are observed with an increasing RIL content (Figure 49). In general, the elongation at break value increases, as well as both stress at break and elastic modulus (E) decrease with the raise of the RIL content. This result confirms the plasticization effect of RIL in the case of CAP membrane materials. Such plasticization effect of ionic liquid on polymer membranes was observed also by Schmidt et al [87]. Researchers found that the incorporation of ionic liquids based on imidazolium cation to Nafion® 117 membrane resulted in the plasticization of polymer matrix. This fact was confirmed by the diminished Young's modulus value compared to the pristine Nafion® 117 membrane [87]. Due to the presence of ionic liquid with butyl and hexyl alkyl side chains of remarkable flexibility, the ductility of impregnated Nafion® membrane was improved. It was also pointed out that the ionic liquids incorporation weaken the hydrogen bonds between sulfonic groups in Nafion® membrane [87]. The similar phenomenon of polymer membrane plasticization by ionic liquid incorporation was

reported by Chen et al. for sulfonated poly(ether ether ketone) (SPEEK) membranes blended with 1-ethyl-3-methylimidazole tetrafluoroborate or 1-butyl-3-methylimidazole methanesulfonate ionic liquids [212].

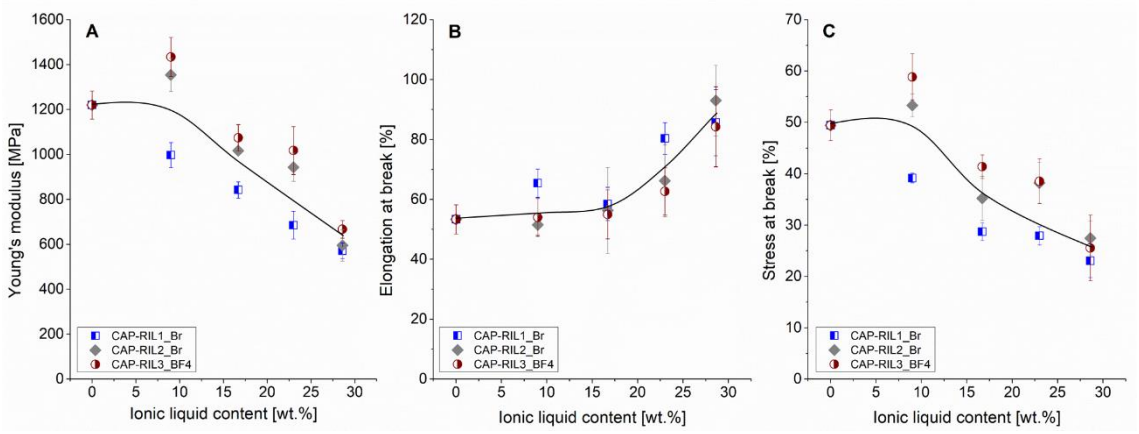

Figure 49. Young's modulus (A), stress at break (B), and elongation at break (C) of the CAP-based membranes modified with RILs. The solid lines are only to guide an eye.

In the case of CAP-PIL membranes, the similar results were obtained, *i.e.* the amelioration of the mechanical properties of CAP-based membranes due to the improvement of the membranes softness and reduced membranes brittleness (Figure 50). The PIL content increase up to 44.4 wt.% led to the drop of E to 451 ± 24 MPa. It was observed that elongation at break reached its maximum value (67 ± 11 %) for CAP-based membrane modified with 28.6 wt.% of PIL. Besides, this membrane possessed the maximum elongation among all tested CAP-PIL membranes. On the other hand, the PIL incorporation did not influence significantly the stress at break (σ_{max}) values in comparison to pristine CAP membrane. It was found that CAP-based membranes with the highest PIL content equal to 44.4 wt.% showed deteriorated mechanical properties among all tested CAP-PIL membranes. The incorporation of high content of PIL increased the inner stress in CAP-44.4-PIL membrane and led to the decrease of the stress at break to 12 ± 2 MPa and to the decrease of the elongation at break to 37 ± 9 %. The results of tensile tests indicate that Young's modulus and elongation at break parameters and, thus, mechanical properties of CAP-based membranes are highly dependent on the content of the incorporated PIL.

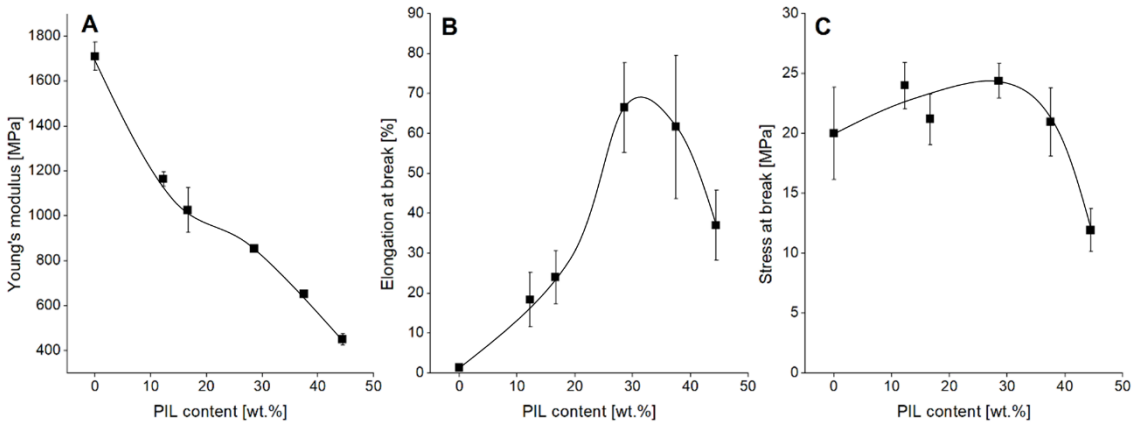

Figure 50. Young's modulus (A), stress at break (B), and elongation at break (C) of the CAP-PIL membranes. The solid lines are drawn to guide an eye only.

The comparison of the mechanical behavior of CAP-ILs membranes and CAP-based membranes modified with commercial plasticizers (TBA and ATBC) reveals that the ILs (both RILs and PIL) plasticize the CAP membranes. As in the case of the CAP membranes modified with traditional plasticizers (Table 17), the plasticization of CAP-based membranes with ILs results in the increased flexibility of the tested membranes. The measured Young's modulus (E), elongation at break (ε_{max}), and stress at break (σ_{max}) parameters are comparable to those obtained for CAP-TBC and CAP-ATBC membranes. The flexibility and softness of CAP-based membranes was improved whatever the compound used (IL or commercial plasticizer). For example, the Young's modulus values of membranes with 23 wt.% of plasticizing compound were equal to 685 ± 62 MPa (CAP-23-RIL), 721 ± 22 MPa (CAP-23-ATBC), and 571 ± 20 MPa (CAP-23-TBC) (Table 17). The higher elongation of CAP membranes containing ILs (RILs and PILs) compared to CAP membranes plasticized with TBC and ATBC is related to the difference in the structure of used additives (plasticizers and ILs) (Figure 18 – Figure 21). The shorter aliphatic segments in the IL structure deshield dipoles in CAP polymer structure which resulted in the enhanced interactions between CAP and ILs compared to those between CAP and plasticizers (TBC and ATBC). Harte et al. noticed the similar behavior in the case of PDLLA membranes modified with TEC, TBC, and ATBC [202]. It was found that the increase of the length of aliphatic nonpolar segments in TBC and ATBC compared to TEC decreased the interactions between plasticizer molecules and PDLLA. Therefore, the decrease in the elongation for PDLLA with TBC and ATBC compared to PDLLA with TEC was observed.

The incorporation of at least 9 wt.% of ionic liquids (RILs and PIL) or plasticizers (TBC and ATBC) to CAP-based membranes resulted in more advantageous mechanical performance than the use of other components, such as essential oils [66], PTS, PTG, and DOA [201]. The comparison of the results shows that CAP-based membranes containing 10% and 20% (v/w) of lemongrass and basil oil possess the elasticity comparable to pure CAP [201]. In this work, the plasticized CAP-based membranes possess higher values of stress at break parameter that corresponds to the higher mechanical strength. CAP-9-RIL1_Br membrane (*i.e.* membrane containing 9 wt.% of RIL1_Br) has the highest improvement of membrane elasticity than membranes containing 27 wt.% of PTS, namely CAP-9-RIL1_Br shows more than twice higher elongation than CAP-27-PTS (29%) [201]. CAP-based membranes with 9 and 23 wt.% of RILs also possess preferable mechanical properties in the comparison to CAB-tetraethoxysilane (TEOS) hybrid membranes with incorporated DOP (52%) [80].

Table 17. The comparison of mechanical performance of studied CAP-based membranes.

Type of plasticizer	Elongation at break (ε_{max})	Stress at break (σ_{max})	Young's modulus (E)
	[%]	[MPa]	[MPa]
CAP pure	2 ± 1	50 ± 3	1710 ± 64
CAP-9-RIL1_Br	65 ± 5	39 ± 1	998 ± 56
CAP-9-RIL2_Br	52 ± 3	53 ± 2	1324 ± 74
CAP-9-RIL3_BF4	54 ± 6	59 ± 4	1435 ± 87
CAP-12.3-PIL	18 ± 7	24 ± 2	1164 ± 31
CAP-9-ATBC	8 ± 6	34 ± 11	1329 ± 226
CAP-9-TBC	9 ± 6	28 ± 6	1162 ± 44
CAP-23-RIL1_Br	80 ± 5	28 ± 2	685 ± 62
CAP-23-RIL2_Br	66 ± 12	38 ± 4	944 ± 63
CAP-23-RIL3_BF4	63 ± 8	39 ± 4	1018 ± 107
CAP-28.6-PIL	67 ± 11	24 ± 1	853 ± 14
CAP-23-ATBC	61 ± 4	32 ± 2	721 ± 22
CAP-23-TBC	50 ± 8	20 ± 3	571 ± 20

4.2.3 Thermal Stability

The thermal properties of CAP-based membranes with different incorporated ionic liquids (RIL1_Br, RIL2_Br, RIL3_BF4) were tested by thermogravimetric analysis and the obtained results are depicted by TG and DTG curves (Figure 51). The thermal degradation profiles of pure CAP as well as RIL1_Br and RIL2_Br were described in detail in section 4.1.2 and 3.2.2, respectively.

The thermal degradation profile of RIL3_BF4 shows three degradation stages. The first step at T_{onset} = 58°C corresponds to the release of the moisture absorbed by the pure RIL. The second step is related to the decomposition of ester groups at T_{onset} = 209°C. The third step is the decomposition of imidazolium ring at T_{onset} = 279°C (Figure 51C). The thermal degradation of RIL3_BF4 was accompanied by the formation of methylimidazole, fluoromethane, and boron trifluoride as reported by Ohtani et al. [191] and Erdmenger et al. [213]. Ohtani et al. pointed out that the thermal decomposition of ILs containing tetrafluoroborate as anion carried out according to the thermal cleavage of C–N bond in imidazolium ring in contrast to ILs containing halides as anion that initiated the nucleophilic attack [191].

The comparison of thermograms of studied IL reveals that the RIL1_Br decomposition starts at lower temperature comparing to RIL2_Br and RIL3_BF4 (compare Figure 51A with Figure 51B, and Figure 51C, respectively). This is mainly related to the more branched structure of RIL1_Br imidazolium cation (Figure 19) as well as to the presence of strongly coordination bromide anion [214, 215]. Raj et al. [214] and Cao and Mu [215] emphasized the importance of the IL anion nature on the thermal stability. Cao and Mu [215] reported that the IL degradation temperature decreased due to the presence of strongly coordinating anions, such as halogen (Cl^-, Br^- or I^-), whereas weakly coordinating anions (e.g. BF_4^-, PF_6^-) increased the IL decomposition temperature.

Thermograms of CAP-RIL membranes reveal that the RIL incorporation to CAP structure shifts the degradation temperature to lower values because of the formation of ester bonds between RIL and CAP polymer during the polymer modification by transesterification reaction (Figure 48). The created ester bonds are characterized by lower thermal stability and higher ease to break during thermal degradation [61].

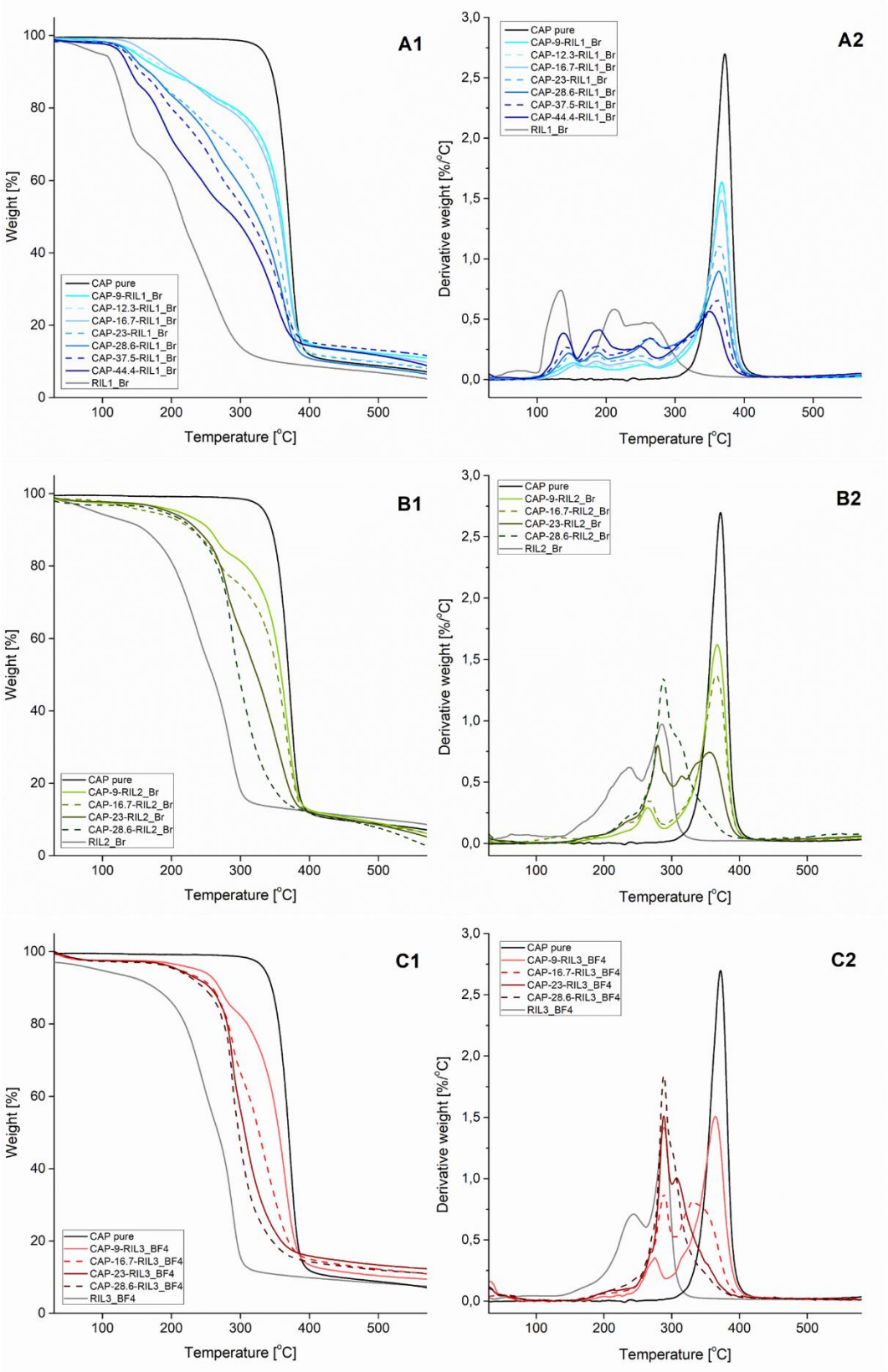

Figure 51. Thermogravimetric analysis of (A) CAP-RIL1_Br, (B) CAP-RIL2_Br, and (C) CAP-RIL3_BF4 membranes: (A1, B1, C1) TG and (A2, B2, C2) DTG curves.

The thermograms of CAP-RIL membranes (Figure 51) as well as the degradation temperatures at 5 and 10% weight loss (Table 18) reveal the dependence of thermal stability of CAP-based membranes on the RIL concentration. The increasing content of RIL leads to the substitution of more side chains of CAP, which is in accordance with the systematically diminished thermal stability of CAP-RIL membranes. For example, the raise of RIL1_Br content from 9 to 28.6 wt.% decreases the degradation temperature at 5% weight loss from 168 to 138°C (Table 18).

Table 18. Characteristic degradation temperature of studied CAP, CAP-RIL1_Br, CAP-RIL2_Br, and CAP-RIL3_BF4 membranes.

Membrane	Degradation temperature [°C]	
	at 5% weight loss	at 10% weight loss
CAP pure	325 ± 2	340 ± 2
CAP-9-RIL1_Br	168 ± 2	205 ± 2
CAP-16.7- RIL1_Br	149 ± 2	192 ± 2
CAP-23- RIL1_Br	140 ± 2	168 ± 2
CAP-28.6- RIL1_Br	138 ± 2	166 ± 2
CAP-9- RIL2_Br	210 ± 2	255 ± 2
CAP-16.7- RIL2_Br	197 ± 2	238 ± 2
CAP-23- RIL2_Br	188 ± 2	232 ± 2
CAP-28.6- RIL2_Br	197 ± 2	238 ± 2
CAP-9- RIL3_BF4	239 ± 2	270 ± 2
CAP-16.7- RIL3_BF4	211 ± 2	260 ± 2
CAP-23- RIL3_BF4	210 ± 2	256 ± 2
CAP-28.6- RIL3_BF4	207 ± 2	247 ± 2

DTG curve of PIL (Figure 52) shows four peaks. The peak at T_{onset} = 64°C corresponds to the loss of absorbed moisture, whereas peaks in the temperature range from 250-350°C are related to the decomposition of the imidazole group [216]. The weight loss of PIL at T_{onset} 442°C is ascribed to the degradation of vinyl benzyl group [216].

The increase of the peak intensity at T_{onset} = 65°C for CAP-PIL membranes is observed with the PIL content increasing. This result is related to the hydrophilic PIL

nature that leads to the higher moisture absorption. Also, the increase of the PIL content leads to the raise of peaks intensity at the onset degradation temperatures equal to 255 and 442°C.

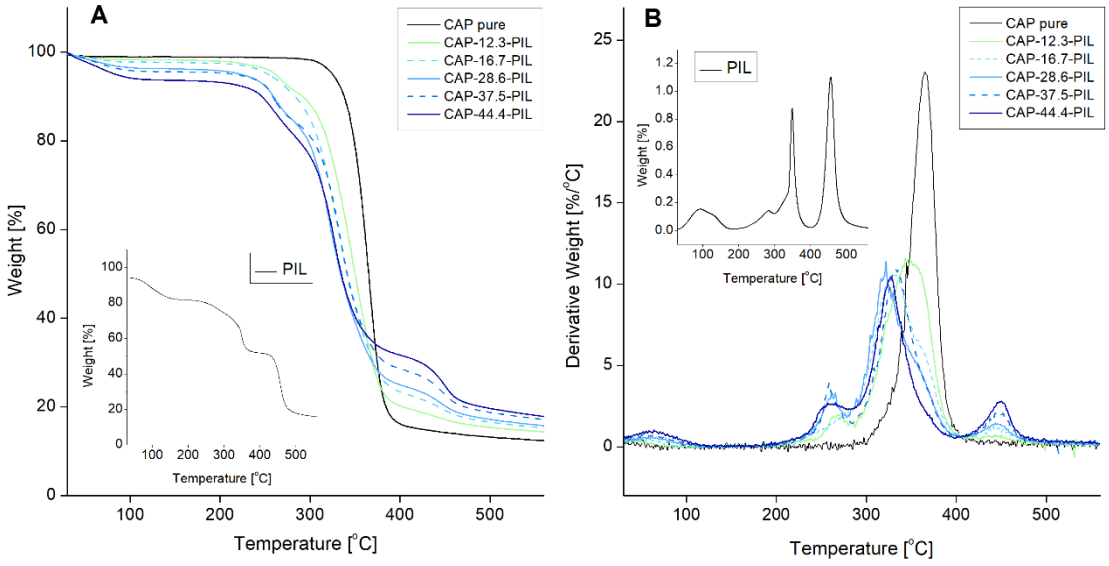

Figure 52. Thermogravimetric analysis of the CAP-PIL membranes: (A) TG and (B) DTG curves.

The incorporation of PIL in CAP-based membranes results also in the shift of the degradation temperature to the lower values comparing to pure CAP membrane (Figure 52). Such behavior indicates the successful immobilization of PIL into CAP matrix [155, 217] and is in accordance with the findings of Kadokawa et al. [218]. Researchers reported that the incorporation of the polymerizable ionic liquid possessing styril and vinyl groups to cellulose-based composite decreased the onset weight loss temperature to 245°C in comparison with pristine cellulose (300°C) and PIL (260°C) [218].

The performed thermogravimetric analysis reveals that CAP membranes modified with PIL possess the highest thermal stability among tested CAP-based membranes (Table 18 and Table 19). The initial thermal degradation of CAP-PIL membranes starts at around 200°C. CAP membranes with RIL2_Br and RIL3_BF4 ionic liquids have the comparable thermal stability to CAP-based membranes modified with TBC and ATBC (Figure 40, Figure 51, Figure 52) and improved thermal stability compared CAP-RIL1_Br membranes. It is found that thermal stability of CAP-based membranes is highly influenced by the concentration of a given additive (ionic liquid or plasticizer). However,

the raise of the ionic liquid or plasticizer content shifts systematically the membrane degradation temperature to lower values whatever the additive.

Table 19. Characteristic degradation temperature of studied CAP-PIL membranes.

Membrane	Degradation temperature [°C]	
	at 5% weight loss	at 10% weight loss
CAP pure	325 ± 2	340 ± 2
CAP-12.3-PIL	261 ± 2	292 ± 2
CAP-16.7- PIL	253 ± 2	283 ± 2
CAP-28.6- PIL	222 ± 2	259 ± 2
CAP-37.5- PIL	214 ± 2	258 ± 2
CAP-44.4- PIL	83 ± 2	246 ± 2

It can be pointed out that the type and the content of the additive have a significant impact on the initial degradation temperature of CAP-based membranes. It should be also noted that the studied CAP-based membranes revealed the significant thermal stability up to at least 120°C. Such thermal stability is sufficient taking into account the requirements for polymer membranes applications in various separation processes, including pervaporation, gas separation, and metal ions transport [219].

4.3.4 Morphology and Surface Characterization

It is known that membrane components should be compatible in order to obtain homogenous films. The compatibility between CAP and ionic liquids (RILs and PILs) was studied by the SEM analysis (Figure 53). As it can be seen from the surface and cross-section view of pristine CAP and CAP-based membranes modified with RILs, the dense structure is formed in the case of all membranes. The CAP-based membranes with the low RIL content possess the membrane surface comparable to the native CAP. However, the morphological study of CAP-RIL membranes showed the increasing heterogeneity of the membrane structure as a result of the increased ionic liquid content up to 23 wt.%. This was reflected by the presence of RIL-rich and CAP-rich domains on the membrane surface as well as by the appearance of unconnected small pores, particularly in the case of CAP-RIL2_Br and CAP-RIL3_BF4 membranes (Figure 53B and Figure 54C, respectively). In the case of RIL1_Br, the increase of ionic liquid content

up to 28 wt.% results in the appearance of the IL domains on the membrane surface. This fact may be explained by the partial compatibility of CAP with RIL1_Br. The varied CAP-based membrane surface can evidence the difference in the substitution ability of CAP with RIL.

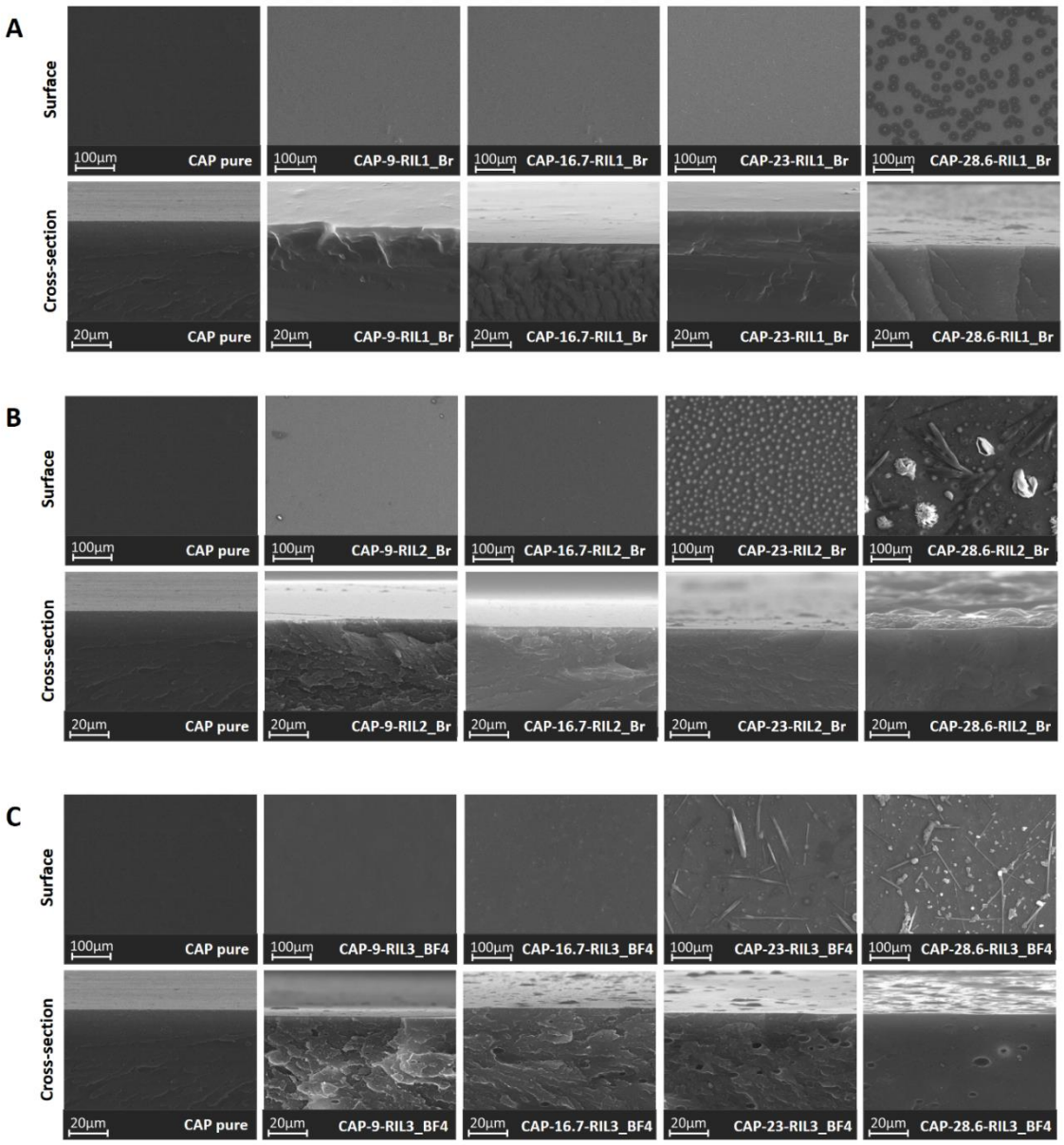

Figure 53. SEM images of surface and cross-section of (A) CAP-RIL1_Br; (B) CAP-RIL2_Br, and (C) CAP_RIL3_BF4 membranes.

The surface and cross-section images of CAP-PIL reveal the influence of the PIL incorporation on the morphology of the CAP-based membranes (Figure 54). It is found that the PIL incorporation also results in the heterogeneity of the membrane structure as

the presence of small non-interconnected pores or CAP-rich and PIL-rich domains can be observed (CAP-44.4-PIL membrane in Figure 54).

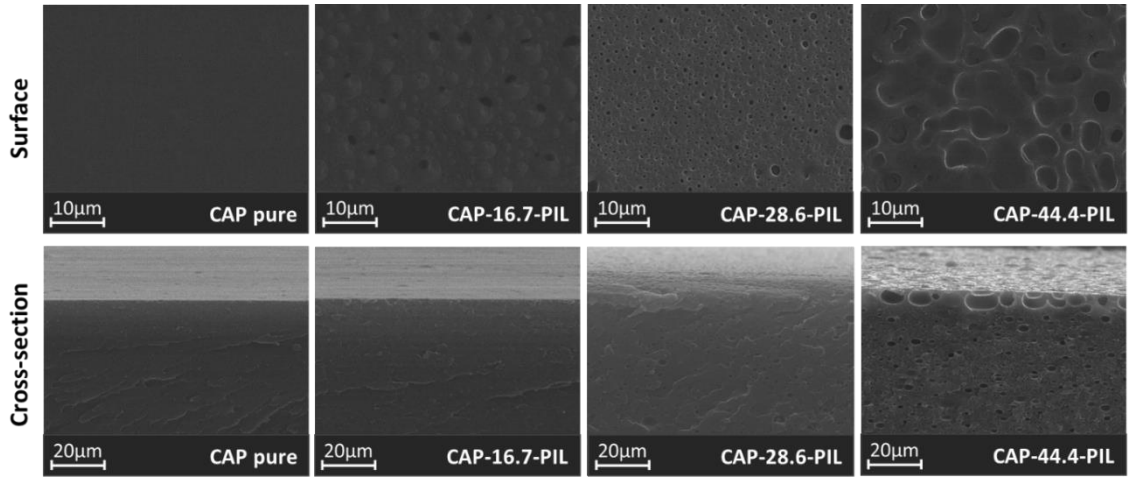

Figure 54. SEM surface and cross-section micrographs of CAP-PIL membranes.

CAP-based membranes were elaborated according to the same procedure; therefore, the presence of IL agglomerates can be linked to the difference in the polymer-IL interactions and IL viscosity. Such behavior was reported by de los Rios for Nylon®- and Mitex-based supported liquid membranes with 1-butyl-3-methylimidazolium hexafluorophosphate [BMIM][PF6], 1-butyl-3-methylimidazolium tetrafluoroborate [BMIM][BF4], and 1-butyl-3-methylimidazolium bis(trifluoromethanesulfonyl)imide, [BMIM][Tf2N] [220]. The IL agglomerates with various size were observed on Mitex and Nylon® membranes surface despite using the identical elaboration procedure for all polymer-IL systems. As a result, the heterogeneity of Mitex-IL and Nylon®-IL membranes was correlated to the difference in ILs viscosity and fluidity. The amount of IL agglomerates on the membranes surface increases with the raise of the IL viscosity according to the following order: [BMIM][PF6] > [BMIM][BF4] > [BMIM][Tf2N] [220]. The researchers also pointed out the importance of the IL hydrophilicity as this property could significantly influence the polymer-IL compatibility. It was found that the good homogeneity and the better compatibility between Nylon® and studied ILs was correlated to their hydrophilic nature in contrast to the hydrophobic Mitex membranes. The highly hydrophobic nature of Mitex restricted its interactions with hydrophilic ILs [220].

The results of the SEM analysis were also evaluated taking into consideration the ratio between the polymer and RIL. In principle, the transesterification reaction could

theoretically take place between three ester groups in AGU unit and one ester group in RIL2_Br and RIL3_BF4 ionic liquids. Therefore, the ratio between CAP and RIL required for the total substitution of CAP ester by RIL2_Br or RIL3_BF4 is 1 to 3 that corresponds to ca. 29 wt.% of ionic liquid in the polymer matrix. The content of ionic liquid in CAP films exceeding this ratio may result in the release of ionic liquid excess and the formation of RIL-rich domains on the membrane surface. RIL-rich agglomerates can be seen for CAP-RIL2 and CAP-RIL3 films containing at least 23 wt.% of RIL (Figure 53B and Figure 53C). These results suggest that the substitution reaction is not completed and only two ester groups in AGU could possibly be substituted by RIL2_Br or RIL3_BF4. Thus, the ratio between polymer and ionic liquid can be 1:2, which corresponds to maximum 21 wt.% of ionic liquid in the polymer matrix. These assumptions are in accordance with the results of the SEM analysis.

Assuming that the transesterification reaction can take place between two ester group in RIL1_Br and three ester groups in AGU unit, the polymer:RIL1_Br ratio is 2:3, what corresponds to 21 wt.% of RIL1_Br in the polymer matrix. CAP film with the RIL1_Br content equal to 23 wt.% does not have remarkable visible changes on the film surface, thus confirming the full substitution and the high compatibility between CAP and RIL1_Br in agreement with high degree of substitution (Table 16). On the other hand, the polymer:RIL1_Br ratio may be 1:3, taking into account the steric hindrance that might result from the branched structure of ionic liquid (Figure 19). In this case, the content of ionic liquid bounded in the polymer matrix is equal to 28.9 wt.%.

Figure 55 presents the EDX images of native CAP and CAP-based membranes modified with RILs. SEM-EDX mapping of pure CAP film confirmed the presence of carbon and oxygen elements in the chemical composition of polymer. The performed mapping of modified membranes reveals the new bromine signal for CAP-RIL1_Br and CAP-RIL2_Br confirming the uniform distribution of RILs in a polymer matrix. De los Rios et al. [220] presented the SEM-EDX line profiles of fluorine (F) recorded at the membrane cross-section that confirmed the homogeneous distribution of the studied imidazolium-based ionic liquids within Nylon® membranes. Xi et al. [189] reported the homogeneous dispersion of 1-ethyl-3-methylimidazolium hexafluorophosphate [EMIM][PF6] in the WPU membranes up to 10 wt.% of [EMIM][PF6]. However, it was found that the increase of the [EMIM][PF6] content above 10 wt.% resulted in the formation of IL-rich domains dispersed in the WPU matrix as it was noted from the results of SEM-EDX mapping [189].

Besides, the RIL-rich domains are observed on the surface of CAP-RIL2_Br membranes with 23 wt.% and 28.6 wt.% of RIL (Figure 55B). The mapping of CAP-RIL_BF4 films is not shown as boron atom cannot be detected due to the limitation of SEM-EDX analysis.

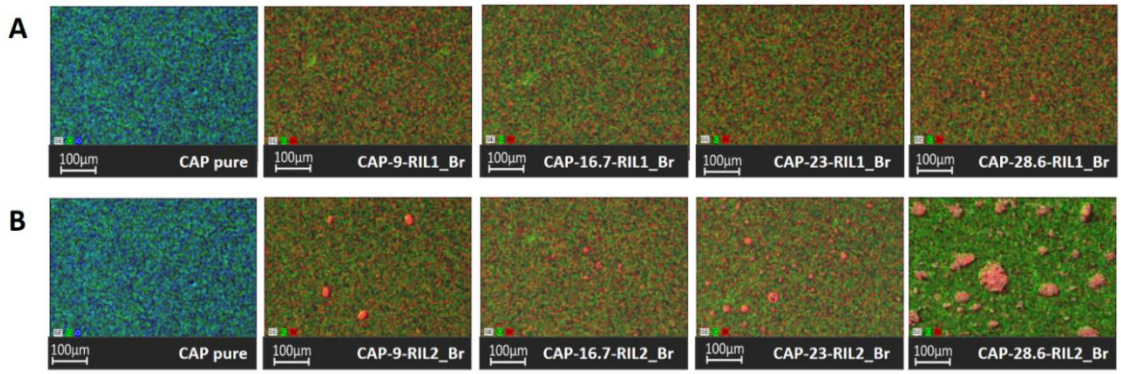

Figure 55. SEM-EDX images of film surface: (A) CAP-RIL1_Br and (B) CAP-RIL2_Br (green – carbon atoms, red – bromine atoms, and blue – oxygen atoms).

AFM analysis was performed to study and visualize the CAP-based membranes' surface morphology. The obtained results were discussed based on the roughness average parameter (R_a) (Figure 56 and Table 20). The obtained results showed the influence of the RIL addition on the membrane surface roughness (Figure 56). It was found that the increase of the RIL2_Br and RIL3_BF4 content resulted in the greater surface roughness of CAP-RIL membranes. This was reflected by the increased values of R_a and R_q parameters (Table 20). Such effect was the most pronounced in the case of CAP-based membranes with the RIL3_BF4 incorporation. The increase of the RIL3_BF4 content from 9 to 23 wt.% resulted in the increase of the R_a parameter value from 16.8 ± 12.7 to 103.2 ± 14.2 nm, whereas the R_a for pure CAP is equal to 5.3 ± 1.4 nm. The increased surface roughness can be correlated to the presence of the RIL-rich domains on the surface of the tested membrane materials that is in accordance with the results obtained by SEM analysis (Figure 53). The enhanced surface roughness of WPU-based membranes with IL content increasing was also observed using AFM analysis by Xi et al [189]. The researchers found that the presence of [EMIM][PF6] disrupts the polymer chains order that leads to the rougher surface of WPU-[EMIM][PF6] membranes compared to the flat surface of pristine WPU. For example, the value of R_a parameter increased from 0.8 nm for pure WPU up to 6.9 nm for WPU membrane with 15 wt.% of [EMIM][PF6] [189]. Moreover, it is pointed out that the high IL content in WPU-based membranes results in

the phase separation reflected by the appearance of the [EMIM][PF6]-rich domains precipitated on the membrane surface [189].

Considering the CAP-RIL1_Br membranes, the presence of RIL1_Br led to the decrease of the membrane surface roughness that was reflected by the decreasing roughness parameters values (R_q equal to 4.9 ± 0.4 μm for CAP-23-RIL1_Br) comparing to pure CAP (R_q equal to 8.4 ± 1.7 μm). Such behavior can be correlated to the higher *DS* of CAP-RIL1_Br membranes in comparison to CAP-RIL2_Br membranes (Table 16). The higher substitution degree of RIL1_Br was associated with more homogenous membrane structure. This result is in accordance to the results of SEM analysis revealing the more uniform membrane surface in respect to the CAP-based membranes with RIL2_Br and RIL3_BF4 (Figure 53).

Table 20. Roughness parameters: R_q and R_a of pristine CAP and CAP-based membranes with RIL1_Br, RIL2_Br, and RIL3_BF4 ionic liquids.

Parameter	R_q [nm]	R_a [nm]	R_q [nm]	R_a [nm]
Scanning area	5 μm x 5 μm		10 μm x 10 μm	
CAP pure	3.4 ± 0.7	2.6 ± 0.6	8.4 ± 1.7	5.3 ± 1.4
CAP-9-RIL1_Br	3.7 ± 0.3	2.8 ± 0.3	8.8 ± 0.7	6.0 ± 0.9
CAP-16.7-RIL1_Br	4.1 ± 0.6	3.1 ± 0.4	6.1 ± 1.0	4.5 ± 0.4
CAP-23-RIL1_Br	6.0 ± 1.2	4.5 ± 0.7	4.9 ± 0.4	3.6 ± 0.1
CAP-9-RIL2_Br	2.9 ± 0.1	2.4 ± 0.4	7.4 ± 2.5	5.6 ± 1.9
CAP-16.7-RIL2_Br	3.2 ± 0.6	2.4 ± 0.4	9.8 ± 5.0	6.7 ± 2.6
CAP-23-RIL2_Br	4.8 ± 0.8	3.1 ± 0.3	10.3 ± 3.2	7.9 ± 1.6
CAP-9-RIL3_BF4	6.1 ± 0.9	4.7 ± 0.4	30.3 ± 16.5	16.9 ± 12.7
CAP-16.7-RIL3_BF4	6.6 ± 1.1	4.8 ± 0.5	139.6 ± 26.7	86.7 ± 16.6
CAP-23-RIL3_BF4	7.4 ± 2.1	5.2 ± 1.0	139.9 ± 11.2	103.2 ± 14.2

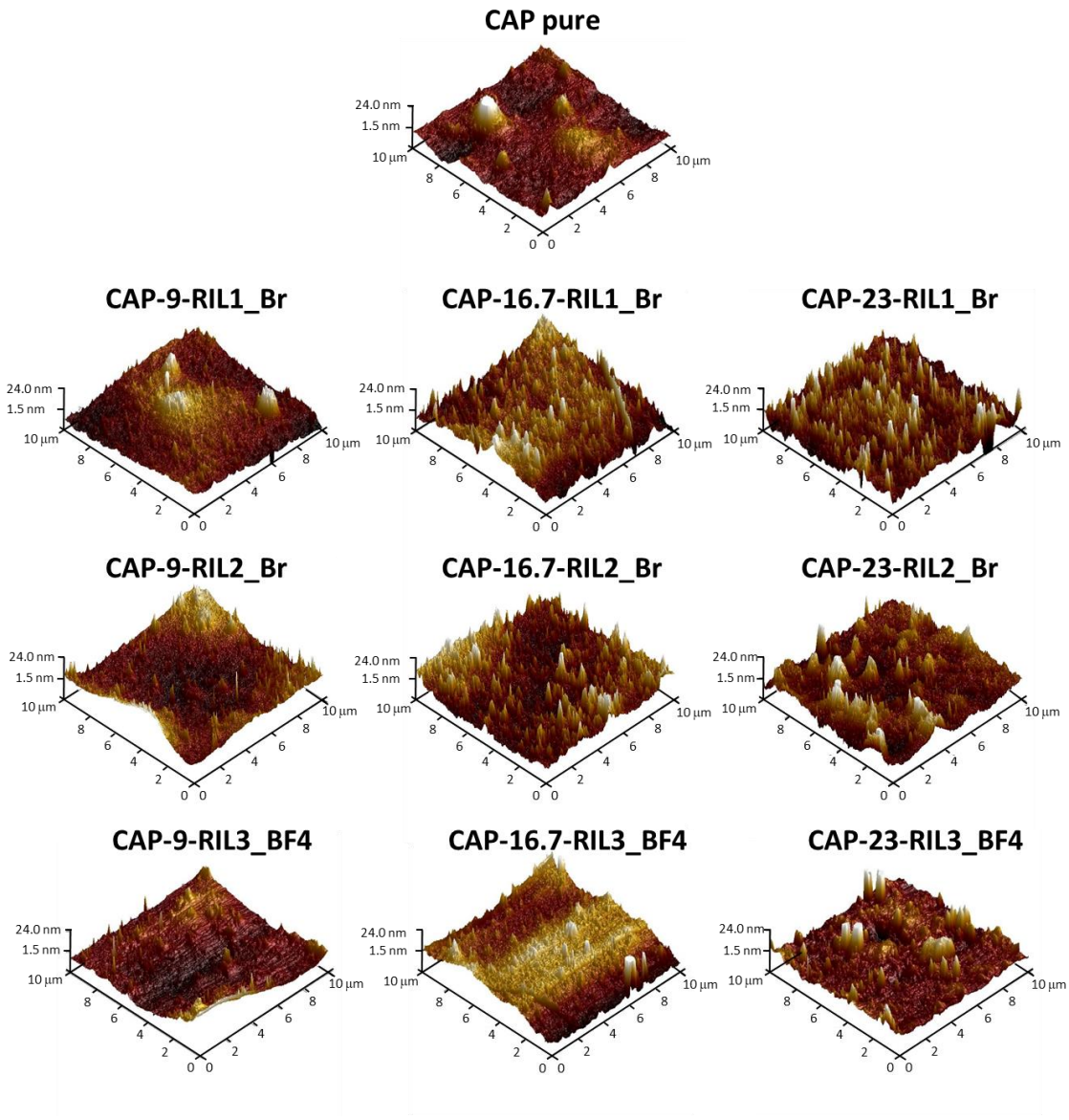

Figure 56. 3D profile of pristine CAP and CAP-RILs membranes.

4.2.5 Equilibrium Properties

The contact angle (Figure 57) and swelling measurements (Figure 58, Table 22) of the CAP-based membranes with different ionic liquids (RILs and PIL) were performed in order to study the affinity between polymer and solvents of various polarity. The molecules permeation during the pervaporation process consists of three consecutive steps: sorption, diffusion, and desorption that are described by the solution-diffusion mechanism [2, 4, 41]. Sorption and diffusion phenomena play a crucial role in the molecules permeation. Therefore, the studies of polymer membrane-permeates

interaction can provide the important information about appropriate membrane material for a given separation process.

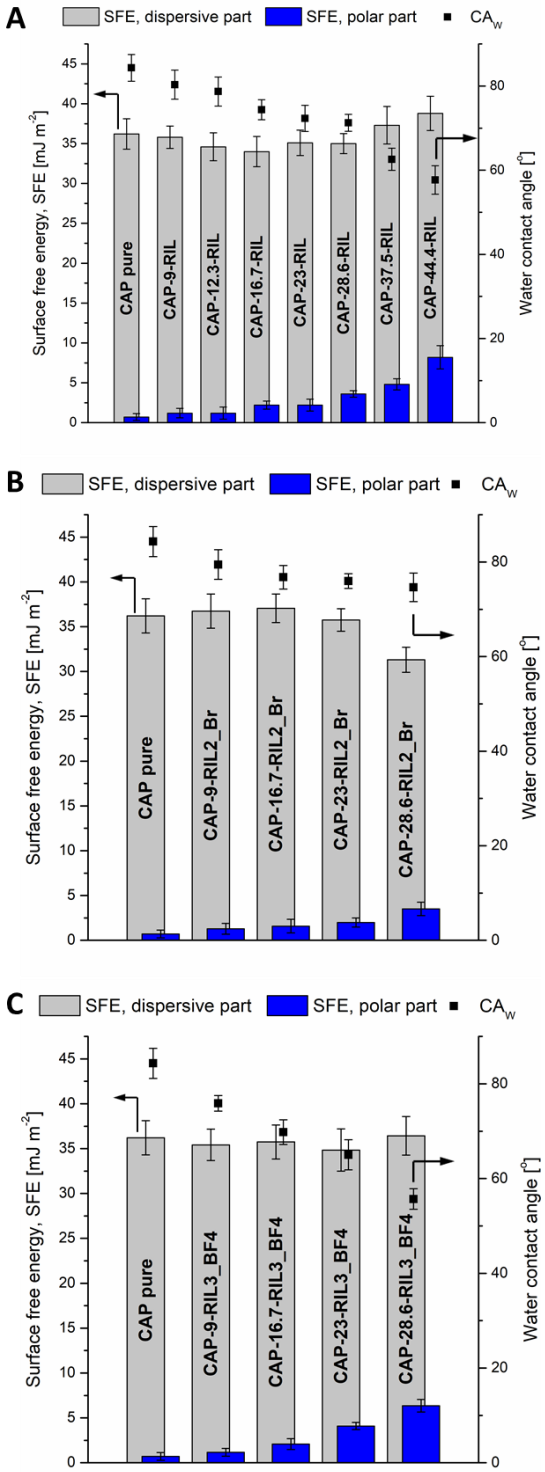

Figure 57. Water contact angle, dispersive γ^D and polar γ^P components, and surface free energy (*SFE*) of (A) CAP-RIL1_Br, (B) CAP-RIL2_Br, and (C) CAP-RIL3_BF4 membranes.

The contact angle measurements revealed the decreased value of water contact angle of CAP-RIL membranes as compared to pristine CAP (Figure 57). For example, CAP-based membrane with 44 wt.% RIL1_Br possessed the water contact angle decreased to 59°, comparing to 86° for pristine CAP membrane (Figure 57A). The incorporation of RILs improves the hydrophilicity of the CAP membranes surface due to the raised number of hydrophilic groups, which enhances the hydrogen bonding between the membrane surface and water molecules [74]. Consequently, the wettability of the CAP-RIL membrane surface is improved. Such behavior is in accordance with the results of AFM analysis indicating the increase of the membrane surface roughness with the increasing RILs content. As a result, the enhanced roughness of CAP-RIL membranes results in more hydrophilic membrane surface.

This result is also confirmed by the raised values of polar component as a function of RIL content (Figure 57). Such behavior was related to the enhanced hydrophilicity of the membrane surface due to the hydrophilic nature of ionic liquids. Moreover, the presence of RIL practically did not influence the dispersive part of surface free energy. This fact indicates that RILs possess the predominant influence on the surface hydrophilicity of CAP-based membranes [221]. It should be mentioned that the obtained membranes are highly desirable for the hydrophilic pervaporation.

The membrane sorption is an important step in the pervaporation process that can be influenced by the membrane morphology and the solvation ability of functional groups in studied membranes [4].

The polymer-solvent interactions can be also assessed based on the Hansen's Solubility Parameters δ [222]. According to Hansen's approach [222], the cohesion energy of a liquid (δ value) can be divided into three separate parts – quantitatively describing the nonpolar, atomic (dispersion) interactions (δ_d), the permanent dipole–dipole interactions (δ_p) and the hydrogen bonding interactions (δ_h). The Hansen's cohesion energy is the total cohesion energy of a liquid (E) divided by the molar volume (V_i) [222]:

$$\delta = \sqrt{\frac{E}{V_i}} \tag{54}$$

Taking into account the partial solubility parameters δ_i of investigated pure solvents and polymer as well as feed mixture and polymer, the distance parameter $\Delta_{i,j}$ was calculated (Eq. (6), Table 21) [4, 222, 223].

In general, the higher affinity between two components corresponds to the lower value of distance parameter $\Delta_{i,j}$ [26]. The dispersion parameter δ_d is similar for all solvents and, hence, δ_d does not influence the polymer-solvent interactions. Simultaneously, the polar δ_p and hydrogen bonding δ_h parameters possess the predominant influence on the interactions between investigated components.

Table 21. Hansen's solubility parameters and distance parameter of CAP [223] and solvents [222] used in sorption measurements.

Solvent	Hansen's Solubility Parameters [MPa$^{1/2}$]			Distance parameter Δ [MPa$^{1/2}$]
	δ_d	δ_p	δ_h	
CAP	27.3	10.6	6.5	-
H_2O	15.5	16.0	42.3	38.1
EtOH	15.8	8.8	19.4	17.4
IPA	15.8	6.1	16.4	15.8
H_2O-IPA*	15.8	7.0	18.9	17.3
H_2O-IPA**	15.8	7.3	18.9	17.8
H_2O-EtOH*	15.8	9.5	21.5	19.0

*Data corresponds to tested binary feed mixture containing 9.25 wt.% of water.

**Data corresponds to tested binary feed mixture containing 12 wt.% of water.

The individual contributions of Hansen's solubility parameters (δ_d, δ_p, and δ_h) for binary mixture (δ_m) used in pervaporation containing 9.25 and 12 wt.% of water was calculated according to:

$$\delta_m = [dD, dP, dH] = \frac{(a \cdot dD_1 + b \cdot dD_2), (a \cdot dP_1 + b \cdot dP_2), (a \cdot dH_1 + b \cdot dH_2)}{a+b} \quad (55)$$

where dD_1, dP_1, dH_1 are dispersive, polar and hydrogen bonding interactions, respectively, for first component (water), dD_2, dP_2, dH_2 are dispersive, polar and hydrogen bonding interactions, respectively, for second component (propan-2-ol), and a and b are parameters describing mixture composition [224].

The swelling ability in water, ethanol, and propan-2-ol of native CAP membrane and CAP membranes modified with RILs and PIL was assessed based on the molar swelling degree SD_M value (Figure 58 and Table 22). In principal, the higher value of SD_M for pure CAP corresponds to lower value of distance parameter $\Delta_{i,j}$ between CAP and tested solvents (Table 21).

It can be seen that the lowest SD_M value was found in the case of CAP membrane equilibrated with water (Figure 58), which is in accordance with the significantly higher distance parameter $\Delta_{i,j}$ between CAP and water as compared to ethanol and IPA (Table 21). On the other hand, it can be noticed that SD_M of pure CAP membrane equilibrated with IPA is the highest one, despite the higher affinity between CAP and IPA reflected by the lowest distance parameter. This difference can be related to the lower molar volume of ethanol and, thus, to the better accessibility of the CAP functional groups for ethanol molecules.

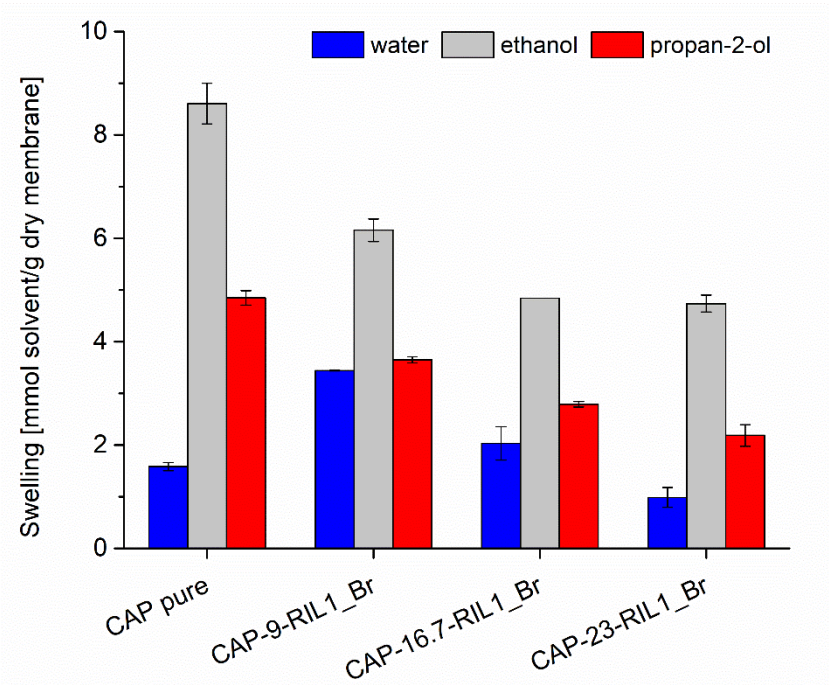

Figure 58. The molar swelling degree SD_M of CAP and CAP-RIL membranes.

CAP modification with RILs influences the CAP-RIL membranes swelling ability, namely, the RIL incorporation into CAP-based membranes raises their water swelling comparing to pristine CAP membrane (Figure 58). Also, it can be seen that CAP-based membranes possess the decreased swelling in the contact with organic solvents (ethanol and propan-2-ol) because of the RIL incorporation. Such tendency can be correlated to

the hydrophilic character of tested RIL [21]. These findings are in accordance with the obtained in this work water contact angles and calculated values of *SFE* (Figure 57). Ye et al. [21] reported that the IL hydrophilic/hydrophobic character and, thus, its affinity to solvents of different polarity, is influenced by the type of IL anion [21].

Taking into consideration the hydrophilicity of studied RILs and low polarity of ethanol and propan-2-ol (relative permittivity: 25.16 and 20.18, respectively (Table 23)), it is found that studied CAP-based membranes are less compatible with organic solvents comparing to water (value of relative permittivity for water is equal to 80.20 (Table 23)). Moreover, the smaller molar volume of water molecules results in its better affinity and facilitated penetration into transport channels that can be formed in ionic liquid [225].

Table 22. The molar swelling degree SD_M of native CAP and CAP-PIL membranes.

Sample name	SD_M [mmol solvent/g dry membrane]		
	H_2O	EtOH	Propan-2-ol
CAP pure	1.7	7.0	5.3
CAP-12.3 wt.% PIL	3.6	6.4	4.4
CAP-16.7 wt.% PIL	3.6	6.7	3.9
CAP-28.6 wt.% PIL	5.6	7.5	4.4
CAP-37.5 wt.% PIL	9.9	12.3	6.9
CAP-44.4 wt.% PIL	16.9	19.9	9.1

The swelling behavior of CAP-PIL membrane reflected by the values of molar swelling degree is presented in Table 22. It can be seen that the addition of PIL into CAP-based membranes increased the SD_M values for all studied solvents, whereas the CAP-PIL membranes equilibrated with water and ethanol revealed the most pronounced improvement of the membranes swelling. In addition, CAP-based membranes with the PIL content above 16.7 wt. % possess SD_M for water exceeding those for IPA, whereas the water SD_M is similar to that in EtOH. This behavior can be correlated to the PIL hydrophilicity and it confirms the predominant influence of the IL and its nature on the polymer-based membranes properties.

Luo et al. [77] investigated the effect of the temperature and EtOH concentration in the feed EtOH–ethyl *tert*-butyl ether (ETBE) mixture on the swelling of the CAP

membrane. The increasing EtOH content in the feed mixture resulted in the raise of the swelling ratio reaching the maximum for around 40 wt. % of EtOH. The swelling ratio of the CAP membrane equilibrated with pure EtOH was higher than that observed in this work. It was equal to around 14 g EtOH/g dry membrane, which corresponds to 304.3 mmol EtOH/g dry membrane. It was noticed that upon rising the temperature from 40 to 60°C the swelling ratio increased because of weaker interactions and increased distance between polymer chains.

Table 23. Physicochemical properties of water, ethanol, and propan-2-ol.

Solvent	Molar volume (at 293.15 K)	Molar mass	Boiling temperature	Relative permittivity (at 293.15 K)	Density (at 293.15 K)
	V_m	M	T	ε	d
	[$cm^3\ mol^{-1}$]	[$g\ mol^{-1}$]	[°C]	[-]	[$g\ cm^{-3}$]
Water	18.1	18.0	100	80.20 [226]	0.9982
Ethanol	56.9	46.1	78	25.16 [226]	0.81 *
Propan-2-ol	77.1	60.1	82	20.18 *	0.78 *

* Information supplied by the producer.

4.2.6 Transport Properties

Taking into consideration the results of swelling measurements as well as the PIL insolubility in water and its negligible solubility in propan-2-ol, water-propan-2-ol was chosen as a testing mixture for pervaporation performance.

CAP-RIL and CAP-PIL membranes were studied in the pervaporative dehydration of propan-2-ol with the water concentration range in the feed mixture varied from 7 to 14 wt. %. The membrane effectiveness was evaluated in terms of separation factor β (Eq. (24)) and thickness-normalized process separation index (PSI_N) (Eq. (25)). The special attention was paid to the pervaporation effectiveness of CAP-based membranes in contact with the azeotropic composition of water-propan-2-ol feed mixture (*i.e.* containing 12 wt. % of water). The obtained results are gathered in Figure 59 – Figure 61.

All tested CAP-based membranes are selective towards water as the increase of the water content is observed in permeate with the increase of the water content in feed

mixture. The high affinity between the native CAP membrane and water-propan-2-ol mixture corresponds to the low value of distance parameter $\Delta_{i,j}$ (Table 21). Moreover, the enhanced transport of water molecules through the membrane can be seen (Figure 59). Simultaneously, the water content in permeate for CAP pure membrane increased from 12 to 60 wt.%.

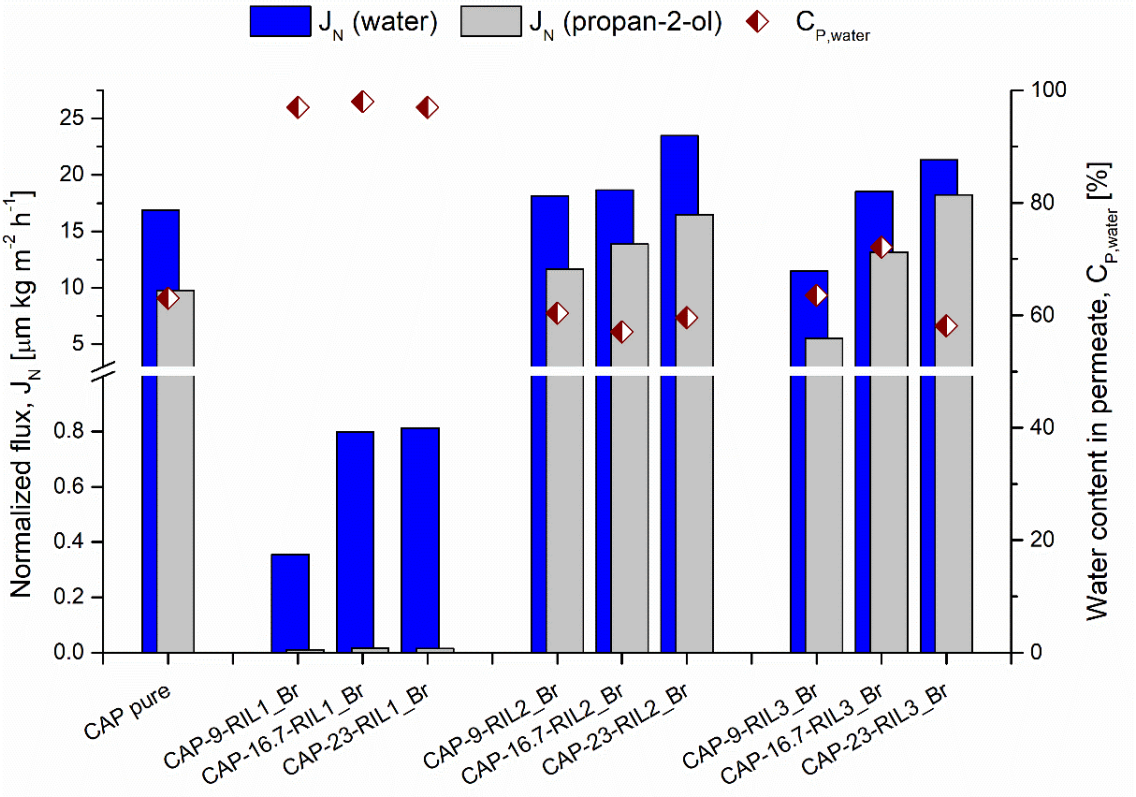

Figure 59. Thickness-normalized flux of water and propan-2-ol and water content in permeate for CAP and CAP-RIL membranes in contact with water-propan-2-ol mixture containing 12 wt. % of water (azeotropic mixture). T = 35°C.

The CAP modification with RIL1_Br leads to the great improvement of separation factor β: from 12 (for pristine CAP membrane) to ca. 380 (for CAP-16.7-RIL1_Br membrane) (Figure 60). Unfortunately, the addition of RIL1_Br reduced the transport properties of tested CAP-RIL1_Br membranes as compared to the pure CAP membrane. This behavior was reflected by the remarkable drop of water thickness-normalized fluxes (Figure 60), despite the fact that the CAP-RIL1_Br membranes possess enhanced water swelling in comparison to pristine CAP membrane. Such hindered permeate transport can be correlated to the chemical modification of CAP with RIL. The presence of RIL1_Br decreases the free volume of CAP-RIL1_Br membranes because of the enhanced

chemical interaction between polymer and IL. However, it is noteworthy that CAP-RIL1_Br membranes are efficient in propan-2-ol dehydration that allows breaking the water-propan-2-ol azeotrope. The maximum water content in permeate was reached for CAP-16.7-RIL membrane and it was equal to 98.1 wt. % (Figure 59). Ong and Tan [130] reported the effective separation of the ternary azeotropic mixture of ethyl acetate, ethanol, and water in contact with for buckypaper membranes based on PVA immobilized with 1-butyl-3-methylimidazolium tetrafluoroborate ionic liquid. The pervaporation performance at 30 °C revealed a total permeation flux of 0.385 $kg \cdot m^{-2} \cdot h^{-1}$ and a separation factor equal to ca. 250 [130].

On the other hand, the analysis of the overall pervaporation efficiency for CAP-RIL1_Br membranes reflected by the pervaporation separation index *PSI* witnesses to the occurrence of the typical trade-off between the separation and transport properties of the CAP-RIL1_Br membranes. The decreasing PSI_N value for CAP-RIL1_Br membranes comparing to pure CAP reflects the diminished membranes efficiency as a result of the RIL1_Br presence (Figure 60).

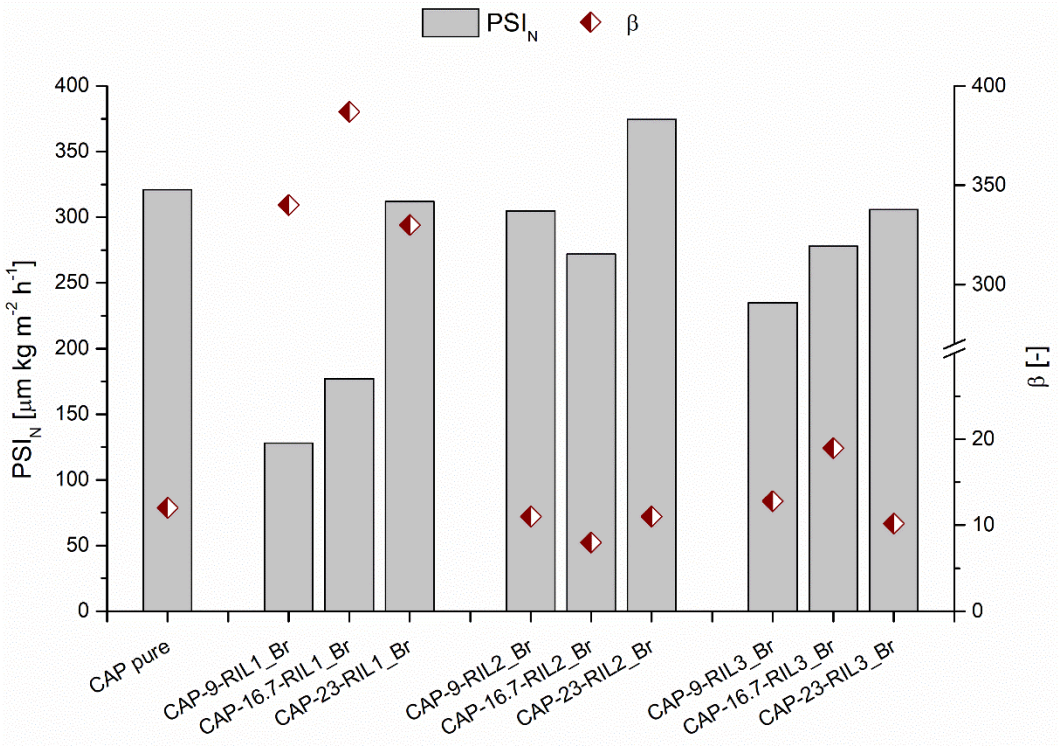

Figure 60. Efficiency of CAP and CAP-RIL membranes in contact with water-propan-2-ol mixture containing 12 wt. % of water (azeotropic mixture). T = 35°C.

Considering the CAP-RIL2_Br and CAP-RIL3_BF4 membranes, it was found that RIL2_Br and RIL3_BF4 did not significantly influence the separation effectiveness and transport properties of the CAP-based membranes (Figure 59 and Figure 60). CAP-RIL2_Br and CAP-RIL3_BF4 membranes possess the values of separation factor β and thickness-normalized permeate fluxed comparable to those for pure CAP membrane. Taking into account the *PSI* values, it was found that RIL2_Br and RIL3_BF4 did not influenced the overall membranes efficiency in the dehydration of propan-2-ol.

In the case of CAP-PIL membranes, the increasing PIL content in the CAP-based membranes resulted in the remarkable enhancement of membrane transport properties (Figure 61).

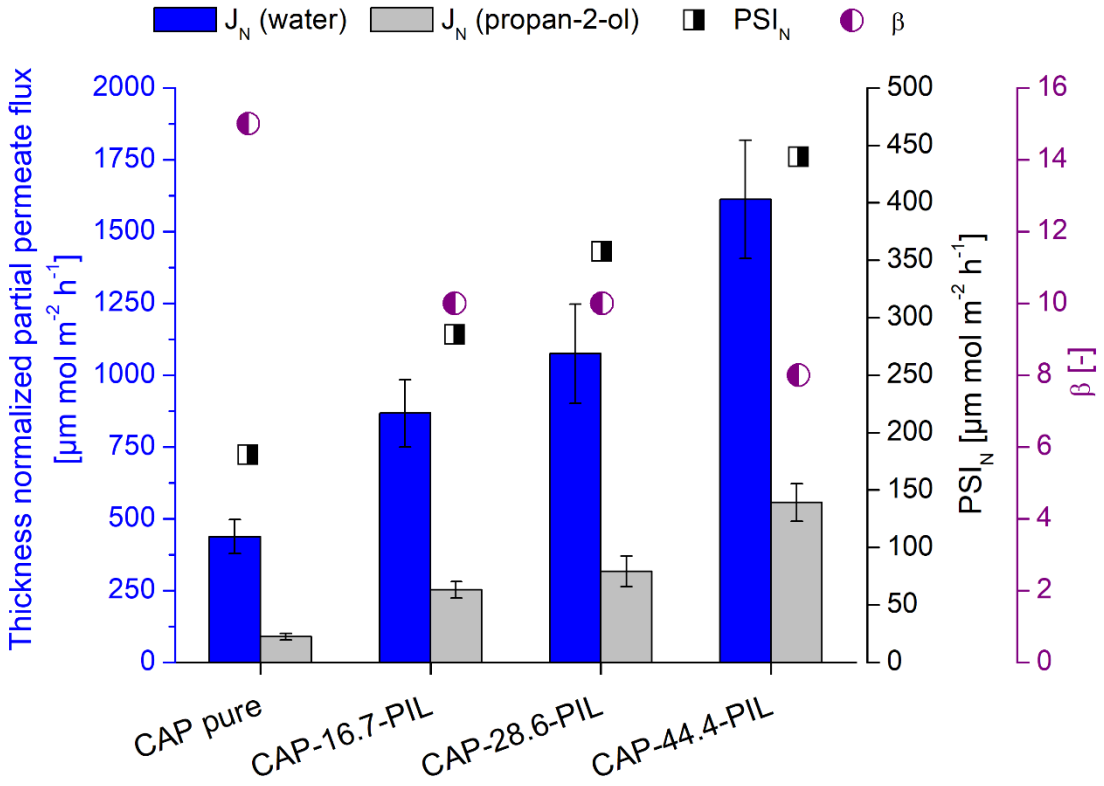

Figure 61. Thickness-normalized flux of water and propan-2-ol and efficiency of CAP and CAP-PIL membranes in contact with water-propan-2-ol mixture containing 12 wt. % of water (azeotropic mixture). T = 35°C.

The CAP-based membranes containing PIL increased the CAP-PIL membranes hydrophilicity as it was revealed by sorption behavior and, therefore, the increased thickness-normalized partial permeate flux of water was observed. In addition, the increasing PIL content in the CAP-based membranes improved the separation

effectiveness of the investigated membranes expressed by PSI_N. The membrane performance was enhanced more than 2.4 times comparing to the pristine membrane. On the other hand, the further raise of PIL content (up to 44.4 wt.%) resulted in the mitigation of separation properties expressed by separation factor β (Figure 61).

The transport properties of CAP-RIL membranes were also investigated by studying the permeation of liquid water and chosen gases with various diameter and critical temperature (N_2, O_2, and CO_2) (Table 24).

Considering the water permeation kinetics, the experimental curves of water flux were fitted taking into account the possible water plasticization effect in CAP-based membranes as a function of local water concentration C according to the following equation:

$$D = D_0 e^{\gamma C} \tag{56}$$

where D_0 is the diffusion coefficient when the water concentration tends to 0, γ is the plasticization factor, and C is the local water concentration in the membrane [34, 227].

Figure 62 presents the curves of water flux in a dimensionless scale of flux and time for the CAP-9-RIL1_Br membrane as an example of the very good fitting of the experimental water flux for studied CAP-based membranes.

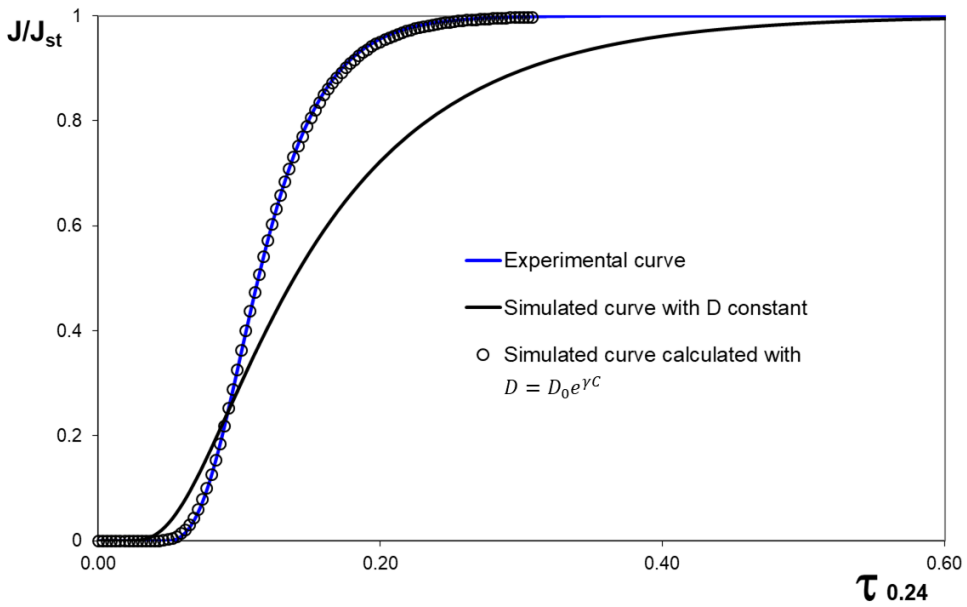

Figure 62. Curves of experimental and simulated water flux obtained for CAP-9-RIL1_Br membrane.

It was found that the water barrier properties decreased with the increasing RIL content in the CAP-based membranes whatever the used RIL type. CAP-RIL2_Br membranes were found to be the most permeable among the tested CAP-based membranes (Figure 63). This is in accordance with the pervaporation results and the fact that the highest thickness-normalized water permeation fluxes were in the case of CAP-based membranes containing RIL2_Br.

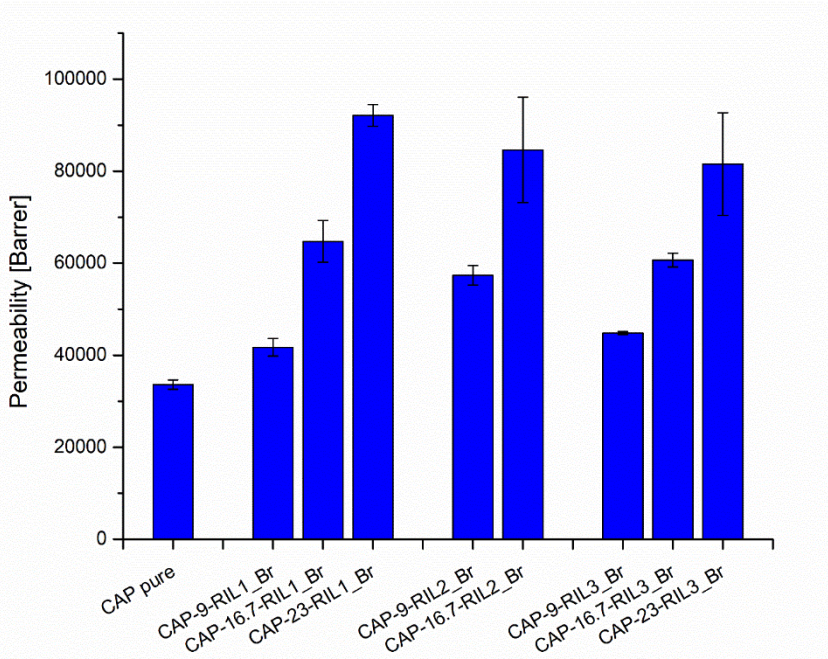

Figure 63. Water permeability of pure CAP and CAP-RIL membranes as a function of RIL content.

Figure 64 presents the gas permeation results carried out at 25 ± 1 ° C for CAP-based membranes modified with RILs. Unlike water molecules, the small permanent gas molecules, such as N_2, O_2, and CO_2, have no or very few interactions with polymers and they can be used as probes of the molecular architecture and the microstructure of materials. As it was described in section 1.2, the gas transport through the dense membranes is described by the solution-diffusion mechanism. Therefore, the obtained results of the gas permeation measurements were evaluated taking into account the permeability *P* as a product of the solubility *S* and the diffusivity *D* (Eq. (5)) [27]. The results of permeability *P*, diffusion *D*, and solubility *S* coefficients as well as the ideal selectivity were presented in Figure 64 and Table 25 as a function of RIL content.

The obtained results of N_2, O_2, and CO_2 permeation measurements for the native CAP membrane showed that the values of permeability *P*, diffusion *D*, and solubility *S*

coefficients are comparable with the literature results for the native CAB membrane [228] (Figure 64).

It can be seen that the values of permeability coefficient *P* for tested CAP-based membranes exhibit the well-known tendency discussed in section 1.2.1.2: $P_{N2} < P_{O2} < P_{CO2}$. Such behavior is related to the correlation of permeability with diffusivity (kinetic parameter) which is dependent on molecular size and solubility (thermodynamic parameter) which is dependent on the critical temperature T_c (Table 24).

The order of Van der Waals molar volumes of gaseous molecules, $V_m\text{-}VdW_{O2} < V_m\text{-}VdW_{N2} < V_m\text{-}VdW_{CO2}$, is inverse to that of the gas diffusion coefficients *D*, as shown in Figure 64B. The solubility coefficients *S* follow the order of the critical permeate temperatures, $T_{c,N2} < T_{c,O2} < T_{c,CO2}$, as shown in Figure 64C. Thus, the very low N_2 critical temperature associated with a large Van der Waals molar volume (Table 24) leads to lower membrane permeability to nitrogen than to oxygen and carbon dioxide (Figure 64A). The experimental values collected in Figure 64 are in a good agreement with the theory.

Table 24. Dynamic diameter ϕ_d, Van der Waals molar volume $V_m\text{-}VdW$, and critical temperature T_c of N_2, O_2, and CO_2 gases.

Permeant	ϕ_d [Å] [229]	$V_m\text{-}VdW$ [$cm^3\ mol^{-1}$] [230]	T_c [°C] [231]
N_2	3.64	39.13	-146.94
O_2	3.46	31.83	-118.56
CO_2	3.30	42.46	31.15

As it can be seen, the type of the imidazolium-based cation does not alter the permeability of the CAP-based films. The presence of 9 and 16.7 wt. % of RIL1_Br and RIL2_Br in CAP membranes slightly reduced the diffusion coefficient *D* for tested gases (Figure 64B). Simultaneously, CAP-based membranes with 9 and 16.7 wt. % of RIL1_Br and RIL2_Br showed lower permeability and, thus, higher barrier properties reflected by lower permeability coefficients comparing to the native CAP membrane (Figure 64A). The reduced transport of gas molecules through the membrane can be associated with a reduction of the free volume in the polymer membrane because of the RIL presence. On the other hand, concerning the CAP-RIL1_Br membranes, it can be seen that the CAP-based membranes become more permeable and less selective with the increasing content

of RIL1_Br, what is reflected by the increase of the permeability *P* and the decrease of the ideal selectivity values (Table 25).

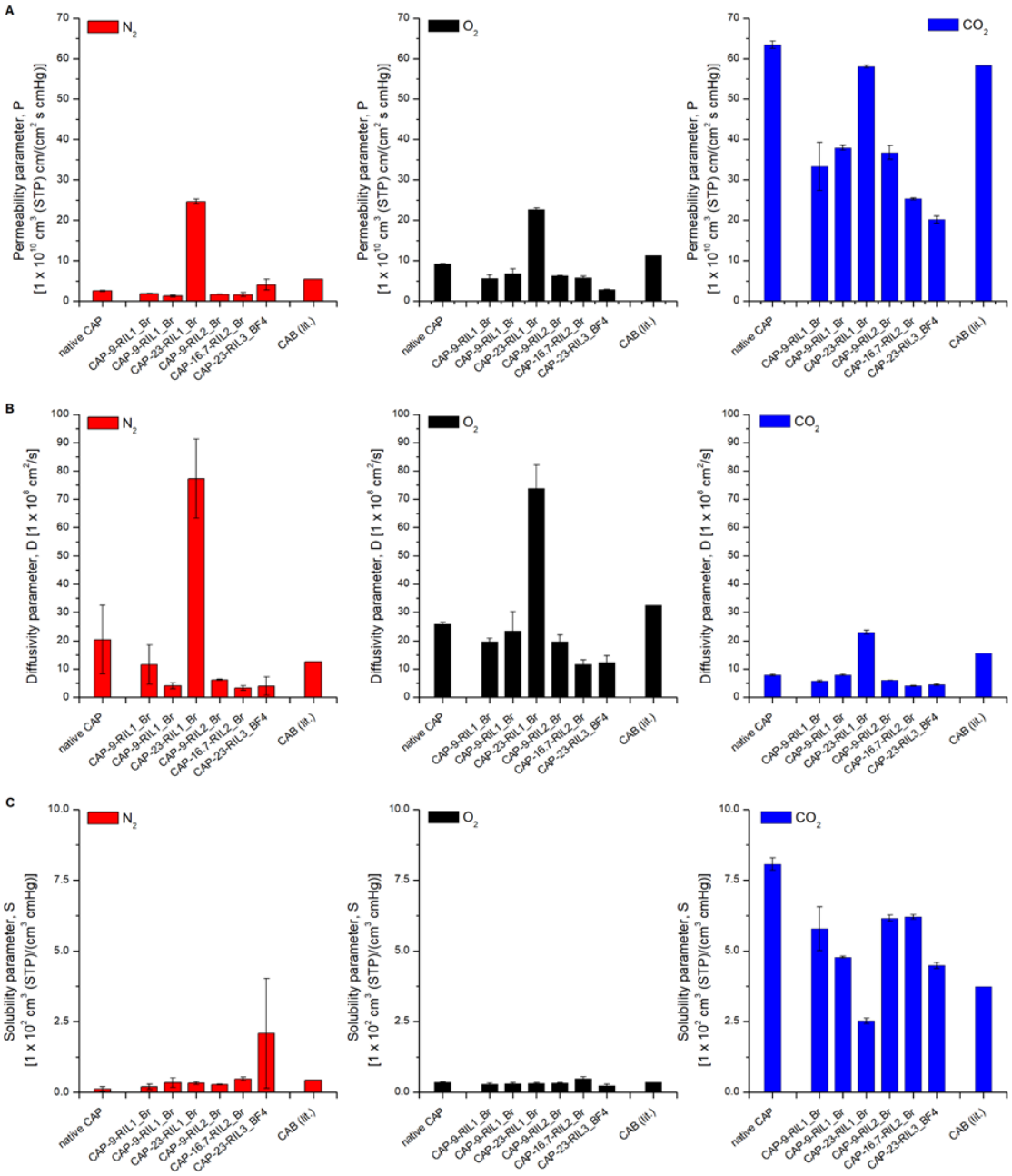

Figure 64. Permeability (A), diffusion (B), and solubility (C) coefficients for CAP-RIL membranes compared to literature data for a native CAB membrane [228].

A further increase of RIL1_Br content (23 wt.%) caused a significant increase of the diffusion coefficient *D* values for all tested gases, as well as an increase of the permeability coefficient *P* values for O_2 and N_2. The facilitated gas transport through the CAP-23-RIL1_Br membrane can be due to the fact that a higher RIL1_Br content in the CAP based membrane resulting in the formation of RIL-rich domains that act as a

transport channels for gas molecules. It was also found that the presence of 23 wt. % of the RIL1_Br leads to CAP-based membrane plasticization, as the significant increase in ε_{max} and the decrease in *E* was observed indicating the influence of RIL on CAP-RIL membranes flexibility. The presence of RIL-rich domains was observed by SEM and AFM analysis. It is found that the type of anion influences the membrane permeability and diffusivity of CAP-based membranes containing 23 wt. % of RIL. CAP-23-RIL3_BF4 is the most barrier membrane towards studied gases.

Table 25. Pure gas permeability *P* and ideal gas selectivity in respect to nitrogen (P/P_{N2}) for CAP and CAP-RIL membranes.

Membrane	Gas	*P* [Barrer]	P/P_{N2} [-]
native CAP	N_2	2.6	-
	O_2	9.2	3.6
	CO_2	63.4	24.8
CAP-9-RIL1_Br	N_2	1.9	-
	O_2	5.6	3.0
	CO_2	33.3	17.6
CAP-16.7-RIL1_Br	N_2	1.2	-
	O_2	6.8	5.5
	CO_2	38.0	30.4
CAP-23-RIL1_Br	N_2	24.6	-
	O_2	22.7	0.9
	CO_2	58.1	2.4
CAP-9-RIL2_Br	N_2	1.7	-
	O_2	6.2	3.7
	CO_2	36.8	22.0
CAP-16.7-RIL2_Br	N_2	1.6	-
	O_2	5.8	3.6
	CO_2	25.3	15.8
CAP-23-RIL3_BF4	N_2	4.1	-
	O_2	2.9	0.7
	CO_2	20.2	5.0

1 Barrer = $\frac{10^{-10} cm^3(STP)\cdot(cm\ membrane\ thickness)}{(cm^2\ membrane\ area)\cdot(cmHg\ pressure)\cdot s}$

4.3.7 Conclusions

In this study, the alteration of the physicochemical, transport, and separation properties of CAP-based membranes was achieved by the incorporation of RILs and PIL into CAP membrane. CAP-based membranes chemically modified with RIL and blended with PIL possessed the improved mechanical properties. The obtained results confirmed the CAP plasticization using RILs and PIL. Moreover, the improved mechanical strength of CAP-RIL membranes in comparison to CAP-based membranes with commercial plasticizers was observed. The obtained results demonstrated the predominant influence of the RIL and PIL incorporation on enhancement of hydrophilic properties of CAP-based membranes surface. CAP-RIL and CAP-PIL membranes were water selective in the pervaporative dehydration of propan-2-ol. It is found that the immobilization of RIL enhances separation properties of CAP-based membranes, simultaneously diminishing its transport properties in the pervaporative dehydration of propan-2-ol.

General Conclusions & Prospects

The aim of the present PhD thesis was to elaborate PVA and CAP-based membranes with enhanced transport and separation behavior. For this purpose, the influence of the polymer modification with RILs and PIL on the physicochemical, equilibrium, barrier, and transport properties of the PVA- and CAP-based membranes was investigated. Furthermore, the chosen membranes were tested in pervaporation process in contact with water-propan-2-ol mixture. In order to understand the phenomena occurring in the polymer-IL membranes, the several types of membranes were prepared and investigated: PVA-RIL1_Br, PVA-RIL2_Br, CAP-RIL1_Br, CAP-RIL2_Br, and CAP-RIL3_BF4. The choice of these polymer-IL systems resulted from the solubility and miscibility of the polymer and ILs. The selection of polymers was based on their biodegradable and harmless nature. Imidazolium-based ILs were chosen because of the tunable structure of imidazolium cation.

The two-step crosslinking approach (*i.e.* the esterification reaction and the subsequent heat-treatment) of PVA-based membranes was efficient and it influenced the physicochemical characteristics of PVA-based materials. It was found by the FTIR-ATR analysis that the increase of the SSA concentration and crosslinking temperature decreases the intensity of bands corresponding to the vibration of -OH groups and increases the intensity of ester bond bands between PVA and SSA due to the esterification reaction, which confirms the efficiency of crosslinking. The increasing SSA content significantly raised the crosslinking density what resulted in the membrane reinforcement and the improvement of the membranes resistance towards liquid water. Studies of mechanical properties of PVA-SSA membranes by tensile test showed that the increase of the SSA content reduced the elongation at break (from 316% to 98% for pure PVA membrane and membrane containing 33 wt.% SSA and crosslinked at 160°C, respectively). The sorption studies of the elaborated membranes performed in pure water, methanol and propan-2-ol revealed the decreasing membrane swelling with the raised SSA concentration for all studied crosslinking temperatures. The swelling of PVA-SSA membranes was the highest in water and the lowest in propan-2-ol, i.e. the swelling in water was around 4000-fold and 16-fold higher than in propan-2-ol and methanol, respectively. These results, i.e. high swelling water ability, explain also the difficulty to perform liquid water permeation study. For this reason the water vapour permeation

measurement at different relative humidity levels was carried out. The crosslinking at 120°C and the low concentration of SSA (5 and 9 wt.%) were not sufficient for complete crosslinking, wherein 50 wt.% SSA was too high, thus decreasing the membranes stability in contact with solvents. Therefore, the optimised conditions for the crosslinking are: 9 and 23 wt.% SSA and 140 and 160°C for thermal crosslinking.

The CAP-based membranes were plasticized using citrate esters what was reflected by the decrease of the membranes rigidity and the increase of the elastic properties of tested CAP-based materials. The increase of both elongation at break and stress at break, and the decrease of Young's modulus with the increasing content of plasticiser testified to the improved mechanical properties of the membranes. TBC and ATBC plasticizers possessed the influence on the CAP-based membranes' surface hydrophilicity. The addition of plasticizers decreased the water contact angle of the plasticized CAP-based films compared to the native CAP membrane. Moreover, the increase of the plasticiser content reduced swelling ability of the membranes in water.

The two-step approach combining chemical crosslinking and the thermal treatment is an efficient, but relatively time-consuming method for the reinforcement of PVA-based membrane material and tailoring its physicochemical properties. On the other hand, the use of commercial plasticizers is an efficient method for the plasticization of CAP-based membrane material. However, the addition of TBC and ATBC does not influence the CAP-based membranes swelling in water that restricts their further application in hydrophilic pervaporation. Moreover, it is known that citrate esters can migrate and they can be released from the polymer-based materials [55]. Therefore, the other approach, namely, the use of ILs was also studied in this work. Besides, the influence of the IL structure on the membrane properties is investigated.

The studies of PVA- and CAP-based membranes elaborated with compatible ester-functionalized imidazolium-based ionic liquids revealed the predominant influence of RIL content on the membranes physicochemical properties. The FTIR-ATR analysis of PVA-RILs membranes showed the formation of the physical junctions induced by the hydrogen bond interactions between PVA and RILs (RIL1_Br and RIL2_Br) which partially replaced the intermolecular interactions of PVA chains. It is reflected by the fact that the increase of RIL content leads to the intensity increase of C=O and C-O stretching vibration bands of -COO- ester groups in PVA-RIL membranes, as well as the stretching vibration band of -OH groups attached to the main chain of PVA.

The enhancement of the intramolecular interactions between RIL and PVA influenced the mechanical properties of PVA-RILs membranes. It was found that PVA-RILs membranes with low RIL content were more rigid compared to pure PVA because of the physical crosslinking. In the presence of RIL with high content (23 wt.%), PVA-RIL membranes with increased elastic properties were obtained. The observed dual functions of RIL (as a promoter of physical crosslinking and plasticizer) depending on the RIL content provide the possibility for obtaining of PVA-RIL materials with tailored mechanical and thermal properties. It was found that the most reinforced PVA-9-RIL membrane possessed the most improved thermal stability among all tested membranes.

Considering the CAP-IL membranes, the increasing IL content enhanced elongation and reduced brittleness of studied CAP-based materials. In general, the elongation at break value increased, as well as both stress at break and elastic modulus decreased with the raise of the RIL content. Such behavior confirmed the plasticization effect of RIL for CAP-based membrane materials. It was noted that the presence of the highest PIL content equal to 44.4 wt.% deteriorated the mechanical properties of CAP-based membrane because of the increased inner stress in CAP-44.4-PIL membrane.

In general, ILs possess the remarkable influence on the thermal stability of PVA- and CAP-based membranes with higher IL content. In the case of CAP-RIL membranes, RIL incorporation to CAP structure diminishes the degradation temperature because of the formation of ester bonds during the polymer modification by transesterification reaction. The comparison of the thermograms for CAP-RIL membranes revealed also the influence of the RIL structure on the thermal stability of studied materials. The membranes with RIL1_Br possessed the lower decomposition temperature comparing to the ones with RIL2_Br and RIL3_BF4. Such behavior was correlated to the more branched structure of RIL1_Br imidazolium cation and the presence of strongly coordinated bromide anion.

All studied RILs improved the hydrophilicity of the CAP-RILs membrane surface what was reflected by the decrease of water contact angle and by the increase of polar part of *SFE*. However, only the addition of RIL1_Br with two active sites to CAP-based membranes led to the great improvement of separation factor β: from 12 (for pristine CAP membrane) to ca. 380 (for CAP-16.7-RIL1_Br membrane). The reduced transport properties of tested CAP-RIL1_Br membranes comparing to the pure CAP membrane were also observed. The presence of RIL1_Br decreased the free volume of CAP-

RIL1_Br membranes because of the enhanced chemical interaction between polymer and IL due to the chemical modification of CAP with RIL.

The chemical modification of CAP-based membranes with RIL was confirmed based on the results of NMR analysis of CAP-RIL1_Br and CAP-RIL2_Br membranes comparing to the pure RILs. The successful transesterification reaction between the RIL and CAP was evidenced by the shift of the signals corresponding to the proton at C2 carbon as well as at C4 and C5 in the imidazole ring. It is observed that reaction between CAP and RIL leads to the various partial substitution of ester groups in RILs as different *DS* values are obtained. The quantitative assessment of the transesterification reaction between RILs and CAP revealed, however, that the transesterification reaction was more efficient in the case of the RIL1_Br with two ester groups in the structure. This result was reflected by the higher *DS* value for CAP-RIL1_Br membranes compared to CAP-RIL2_Br ones.

The partial substitution of ester groups in RIL resulted in the appearance of the RIL-rich domains as observed from the results of SEM and AFM analysis. The increasing RILs content up to 23 wt.% revealed the increased heterogeneity of the membrane structure, that additionally evidenced the difference in the substitution ability of CAP with RIL.

The results obtained in this work gives the new insight to the knowledge about tailoring of the membrane properties, in particular the mechanical, equilibrium, and transport properties, which can be important for the membrane development for pervaporative separation of liquid-liquid mixtures. Knowing the accomplishments in this work, the numerous prospects could be proposed for further study. Some suggestions are listed below. They are based on the results reported in this thesis and on related issues that arose, but were not explored, during the course of this research.

- Because of the possibility of the IL leaching from the membrane structure, the importance of interactions between polymer and RILs and PIL was underlined in this work. However, the further studies concerning the polymerization of PIL monomers with simultaneous controlling the polymerization degree will be required.
- More detailed study on the influence of the ILs structure on the membrane functional properties is needed in order to understand how various properties of the polymer materials can be optimized. It must be remembered that the structure of ILs should be tailored in order to achieve IL combining the sufficiently high

viscosity (in order to prevent IL leaching) and relatively high mobility (in order to ensure the transport properties). Therefore, in order to better understand the influence of the IL structure on the properties of the investigated membranes, the studies of ILs viscosity as a function of temperature and the IL composition could be performed.

- In order to achieve industrially acceptable membranes, the transport properties of the membranes must be improved. For this purpose, the membrane morphology could be changed. For example, the supported membranes, *i.e.* the membrane composed of porous support and thin dense layer, can be elaborated. In this case the porous support will assure the high transport flux and dense layer will provide high separation behavior. In addition, the pore size of membrane should be optimized for better control of permeant transport.
- The more detailed studies of the separation effectiveness of the elaborated polymer-IL membranes could be performed by investigating the influence of the feed temperature as well as by studying the other feed mixture (*e.g.* organic-organic).
- The aging behavior of the elaborated polymer-IL membranes should be also studied in order to estimate the possible membrane duration under the experimental conditions.

References

References

[1] B. Pospiech, W. Kujawski, Ionic liquids as selective extractants and ion carriers of heavy metal ions from aqueous solutions utilized in extraction and membrane separation, Rev. Chem. Eng., 31 (2015) 179-191.
[2] W. Kujawski, M. Staniszewski, T.Q. Nguyen, Transport parameters of alcohol vapors through ion-exchange membranes, Sep. Purif. Technol., 57 (2007) 476-482.
[3] L. Karpenko-Jereb, E. Rynkowska, W. Kujawski, S. Lunghammer, J. Kujawa, S. Marais, K. Fatyeyeva, C. Chappey, A.M. Kelterer, Ab initio study of cationic polymeric membranes in water and methanol, Ionics, 22 (2016) 357-367.
[4] E. Rynkowska, J. Kujawa, C. Chappey, K. Fatyeyeva, L. Karpenko-Jereb, A.-M. Kelterer, S. Marais, W. Kujawski, Effect of the polar–nonpolar liquid mixtures on pervaporative behavior of perfluorinated sulfonic membranes in lithium form, J. Membr. Sci., 518 (2016) 313-327.
[5] C. Chappey, K. Fatyeyeva, E. Rynkowska, W. Kujawski, L. Karpenko-Jereb, A.M. Kelterer, S. Marais, Sulfonic membrane sorption and permeation properties: Complementary approaches to select a membrane for pervaporation, J. Phys. Chem. B, 121 (2017) 8523-8538.
[6] Membrane modification. Technology and applications, CRC Press, 2012.
[7] B. Smitha, D. Suhanya, S. Sridhar, M. Ramakrishna, Separation of organic-organic mixtures by pervaporation - a review, J. Membr. Sci., 241 (2004) 1-21.
[8] N.K. Acharya, V. Kulshrestha, K. Awasthi, A.K. Jain, M. Singh, Y.K. Vijay, Hydrogen separation in doped and blend polymer membranes, Int. J. Hydrogen Energy, 33 (2008) 327-331.
[9] Membrane technology benefits the food processing industry, Filtr. Sep., 41 (2004) 32-33.
[10] E.M.V. Hoek, V. Tarabara, Encyclopedia of membrane science and technology, John Wiley and Sons, Inc., Hoboken, NJ, 1999.
[11] R.W. Baker, Membrane technology and applications, Second ed., John Wiley & Sons, Ltd, 2004.
[12] H. Strathmann, Introduction to Membrane Science and Technology, Wiley-VCH, 2011.
[13] M. Mulder, Basic principles of membrane technology, Second ed., Kluwer Academic Publishers, Dordrecht, 1996.
[14] W. Kujawski, Application of pervaporation and vapor permeation in environmental protection, Pol. J. Environ. Stud., 1 (2000) 13-26.
[15] M. Ulbricht, Advanced functional polymer membranes, Polymer, 47 (2006) 2217-2262.
[16] S. Roy, N. Singha, Polymeric nanocomposite membranes for next generation pervaporation process: strategies, challenges and future prospects, Membranes, 7 (2017) 53.
[17] N. Hilal, A.F. Ismail, C.J. Wright, Membrane Fabrication, CRC Press, 2015.
[18] J. Ren, R. Wang, Preparation of polymeric membranes, in: L.K. Wang, J.P. Chen, Y.-T. Hung, N.K. Shammas (Eds.) Membrane and Desalination Technologies, Humana Press, Totowa, NJ, 2011, pp. 47-100.
[19] I. Pinnau, B.D. Freeman, Formation and modification of polymeric membranes: overview, in: Membrane Formation and Modification, American Chemical Society, Washington, DC, 1999, pp. 1-22.

[20] B. Bolto, T. Tran, M. Hoang, Z. Xie, Crosslinked poly(vinyl alcohol) membranes, Prog. Polym. Sci., 34 (2009) 969-981.
[21] Y.-S. Ye, J. Rick, B.-J. Hwang, Ionic liquid polymer electrolytes, J. Mater. Chem. A, 1 (2013) 2719-2743.
[22] K.C. Khulbe, C. Feng, T. Matsuura, The art of surface modification of synthetic polymeric membranes, J. Appl. Polym. Sci., 115 (2010) 855-895.
[23] S.S. Hosseini, E. Bringas, N.R. Tan, I. Ortiz, M. Ghahramani, M.A. Alaei Shahmirzadi, Recent progress in development of high performance polymeric membranes and materials for metal plating wastewater treatment: A review, J. Water Process Eng., 9 (2016) 78-110.
[24] J.G.A. Bitter, Transport mechanisms in membrane separation processes, Springer Science+Business Media New York, New York, 1991.
[25] T.d. Naylor, Permeation properties, in: J.C. Bevington (Ed.) Comprehensive Polymer Science and Supplements, Pergamon, Amsterdam, 1989, pp. 643-668.
[26] A. Rozicka, J. Niemistö, R.L. Keiski, W. Kujawski, Apparent and intrinsic properties of commercial PDMS based membranes in pervaporative removal of acetone, butanol and ethanol from binary aqueous mixtures, J. Membr. Sci., 453 (2014) 108-118.
[27] J. Crank, The mathematics of diffusion, Second ed., Oxford University Press, 1975.
[28] G. Jyoti, A. Keshav, J. Anandkumar, Review on pervaporation: theory, membrane performance, and application to intensification of esterification reaction, J. Eng., (2015) 1-24.
[29] D.W. van Krevelen, Properties of polymers: their correlation with chemical structure; their numerical estimation and prediction from additive group contributions, 4th ed., Elsevier B.V, Slovenia, 2009.
[30] A.Y. Houde, S.A. Stern, Solubility and diffusivity of light gases in ethyl cellulose at elevated pressures Effects of ethoxy content, J. Membr. Sci., 127 (1997) 171-183.
[31] A.S. Michaels, H.J. Bixler, Solubility of gases in polyethylene, J. Polym. Sci., 50 (1961) 393-412.
[32] T.C. Merkel, V.I. Bondar, K. Nagai, B.D. Freeman, I. Pinnau, Gas sorption, diffusion, and permeation in poly(dimethylsiloxane), J. Polym. Sci., Part B: Polym. Phys., 38 (2000) 415-434.
[33] T. Messin, N. Follain, A. Guinault, G. Miquelard-Garnier, C. Sollogoub, N. Delpouve, V. Gaucher, S. Marais, Confinement effect in PC/MXD6 multilayer films: Impact of the microlayered structure on water and gas barrier properties, J. Membr. Sci., 525 (2017) 135-145.
[34] S. Charlon, N. Follain, C. Chappey, E. Dargent, J. Soulestin, M. Sclavons, S. Marais, Improvement of barrier properties of bio-based polyester nanocomposite membranes by water-assisted extrusion, J. Membr. Sci., 496 (2015) 185-198.
[35] P.D. Chapman, T. Oliveira, A.G. Livingston, K. Li, Membranes for the dehydration of solvents by pervaporation, J. Membr. Sci., 318 (2008) 5-37.
[36] J.G. Crespo, C. Brazinha, 1 - Fundamentals of pervaporation, in: A. Basile, A.F. Khayet (Eds.) Pervaporation, Vapour Permeation and Membrane Distillation, Woodhead Publishing, Oxford, 2015, pp. 3-17.
[37] I.L. Borisov, V.V. Volkov, V.A. Kirsh, V.I. Roldugin, Simulation of the temperature-driven pervaporation of dilute 1-butanol aqueous mixtures through a PTMSP membrane in a cross-flow module, Pet. Chem., 51 (2011) 542-554.
[38] W. Kujawski, S.R. Krajewski, Sweeping gas pervaporation with hollow-fiber ion-exchange membranes, Desalination, 162 (2004) 129-135.

[39] J. Kujawski, A. Rozicka, M. Bryjak, W. Kujawski, Pervaporative removal of acetone, butanol and ethanol from binary and multicomponent aqueous mixtures, Sep. Purif. Technol., 132 (2014) 422-429.
[40] R.W. Baker, J.G. Wijmans, Y. Huang, Permeability, permeance and selectivity: A preferred way of reporting pervaporation performance data, J. Membr. Sci., 348 (2010) 346-352.
[41] J.G. Wijmans, R.W. Baker, The solution-diffusion model - a review, J. Membr. Sci., 107 (1995) 1-21.
[42] Y. Yampolskii, Polymeric gas separation membranes, Macromolecules, 45 (2012) 3298-3311.
[43] K. Friess, M. Lanč, K. Pilnáček, V. Fíla, O. Vopička, Z. Sedláková, M.G. Cowan, W.M. McDanel, R.D. Noble, D.L. Gin, P. Izak, CO_2/CH_4 separation performance of ionic-liquid-based epoxy-amine ion gel membranes under mixed feed conditions relevant to biogas processing, J. Membr. Sci., 528 (2017) 64-71.
[44] L.-H. Cheng, M.S.A. Rahaman, R. Yao, L. Zhang, X.-H. Xu, H.-L. Chen, J.-Y. Lai, K.-L. Tung, Study on microporous supported ionic liquid membranes for carbon dioxide capture, Int. J. Greenhouse Gas Control, 21 (2014) 82-90.
[45] H. Bum Park, E.M.V. Hoek, V.V. Tarabara, Gas Separation Membranes, in: Encyclopedia of Membrane Science and Technology, John Wiley & Sons, Inc., 2013.
[46] L.M. Robeson, The upper bound revisited, J. Membr. Sci., 320 (2008) 390-400.
[47] M.L. Jue, R.P. Lively, Targeted gas separations through polymer membrane functionalization, React. Funct. Polym., 86 (2015) 88-110.
[48] Y.Y. Gu, T.P. Lodge, Synthesis and gas separation performance of triblock copolymer ion gels with a polymerized ionic liquid mid-block, Macromolecules, 44 (2011) 1732-1736.
[49] L.M. Robeson, B.D. Freeman, D.R. Paul, B.W. Rowe, An empirical correlation of gas permeability and permselectivity in polymers and its theoretical basis, J. Membr. Sci., 341 (2009) 178-185.
[50] K. Hunger, N. Schmeling, H.B.T. Jeazet, C. Janiak, C. Staudt, K. Kleinermanns, Investigation of cross-linked and additive containing polymer materials for membranes with improved performance in pervaporation and gas separation, Membranes, 2 (2012) 727-763.
[51] L. Chen, J. Chen, Asymmetric membrane containing ionic liquid [A336][P507] for the preconcentration and separation of heavy rare earth lutetium, ACS Sustainable Chem. Eng., 4 (2016) 2644-2650.
[52] D.R. Greer, A.E. Ozcam, N.P. Balsara, Pervaporation of organic compounds from aqueous mixtures using polydimethylsiloxane-containing block copolymer membranes, AIChE J., 61 (2015) 2789-2794.
[53] X. Li, K.Y. Wang, B. Helmer, T.S. Chung, Thin-film composite membranes and formation mechanism of thin-film layers on hydrophilic cellulose acetate propionate substrates for forward osmosis processes, Ind. Eng. Chem. Res., 51 (2012) 10039-10050.
[54] C.-W. Liew, K.H. Arifin, J. Kawamura, Y. Iwai, S. Ramesh, A.K. Arof, Electrical and structural studies of ionic liquid-based poly(vinyl alcohol) proton conductors, J. Non-Cryst. Solids, 425 (2015) 163-172.
[55] H.-M. Park, M. Misra, L.T. Drzal, A.K. Mohanty, “Green” nanocomposites from cellulose acetate bioplastic and clay: Effect of eco-friendly triethyl citrate plasticizer, Biomacromolecules, 5 (2004) 2281-2288.
[56] S. Wang, A. Lu, L. Zhang, Recent advances in regenerated cellulose materials, Prog. Polym. Sci., 53 (2016) 169-206.

[57] H. Kamal, F.M. Abd-Elrahim, S. Lotfy, Characterization and some properties of cellulose acetate-co-polyethylene oxide blends prepared by the use of gamma irradiation, J. Radiat. Res. Appl. Sci., 7 (2014) 146-153.
[58] K.J. Edgar, C.M. Buchanan, J.S. Debenham, P.A. Rundquist, B.D. Seiler, M.C. Shelton, D. Tindall, Advances in cellulose ester performance and application, Prog. Polym. Sci., 26 (2001) 1605-1688.
[59] L. Wang, J. Li, Y. Lin, C. Chen, Separation of dimethyl carbonate/methanol mixtures by pervaporation with poly(acrylic acid)/poly(vinyl alcohol) blend membranes, J. Membr. Sci., 305 (2007) 238-246.
[60] C. Moreau, A. Villares, I. Capron, B. Cathala, Tuning supramolecular interactions of cellulose nanocrystals to design innovative functional materials, Ind. Crops Prod., 93 (2016) 96-107.
[61] P.A. Dantas, V.R. Botaro, Synthesis and characterization of a new cellulose acetate-propionate gel: crosslinking density determination, Open J. Polym. Chem., 2 (2012) 144-151.
[62] K.L. Huang, B. Wang, Y. Cao, H.Q. Li, J.S. Wang, W.J. Lin, C.S. Mu, D.K. Liao, Homogeneous preparation of cellulose acetate propionate (CAP) and cellulose acetate butyrate (CAB) from sugarcane bagasse cellulose in ionic liquid, J. Agric. Food Chem., 59 (2011) 5376-5381.
[63] J.-I. Kadokawa, Preparation of polysaccharide-based materials compatibilized with ionic liquids, in: A. Kokorin (Ed.) Ionic Liquids: Applications and Perspectives, InTech, Rijeka, 2011.
[64] A. Schenzel, A. Hufendiek, C. Barner-Kowollik, M.A.R. Meier, Catalytic transesterification of cellulose in ionic liquids: sustainable access to cellulose esters, Green Chem., 16 (2014) 3266-3271.
[65] M. Schilling, M. Bouchard, H. Khanjian, T. Learner, A. Phenix, R. Rivenc, Application of chemical and thermal analysis methods for studying cellulose ester plastics, Acc. Chem. Res., 43 (2010) 888-896.
[66] M.d.S.R. Bastos, L.d.S. Laurentino, K.M. Canuto, L.G. Mendes, C.M. Martins, S.M.F. Silva, R.F. Furtado, S. Kim, A. Biswas, H.N. Cheng, Physical and mechanical testing of essential oil-embedded cellulose ester films, Polym. Test., 49 (2016) 156-161.
[67] R.G. Candido, G.G. Godoy, A.R. Gonçalves, Characterization and application of cellulose acetate synthesized from sugarcane bagasse, Carbohydr. Polym., 167 (2017) 280-289.
[68] P. Číhal, O. Vopička, M. Lanč, M. Kludský, J. Velas, Z. Hrdlička, A. Michalcová, M. Dendisová, K. Friess, Poly(butylene succinate)-cellulose triacetate blends: permeation, pervaporation, sorption and physical structure, Polym. Test., 65 (2018) 468-479.
[69] M.E. Abd Manaf, M. Tsuji, S. Nobukawa, M. Yamaguchi, Effect of moisture on the orientation birefringence of cellulose esters, Polymers, 3 (2011) 955-966.
[70] G. Burwell, N. Smith, O. Guy, Investigation of the utility of cellulose acetate butyrate in minimal residue graphene transfer, lithography, and plasma treatments, Microelectron. Eng., 146 (2015) 81-84.
[71] M.S. Marques, K.M. Zepon, F.C. Petronilho, V. Soldi, L.A. Kanis, Characterization of membranes based on cellulose acetate butyrate/poly(caprolactone)triol/doxycycline and their potential for guided bone regeneration application, Mater. Sci. Eng., 76 (2017) 365-373.
[72] E. Rynkowska, K. Dzieszkowski, A. Lancien, K. Fatyeyeva, A. Szymczyk, J. Kujawa, S. Koter, S. Marais, A. Wolan, W. Kujawski, Physicochemical properties and pervaporation performance of dense membranes based on cellulose acetate propionate

(CAP) and containing polymerizable ionic liquid (PIL), J. Membr. Sci., 544 (2017) 243-251.
[73] E. Rudnik, Compostable polymer materials, Elsevier, Hungary, 2008.
[74] E.S. Carvalho, R.J. Sánchez, M.I.B. Tavares, Á.C. Lamônica, Characterization and properties of hydrophilic cellulose acetate propionate derivative, J. Polym. Environ., 18 (2010) 661-667.
[75] M. Chanda, S.K. Roy, Plastics technology handbook, Taylor & Francis Group, LCC, 2007.
[76] A.J. Guiomar, S.D. Evans, J. Guthrie, Evaluation of the permeability of modified cellulose acetate propionate membranes for use in biosensors based on hydrogen peroxide detection, Cellulose, 8 (2002) 297–301.
[77] G.S. Luo, M. Niang, P. Schaetzel, Development of cellulose acetate propionate membrane for separation of ethanol and ethyl tert-butyl ether mixtures, Sep. Sci. Technol., 32 (1997) 1143-1156.
[78] C.M. Buchanan, S.C. Gedon, A.W. White, M.D. Wood, Cellulose acetate propionate and poly(tetramethylene glutarate) blends, Macromolecules, 26 (1993) 2963-2967.
[79] T. Mekonnen, P. Mussone, H. Khalil, D. Bressler, Progress in bio-based plastics and plasticizing modifications, J. Mater. Chem. A, 1 (2013) 13379-13398.
[80] P. Wojciechowska, The effect of concentration and type of plasticizer on the mechanical properties of cellulose acetate butyrate organic-inorganic hybrids, in: D.M. Luqman (Ed.) Recent Advances in Plasticisers, InTech, Rijeka, 2012, pp. 141-164.
[81] E. Rynkowska, K. Fatyeyeva, J. Kujawa, K. Dzieszkowski, A. Wolan, W. Kujawski, The effect of reactive ionic liquid or plasticizer incorporation on the physicochemical and transport properties of cellulose acetate propionate-based membranes, Polymers, 10 (2018) 86.
[82] M.G.A. Vieira, M.A. da Silva, L.O. dos Santos, M.M. Beppu, Natural-based plasticizers and biopolymer films: A review, Eur. Polym. J., 47 (2011) 254-263.
[83] A. Bendaoud, Y. Chalamet, Plasticizing effect of ionic liquid on cellulose acetate obtained by melt processing, Carbohydr. Polym., 108 (2014) 75-82.
[84] P. Liu, X. Guo, F. Nan, Y. Duan, J. Zhang, Modifying mechanical, optical properties and thermal processability of iridescent cellulose nanocrystal films using ionic liquid, ACS Appl. Mater. Interfaces, 9 (2017) 3085-3092.
[85] W. Ning, Z. Xingxiang, L. Haihui, H. Benqiao, 1-Allyl-3-methylimidazolium chloride plasticized-corn starch as solid biopolymer electrolytes, Carbohydr. Polym., 76 (2009) 482-484.
[86] K. Matsumoto, T. Endo, Confinement of ionic liquid by networked polymers based on multifunctional epoxy resins, Macromolecules, 41 (2008) 6981-6986.
[87] C. Schmidt, T. Glück, G. Schmidt-Naake, Modification of Nafion membranes by impregnation with ionic liquids, Chem. Eng. Technol., 31 (2008) 13-22.
[88] L.W. Chan, J.S. Hao, P.W.S. Heng, Evaluation of permeability and mechanical properties of composite polyvinyl alcohol films, Chem. Pharm. Bull., 47 (1999) 1412-1416.
[89] O.W. Guirguis, M.T.H. Moselhey, Thermal and structural studies of poly (vinyl alcohol) and hydroxypropyl cellulose blends, Nat. Sci., 4 (2012) 57-67.
[90] C. López-de-Dicastillo, M. Jordá, R. Catalá, R. Gavara, P. Hernández-Muñoz, Development of active polyvinyl alcohol/β-cyclodextrin composites to scavenge undesirable food components, J. Agric. Food Chem., 59 (2011) 11026-11033.
[91] A. Martínez-Felipe, C. Moliner-Estopiñán, C.T. Imrie, A. Ribes-Greus, Characterization of crosslinked poly(vinyl alcohol)-based membranes with different

hydrolysis degrees for their use as electrolytes in direct methanol fuel cells, J. Appl. Polym. Sci., 124 (2012) 1000-1011.
[92] J.-W. Rhim, H.B. Park, C.-S. Lee, J.-H. Jun, D.S. Kim, Y.M. Lee, Crosslinked poly(vinyl alcohol) membranes containing sulfonic acid group: proton and methanol transport through membranes, J. Membr. Sci., 238 (2004) 143-151.
[93] S.M. Mahdi Dadfar, G. Kavoosi, S.M. Ali Dadfar, Investigation of mechanical properties, antibacterial features, and water vapor permeability of polyvinyl alcohol thin films reinforced by glutaraldehyde and multiwalled carbon nanotube, Polym. Compos., 35 (2014) 1736-1743.
[94] S.-A. Riyajan, S. Chaiponban, K. Tanbumrung, Investigation of the preparation and physical properties of a novel semi-interpenetrating polymer network based on epoxised NR and PVA using maleic acid as the crosslinking agent, Chem. Eng. J., 153 (2009) 199-205.
[95] Y. Wang, Y.-L. Hsieh, Crosslinking of polyvinyl alcohol (PVA) fibrous membranes with glutaraldehyde and PEG diacylchloride, J. Appl. Polym. Sci., 116 (2010) 3249-3255.
[96] S. Bano, A. Mahmood, K.-H. Lee, Vapor permeation separation of methanol–water mixtures: effect of experimental conditions, Ind. Eng. Chem. Res., 52 (2013) 10450-10459.
[97] K.-J. Kim, S.-B. Lee, N.-W. Han, Kinetics of crosslinking reaction of PVA membrane with glutaraldehyde, Korean J. Chem. Eng., 11 (1994) 41-47.
[98] K.C.S. Figueiredo, T.L.M. Alves, C.P. Borges, Poly(vinyl alcohol) films crosslinked by glutaraldehyde under mild conditions, J. Appl. Polym. Sci., 111 (2009) 3074-3080.
[99] Y. Zhang, P.C. Zhu, D. Edgren, Crosslinking reaction of poly(vinyl alcohol) with glyoxal, J. Polym. Res., 17 (2010) 725-730.
[100] C. Birck, S. Degoutin, N. Tabary, V. Miri, M. Bacquet, New crosslinked cast films based on poly(vinyl alcohol): Preparation and physico-chemical properties, eXPRESS Polym. Lett., 8 (2014) 941-952.
[101] Y. Kudoh, T. Kojima, M. Abe, M. Oota, T. Yamamoto, Proton conducting membranes consisting of poly(vinyl alcohol) and poly(styrene sulfonic acid): Crosslinking of poly(vinyl alcohol) with and without succinic acid, Solid State Ionics, 253 (2013) 189-194.
[102] C. Ajith, A.P. Deshpande, S. Varughese, Proton conductivity in crosslinked hydrophilic ionic polymer system: Competitive hydration, crosslink heterogeneity, and ineffective domains, J. Polym. Sci., Part B: Polym. Phys., 54 (2016) 1087-1101.
[103] L. Wang, J. Li, Y. Lin, C. Chen, Crosslinked poly(vinyl alcohol) membranes for separation of dimethyl carbonate/methanol mixtures by pervaporation, Chem. Eng. J., 146 (2009) 71-78.
[104] K. Kumeta, I. Nagashima, S. Matsui, K. Mizoguchi, Crosslinking reaction of poly(vinyl alcohol) with poly(acrylic acid) (PAA) by heat treatment: Effect of neutralization of PAA, J. Appl. Polym. Sci., 90 (2003) 2420-2427.
[105] Y.-L. Wang, H. Yang, Z.-L. Xu, Influence of post-treatments on the properties of porous poly(vinyl alcohol) membranes, J. Appl. Polym. Sci., 107 (2008) 1423-1429.
[106] N. Follain, J.M. Valleton, L. Lebrun, B. Alexandre, P. Schaetzel, M. Metayer, S. Marais, Simulation of kinetic curves in mass transfer phenomena for a concentration-dependent diffusion coefficient in polymer membranes, J. Membr. Sci., 349 (2010) 195-207.
[107] M.P. Singh, R.K. Singh, S. Chandra, Ionic liquids confined in porous matrices: physicochemical properties and applications, Prog. Mater. Sci., 64 (2014) 73-120.
[108] N.V. Plechkova, K.R. Seddon, Applications of ionic liquids in the chemical industry, Chem. Soc. Rev., 37 (2008) 123-150.

[109] T. Peppel, M. Köckerling, M. Geppert-Rybczyńska, R.V. Ralys, J.K. Lehmann, S.P. Verevkin, A. Heintz, Low-viscosity paramagnetic ionic liquids with doubly charged $[Co(NCS)_4]_2^-$ Ions, Angew. Chem., Int. Ed., 49 (2010) 7116-7119.
[110] A. Takegawa, M. Murakami, Y. Kaneko, J. Kadokawa, A facile preparation of composites composed of cellulose and polymeric ionic liquids by in situ polymerization of ionic liquids having acrylate groups, Polym. Compos., 30 (2009) 1837-1841.
[111] M. Diaz, A. Ortiz, M. Isik, D. Mecerreyes, I. Ortiz, Highly conductive electrolytes based on poly(HSO_3-BVIm TfO)/HSO_3-BMIm TfO mixtures for fuel cell applications, Int. J. Hydrogen Energy, 40 (2015) 11294-11302.
[112] J. Lemus, A. Eguizábal, M.P. Pina, UV polymerization of room temperature ionic liquids for high temperature PEMs: Study of ionic moieties and crosslinking effects, Int. J. Hydrogen Energy, 40 (2015) 5416-5424.
[113] M. Díaz, A. Ortiz, I. Ortiz, Progress in the use of ionic liquids as electrolyte membranes in fuel cells, J. Membr. Sci., 469 (2014) 379-396.
[114] C.B. Yue, D. Fang, L. Liu, T.F. Yi, Synthesis and application of task-specific ionic liquids used as catalysts and/or solvents in organic unit reactions, J. Mol. Liq., 163 (2011) 99-121.
[115] Z. Dai, R.D. Noble, D.L. Gin, X. Zhang, L. Deng, Combination of ionic liquids with membrane technology: A new approach for CO_2 separation, J. Membr. Sci., 497 (2016) 1-20.
[116] A. Fernicola, B. Scrosati, H. Ohno, Potentialities of ionic liquids as new electrolyte media in advanced electrochemical devices, Ionics, 12 (2006) 95-102.
[117] K. Dong, X. Liu, H. Dong, X. Zhang, S. Zhang, Multiscale studies on ionic liquids, Chem. Rev., 117 (2017) 6636-6695.
[118] K.N. Marsh, J.A. Boxall, R. Lichtenthaler, Room temperature ionic liquids and their mixtures - a review, Fluid Phase Equilib., 219 (2004) 93-98.
[119] C.-W. Liew, S. Ramesh, A.K. Arof, Good prospect of ionic liquid based-poly(vinyl alcohol) polymer electrolytes for supercapacitors with excellent electrical, electrochemical and thermal properties, Int. J. Hydrogen Energy, 39 (2014) 2953-2963.
[120] C.-W. Liew, S. Ramesh, A.K. Arof, A novel approach on ionic liquid-based poly(vinyl alcohol) proton conductive polymer electrolytes for fuel cell applications, Int. J. Hydrogen Energy, 39 (2014) 2917-2928.
[121] R.L. Vekariya, A review of ionic liquids: applications towards catalytic organic transformations, J. Mol. Liq., 227 (2017) 44-60.
[122] R. Zarrougui, R. Mdimagh, N. Raouafi, Highly efficient extraction and selective separation of uranium(VI) from transition metals using new class of undiluted ionic liquids based on H-phosphonate anions, J. Hazard. Mater., 342 (2018) 464-476.
[123] J. Lu, F. Yan, J. Texter, Advanced applications of ionic liquids in polymer science, Prog. Polym. Sci., 34 (2009) 431-448.
[124] E. Rynkowska, K. Fatyeyeva, W. Kujawski, Application of polymer-based membranes containing ionic liquids in membrane separation processes: a critical review, Rev. Chem. Eng., 34 (2018) 341–363.
[125] T. Makanyire, S. Sanchez-Segado, A. Jha, Separation and recovery of critical metal ions using ionic liquids, Adv. Manuf., 4 (2016) 33-46.
[126] D.d. Agreda, I. Garcia-Diaz, F.A. López, F.J. Alguacil, Supported liquid membranes technologies in metals removal from liquid effluents, Rev. Metal., 47 (2011) 146-168.
[127] J. Grünauer, V. Filiz, S. Shishatskiy, C. Abetz, V. Abetz, Scalable application of thin film coating techniques for supported liquid membranes for gas separation made from ionic liquids, J. Membr. Sci., 518 (2016) 178-191.

[128] J. Wang, J. Luo, S. Feng, H. Li, Y. Wan, X. Zhang, Recent development of ionic liquid membranes, Green Energ. Environ., 1 (2016) 43-61.
[129] T. Uragami, E. Fukuyama, T. Miyata, Selective removal of dilute benzene from water by poly(methyl methacrylate)-graft-poly(dimethylsiloxane) membranes containing hydrophobic ionic liquid by pervaporation, J. Membr. Sci., 510 (2016) 131-140.
[130] Y.T. Ong, S.H. Tan, Pervaporation separation of a ternary azeotrope containing ethyl acetate, ethanol and water using a buckypaper supported ionic liquid membrane, Chem. Eng. Res. Des., 109 (2016) 116-126.
[131] A.S. Shaplov, R. Marcilla, D. Mecerreyes, Recent advances in innovative polymer electrolytes based on poly(ionic liquid)s, Electrochim. Acta, 175 (2015) 18-34.
[132] Y. Yang, H. Gao, L. Zheng, Anhydrous proton exchange membranes at elevated temperatures: effect of protic ionic liquids and crosslinker on proton conductivity, RSC Adv., 5 (2015) 17683-17689.
[133] E.I. Izgorodina, D.R. MacFarlane, Nature of hydrogen bonding in charged hydrogen-bonded complexes and imidazolium-based ionic liquids, J. Phys. Chem. B, 115 (2011) 14659-14667.
[134] M.D. Green, T.E. Long, Designing Imidazole-Based Ionic Liquids and Ionic Liquid Monomers for Emerging Technologies, Polym. Rev., 49 (2009) 291-314.
[135] S. Imaizumi, H. Kokubo, M. Watanabe, Polymer actuators using ion-gel electrolytes prepared by self-assembly of ABA-triblock copolymers, Macromolecules, 45 (2012) 401-409.
[136] T.P. Lodge, A unique platform for materials design, Science, 321 (2008) 50-51.
[137] M.K. Mistry, S. Subianto, N.R. Choudhury, N.K. Dutta, Interfacial interactions in aprotic ionic liquid based protonic membrane and its correlation with high temperature conductivity and thermal properties, Langmuir, 25 (2009) 9240-9251.
[138] S. Uk Hong, D. Park, Y. Ko, I. Baek, Polymer-ionic liquid gels for enhanced gas transport, Chem. Commun., (2009) 7227-7229.
[139] B. Pospiech, Facilitated transport of palladium(II) across polymer inclusion membrane with ammonium ionic liquid as effective carrier, Chem. Pap., 72 (2018) 301-308.
[140] S. Kasahara, E. Kamio, T. Ishigami, H. Matsuyama, Effect of water in ionic liquids on CO_2 permeability in amino acid ionic liquid-based facilitated transport membranes, J. Membr. Sci., 415–416 (2012) 168-175.
[141] M.I.G.S. Almeida, R.W. Cattrall, S.D. Kolev, Recent trends in extraction and transport of metal ions using polymer inclusion membranes (PIMs), J. Membr. Sci., 415–416 (2012) 9-23.
[142] M. Matsumoto, Y. Murakami, K. Kondo, Separation of 1-butanol by pervaporation using polymer inclusion membranes containing ionic liquids, Solvent Extr. Res. Dev., Jpn., 18 (2011) 75-83.
[143] M. Diaz, A. Ortiz, M. Vilas, E. Tojo, I. Ortiz, Performance of PEMFC with new polyvinyl-ionic liquids based membranes as electrolytes, Int. J. Hydrogen Energy, 39 (2014) 3970-3977.
[144] T. Yasuda, S. Nakamura, Y. Honda, K. Kinugawa, S.Y. Lee, M. Watanabe, Effects of polymer structure on properties of sulfonated polyimide/protic ionic liquid composite membranes for nonhumidified fuel cell applications, ACS Appl. Mater. Interfaces, 4 (2012) 1783-1790.
[145] H.R. Cascon, S.K. Choudhari, 1-Butanol pervaporation performance and intrinsic stability of phosphonium and ammonium ionic liquid-based supported liquid membranes, J. Membr. Sci., 429 (2013) 214-224.

[146] Y. Dong, H. Guo, Z. Su, W. Wei, X. Wu, Pervaporation separation of benzene/cyclohexane through AAOM-ionic liquids/polyurethane membranes, Chem. Eng. Process., 89 (2015) 62-69.
[147] A. Samadi, R.K. Kemmerlin, S.M. Husson, Polymerized ionic liquid sorbents for CO_2 separation, Energy Fuels, 24 (2010) 5797-5804.
[148] P. Izák, U. Kragl, M. Köckerling, Multiphase membrane, in: U.o. Rostock (Ed.), Germany, 2006.
[149] P. Bernardo, J.C. Jansen, F. Bazzarelli, F. Tasselli, A. Fuoco, K. Friess, P. Izák, V. Jarmarová, M. Kačírková, G. Clarizia, Gas transport properties of Pebax®/room temperature ionic liquid gel membranes, Sep. Purif. Technol., 97 (2012) 73-82.
[150] K. Friess, J.C. Jansen, F. Bazzarelli, P. Izák, V. Jarmarová, M. Kačírková, J. Schauer, G. Clarizia, P. Bernardo, High ionic liquid content polymeric gel membranes: Correlation of membrane structure with gas and vapour transport properties, J. Membr. Sci., 415–416 (2012) 801-809.
[151] J.C. Jansen, G. Clarizia, P. Bernardo, F. Bazzarelli, K. Friess, A. Randová, J. Schauer, D. Kubicka, M. Kacirková, P. Izak, Gas transport properties and pervaporation performance of fluoropolymer gel membranes based on pure and mixed ionic liquids, Sep. Purif. Technol., 109 (2013) 87-97.
[152] F. Hassan Hassan Abdellatif, J. Babin, C. Arnal-Herault, L. David, A. Jonquieres, Grafting of cellulose acetate with ionic liquids for biofuel purification by a membrane process: Influence of the cation, Carbohydr. Polym., 147 (2016) 313-322.
[153] A.S. Shaplov, P.S. Vlasov, E.I. Lozinskaya, D.O. Ponkratov, I.A. Malyshkina, F. Vidal, O.V. Okatova, G.M. Pavlov, C. Wandrey, A. Bhide, M. Schönhoff, Y.S. Vygodskii, Polymeric ionic liquids: comparison of polycations and polyanions, Macromolecules, 44 (2011) 9792-9803.
[154] M. Li, B. Yang, L. Wang, Y. Zhang, Z. Zhang, S. Fang, Z. Zhang, New polymerized ionic liquid (PIL) gel electrolyte membranes based on tetraalkylammonium cations for lithium ion batteries, J. Membr. Sci., 447 (2013) 222-227.
[155] M.-a. Murakami, Y. Kaneko, J.-i. Kadokawa, Preparation of cellulose-polymerized ionic liquid composite by in-situ polymerization of polymerizable ionic liquid in cellulose-dissolving solution, Carbohydr. Polym., 69 (2007) 378-381.
[156] J.E. Bara, S. Lessmann, C.J. Gabriel, E.S. Hatakeyama, R.D. Noble, D.L. Gin, Synthesis and performance of polymerizable room-temperature ionic liquids as gas separation membranes, Ind. Eng. Chem. Res., 46 (2007) 5397-5404.
[157] M.G. Cowan, D.L. Gin, R.D. Noble, Poly(ionic liquid)/ionic liquid ion-gels with high “free” ionic liquid content: platform membrane materials for CO_2/light gas separations, Acc. Chem. Res., 49 (2016) 724-732.
[158] R. Marcilla, F. Alcaide, H. Sardon, J.A. Pomposo, C. Pozo-Gonzalo, D. Mecerreyes, Tailor-made polymer electrolytes based upon ionic liquids and their application in all-plastic electrochromic devices, Electrochem. Commun., 8 (2006) 482-488.
[159] K. Põhako-Esko, M. Timusk, K. Saal, R. Lõhmus, I. Kink, U. Mäeorg, Increased conductivity of polymerized ionic liquids through the use of a nonpolymerizable ionic liquid additive, J. Mater. Res., 28 (2013) 3086-3093.
[160] D. Mecerreyes, Applications of ionic liquids in polymer science and technology, Springer, Berlin, 2015.
[161] Y.F. Rongrong Wang, Menghua Qin, Zhiyong Shao, Qinghua Xu, Homogeneous acylation and regioselectivity of cellulose with 2-chloro-2-phenylacetyl chloride in ionic liquid, BioResources, 9 (2014) 5134-5146.

[162] J. Kujawa, A. Rozicka, S. Cerneaux, W. Kujawski, The influence of surface modification on the physicochemical properties of ceramic membranes, Colloids Surf., A, 443 (2014) 567-575.
[163] M. Gindl, G. Sinn, W. Gindl, A. Reiterer, S. Tschegg, A comparison of different methods to calculate the surface free energy of wood using contact angle measurements, Colloids Surf., A, 181 (2001) 279-287.
[164] D.K. Owens, R.C. Wendt, Estimation of the surface free energy of polymers, J. Appl. Polym. Sci., 13 (1969) 1741-1747.
[165] F.M. Fowkes, Dispersion force contributions to surface and interfacial tensions, contact angles, and heats of immersion, in: Contact Angle, Wettability, and Adhesion, American Chemical Society, 1964, pp. 99-111.
[166] C. Joly, D. Le Cerf, C. Chappey, D. Langevin, G. Muller, Residual solvent effect on the permeation properties of fluorinated polyimide films, Sep. Purif. Technol., 16 (1999) 47-54.
[167] ICH Harmonised Tripartite Guideline, in: Validation of Analytical Procedures: Text and Methodology Q2(R1), 1994, pp. 1-13.
[168] A. Kujawska, K. Knozowska, J. Kujawa, W. Kujawski, Influence of downstream pressure on pervaporation properties of PDMS and POMS based membranes, Sep. Purif. Technol., 159 (2016) 68-80.
[169] C.-E. Tsai, C.-W. Lin, B.-J. Hwang, A novel crosslinking strategy for preparing poly(vinyl alcohol)-based proton-conducting membranes with high sulfonation, J. Power Sources, 195 (2010) 2166-2173.
[170] M.S. Boroglu, S.U. Celik, A. Bozkurt, I. Boz, Proton-conducting blend membranes of crosslinked poly(vinyl alcohol)–sulfosuccinic acid ester and poly(1-vinyl-1,2,4-triazole) for high temperature fuel cells, Polym. Eng. Sci., 53 (2013) 153-158.
[171] J. Zhou, Y. Ma, L. Ren, J. Tong, Z. Liu, L. Xie, Preparation and characterization of surface crosslinked TPS/PVA blend films, Carbohydr. Polym., 76 (2009) 632-638.
[172] P. Vashisth, V. Pruthi, Synthesis and characterization of crosslinked gellan/PVA nanofibers for tissue engineering application, Mater. Sci. Eng. C, 67 (2016) 304-312.
[173] J.S. Won, J.E. Lee, D.Y. Jin, S.G. Lee, Mechanical properties and biodegradability of the kenaf/soy protein isolate-PVA biocomposites, Int. J. Polym. Sci., 2015 (2015) 1-11.
[174] R.W. Korsmeyer, N.A. Peppas, Effect of the morphology of hydrophilic polymeric matrices on the diffusion and release of water soluble drugs, J. Membr. Sci., 9 (1981) 211-227.
[175] L. Rey, J. Duchet, J. Galy, H. Sautereau, D. Vouagner, L. Carrion, Structural heterogeneities and mechanical properties of vinyl/dimethacrylate networks synthesized by thermal free radical polymerisation, Polymer, 43 (2002) 4375-4384.
[176] A.V. Penkova, S.F.A. Acquah, M.E. Dmitrenko, B. Chen, K.N. Semenov, H.W. Kroto, Transport properties of cross-linked fullerenol–PVA membranes, Carbon, 76 (2014) 446-450.
[177] O. Farid, F. Mansour, M. Habib, J. Robinson, S. Tarleton, Investigating the sorption influence of poly(vinyl alcohol) (PVA) at different crosslinking content, J. Environ. Chem. Eng., 4 (2016) 293-298.
[178] Y. Salt, E. Arçevik, B. Ekinci, Sorption and pervaporation results of clinoptilolite filled poly(vinylalcohol) membrane prepared for dehydration of aqueous organic mixtures, Can. J. Chem. Eng., 92 (2014) 503-510.
[179] M. Kárászová, M. Kacirková, K. Friess, P. Izák, Progress in separation of gases by permeation and liquids by pervaporation using ionic liquids: A review, Sep. Purif. Technol., 132 (2014) 93-101.

[180] H. Gui, Y. Li, S. Chen, P. Xu, B. Zheng, Y. Ding, Effects of biodegradable imidazolium-based ionic liquid with ester group on the structure and properties of PLLA, Macromol. Res., 22 (2014) 583-591.
[181] J. Yoon, H.J. Lee, C.M. Stafford, Thermoplastic elastomers based on ionic liquid and poly(vinyl alcohol), Macromolecules, 44 (2011) 2170-2178.
[182] S. Patachia, C. Friedrich, C. Florea, C. Croitoru, Study of the PVA hydrogel behaviour in 1-butyl-3-methylimidazolium tetrafluoroborate ionic liquid, eXPRESS Polym. Lett., 5 (2011) 197–207.
[183] N.N. Rozik, A.A. Ward, A novel approach on poly(ionic liquid)-based poly(vinyl alcohol) as a hydrophilic/hydrophobic conductive polymer electrolytes, Polym. Bull., 75 (2018) 267-287.
[184] A.L. Saroj, S. Krishnamoorthi, R.K. Singh, Structural, thermal and electrical transport behaviour of polymer electrolytes based on PVA and imidazolium based ionic liquid, J. Non-Cryst. Solids, 473 (2017) 87-95.
[185] K. Donato, L. Matějka, R. Mauler, R. Donato, Recent applications of ionic liquids in the sol-gel process for polymer–silica nanocomposites with ionic interfaces, Colloids Surf., 1 (2018) 5.
[186] J.C. Geng, L. Qin, X. Du, S.L. Xiao, G.H. Cui, Synthesis, crystal structures, and catalytic properties of silver(I) and cobalt(II) coordination polymers based on flexible bis(benzimidazole) with pyridine-2, 6-dicarboxylate, Z. Anorg. Allg. Chem., 638 (2012) 1233-1238.
[187] P.A. Hunt, C.R. Ashworth, R.P. Matthews, Hydrogen bonding in ionic liquids, Chem. Soc. Rev., 44 (2015) 1257-1288.
[188] T. Schafer, R.E.D. Paolo, R. Franco, J.G. Crespo, Elucidating interactions of ionic liquids with polymer films using confocal Raman spectroscopy, Chem. Commun., 0 (2005) 2594-2596.
[189] T. Xi, L. Tang, W. Hao, L. Yao, P. Cui, Morphology and pervaporation performance of ionic liquid and waterborne polyurethane composite membranes, RSC Adv., 8 (2018) 7792-7799.
[190] R.L. Weber, Y. Ye, S.M. Banik, Y.A. Elabd, M.A. Hickner, M.K. Mahanthappa, Thermal and ion transport properties of hydrophilic and hydrophobic polymerized styrenic imidazolium ionic liquids, J. Polym. Sci., Part B: Polym. Phys., 49 (2011) 1287-1296.
[191] H. Ohtani, S. Ishimura, M. Kumai, Thermal decomposition behaviors of imidazolium-type ionic liquids studied by pyrolysis-gas chromatography, Anal. Sci., 24 (2008) 1335-1340.
[192] M.T. Garcia, I. Ribosa, L. Perez, A. Manresa, F. Comelles, Aggregation behavior and antimicrobial activity of ester-functionalized imidazolium- and pyridinium-based ionic liquids in aqueous solution, Langmuir, 29 (2013) 2536-2545.
[193] E.S. Gadelmawla, M.M. Koura, T.M.A. Maksoud, I.M. Elewa, H.H. Soliman, Roughness parameters, J. Mater. Process. Technol., 123 (2002) 133-145.
[194] J. Deng, L. Bai, S. Zeng, X. Zhang, Y. Nie, L. Deng, S. Zhang, Ether-functionalized ionic liquid based composite membranes for carbon dioxide separation, RSC Adv., 6 (2016) 45184-45192.
[195] K. Hooshyari, M. Javanbakht, M. Adibi, Novel composite membranes based on dicationic ionic liquid and polybenzimidazole mixtures as strategy for enhancing thermal and electrochemical properties of proton exchange membrane fuel cells applications at high temperature, Int. J. Hydrogen Energy, 41 (2016) 10870-10883.
[196] M. Erceg, T. Kovačić, I. Klarić, Thermal degradation of poly(3-hydroxybutyrate) plasticized with acetyl tributyl citrate, Polym. Degrad. Stab., 90 (2005) 313-318.

[197] M. Maiza, M.T. Benaniba, G. Quintard, V. Massardier-Nageotte, Biobased additive plasticizing Polylactic acid (PLA), Polimeros, 25 (2015) 581-590.
[198] S. Ramesh, R. Shanti, E. Morris, Plasticizing effect of 1-allyl-3-methylimidazolium chloride in cellulose acetate based polymer electrolytes, Carbohydr. Polym., 87 (2012) 2624-2629.
[199] Y. Wang, C. Zhou, Y. Xiao, S. Zhou, C. Wang, X. Chen, K. Hu, X. Fu, J. Lei, Preparation and evaluation of acetylated mixture of citrate ester plasticizers for poly(vinyl chloride), Iran. Polym. J., 27 (2018) 423-432.
[200] P. Berman, N. Meiri, L.A. Colnago, T.B. Moraes, C. Linder, O. Levi, Y. Parmet, M. Saunders, Z. Wiesman, Study of liquid-phase molecular packing interactions and morphology of fatty acid methyl esters (biodiesel), Biotechnol. Biofuels, 8 (2015) 12.
[201] A.W. White, C.M. Buschanan, B.G. Pearcy, M.D. Wood, Mechanical properties of cellulose acetate propionate/aliphatic polyester blends, J. Appl. Polym. Sci., 52 (1994) 525-530.
[202] I. Harte, C. Birkinshaw, E. Jones, J. Kennedy, E. DeBarra, The effect of citrate ester plasticizers on the thermal and mechanical properties of poly(DL-lactide), J. Appl. Polym. Sci., 127 (2013) 1997-2003.
[203] J.F. Shackelford, Y.-H. Han, S. Kim, S.-H. Kwon, CRC Materials science and engineering handbook, Fourth ed., CRC Press, Boca Raton, 2015.
[204] S. Kalachandra, D.T. Turner, Water sorption of poly(methyl methacrylate): 3. Effects of plasticizers, Polymer, 28 (1987) 1749-1752.
[205] M.L. Sanyang, S.M. Sapuan, M. Jawaid, M.R. Ishak, J. Sahari, Effect of plasticizer type and concentration on physical properties of biodegradable films based on sugar palm (arenga pinnata) starch for food packaging, J. Food Sci. Technol., 53 (2016) 326-336.
[206] Y. Shuto, H. Taniguchi, Cellulose acetate propionate, in, Google Patents, 1999.
[207] J.A. Brydson, Plastics materials, Seventh ed., Butterworth-Heinemann, 1999.
[208] S. Chen, R. Vijayaraghavan, D.R. MacFarlane, E.I. Izgorodina, Ab initio prediction of proton NMR chemical shifts in imidazolium ionic liquids, J. Phys. Chem. B, 117 (2013) 3186-3197.
[209] S. Scheiner, Assessment of the presence and strength of H-bonds by means of corrected NMR, Molecules, 21 (2016) 1426.
[210] N. Shin, S. Kwon, S. Moon, C.H. Hong, Y.G. Kim, Ionic liquid-mediated deoxydehydration reactions: Green synthetic process for bio-based adipic acid, Tetrahedron, 73 (2017) 4758-4765.
[211] L. Crépy, L. Chaveriat, J. Banoub, P. Martin, N. Joly, Synthesis of cellulose fatty esters as plastics - influence of the degree of substitution and the fatty chain length on mechanical properties, ChemSusChem, 2 (2009) 165-170.
[212] J. Chen, Q. Guo, D. Li, J. Tong, X. Li, Properties improvement of SPEEK based proton exchange membranes by doping of ionic liquids and Y_2O_3, Prog. Nat. Sci., 22 (2012) 26-30.
[213] T. Erdmenger, J. Vitz, F. Wiesbrock, U.S. Schubert, Influence of different branched alkyl side chains on the properties of imidazolium-based ionic liquids, J. Mater. Chem. A, 18 (2008) 5267-5273.
[214] J.J. Raj, C.D. Wilfred, S.N. Shah, M. Pranesh, M.I. Abdul Mutalib, K.C. Lethesh, Physicochemical and thermodynamic properties of imidazolium ionic liquids with nitrile and ether dual functional groups, J. Mol. Liq., 225 (2017) 281-289.
[215] Y. Cao, T. Mu, Comprehensive Investigation on the Thermal Stability of 66 Ionic Liquids by Thermogravimetric Analysis, Ind. Eng. Chem. Res., 53 (2014) 8651-8664.

[216] W. Li, J. Fang, M. Lv, C. Chen, X. Chi, Y. Yang, Y. Zhang, Novel anion exchange membranes based on polymerizable imidazolium salt for alkaline fuel cell applications, J. Mater. Chem., 21 (2011) 11340-11346.
[217] Shalu, S.K. Chaurasia, R.K. Singh, S. Chandra, Thermal stability, complexing behavior, and ionic transport of polymeric gel membranes based on polymer PVdF-HFP and ionic liquid, [BMIM][BF_4], J. Phys. Chem. B, 117 (2013) 897-906.
[218] J.I. Kadokawa, M.A. Murakami, Y. Kaneko, A facile method for preparation of composites composed of cellulose and a polystyrene-type polymeric ionic liquid using a polymerizable ionic liquid, Compos. Sci. Technol., 68 (2008) 493-498.
[219] M.T. Sanz, J. Gmehling, Study of the dehydration of isopropanol by a pervaporation-based hybrid process, Chem. Eng. Technol., 29 (2006) 473-480.
[220] A.P.d.l. Ríos, F.J. Hernández-Fernández, F. Tomás-Alonso, J.M. Palacios, D. Gómez, M. Rubio, G. Víllora, A SEM–EDX study of highly stable supported liquid membranes based on ionic liquids, J. Membr. Sci., 300 (2007) 88-94.
[221] M.M. Pereira, K.A. Kurnia, F.L. Sousa, N.J.O. Silva, J.A. Lopes-da-Silva, J.A.P. Coutinhoa, M.G. Freire, Contact angles and wettability of ionic liquids on polar and non-polar surfaces, Phys. Chem. Chem. Phys., 17 (2015) 31653-31661.
[222] C.M. Hansen, Hansen solubility parameters. A user's book, second ed., CRC Press, London, New York, 2007.
[223] S. Ramanaiah, P.R. Rani, K.S. Reddy, Hansen solubility parameters for the solid surface of cellulose acetate propionate by inverse gas chromatography, J. Macromol. Sci., Part B: Phys., 51 (2012) 2191-2200.
[224] M.O. Mavukkandy, M.R. Bilad, J. Kujawa, S. Al-Gharabli, H.A. Arafat, On the effect of fumed silica particles on the structure, properties and application of PVDF membranes, Sep. Sci. Technol., 187 (2017) 365-373.
[225] D. Mecerreyes, Polymeric ionic liquids: Broadening the properties and applications of polyelectrolytes, Prog. Polym. Sci., 36 (2011) 1629-1648.
[226] M. Mohsen-Nia, H. Amiri, B. Jazi, Dielectric constants of water, methanol, ethanol, butanol and acetone: measurement and computational study, J. Solution Chem., 39 (2010) 701-708.
[227] S. Marais, M. Métayer, Q.T. Nguyen, M. Labbé, D. Langevin, New methods for the determination of the parameters of a concentration-dependent diffusion law for molecular penetrants from transient permeation or sorption data, Macromol. Theory Simul., 9 (1999) 207-214.
[228] J. Chen, J.-m. Zhang, Y. Feng, J.-s. He, J. Zhang, Effect of molecular structure on the gas permeability of cellulose aliphatate esters, Chin. J. Polym. Sci., 32 (2014) 1-8.
[229] R.W. Baker, J.G. Wijmans, Membrane separation of organic vapors from gas streams, in: D.R. Paul, Y.P. Yampol'skii (Eds.) Polymeric Gas Separation Membranes, CRC Press, Boca Raton, Florida, 1994.
[230] W.J. Koros, D.R. Paul, Synthetic membranes, Harwood Academic, New York, 1986.
[231] D.R. Lide, CRC Handbook of chemistry and physics, 84th ed., CRC Press, 2003.

Abstract

In the last decades, membrane separation has played an important role in many industrial processes thanks to its versatility, low energy consumption, high performances of membranes, as well as a possibility of combining membrane technologies with other separation processes. Membrane technologies gave a great contribution to the improvement of separation processes in the industrial scale thanks to a number of advantages, such as the high selectivity of the separation, the opportunity to work with thermolabile compounds, and low energy demand.

Pervaporation process is an important membrane separation technique used to separate binary or multicomponent liquid mixtures including close boiling solvents, azeotrope mixtures, and isomers. During pervaporation, feed components are in the direct contact with one side of the lyophilic membrane, while the selected components are preferentially transported across the membrane to the permeate side.

Membranes used in pervaporation must be characterized by high selectivity, chemical stability, and mechanical strength at high temperatures. Selectivity and transport properties of the membrane determine the overall efficiency of the separation process. The comprehensive characterization of membranes is the crucial approach and can lead to broaden the knowledge about the influence of the membrane structure and membrane preparation conditions on the equilibrium, separation, and transport characteristics of the studied membranes, in order to develop new polymer materials with the expected efficiency of the separation process.

Research has been also focused on the development of the membranes filled with ILs in order to tailor the separation properties of the developed membranes used in liquid separation by pervaporation, gas separation, and separation of metal ions as well as the conducting barriers in fuel cells. ILs are characterized by good thermal stability, high ionic conductivity, negligible vapor pressure, and low melting point. Due to their numerous unique properties, polymer membranes containing ILs (polymer-ILs) possess wide range of advantages, like better separation properties than the classical polymer membranes. This fact is related with much higher molecular diffusion in ionic liquid than in polymers. Therefore, the use of polymer-ILs in separation processes would result in superior separation behavior and higher fluxes. Morphology and physicochemical properties of ILs can be “tailored” depending on the separated system in order to obtain

a suitable polymer material for a given separation process without preparation of a chemically new membrane.

Even though there is a growing interest in the application of polymer membranes filled with ILs, the polymer-ILs based separation processes are limited due to the losses of the unbound ionic liquid in the course of the exploitation.

The PhD is realized in the frame of "co-tutelle" system between the Faculty of Chemistry at the Nicolaus Copernicus University (NCU) in Toruń, Poland (Membranes and Membrane Separation Processes Research Group) and the University of Rouen Normandy, France (Barrier Polymer Materials and Membranes (MPBM) Research Group of the Laboratory of Polymers, Biopolymers, Surfaces (PBS)).

The main aim of the present PhD thesis is to elaborate novel dense membranes based on poly(vinyl alcohol) (PVA) and cellulose acetate propionate (CAP) filled with various reactive and polymerizable ILs in order to obtain the polymer-ionic liquid system in which ionic liquids are linked inside the polymer structure. The investigation of physicochemical characteristics and study of the equilibrium, barrier, and transport properties of the obtained membranes was carried out. Furthermore, the selected membranes were tested in pervaporation process in contact with water-propan-2-ol mixture, water and gas permeation measurements.

The novelty of this work was the formation of membrane materials containing ionic liquids firmly linked to the polymer matrix. The ionic liquid attachment was achieved by the creation of chemical bonds with polymer using RILs. The chemical modification was performed between CAP and ester-functionalized imidazolium-based RILs through the transesterification reaction. The studied approach led to the formation of covalent bonds between polymer and RIL.

The preliminary results revealed that the pristine CAP was brittle whereas PVA was soluble in liquid water, therefore a kind of plasticization and crosslinking were required, respectively. In the first step, PVA was crosslinked using a two-step approach: chemically with SSA and thermally at various temperature (120, 140, and 160^{o}C). The chemical crosslinking combined with the thermal treatment of PVA-based membranes provide the membrane with enhanced crosslinking efficiency and improved resistance in contact with liquid water. It was found by the FTIR-ATR analysis that the increase of the SSA concentration and crosslinking temperature resulted in the increase of the intensity of ester bond bands between PVA and SSA due to the esterification reaction. Moreover, the increase of the SSA content reduces the elongation at break (from 316% to 98% for

pure PVA membrane and membrane containing 33 wt.% SSA and crosslinked at 160°C, respectively). Additionally, TGA analysis of the pure and PVA-SSA membranes testifies that the increase of crosslinking temperature for a given SSA concentration from 120 to 160°C enhanced the thermal stability of the membranes up to 16°C. The sorption studies of the elaborated membranes were performed in contact with solvents of various polarity, i.e. water, methanol, and 2-propanol. The swelling of the PVA-SSA membranes was found to be the highest in water and the lowest for the membranes in contact with 2-propanol, i.e. the swelling in water was around 4000-fold and 16-fold higher than in 2-propanol and methanol, respectively. Moreover, the water vapor permeation studies were carried out at the different relative humidity. The obtained results agree well with the swelling studies and have shown the water vapor influence on the crosslinked PVA membranes.

Considering the PVA-RIL membranes, FTIR-ATR analysis revealed intramolecular interactions based on the hydrogen bonds between PVA and RILs. Due to the amphiphilic nature of studied RILs that is related to the presence of the hydrophobic ethyl substituents attached to the hydrophilic ester-functionalized imidazolium ring, the occurrence of hydrogen bond, as well as van der Waals and π-π stacking interactions is observed. From the analysis of the mechanical properties of the PVA-RIL films, the dual function of RIL (as a physical junction promoter and as a plasticizer) can be seen. The initial doping of PVA with 9 wt.% RILs influenced the PVA chains mobility that corresponds to the physical crosslinking between PVA and RIL due to the enhanced hydrogen bond interactions. This resulted in the increase of the film stiffness reflected by the increase of Young's modulus (E) and stress at break (σ_{max}) and the decrease of elongation at break (ε_{max}) values compared to pristine PVA. The presence of the higher RIL content (23 wt.%) led to the decrease of E and σ_{max} and to the increase of ε_{max} indicating the influence of RILs on PVA-RILs films elasticity. Simultaneously, the good compatibility between PVA and RIL evidenced by SEM and AFM analysis was found confirming that RIL can play role of a plasticizer. Thermogravimetric analysis showed that the increase of the RIL content led to the shift of the degradation temperature towards lower values compared to the native PVA film. Nevertheless, it was noted that the degradation onset temperature (T_{onset}) for PVA-based films was around 230°C whatever used RIL. Such thermal stability is sufficient from the point of view of the potential further application in the pervaporation process. Moreover, it is found that the increase of the RIL content decreases the molar swelling degree of the PVA-based films. Such

behaviour may be related to the decrease of the free volume of polymer network, namely, the capability of polymer to swell in water progressively decreases. That result is in accordance with the results of FTIR-ATR and tensile tests revealing that RIL can play role of a physical junction promoter.

The various physicochemical, mechanical, equilibrium, and transport properties of CAP-RIL membranes were determined and compared with the properties of CAP membranes modified with traditional plasticizers, i.e. TBC and ATBC. TGA testified that CAP-RIL membranes as well as CAP membranes modified with TBC and ATBC are thermally stable up to at least 120°C. The tensile tests of membranes revealed the improved mechanical properties reflected by the reduced brittleness and increased elongation at break achieved for CAP-RIL membranes in contrast to pristine CAP membrane. RIL plasticizes CAP matrix and CAP-RIL membranes possess preferable mechanical properties in comparison to membranes with investigated plasticizers. The incorporation of RIL to CAP membranes tuned the surface properties of CAP membranes enhancing their hydrophilic character. Moreover, the addition of RIL into CAP resulted in an excellent improvement of separation factor in comparison to pristine CAP membrane in pervaporation dehydration of propan-2-ol. The separation factor β increased from ca. 10 for pristine CAP membrane to ca. 380 for CAP-16.7-RIL membranes contacting an azeotropic composition of water-propan-2-ol mixture (i.e. 12 wt. % water).

Streszczenie

W ostatnich dziesięcioleciach separacja membranowa odegrała ważną rolę w wielu procesach przemysłowych dzięki swojej wszechstronności, niskiemu zużyciu energii, wysokiej wydajności membran, możliwości pracy ze związkami termolabilnymi, a także możliwości łączenia technologii membranowych z innymi procesami separacji.

Jedną z istotnych technik separacji membranowej jest proces perwaporacji, który stosuje się do rozdzielania dwuskładnikowych lub wieloskładnikowych mieszanin ciekłych, w tym rozpuszczalników o małej temperaturze wrzenia, mieszanin azeotropowych i izomerów. Podczas perwaporacji nadawa jest w bezpośrednim kontakcie z jedną stroną liofilowej membrany, podczas gdy wybrane jej składniki są preferencyjnie transportowane przez membranę.

Membrany stosowane w perwaporacji powinny charakteryzować się wysoką selektywnością, stabilnością chemiczną i wytrzymałością mechaniczną w wysokich temperaturach. Selektywność i właściwości transportowe membrany decydują o ogólnej wydajności procesu separacji. Przeprowadzenie kompleksowej charakterystyki membran może prowadzić do poszerzenia wiedzy na temat wpływu struktury i warunków przygotowania membrany na jej właściwości równowagowe, separacyjne i transportowe. Uzyskana wiedza pozwala na opracowanie nowych materiałów polimerowych o oczekiwanej efektywności w procesie separacji.

Badania nad rozwojem membran do procesów separacyjnych skupiają się również nad przygotowaniem materiałów zawierających ciecze jonowe w celu dostosowania właściwości separacyjnych opracowanych membran wykorzystywanych w perwaporacji, separacji gazów, rozdziale jonów metali oraz służących jako materiały barierowe w ogniwach paliwowych. Ciecze jonowe charakteryzują się dobrą stabilnością termiczną, wysoką przewodnością jonową, znikomą prężnością pary i niską temperaturą topnienia. Ze względu na swoje wyjątkowe właściwości, membrany polimerowe zawierające ciecze jonowe (polimer-ciecz jonowa) mogą posiadać lepsze właściwości separacyjne niż klasyczne membrany polimerowe. Związane jest to ze zwiększoną dyfuzją molekuł w cieczy jonowej w stosunku do polimerów, dlatego wykorzystanie materiałów polimerowych zawierających ciecze jonowe w procesach rozdzielania może skutkować poprawą separacji i wyższymi strumieniami. W celu uzyskania odpowiedniego materiału polimerowego dla danego procesu rozdzielania, morfologia i właściwości

fizykochemiczne cieczy jonowych mogą być dostosowane w zależności od rozdzielanego układu.

Pomimo, że obserwuje się rosnące zainteresowanie zastosowaniem membran polimerowych zawierających ciecze jonowe, procesy separacji oparte na tych materiałach są ograniczone, ze względu na straty niezwiązanej cieczy jonowej w trakcie eksploatacji.

Badania niniejszej rozprawy doktorskiej realizowane są w ramach systemu "co-tutelle" pomiędzy Wydziałem Chemii Uniwersytetu Mikołaja Kopernika w Toruniu (Polska) a Uniwersytetem w Rouen Normandie (Francja). Prace badawcze zostały przeprowadzone w grupie badawczej MPBM w laboratorium Polimerów, Biopolimerów, Powierzchni na Uniwersytecie w Rouen Normandie oraz w Zespole Membran i Technik Membranowych na Wydziale Chemii Uniwersytetu Mikołaja Kopernika w Toruniu.

Głównym celem niniejszej rozprawy doktorskiej jest otrzymanie gęstych membran opartych na poli(alkoholu winylowym) (PVA) i octanie-propionianie celulozy (CAP) zawierających reaktywne i polimeryzowalne ciecze jonowe, w celu uzyskania systemu polimer-ciecz jonowa, w którym ciecz jonowa jest związana wewnątrz struktury polimeru. W ramach niniejszej pracy zbadano charakterystykę fizykochemiczną oraz właściwości równowagowe, barierowe i transportowe otrzymanych membran. Ponadto, wybrane membrany przetestowano w procesie perwaporacji w kontakcie z mieszaniną woda-propan-2-ol.

Nowością tej pracy było wytworzenie materiałów membranowych zawierających ciecze jonowe połączone z matrycą polimerową. Modyfikację chemiczną polimerów przeprowadzono w oparciu o reakcję transestryfikacji w wyniku czego powstały wiązania kowalencyjne pomiędzy polimerem i reaktywnymi cieczami jonowymi.

Wstępne wyniki badań wykazały, że natywna membrana na bazie CAP jest krucha, natomiast natywna membrana na bazie PVA jest rozpuszczalna w wodzie, dlatego wymagane było zastosowanie odpowiednio plastyfikatorów i związków sieciujących. W pierwszym etapie pracy PVA był sieciowany: chemicznie przy użyciu SSA, a następnie termicznie w różnych temperaturach (120, 140 i 160°C). Połączenie chemicznego i termicznego sieciowania membran opartych na PVA zapewnia zwiększoną wydajność sieciowania, a także zwiększoną odporność membran w kontakcie z wodą. W analizie FTIR-ATR stwierdzono, że wzrost stężenia SSA i temperatury sieciowania powodował wzrost intensywności pasm pochodzących od wiązania estrowego powstałego w wyniku reakcji estryfikacji PVA i SSA. Co więcej, wzrost zawartości SSA zmniejszył wartość wydłużenia przy zerwaniu (odpowiednio z 316% dla

czystej membrany PVA do 98% dla membrany zawierającej 33% mas. SSA, a następnie usieciowanej w temperaturze 160°C). Analiza TGA dla natywnej membrany PVA i membran PVA-SSA dowodzi, że wzrost temperatury sieciowania z 120 do 160°C dla danego stężenia SSA poprawił stabilność termiczną membran o 16°C. Badania sorpcji opracowanych membran przeprowadzono w kontakcie z rozpuszczalnikami o różnej polarności, tj. wodą, metanolem i propan-2-olem. Na ich podstawie stwierdzono, że pęcznienie membran PVA-SSA osiąga najwyższą wartość w wodzie, a najniższą w propan-2-olu, tj. pęcznienie w wodzie było odpowiednio około 4000-krotnie i 16-krotnie wyższe niż w propan-2-olu i metanolu. Ponadto, przeprowadzono badania przenikania pary wodnej dla opisanych wyżej membran przy różnej wilgotności względnej. Uzyskane wyniki przenikalności dobrze korelują z wynikami otrzymanymi w trakcie badań pęcznienia.

Biorąc pod uwagę membrany PVA-RIL, analiza FTIR-ATR ujawniła wewnątrzcząsteczkowe oddziaływania oparte na wiązaniach wodorowych między PVA i RIL. Ze względu na amfifilową naturę badanych RIL, która jest związana z obecnością hydrofobowych podstawników etylowych przyłączonych do hydrofilowego pierścienia imidazolowego zawierającego grupy estrowe, obserwuje się występowanie wspomnianego wiązania wodorowego, jak również oddziaływania van der Waalsa i π-π. Na podstawie analizy właściwości mechanicznych filmów PVA-RIL można zaobserwować podwójną funkcję RIL (jako promotora fizycznego sieciowania oraz jako plastyfikatora). Początkowe wprowadzenie 9% mas. RIL do membrany na bazie PVA zmniejszyło ruchliwość łańcuchów PVA, która odpowiada fizycznemu sieciowaniu PVA za pomocą RIL, ze względu na wzmożone interakcje oparte na powstałych wiązaniach wodorowych. Doprowadziło to do zwiększenia sztywności badanych filmów, co było odzwierciedlone przez wzrost wartości modułu Younga (E) i naprężenia przy zerwaniu (σ_{max}) oraz zmniejszenie wartości wydłużenia przy zerwaniu (ε_{max}) w porównaniu z natywnym filmem na bazie PVA. Obecność wyższej zawartości RIL (23% mas.) w układzie PVA-RIL doprowadziła do spadku E i σ_{max} oraz do wzrostu ε_{max} wskazującego na wpływ RIL na elastyczność filmów PVA-RIL. Równocześnie stwierdzono dobrą kompatybilność pomiędzy PVA i RIL, potwierdzoną analizą SEM i AFM. Analiza termograwimetryczna membran PVA-RIL wykazała, że wzrost zawartości RIL prowadzi do przesunięcia temperatury degradacji w kierunku niższych wartości w porównaniu z natywnym filmem na bazie PVA. Niemniej jednak zauważono, że temperatura początku rozkładu (T_{onset}) dla filmów opartych na PVA wynosiła około 230°C, niezależnie od

rodzaju stosowanej RIL. Otrzymana stabilność termiczna badanych filmów PVA-RIL jest wystarczająca z punktu widzenia potencjalnego dalszego zastosowania w procesie perwaporacji. Ponadto stwierdzono, że wzrost zawartości RIL zmniejsza stopień pęcznienia filmów na bazie PVA. Takie zachowanie może być związane ze zmniejszeniem wolnej objętości sieci polimerowej, a mianowicie zdolność polimeru do pęcznienia w wodzie progresywnie maleje. Wynik ten jest zgodny z wynikami FTIR-ATR i analizą właściwości mechanicznych wskazującymi, że RIL może odgrywać rolę promotora fizycznego sieciowania.

W pracy określono również szereg właściwości fizykochemicznych, mechanicznych, równowagowych i transportowych membran CAP-RIL i porównano je z właściwościami membran na bazie CAP zmodyfikowanych plastyfikatorami, tj. TBC i ATBC. Analiza wyników TGA wykazała, że membrany CAP-RIL, jak również membrany CAP zmodyfikowane za pomocą TBC i ATBC, są stabilne termicznie do co najmniej 120°C. Membrany CAP-RIL poddane badaniu właściwości mechanicznych charakteryzowały się zmniejszoną kruchością i zwiększonym wydłużeniem przy zerwaniu w przeciwieństwie do natywnej membrany na bazie CAP. Ponadto, zaobserwowano, iż membrany CAP-RIL posiadają również korzystniejsze właściwości mechaniczne w porównaniu do membran z badanymi plastyfikatorami. Mianowicie, membrany CAP-RIL posiadały wyższe wartości E i ε_{max} dla w odniesieniu do membran CAP zawierających TBC i ATBC. Należy również wspomnieć, że dodatek RIL spowodował wzrost właściwości hydrofilowych membran na bazie CAP, co zostało uwidocznione spadkiem wartości kątów zwilżania dla wody wraz ze wzrostem zawartości RIL. Membrany CAP zawierające RIL1_Br wykazały wyraźną poprawę właściwości separacyjnych w porównaniu z natywną membraną CAP w perwaporacyjnym odwadnianiu propan-2-olu, na co wskazywał wzrost wartości współczynnika podziału β z ok. 10 dla natywnej membrany CAP do ok. 380 dla membrany CAP-16,7-RIL.

Resumé

Au cours des dernières décennies, les technologies membranaires ont largement contribué à l'amélioration des procédés de séparation à l'échelle industrielle grâce à de nombreux avantages, tels que la sélectivité de la séparation élevée, la possibilité de travailler avec des composés thermolabiles et la faible demande en énergie, ainsi que la possibilité de combiner les technologies membranaires avec d'autres procédés de séparation.

Le procédé de pervaporation est une technique de séparation membranaire importante utilisée pour séparer les mélanges liquides binaires ou multicomposants, y compris les solvants à point d'ébullition proche, les mélanges azéotropes et les isomères. Il s'agit du transfert sélectif de matière à travers une membrane dense. Au cours de cette opération, le perméat sous forme vapeur est condensé sur une paroi froide, mais, contrairement à la distillation, seule une faible partie de la charge subit ce changement d'état.

Les membranes utilisées dans la pervaporation doivent posséder une forte sélectivité, une stabilité chimique et une résistance mécanique à haute température élevées. La sélectivité et les propriétés de transport de la membrane déterminent l'efficacité globale du processus de séparation. La caractérisation approfondie des membranes est cruciale pour bien comprendre l'influence de la structure de la membrane et des conditions de préparation de la membrane sur les caractéristiques d'équilibre, de séparation et de transport des membranes étudiées, en vue de développer de nouveaux matériaux polymères efficaces.

Les nombreuses recherches ont également été menées sur le développement des membranes avec de liquides ioniques (LIs) afin de personnaliser les propriétés de séparation des membranes utilisées dans la séparation des liquides par pervaporation, la séparation des gaz et la séparation des ions métalliques ainsi que les membranes conductrices dans les piles à combustible. Les LIs sont caractérisés par une bonne stabilité thermique, une conductivité ionique élevée, une pression de vapeur négligeable et un point de fusion assez bas. En raison de leurs nombreuses propriétés uniques, les membranes polymères contenant des LIs possèdent une large gamme d'avantages, comme de meilleures propriétés de séparation que les membranes polymères classiques. Ce fait est lié à une diffusion moléculaire beaucoup plus élevée dans un liquide ionique que dans

des polymères. Par conséquent, l'utilisation de membranes à base de polymères et LIs dans les processus de séparation permettrait une sélectivité de séparation élevée et des flux plus importants. La structure et les propriétés physicochimiques des LIs peuvent être ciblées en fonction de l'application afin d'obtenir un matériau polymère approprié.

En revanche, même si l'application de membranes hybrides à base de polymères et LIs suscite un intérêt croissant, leur utilisation dans les procédés de séparation reste limitée en raison des pertes de LI non lié.

Cette thèse de doctorat en co-tutelle est réalisée entre la Faculté de Chimie de l'Université Nicolaus Copernicus (NCU) à Toruń (Pologne) et le Laboratoire Polymères, Biopolymères, Surfaces UMR 6270 CNRS de l'Université de Rouen Normandie (France).

L'objectif principal de la thèse est d'élaborer de nouvelles membranes denses à base de poly (alcool vinylique) (PVA) et d'acétate-propionate de cellulose (CAP) et de divers LIs réactifs et polymérisables ceci afin d'obtenir un système polymère-liquide ionique dans lequel le LI est stabilisé par liaison covalente avec les chaînes macromoléculaires du polymère. L'étude des propriétés physicochimiques et d'équilibre des membranes a été effectuée ainsi que l'analyse de leurs propriétés de transport. De plus, les membranes sélectionnées ont été testées dans un processus de pervaporation en contact avec le mélange eau-propane-2-ol.

La nouveauté de ce travail réside dans la formation de matériaux membranaires contenant des liquides ioniques liés à la matrice polymère. La modification chimique par la réaction de transestérification a été effectuée entre le CAP et des LIs à base d'imidazolium fonctionnalisés par un ester. L'approche utilisée a conduit à la formation de liaisons covalentes entre le polymère et le LI.

Les résultats préliminaires ont révélé que le CAP vierge était fragile, alors que le PVA était soluble dans l'eau liquide ; il devenait donc indispensable effectuer la réticulation de membranes. Dans le cas du PVA, le polymère a été réticulé selon une approche en deux étapes : chimiquement avec de l'acide sulfosuccinique (SSA) et thermiquement à différentes températures (120, 140 et 160 °C). La réticulation chimique associée au traitement thermique des membranes à base de PVA confère à la membrane une résistance améliorée au contact de l'eau liquide. L'analyse infrarouge a révélé que l'augmentation de la concentration de SSA et de la température de réticulation entraînait une augmentation de l'intensité des bandes de liaison ester entre le PVA et le SSA du fait de la réaction d'estérification. De plus, l'augmentation de la teneur en SSA réduit

l'allongement à la rupture (passant de 316% pour les membranes de PVA pur à 98% pour les membranes contenant 33% en poids de SSA et réticulées à 160 °C). De plus, les résultats d'analyse thermogravimétrique des membranes montrent que l'augmentation de la température de réticulation de 120 à 160 °C pour une concentration de SSA donnée a amélioré la stabilité thermique des membranes jusqu'à 16 °C de plus. Les mesures de sorption des membranes élaborées ont été réalisées au contact de solvants de polarité différente, à savoir de l'eau, du méthanol et du 2-propanol. Le gonflement des membranes PVA-SSA s'est avéré le plus élevé dans l'eau et le plus faible pour les membranes en contact avec le 2-propanol, c'est-à-dire que le gonflement dans l'eau était environ 4000 fois et 16 fois plus élevé que dans le 2-propanol et méthanol, respectivement. De plus, les mesures de perméation à la vapeur d'eau ont été effectuées à différentes taux d'humidité relative. Les résultats obtenus concordent bien avec les résultats de gonflement.

Pour les membranes PVA-LI, l'analyse infrarouge a montré des interactions intramoléculaires causées par des liaisons hydrogène établies entre le PVA et les LIs. En raison de la nature amphiphile des LIs étudiés, qui est liée à la présence des substituants hydrophobes d'éthyle liés au cycle imidazolium et à la fonction hydrophile ester ; les liaisons d'hydrogène ainsi que les interactions de van der Waals et les interactions π-π ont été observées. Les résultats des essais mécaniques des membranes PVA-LI ont été expliqués par le double rôle du LI – à la fois promoteur de jonction physique et agent plastifiant. Le rajout de 9% en poids de LI dans la membrane à base de PVA a nettement modifié la mobilité des chaînes de PVA à cause de la réticulation entre le PVA et le LI. Ceci a eu pour conséquence l'augmentation de la rigidité de la membrane manifestée par l'augmentation du module de Young (E) et de la contrainte à la rupture (σ_{max}) et la diminution des valeurs d'élongation à la rupture (ε_{max}) par rapport au PVA vierge. A l'inverse, une teneur en LI plus élevée (23% en poids) a conduit à une diminution de E et de σ_{max} et une augmentation de ε_{max} montrant l'influence de la présence de LI sur l'élasticité des membranes PVA-LI. La bonne compatibilité entre le PVA et le LI vérifiée par les analyses microscopiques (MEB et AFM) confirme que le LI agit comme plastifiant. Une analyse thermogravimétrique a montré que l'augmentation de la teneur en LI entraînait une diminution de la température de dégradation. Néanmoins, il a été noté que la température de début de dégradation (T_{onset}) pour les membranes à base de PVA était d'environ 230 °C quelle que soit le LI utilisé. Cette stabilité thermique est largement suffisante compte tenu des applications potentielles visant les processus de pervaporation. De plus, on constate que l'augmentation de la teneur en LI diminue le degré de gonflement

des membranes à base de PVA. Ce comportement peut être lié à la diminution du volume libre du polymère, à savoir que la capacité du polymère à gonfler dans l'eau diminue progressivement. Ce résultat concorde bien avec les résultats de spectroscopie infrarouge et ceux des tests de traction indiquant que le LI peut jouer le rôle de promoteur de jonction physique.

Les propriétés physicochimiques, mécaniques, d'équilibre et de transport des membranes CAP-RIL ont été analysées et comparées à celles des membranes CAP modifiées avec des plastifiants traditionnels comme le TBC ou ATBC. Les résultats d'analyse thermogravimétrique ont montré que les membranes CAP-LI ainsi que les membranes CAP modifiées avec TBC ou ATBC sont thermiquement stables jusqu'à au moins 120 °C. Les mesures de traction des membranes ont révélé l'amélioration des propriétés mécaniques des membranes CAP-RIL à travers la réduction de la fragilité et l'augmentation de l'allongement à la rupture. Le LI plastifie la matrice à base de CAP au point que les membranes CAP-LI possèdent des propriétés mécaniques meilleures par rapport aux membranes contenant des plastifiants classiques. L'incorporation des LIs dans la matrice CAP a permis de modifier les propriétés de surface des membranes renforçant ainsi leur caractère hydrophile. De plus, l'ajout de LI dans le CAP a permis d'obtenir une amélioration significative du facteur de séparation β par rapport à la membrane native de CAP lors de la déshydratation du propan-2-ol par procédé de pervaporation. Pour une composition azéotropique de mélange eau-propane-2-ol (soit 12% en poids d'eau), le facteur de séparation β s'est trouvé très fortement augmenté passant d'environ 10 pour la membrane CAP pur à environ 380 pour les membranes CAP contenant 16,7 % en poids de LI.

Scientific Contributions

Articles (Thesis)

1. **Edyta Rynkowska**, Kateryna Fatyeyeva, Joanna Kujawa, Krzysztof Dzieszkowski, Andrzej Wolan, Wojciech Kujawski, The effect of reactive ionic liquid or plasticizer incorporation on the physicochemical and transport properties of cellulose acetate propionate-based membranes, Polymers 10 (2018) 86 (IF = 2.935). DOI: 10.3390/polym10010086
2. **Edyta Rynkowska**, Kateryna Fatyeyeva, Wojciech Kujawski, Application of polymer based membranes containing ionic liquids in membrane separation processes – a critical review, Reviews in Chemical Engineering 34 (2018) 341-363 (IF = 4.490). DOI: 10.1515/revce-2016-0054
3. **Edyta Rynkowska**, Krzysztof Dzieszkowski, Antoine Lancien, Kateryna Fatyeyeva, Anthony Szymczyk, Joanna Kujawa, Stanisław Koter, Stephane Marais, Andrzej Wolan, Wojciech Kujawski, Physicochemical properties and pervaporation performance of dense membranes based on cellulose acetate propionate (CAP) and containing polymerizable ionic liquid (PIL), Journal of Membrane Science 544 (2017) 243-251 (IF = 6.578). DOI: 10.1016/j.memsci.2017.09.031

Articles (Other)

4. Corinne Chappey, Kateryna Fatyeyeva, **Edyta Rynkowska**, Wojciech Kujawski, Larisa Karpenko-Jereb, Anne-Marie Kelterer, Stephane Marais, Sulfonic Membrane Sorption and Permeation Properties: Complementary Approaches to Select a Membrane for Pervaporation, Journal of Physical Chemistry B 121 (2017) 8523–8538 (IF = 3.146). DOI: 10.1021/acs.jpcb.7b06305
5. Jan Kujawski, Wojciech Kujawski, Henryk Sondej, Karolina Jarzynka, Anna Kujawska, Marek Bryjak, **Edyta Rynkowska**, Katarzyna Knozowska, Joanna Kujawa, Dewatering of 2,2,3,3-tetrafluoropropan-1-ol by hydrophilic pervaporation with poly(vinyl alcohol) based Pervap^{TM} membranes, Separation and Purification Technology 174 (2017) 520-528 (IF = 3.927). DOI: 10.1016/j.seppur.2016.10.041
6. **Edyta Rynkowska**, Joanna Kujawa, Corinne Chappey, Kateryna Fatyeyeva, Larisa Karpenko-Jereb, Anne-Marie Kelterer, Stephane Marais, Wojciech Kujawski, Effect

of the polar–nonpolar liquid mixtures on pervaporative behavior of perfluorinated sulfonic membranes in lithium form, Journal of Membrane Science 518 (2016) 313-327 (IF = 6.035). DOI: 10.1016/j.memsci.2016.07.008

7. Larisa Karpenko-Jereb, **Edyta Rynkowska**, Wojciech Kujawski, Sarah Lunghammer, Joanna Kujawa, Stephane Marais, Kateryna Fatyeyeva, Corinne Chappey, Anne-Marie Kelterer, Ab-initio study of cationic polymeric membranes in water and methanol, Ionics 22 (2016) 357-367 (IF = 2.062). DOI: 10.1007/s11581-015-1551-7

Oral communications

1. E. Rynkowska, K. Fatyeyeva, J. Kujawa, A. Wolan, K. Dzieszkowski, W. Kujawski, Elaboration and characterization of PVA-based composite films with ester-functionalized ionic liquids, XII Copernican International Young Scientists Conference, 28-29.06.**2018**, Toruń (Poland)
2. E. Rynkowska, K. Fatyeyeva, K. Dzieszkowski, J. Kujawa, W. Kujawski, Preparation and characterization of cellulose acetate propionate based membranes functionalized with reactive ionic liquids of various nature, Workshop of Students' Presentations 2017, 18.10.**2017**, Straz pod Ralskem (Czech Republic) – **1st prize awarded**
3. E. Rynkowska, K. Fatyeyeva, K. Dzieszkowski, J. Kujawa, W. Kujawski, Effect of reactive ionic liquid and plasticizer incorporation on physicochemical and transport properties of cellulose acetate propionate-based membranes, 5th International Scientific Conference on Pervaporation, Vapor Permeation, and Membrane Distillation, 20-23.06.**2017**, Toruń (Poland) – **1st prize awarded**
4. K. Dzieszkowski, E. Rynkowska, K. Fatyeyeva, J. Kujawa, A. Wolan, W. Kujawski, Synteza, właściwości i wykorzystanie cieczy jonowych do modyfikacji membran polimerowych, Ogólnopolska Szkoła Chemii, 10-14.11.**2016**, Rozewie (Poland)
5. E. Rynkowska, W. Kujawski, C. Chappey, K. Fatyeyeva, L. Karpenko-Jereb, A.-M. Kelterer, S. Marais, J. Kujawa, Ion-pairs dissociation of sulfonic groups – lithium counter-ions during pervaporation of polar – non-polar binary liquid mixtures using perfluorinated ion-exchange membranes, Membranes and Membrane Processes in Environmental Protection, 15-18.06.**2016**, Zakopane (Poland) – **2nd prize awarded**
6. E. Rynkowska, K. Fatyeyeva, S. Marais, A. Wolan, W. Kujawski, Behaviour of Novel Crosslinked PVA/Ionic Liquid Membranes in Contact with Polar Solvents, The 24th

Annual World Forum on Advanced Materials (Polychar), 9-13.05.**2016**, Poznań (Poland)

Poster communications

1. E. Rynkowska, K. Fatyeyeva, J. Kujawa, A. Wolan, K. Dzieszkowski, W. Kujawski, Tailoring of polymer membranes properties with reactive ionic liquids, Euromembrane 2018, 09-13.07.**2018**, Valencia (Spain)
2. E. Rynkowska, K. Fatyeyeva, J. Kujawa, A. Wolan, K. Dzieszkowski, W. Kujawski, The Effect of Reactive Ionic Liquid or Plasticizer Incorporation on Physicochemical, Equilibrium, and Transport Properties of Cellulose Acetate Propionate-Based Membranes, Polymers: Design, Function and Application, 21-23.03.**2018**, Barcelona (Spain)
3. E. Rynkowska, K. Fatyeyeva, K. Dzieszkowski, J. Kujawa, A. Wolan, S. Marais, W. Kujawski, Cellulose acetate propionate based membranes with poly(ionic liquid): elaboration and characterization, XIV Szkoła Membranowa Od badań podstawowych do wdrożenia, 22-25.10.**2017**, Wilga k. Warszawy (Poland)
4. E. Rynkowska, K. Fatyeyeva, S. Marais, K. Dzieszkowski, A. Wolan, J. Kujawa, W. Kujawski, Properties of novel cellulose acetate propionate based materials containing reactive ionic liquid or plasticizer, 2017 International Congress on Membranes and Membrane Processes (ICOM), 29.07.-04.08.**2017**, San Francisco (USA)
5. E. Rynkowska, K. Fatyeyeva, A. Wolan, S. Marais, J. Kujawa, W. Kujawski, Properties of novel polymer based materials containing polymerisable ionic liquid, The 2016 European Membrane Society Summer School on Membranes and Membrane Processes Design, 26.06.-01.07.**2016**, Bertinoro (Italy)
6. W. Kujawski, E. Rynkowska, K. Fatyeyeva, A. Wolan, K. Dzieszkowski, J. Kujawa, Properties of poly(vinyl alcohol) based materials containing reactive ionic liquids, Ionothermal Synthesis Symposium: Exploiting Ionic Liquids for Advanced Materials Synthesis & Design, 28-30.09.**2016**, Potsdam (Germany)
7. W. Kujawski, A. Kraslawski, A. Kujawska, K. Knozowska, E. Rynkowska, K. Jarzynka, M. Bryjak, J. Kujawski, J. Kujawa, Impact of organic component on separation efficiency of hydrophilic pervaporation with polymeric membranes, 4th International Conference on Methods and Materials for Separation Processes, 04-08.09.**2016**, Brunów/Lwówek Śląski (Poland)

8. L. Karpenko-Jereb, E. Rynkowska, A.-M. Kelterer, W. Kujawski, Effect of counter-ions on the water state in the polymer electrolytes: computational study, Ion Transport in Organic and Inorganic Membranes, 23-28.05.**2016**, Sochi (Russia)
9. E. Rynkowska, A. Lancien, K. Fatyeyeva, A. Szymczyk, A. Wolan, S. Koter, W. Kujawski, Preliminary Studies on the Properties of Novel Polymer Based Materials Containing Polymerisable Ionic Liquid, XIII Polish Membrane School, 18-21.10.**2015**, Przysiek k/Torunia (Poland)
10. L. Karpenko-Jereb, E. Rynkowska, W. Kujawski, C. Chappey, K. Fatyeyeva, S. Marais, A.-M. Kelterer, Ab-initio study of cation-exchange membranes in water and methanol, Euromembrane 6-10.09.**2015**, Aachen (Germany)